Search for new physics with atoms and molecules

M. S. Safronova

University of Delaware, Newark, Delaware 19716, USA
and Joint Quantum Institute, National Institute of Standards and Technology
and the University of Maryland, College Park, Maryland 20742, USA

D. Budker

Helmholtz Institute, Johannes Gutenberg University, Mainz, Germany,
University of California, Berkeley, California 94720, USA,
and Nuclear Science Division, Lawrence Berkeley National Laboratory,
Berkeley, California 94720, USA

D. DeMille

Yale University, New Haven, Connecticut 06520, USA

Derek F. Jackson Kimball

California State University, East Bay, Hayward, California 94542, USA

A. Derevianko

University of Nevada, Reno, Nevada 89557, USA

Charles W. Clark

Joint Quantum Institute, National Institute of Standards and Technology
and the University of Maryland, College Park, Maryland 20742, USA

(published 29 June 2018)

This article reviews recent developments in tests of fundamental physics using atoms and molecules, including the subjects of parity violation, searches for permanent electric dipole moments, tests of the *CPT* theorem and Lorentz symmetry, searches for spatiotemporal variation of fundamental constants, tests of quantum electrodynamics, tests of general relativity and the equivalence principle, searches for dark matter, dark energy, and extra forces, and tests of the spin-statistics theorem. Key results are presented in the context of potential new physics and in the broader context of similar investigations in other fields. Ongoing and future experiments of the next decade are discussed.

CONTENTS

I. INTRODUCTION

A. Recent advances in atomic, molecular, and optical physics

The past two decades have been a transformational era for atomic, molecular, and optical (AMO) physics, due to extraordinary accomplishments in the control of matter and light. Experimental breakthroughs, including laser cooling and trapping of atoms, attainment of Bose-Einstein condensation, optical frequency combs, and quantum control—the subject of Nobel Prizes in Physics in 1997 (Chu, 1998; Cohen-Tannoudji, 1998; Phillips, 1998), 2001 (Cornell and Wieman, 2002; Ketterle, 2002), 2005 (Glauber, 2006; Hall, 2006; Hänsch, 2006), and 2012 (Haroche, 2013; Wineland, 2013), respectively—have led to widespread availability of ultracold (temperature $T < 1\ \mu K$) ions, atoms, and molecules, subject to precise interrogation and control. Revolutionary developments on several fronts have been made possible by these advances, aided by improvements in precision time and frequency metrology, measurement techniques such as atomic magnetometry and interferometry, and first-principles atomic and molecular theory. These advances brought forth a plethora of new AMO applications, including novel tests of the fundamental laws of physics.

B. Problems with the standard model

The standard model (SM) of particle physics (Patrignani *et al.*, 2016) has been exceptionally successful in predicting and describing numerous phenomena and has been extensively tested by a multitude of different approaches spanning most fields of physics. Despite its great success, the SM has major problems. Indeed, it is inconsistent with the very existence of our Universe: the standard model cannot account for the observed imbalance of matter and antimatter (Dine and Kusenko, 2003). In addition, all attempts to combine gravity with the fundamental interactions described by the SM have been unsuccessful.

A long-standing mystery dating back to the 1930s (Zwicky, 1933) is the apparent existence of "dark matter" (DM) that is observed only via its gravitational interactions. This is confirmed by numerous studies of astronomical objects, which show that the particles of the SM make up only $\approx 16\%$ of the total matter present in our Universe. Decades of investigation have not identified the nature of dark matter

(Bertone, 2013). We now know what most of it is not—any of the particles of the SM.

Studies of the type I supernovae which were originally aimed at measuring the deceleration rate of the Universe arrived at a completely unexpected result: the expansion of the Universe is now accelerating (Perlmutter, 2012; Riess, 2012; Schmidt, 2012). This seems to be possible only if our Universe contains a kind of "dark energy" which effectively acts as repulsive gravity. While we do not know what dark matter is, we know even less what such dark energy could be—while vacuum energy is a handy potential candidate, the discrepancy between the sum of known contributions to vacuum energy in the Universe and the cosmologically observed value is 55 orders of magnitude (Solà, 2013). According to the 2015 results of the Planck Mission study of cosmic microwave background radiation (Adam *et al.*, 2016), our present Universe is 69% dark energy, 26% dark matter, and 5% ordinary (standard model) matter.

In summary, we are at an extraordinary point in time for physics discovery. We have found all of the particles of the SM and have tested it extensively, but we do not know what makes 95% of the Universe, nor how ordinary matter survived against annihilation with antimatter in the aftermath of the big bang. This provides strong motivation to search for new particles (and/or the associated fields) beyond those described in the SM.

C. Search for new physics with precision measurements

While one can search for new particles directly with large-scale collider experiments at the TeV energy scale, such as those carried out at the Large Hadron Collider (LHC) at CERN, new physics may also be observed via low-energy precision measurements. An early example of the use of AMO physics in this paradigm, beginning in the 1970s, was the deployment of highly sensitive laser-based techniques to observe parity violation in optical transitions in atoms. This parity violation occurs due to exchange of Z bosons between electrons and nuclei in atoms, and quantitative measurements of the strength of the effect can be used to test the predictions of theoretical models of the electroweak interaction (Khriplovich, 1991). These investigations quickly led to the realization that the accuracy of first-principles theory of atomic structure needed radical improvement in order to interpret the experimental results. This was particularly true for heavy atoms like cesium (Cs, $Z = 55$), which required the development of novel theoretical methodologies enabled by modern computing architecture (Porsev, Beloy, and Derevianko, 2009). Improved computational resources and development of high-precision methodologies have led to essential progress in related theoretical investigations, enabling improved analyses of precision experiments, development of new experimental proposals, and improved theoretical predictions for yet unmeasured quantities. As a result, analyses of the Cs atomic parity violation (APV) experiment (Wood *et al.*, 1997) provided the most accurate to-date tests of the low-energy electroweak sector of the SM and constraints on a variety of scenarios for physics beyond the SM (Porsev, Beloy, and Derevianko, 2009; Dzuba *et al.*, 2012). Combined with the results of high-energy collider experiments, Cs APV

studies confirmed the energy dependence of the electroweak force over an energy range spanning 4 orders of magnitude (Porsev, Beloy, and Derevianko, 2009). Further details are given in Sec. IV.A.

Similarly, for several decades AMO experiments have been employed to search for violation of time-reversal (T) symmetry, as manifested by an electric dipole moment (EDM) along the angular momentum axis of a quantized system. T violation is required to generate a cosmological matter-antimatter asymmetry, and sources beyond those in the SM are required to explain the magnitude of the observed imbalance (Dine and Kusenko, 2003). Extensions to the SM frequently introduce new sources of T violation that are associated with new particles (Barr, 1993). In theories where these new particles have mass at the TeV scale, or sometimes well above it, EDMs are typically predicted with size near the limits set by current AMO experiments (Pospelov and Ritz, 2005; Engel, Ramsey-Musolf, and van Kolck, 2013). Hence these EDM experiments probe commonly predicted physics at similar or higher energy scales than those accessible with the LHC. New experiments based on large enhancements of the observable EDM effects (in experiments using polar molecules or deformed nuclei) hold the promise to increase the energy reach for probing new T-violating physics by an order of magnitude or even more in the near future. Further details are given in Sec. V.

AMO experiments also probe even higher energy scales. A number of theories aiming to unify gravity with other fundamental interactions suggest violations of cornerstones of modern physics such as Lorentz symmetry and combined charge conjugation (C), parity (P), and time-reversal (CPT) invariance (Colladay and Kostelecký, 1998; Kostelecký and Russell, 2011) and imply spatiotemporal variation of fundamental constants (Uzan, 2011). Whereas the energy scale of such physics is much higher than that attainable at present by particle accelerators, Lorentz violation may nevertheless be detectable via precision measurements at low energies.

The unprecedented accuracy of AMO precision measurements coupled with accurate theory predictions facilitated significant expansion of AMO fundamental physics studies. As a result, AMO physics now addresses questions in fields from which it was once quite remote, such as nuclear, particle, gravitational physics, and cosmology.

For example, a number of AMO technologies such as high-precision magnetometery (Pustelny *et al.*, 2013; Budker *et al.*, 2014), atom interferometry (Hamilton *et al.*, 2015), atomic clocks (Derevianko and Pospelov, 2014), and ultrahigh-intensity lasers (Di Piazza *et al.*, 2012) are aimed at the search for axions and other dark matter and dark energy candidates. The principles of a new technique for detecting transient signals of exotic origin using a global network of synchronized optical magnetometers were demonstrated by Pustelny *et al.* (2013). The network may probe stable topological defects (e.g., domain walls) of axionlike fields.

A recent Cs matter-wave interferometry experiment constrained a wide class of dynamical dark energy theories (Hamilton *et al.*, 2015). The exceptional sensitivity of matter-wave interferometers operated with quantum gases has generated new ideas for probing the fundamental concepts of quantum mechanics, tests of general relativity, and gravitational-wave detection (Müntinga *et al.*, 2013; Biedermann

et al., 2015; Hogan and Kasevich, 2016). The first quantum test of the universality of free fall with matter waves of two different atomic species was reported by Schlippert *et al.* (2014).

The accuracy of atomic clocks has improved by a factor of 1000 in the past 10 years, to a fractional frequency uncertainty of 2 parts in 10^{18} (Nicholson *et al.*, 2015; Ushijima *et al.*, 2015) which corresponds to a temporal uncertainty of 1 s in the lifetime of our Universe. As a result, atomic clocks are now used to search for possible time variations of the dimensionless fine-structure constant α and proton-electron mass ratio m_p/m_e (Rosenband *et al.*, 2008; Godun *et al.*, 2014; Huntemann *et al.*, 2014).

A demonstration of the potential of quantum-information techniques in the search for physics beyond the SM was provided by Pruttivarasin *et al.* (2015). Using a pair of trapped calcium (Ca, $Z = 20$) ions in a decoherence-free subspace, they improved by a factor of 100 the bounds on a number of Lorentz-symmetry violating parameters of the standard model extension (SME) for electrons.

D. Scope of this review

These examples show the diversity of recent AMO searches for new physics. Here we review this subject as a whole rather than limit the treatment to a few specific topics, since this field is based on a commonality of approaches that is likely to have even wider applicability in the future, given the growth that we have witnessed recently.

Another active area of AMO physics is the simulation of condensed-matter systems using ultracold atoms in optical potentials. This field has aspects of searches for new physics associated with novel quantum phases, non-Abelian gauge potentials, atomtronics, and the like. Our review will not deal with such topics since they are already addressed by other reviews (Lewenstein *et al.*, 2007; Bloch, Dalibard, and Zwerger, 2008; Bloch, Dalibard, and Nascimbène, 2012; Stamper-Kurn and Ueda, 2013; Windpassinger and Sengstock, 2013; Georgescu, Ashhab, and Nori, 2014; Goldman *et al.*, 2014; Ueda, 2014) and constitute a vast subject in their own right. We will also exclude detailed consideration of quantum mechanics tests with AMO systems which have been recently reviewed as well (Hornberger *et al.*, 2012; Bassi *et al.*, 2013; Aspelmeyer, Kippenberg, and Marquardt, 2014).

Since the field of AMO tests of fundamental physics is a vast subject spanning decades of research, we limit this review to recent developments and proposals. For each topic, we begin with an introduction to its specific relevance to physics beyond the SM. We present recent key results in the context of potential new physics and summarize ongoing and future experiments of the next decade.

II. SEARCH FOR VARIATION OF FUNDAMENTAL CONSTANTS

A. Fundamental constants: An introduction

First we have to define what we mean by "fundamental constants." Opening a textbook on various fields of physics would produce different lists of measured quantities of

specific importance to a given field. In this review, we follow the definition of Uzan (2015): A fundamental constant is *any parameter not determined by the theories in which it appears*. This definition has the following implications:

- the number of fundamental constants depends on a particular theory, and
- the fundamental constants are not predicted by any theory and thus their values must be determined through measurements.

Present physics is described by general relativity (GR) and the SM of particle physics that combines quantum chromodynamics (QCD) with the electroweak theory (Patrignani *et al.*, 2016). The minimal SM has 19 parameters, with somewhat different sets of these parameters given in the literature (Hogan, 2000; Scott, 2006; Uzan, 2013). Following the summary of Scott (2006), the list contains six quark masses, three lepton masses, three quark mixing angles (θ_{12}, θ_{23}, and θ_{13}) and phase δ, three electroweak parameters (fine-structure constant α, Fermi coupling constant G_F, and mass of the Z boson M_Z), Higgs mass, strong combined charge conjugation and parity (*CP*) violating phase, and the QCD coupling constant. The incorporation of the neutrino masses leads to additional parameters.

To reproduce known physics, the SM parameters must be supplemented by the Newtonian constant of gravitation G of GR, the speed of light in vacuum c, and the Planck constant h. We note that this list of fundamental constants lacks any description of either dark matter or dark energy and contains no cosmological information about the Universe. The standard cosmological model adds 12 more parameters, listed by Scott (2006) which include the Hubble constant, baryon, cold dark matter and dark energy densities, and others. Further understanding of these phenomena may increase the required number of fundamental constants, while developing a unified theory might reduce them.

Measurements of fundamental constants and numerous other derived quantities, some of which can be predicted from current theories with varying levels of accuracy, is a vast area of research. We refer the interested reader to the publications of the Committee on Data for Science and Technology (CODATA) (Mohr, Newell, and Taylor, 2016) and the Particle Data Group (PDG) (Patrignani *et al.*, 2016) for measurement techniques, analysis of data, and current recommended values. The data are continuously revised and improved, with critical assessment of various types of experiments carried out prior to new CODATA and PDG publications.

It should be kept in mind that there is *no single experiment* that determines the CODATA recommended value of a given fundamental constant. There is a complex web of deep and sometimes subtle connections between fundamental constants, for example, between the fine-structure constant and the molar Planck constant $N_A h$ (Mohr, Newell, and Taylor, 2016), and the CODATA recommended values are determined by a least-squares adjustment that keeps inconsistencies within limits.

An example of this interdependence, that is highlighted by Mohr, Newell, and Taylor (2016) and is of particular relevance to AMO physics, is the determination of the fine-structure constant

$$\alpha = \frac{1}{4\pi\epsilon_0} \frac{e^2}{\hbar c}, \tag{1}$$

which characterizes the strength of the electromagnetic interaction; see Sec. III. Here e is the elementary charge, $\hbar = h/2\pi$ is the reduced Planck constant, and ϵ_0 is the electric constant. A recent overview of the determinations of fundamental constants from low-energy measurements is given by Karshenboim (2013).

We note that the values of the coupling constants of the SM depend on the energy at which they are measured (the so-called "running" of the coupling constants discussed using the example of $\sin^2\theta_W$ in Sec. IV.A). The fine-structure constant α is defined in the limit of zero momentum transfer.

B. Units of measurement versus fundamental constants

Experimental measurements can be reduced to comparing two physical systems, one of which defines the unit of measurement. For example, the International System of Units (SI) unit of time is defined as follows: "The second is the duration of 9 192 631 770 periods of the radiation corresponding to the transition between the two hyperfine levels of the ground state of the cesium 133 atom" (BIPM, 2014). This definition refers to a Cs atom at rest at a temperature of 0 K. Therefore, absolute values of all other frequencies are determined relative to this Cs frequency and no absolute frequency measurement can be performed with smaller fractional frequency uncertainty than that of the best Cs frequency standard, which is presently on the order of 10^{-16} (Guéna *et al.*, 2010, 2012; Szymaniec *et al.*, 2010; Heavner *et al.*, 2014; Levi *et al.*, 2014). Note that one can still make *relative* comparison of two frequencies to much better precision than the Cs standard provides (Ushijima *et al.*, 2015). To make absolute frequency measurements accurate to, for example, 10^{-18} of a second, we would need to change the definition of the second from the Cs microwave frequency transition to another physical system. Such system must allow for the construction of a frequency standard with 10^{-18} fractional uncertainty in a consistently reproducible way, accompanied by a global technology infrastructure for frequency comparison (Poli *et al.*, 2013; Ludlow *et al.*, 2015).

Changing the values of the constants in such a way that all dimensionless combinations are unchanged will simply change the units. For example, in atomic units of measurement the values of e, the electron mass m_e, and the reduced Planck constant $\hbar$ have the numerical value of 1, and the electric constant ϵ_0 has the numerical value of $1/(4\pi)$. However, the value of the dimensionless fine-structure constant α is still the same as in SI units as given by Eq. (26).

Dimensionless fundamental constants play a special role in discussions of spatiotemporal variations of physical laws. Their values are, by construction, independent of the choice of units of measurement, which are arbitrary conventions that have changed in the past and may change in the future.

For example, it is difficult to see how one could unambiguously measure a time variation in the speed of light c. This may be viewed from the perspective of 1982. Then the second and the meter were defined independently: the second as it is today, a defined multiple of the period of the ground hyperfine

transition of ^{133}Cs, and the meter as a defined multiple of the wavelength of the $2p_{10} - 5d_5$ spectral line of the ^{86}Kr isotope of krypton (Kr, $Z = 36$). On a simple observational basis, if a change in the 1982 value of c was well established on the basis of multiple independent observations, it seems impossible to disentangle that effect from changes in either, or both, of the Cs frequency or the Kr wavelength.

The focus of modern studies of the variation of fundamental constants is thus on dimensionless constants, and as concerns AMO physics, particularly on α and the proton-to-electron mass ratio, $m_{\rm p}/m_{\rm e}$.

C. Theories with varying fundamental constants

While the 2014 CODATA value of fine-structure constant α has a remarkably small 2.3×10^{-10} relative uncertainty, it remains an open question whether the value of α is variable across space and time. In the SM, all fundamental constants are invariable. The dimensionless constants become dynamical (i.e., varying) in a number of theories beyond the SM and GR. A detailed review and references to theories with varying fundamental constants are given by Uzan (2011) so we give only a brief summary here.

Higher-dimensional theories, in particular, string theories, naturally lead to varying fundamental constants. String theories predict the existence of a scalar field, the dilaton, that couples directly to matter (Taylor and Veneziano, 1988). The four-dimensional coupling constants are determined in terms of a string scale and various dynamical fields. As a result, the coupling constants naturally become varying, evaluated as the expectation values of these dynamical fields. The variation of the gauge couplings and of the gravitational constant may also arise from the variation of the size of the extra dimensions.

Many other theories beyond the SM and GR have been proposed in which fundamental constants become dynamic fields. These include discrete quantum gravity (Gambini and Pullin, 2003), loop quantum gravity (Taveras and Yunes, 2008), chameleon models (Khoury and Weltman, 2004a), dark energy models with a nonminimal coupling of a quintessence field (Avelino *et al.*, 2006), and others. As a result, studies of the variation of the fundamental constant may provide some information on the potential origin of dark energy. Analysis of experiments on the variation of fundamental constants also depends on the nature of the particular model. For example, a chameleon field is expected to be more massive in high-density regions on Earth than in low-density regions of the Solar System (Khoury and Weltman, 2004a). Since the constants would be dependent on the local value of the chameleon field, the values of the constants become dependent on their (mass density) environment.

While one can construct models in which only one or a few constants vary, in most realistic current models, all constants vary if one does (Uzan, 2015). In unified theories of fundamental interactions the variations of fundamental constants are correlated. However, including such correlations in the analysis of experiments leads to dependence of the results on the particular model.

It has been pointed out that searching for a variation of fundamental constants is a test of the local position invariance hypothesis and thus of the equivalence principle [see Uzan (2011, 2015), and references therein].

Searches for variation of fundamental constants are conducted in a number of systems including atomic clocks, astrophysical studies of quasar spectra, and the observation of the HI 21 cm line, the Oklo natural nuclear reactor, meteorite dating, stellar physics, cosmic microwave background (CMB), and big bang nucleosynthesis (BBN). A detailed review of these topics is given by Uzan (2011). We limit our coverage to recent results, ongoing experiments, and proposals relevant to AMO physics.

Laboratory tests for the variation of fundamental constants, such as carried out with atomic clocks, are sensitive only to present-day variation, while other searches are probing whether α and other constants were different in the past compared to what they are now, with different look-back times. We discuss this further in Sec. II.H. The analysis of CMB and BBN in terms of constraining the variation of fundamental consistent is also dependent on the cosmological model.

In this section, we consider the "slow-drift" model of variation of fundamental constants, as well as coupling of fundamental constants to a changing gravitational potential, and testing for a dependence of fundamental constants on the mass density of the environment. Searches for oscillatory and transient variation of fundamental constants, and their relevance to the nature of dark matter and dark energy, are discussed in Sec. IX.

D. Tests of fundamental constant variations with atomic clocks

The most precise tests of modern-epoch variation of fundamental constants are carried out using atomic clocks. From the standpoint of metrology and other precision experiments, testing the variation of fundamental constants is necessary to ensure that the experiments are reproducible at the level of their uncertainties. This became particularly important due to exceptional improvement of AMO precision metrology in recent years. If α or $\mu = m_{\rm p}/m_{\rm e}$ are spacetime dependent, so are atomic and molecular spectra. Therefore, the variation of the fundamental constants makes the clock tick rate dependent on location, time, and type of the clock—since frequencies of Cs or Sr depend differently on fundamental constants. We have arrived at a level of precision such that new physics might show up unexpectedly as an irreducible systematic error. An important question for AMO theory is predicting the best systems for dedicated experiments where the variation of fundamental constants is strongly enhanced.

We start with the discussion of the dependence of atomic spectra on the dimensionless constants of interest. The possibility of using atomic spectroscopy to detect variations in the fine-structure constant α is suggested in Dirac's theory of the hydrogen atom. The energies of $E_{n,j}$ of a Dirac electron bound to an infinite-mass point nucleus are given by

$$E_{n,j} = m_{\rm e} c^2 \left[1 + \frac{(Z\alpha)^2}{[n - j - (1/2) + \sqrt{(j+1/2)^2 - (Z\alpha)^2}]^2} \right]^{-1/2},$$

(2)

where Ze is the charge of the nucleus, with e the elementary charge, n is the principal quantum number, and j is the electronic angular momentum in units of $\hbar$ (Greiner, 2000; Johnson, 2007). With reference to the discussion of Sec. II.A, note that the Rydberg constant is given by

$$R_\infty = \frac{1}{hc}\frac{\alpha^2}{2}m_e c^2. \qquad (3)$$

The only fundamental constants present in Eq. (2) are α^2 and the rest mass energy of the electron $m_e c^2$. Expansion of $E_{n,j}$ in powers of α^2 shows that for electronic states with different values of the principal quantum number n, the energy splitting scales with α^2, whereas the splitting scales with α^4 for states with the same n but different j. Thus, ratios of the wavelengths of these two types of transitions are sensitive to variations in α. The dependence of the atomic spectra of more complicated atoms on fundamental constants is discussed next.

1. Dependence of hyperfine and electronic transitions on dimensionless constants

Interaction of atomic electrons with the magnetic and electric multipole fields of the nucleus leads to a splitting of atomic energy levels referred to as hyperfine structure. For example, the nuclear angular momentum of ^{133}Cs is $I = 7/2$ and the ground-state electronic configuration consists of a closed Xe-like core (xenon, $Z = 54$) with an unpaired single valence electron with $j = 1/2$. Therefore, the Cs [Xe]$6s$ ground state splits into two hyperfine levels, with $F = 3$ and 4, where the total angular momentum is $\mathbf{F} = \mathbf{I} + \mathbf{J}$. The frequency of electromagnetic radiation associated with transitions between these levels is conventionally expressed as

$$\nu_{\text{hfs}} \sim cR_\infty A_{\text{hfs}} g_i \frac{m_e}{m_p}\alpha^2 F_{\text{hfs}}(\alpha), \qquad (4)$$

where A_{hfs} is a number depending on the particular atom, and $F_{\text{hfs}}(\alpha)$ is a relativistic correction specific to each hyperfine transition. The dimensionless $g_i = \mu_i/\mu_N$ is the g factor associated with the nuclear magnetic moment μ_i, where $\mu_N = e\hbar/2m_p$ is the nuclear magneton.

The Cs hyperfine $F = 3 - F = 4$ transition frequency ν_{Cs} of ≈ 9 GHz defines the second, and all *absolute* frequency measurements are actually measurements of ν/ν_{Cs} frequency ratios. Atomic clocks based on hyperfine transitions are referred to in the literature as "microwave clocks," specifying the relevant region of the electromagnetic spectrum (Poli *et al.*, 2013; Ludlow *et al.*, 2015).

The transition frequency between electronic energy levels in an atom can be expressed as

$$\nu \sim cR_\infty A F(\alpha), \qquad (5)$$

where A is the numerical factor depending on an atom and $F(\alpha)$ depends upon the particular transition. Atomic clocks based on electronic transitions with frequencies from $\approx 0.4 \times 10^{15}$ to $\approx 1.1 \times 10^{15}$ Hz are referred to in the literature as "optical clocks."

2. Theoretical determination of the sensitivity of atomic transitions to variations of α

The coefficient $F(\alpha)$ in Eq. (5) is obtained by calculating the α dependence of the energies of the two atomic levels involved in the transition. The dependence of electronic energy level E on α is usually parametrized by the coefficient q (Dzuba, Flambaum, and Webb, 1999a, 1999b):

$$E(\alpha) = E_0 + q\left[\left(\frac{\alpha}{\alpha_0}\right)^2 - 1\right], \qquad (6)$$

which can be determined rather accurately (generally to 1%–10%) from atomic-structure computations. Here α_0 is the current CODATA value of α, the measurement of which is discussed in Sec. III.B, and E_0 is the energy corresponding to this value of α_0. The coefficient q depends weakly on electron correlations, so it can be calculated more accurately than the actual energy of a level.

The coefficient q of an atomic state is computed by varying the numerical value of α in the computation of the respective energy level (Dzuba and Flambaum, 2009b). Generally, three energy level calculations are performed which differ only by the values of α. The first calculation uses the current CODATA value of α^2. Two other calculations are performed with α^2 varied by a small but non-negligible amount, commonly selected at $\delta = 0.01$. Then the value of q is derived from a numerical derivative

$$q = \frac{E(\delta) - E(-\delta)}{2\delta}, \qquad (7)$$

where $E(\pm\delta)$ are results of the energy calculations. The additional calculation (with the CODATA value of α) is used to verify that the change in the energy is close to linear.

The parameter q links variation of the transition energy E, and hence the atomic frequency $\nu = E/h$, to the variation of α

$$\frac{\delta E}{E_0} = \frac{2q}{E_0}\frac{\delta\alpha}{\alpha_0} \equiv K\frac{\delta\alpha}{\alpha_0}, \qquad (8)$$

where

$$K = \frac{2q}{E_0} \qquad (9)$$

is a dimensionless sensitivity factor.

In α-variation tests with atomic clocks, the ratio of two clock frequencies is monitored, and the sensitivity to the variation of α is then given by the difference in their respective K values for each clock transition, i.e., $\Delta K = |K_2 - K_1|$. The larger the value of K, the more sensitive is a particular atomic energy level to the variation of α.

A note of caution has to be added here: while small E_0 may lead to large K following Eq. (9), it may also lead to technical difficulties in measuring the relevant frequency with the extremely high accuracy that is required for tests of variation of fundamental constants. Small energy E_0 corresponds to transitions in the infrared, with wavelengths that may exceed 3000 nm. Accurate theory predictions are particularly difficult

for such transitions, as small E_0 is the result of strong cancellations of upper and lower energies, leading to difficulties in locating weak clock transitions. Moreover, the clock instability is inversely proportional to the transition frequency, so lower frequency leads to higher ultimate instability, which is particularly problematic with single-ion clocks. Therefore, the actual transition frequency and other experimental considerations have to be taken into account when designing dedicated experiments. This issue is further discussed in Sec. II.F.

3. Microwave versus optical clock-comparison experiments

At the lowest level of the analysis that requires only atomic structure calculations, measuring the ratios $R = \nu_1/\nu_2$ of two clocks over time may set limits on variation of α, the proton-to-electron mass ratio $\mu = m_p/m_e$, and nuclear g factors, specifically g_{Cs} and g_{Rb} as these correspond to two microwave clocks with the smallest uncertainties. We summarize the dependence of clock-frequency ratios on the dimensionless constants as follows:

- The ratio of two microwave clock frequencies depends on α and g factors of the corresponding nuclei according to Eq. (4). For example, the ratio of Cs to Rb (rubidium, $Z = 37$) clock frequencies is proportional to

$$\frac{\nu_{Cs}}{\nu_{Rb}} \propto \frac{g_{Cs}}{g_{Rb}} \alpha^{K_{Cs}-K_{Rb}} = \frac{g_{Cs}}{g_{Rb}} \alpha^{0.49}, \quad (10)$$

where the K factors defined by Eq. (9) are given in Table I.
- The ratio of frequencies of any two optical clocks depends only upon α, according to Eq. (5).
- The ratio of optical to microwave clock frequencies depends on α, μ, and the g factor of the atomic nucleus of the microwave clock.

Reducing the potential variation of g factors to more fundamental quantities, such as $X_q = m_q/\Lambda_{QCD}$, and calculation of the corresponding dimensionless sensitivity factors κ_{Cs} and κ_{Rb}, requires nuclear structure calculations which are dependent on a particular model (Flambaum and Tedesco, 2006; Dinh *et al.*, 2009; Jackson Kimball, 2015). Here m_q is the average light quark mass and Λ_{QCD} is the QCD energy scale.

TABLE I. Sensitivity factors K to the variation of the fine-structure constant α for clock transitions (Dzuba and Flambaum, 2009b). K is defined by Eq. (9). All transitions except Rb and Cs are optical frequency standards.

Atom	Transition	K
^{87}Rb	Ground hyperfine	0.34
^{133}Cs	Ground hyperfine	0.83
Al$^+$	$3s^2\,^1S_0 - 3s3p\,^3P_0$	0.008
Ca$^+$	$4s\,^2S_{1/2} - 3d\,^2D_{5/2}$	0.15
Sr	$5s^2\,^1S_0 - 5s5p\,^3P_0$	0.06
Sr$^+$	$5s\,^2S_{1/2} - 4d\,^2D_{5/2}$	0.43
Yb	$6s^2\,^1S_0 - 6s6p\,^3P_0$	0.31
Hg$^+$	$6s\,^2S_{1/2} - 5d\,^2D_{5/2}$	−2.94
Yb$^+$ *E*2	$4f^{14}6s\,^2S_{1/2} - 4f^{14}5d\,^2D_{5/2}$	1.03
Yb$^+$ *E*3	$4f^{14}6s\,^2S_{1/2} - 4f^{13}6s^2\,^2F_{7/2}$	−5.95

E. Current limits on α and μ variations from atomic clocks and Dy spectroscopy

At present, the best constraints on temporal variations of α and μ from comparisons of atomic transition frequencies are due to combinations of several experiments tracking ratios of different clock transitions (Godun *et al.*, 2014; Huntemann *et al.*, 2014). The analysis of current α and μ clock constraints of Huntemann *et al.* (2014) is illustrated in Fig. 1. Filled stripes mark 1 standard deviation uncertainty regions of individual measurements and the central blank region is bounded by the standard uncertainty ellipse resulting from the combination of all data. The results obtained from comparing four different optical clocks and Cs clocks provide constraints on both α and μ. The Sr world data show combined constraints from clocks based on neutral St atom (Le Targat *et al.*, 2013); the other three are based on singly charged ions: Hg$^+$ (mercury, $Z = 80$); Yb$^+$ (ytterbium, $Z = 80$), using an electric quadrupole (*E*2) transition (Tamm *et al.*, 2014); and Yb$^+$ using an electric octupole (*E*3) transition (Huntemann *et al.*, 2014). The frequency ratio, $R = \nu/\nu_{Cs}$, of each optical clock compared to a Cs microwave clock was parametrized as

$$\frac{1}{R}\frac{dR}{dt} = (K - K_{Cs} - 2)\frac{1}{\alpha}\frac{d\alpha}{dt} + \frac{1}{\mu}\frac{d\mu}{dt} - \kappa_{Cs}\frac{1}{X_q}\frac{dX_q}{dt}, \quad (11)$$

where the coefficients K for the optical clocks and Cs are listed in Table I. We note that the extra "2" in the parentheses of the first term appears due to the presence of a factor of α^2 in the hyperfine frequency expression given by Eq. (4).

The contribution due to the third term in Eq. (11) was taken to be zero in the analysis of Godun *et al.* (2014). Huntemann *et al.* (2014) accounted for this term by using the result

$$\kappa_{Cs}\frac{1}{X_q}\frac{dX_q}{dt} = 0.14(9) \times 10^{-16}/\text{yr} \quad (12)$$

inferred from the comparison of ^{87}Rb and ^{133}Cs clocks over 14 years reported by Guéna, Abgrall *et al.* (2012).
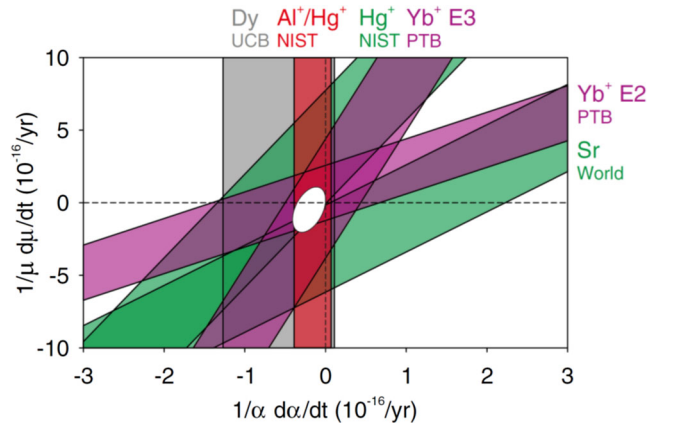

FIG. 1. Constraints on temporal variations of α and μ from comparisons of atomic transition frequencies. Filled stripes mark the 1 standard deviation σ uncertainty regions of individual measurements and the central blank region is bounded by the standard uncertainty ellipse resulting from the combination of all data. From Huntemann *et al.*, 2014.

Figure 1 also includes constraints on the temporal variation of α from comparisons of transition frequencies of Al$^+$ (aluminum, $Z = 13$) and Hg$^+$ optical clocks (Rosenband *et al.*, 2008) and from the measurement of Dy (dysprosium, $Z = 66$) transition frequencies (Leefer *et al.*, 2013). The Al$^+$/Hg$^+$ optical clock comparison (Rosenband *et al.*, 2008) currently provides the most accurate single test of only α variation, setting the limit

$$\frac{\dot{\alpha}}{\alpha} = (-1.6 \pm 2.3) \times 10^{-17} \text{ yr}^{-1}. \tag{13}$$

The Dy limit on α variation comes from spectroscopy of radio-frequency transitions between nearly degenerate, opposite-parity excited states rather than from an atomic clock comparison. These states are sensitive to a variation of α due to large relativistic corrections of opposite sign for the opposite-parity levels. The near degeneracy reduces the relative precision needed to place strict constraints on α variation. We note that filled stripes representing results of both Al$^+$/Hg$^+$ and Dy experiments in Fig. 1 are vertical, since they are sensitive only to a variation of α and not m_p/m_e.

We emphasize that Yb$^+$ has two ultranarrow optical clock transitions at 467 and 436 nm: electric octupole (E3) $4f^{14}6s\,^2S_{1/2} - 4f^{13}6s^2\,^2F_{7/2}$ and electric quadrupole $4f^{14}6s\,^2S_{1/2} - 4f^{14}5d\,^2D_{5/2}$.

The frequency ratio of those two transitions in Yb$^+$ was measured directly for the first time by Godun *et al.* (2014), without reference to the Cs primary standard, and using the same single ion of ^{171}Yb. This measurement is illustrated in Fig. 2. The $E3/E2$ frequency ratio was determined by stabilizing one laser to the $E3$ transition and the other laser to the $E2$ transition and measuring the ratio between the laser
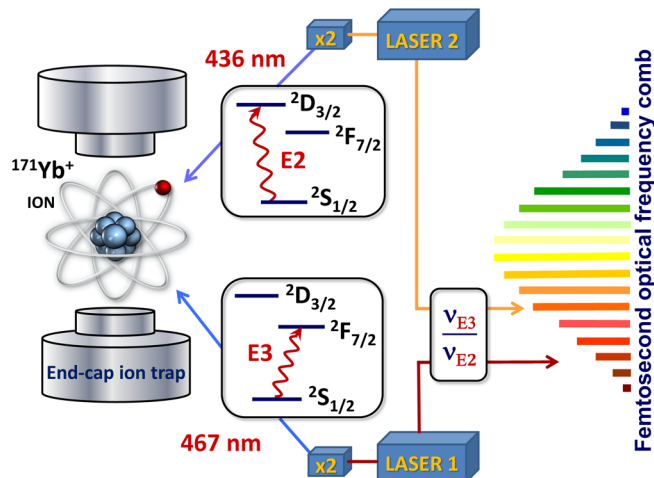
FIG. 2. Schematic experimental arrangement for measuring the $E2$ and $E3$ clock frequencies of a single ^{171}Yb$^+$ ion. The $E3/E2$ frequency ratio was determined by stabilizing one laser to the $E3$ transition and the other laser to the $E2$ transition and measuring the ratio between the laser frequencies with an optical frequency comb. For experimental reasons, the researchers used infrared lasers that have to be frequency doubled to excite the $E2$ and $E3$ optical transitions. Adapted from Safronova, 2014.

frequencies with an optical frequency comb. Both lasers were simultaneously stabilized to their respective transitions in the same ion ensuring experimental simplicity and common-mode rejection of certain systematic effects such as the gravitational redshift and relativistic time dilation. Such direct measurements of the ratio of the two optical frequencies are free from the additional uncertainties introduced by the primary Cs frequency standard.

Combining this measurement with constraints from previous experiments, Godun *et al.* (2014) set the following limits to the present day variation of α and μ:

$$\frac{\dot{\alpha}}{\alpha} = (-0.7 \pm 2.1) \times 10^{-17} \text{ yr}^{-1}, \tag{14}$$

$$\frac{\dot{\mu}}{\mu} = (0.2 \pm 1.1) \times 10^{-16} \text{ yr}^{-1}, \tag{15}$$

which are similar to limits set by the analysis of Huntemann *et al.* (2014).

F. Prospects for the improvement of atomic clock constraints on fundamental constant variations

The limits on the variation of the fundamental constants from comparison of two clock frequencies are determined by (1) uncertainties of both clocks, (2) sensitivity factors of each clock to the variation of different constants, and (3) the time interval over which the ratios are repeatedly measured. Therefore, strategies to improve the limits set by atomic clocks on the variation of fundamental constants may arise from the improvement of any of the three factors: building clocks with lower uncertainties, building conceptually different clocks with higher sensitivities to variation of fundamental constants, and making measurements over longer time intervals.

For example, the Al$^+$/Hg$^+$ clock constraint on α variation reported in 2008 (Rosenband *et al.*, 2008) was obtained from repeated measurements during 1 yr. Even with the same accuracy for both Al$^+$ and Hg$^+$ clocks, repeating the frequency-ratio measurements now would improve the 2008 limit (13) by almost of factor of 10, since a decade has passed since the first measurements. For clock-ratio experiments that have already accumulated more than a decade of data, such as the Cs/Rb ratio (Guéna, Abgrall *et al.*, 2012), only moderate improvements can be achieved in the next decade without the reduction of clock uncertainties. We start with a discussion of the prospects for further improvements in searches for variation of fundamental constants with current clocks and then explore new clock proposals.

1. Improvements of current clocks

Figure 3 illustrates the evolution of fractional frequency uncertainties of atomic frequency standards based on microwave and optical transitions. All microwave data in this figure come from Cs clocks. The figure is adapted from Poli *et al.* (2013) with the addition of recent data up to 2017.

The present-day state-of-the-art Cs microwave clocks are approaching uncertainties of 10^{-16} (Heavner *et al.*, 2014; Levi *et al.*, 2014), which is near their practical limitations. This is a
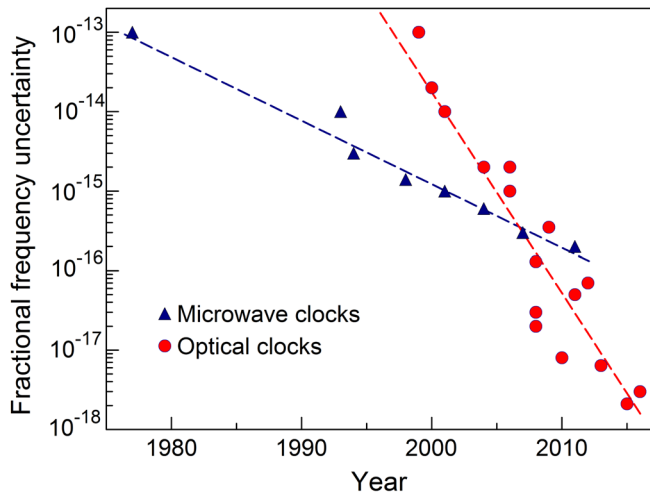
FIG. 3. Evolution of fractional frequency uncertainties of atomic frequency standards based on microwave (Cs clocks) and optical transitions. Data points are from Poli *et al.* (2013), Nicholson *et al.* (2015), and Huntemann *et al.* (2016).

remarkable achievement considering that the Cs atomic clock transition has an intrinsic quality factor Q, defined as the ratio of the absolute frequency of the transition to its natural linewidth of $Q \approx 10^{10}$. The Q factors of optical atomic clocks are 5 orders of magnitude higher than those of microwave clocks, giving optical clocks a tremendous advantage in terms of frequency stability (Poli *et al.*, 2013; Ludlow *et al.*, 2015). Recent progress in the accuracy of the optical clocks has been extraordinary, with the world's best optical lattice atomic clocks approaching fractional frequency uncertainties of 10^{-18} (Nicholson *et al.*, 2015; Ushijima *et al.*, 2015). The smallest uncertainty attained to date is 2×10^{-18} in a strontium (Sr, $Z = 38$) optical lattice clock (Nicholson *et al.*, 2015). In 2016, a systematic uncertainty of 3×10^{-18} was reported in a single-ion atomic clock based on the electric-octupole transition in Yb$^+$ (Huntemann *et al.*, 2016). As a result, the most rapid improvement in this field is expected to come from optical to optical clock comparison, with optical to microwave comparison being limited by the ultimate accuracy of microwave clocks.

Results of experiments measuring the stability of two optical clock-frequency ratios $R = \nu_2/\nu_1$ are parametrized by a simpler version of Eq. (11):

$$\frac{\dot{R}}{R} = (K_2 - K_1)\frac{\dot{\alpha}}{\alpha}, \qquad (16)$$

where K_1 and K_2 are K sensitivity coefficients for clocks 1 and 2. Therefore, the sensitivity of optical clock-frequency ratios to α variation is described by the difference in the corresponding K values, i.e., $\Delta K = |K_2 - K_1|$. The K factors are small (0.008–1.0, see Table I) for most clocks currently in development: Mg, Al$^+$, Ca$^+$, Sr$^+$, Sr, Yb, Yb$^+$ quadrupole transition, and Hg. The K factors for Hg$^+$ and Yb$^+$ octupole clock transitions are -3 and -6, making them the best candidates for one member of a clock-comparison pair, with the other member taken from the previous group. Recently

reported drastic reductions in the fractional frequency uncertainty of the Yb$^+$ octupole clock (Huntemann *et al.*, 2016) are expected to lead to a more accurate test of α variation, with the second clock being perhaps Sr. Future prospects for the development of optical atomic clocks are discussed in recent reviews (Poli *et al.*, 2013; Ludlow *et al.*, 2015), which envisage further decreases in atomic clock uncertainties during the next decade. Comparison of different clock frequencies beyond 10^{-18} accuracy will become more challenging due to the sensitivity to the environment, including temperature and gravitational potential (Ludlow *et al.*, 2015). For example, a clock on the surface of the Earth that is higher by just 1 cm than another identical clock runs faster by $\delta\nu/\nu_0 \approx 10^{-18}$ (Ludlow *et al.*, 2015). The blackbody radiation (BBR) shift has a leading temperature dependence of T^4, making clock frequencies sensitive to the temperature fluctuations. The BBR shift for a given temperature also varies significantly, by orders of magnitude, between different clock transitions. The strategies for reducing BBR shifts in current clocks are discussed by Ludlow *et al.* (2015). Comparisons of clocks based on two transitions in a single ion, such as Yb$^+$ quadrupole to octupole clock comparisons illustrated by Fig. 2 or with two ions held in the same trap, may be used to reduce the environmental sensitivities of the clock ratios.

2. Prospects for optical clocks with highly charged ions

Another pathway toward improved tests of α variation with atomic clocks is the development of frequency standards based on new systems, which have higher K sensitivities, while still enabling highly accurate measurements of the frequency ratios. Put simply, it is much easier to measure large effects, so the search for high-sensitivity systems is a major ongoing effort of AMO theory.

This brings us to a question: what are the requirements for such new systems? If we want to build a clock with accuracy at the present state-of-the-art level, we need at the very least a system with a transition in a laser accessible range with very high Q, at least $Q \approx 10^{15}$. The high-Q requirement means that the upper state of the transition is metastable, i.e., long lived. There are a number of other considerations to ensure small frequency uncertainties by minimizing systematic effects. The system also has to be amenable to cooling and trapping. If we want to use our new clock to search for α variation, the clock transition has to be between states of different electronic configurations, i.e., not between fine- or hyperfine-structure levels since the K factors for such states are similar.

These requirements were formulated in the criteria for good clock transitions proposed by Dzuba, Flambaum, and Katori (2015):
- The transition is in the near-optical region ($230 < \lambda < 2000$ nm or $5000 < 1/\lambda < 43\,000$ cm^{-1}) as such transitions are accessible with available laser systems.
- The lifetime of the clock state is between 100 and $\approx 10^4$ s as this enables high Q.
- There are other relatively strong optical transitions in the same atomic system with a lifetime of the upper level on the order of $\tau \lesssim 1$ ms, which may be useful for laser cooling or optical pumping or probing.

- The clock transition is not sensitive to perturbations caused by blackbody radiation, gradients of external electric fields, etc.

The first requirement seems to limit the potential systems to neutral atoms or singly charged ions, all of which have been considered as potential clock systems. Examination of the National Institute of Standards and Technology (NIST) atomic spectra database (Kramida, Ralchenko, and Reader, 2018) establishes that the energies of the relevant ion transitions involving the ground states tend to be outside of the laser-accessible range with the degree of ionization exceeding 2. Remarkably, selected highly charged ions with degrees of ionization ranging from 9 to 18 actually have potential clock transitions in the optical range between different electronic configurations as discovered by Berengut, Dzuba, and Flambaum (2010). This phenomenon arises from the rearrangement of the order of electronic configurations: as more electrons are removed, the order of levels becomes more hydrogenic, for example, restoring the Coulomb ordering where the $4f$ shell becomes occupied prior to the $5s$ shell. For example, the ground state of cadmium (Cd, $Z = 48$) is $[\mathrm{Kr}]4d^{10}5s^2$. Proceeding along the Cd isoelectronic sequence, the ground state remains in this configuration up to Nd^{12+}, but the ground-state configuration of Sm^{14+} (samarium, $Z = 62$) becomes $[\mathrm{Kr}]4d^{10}4f^2$ (Safronova *et al.*, 2014a). As a result, different electronic configurations move close together for two or three ions in an isoelectronic sequence when the order of levels is rearranged. An example is the Nd^{12+} (neodymium, $Z = 60$), Pm^{13+} (promethium, $Z = 61$), Sm^{14+} (samarium, $Z = 62$) parts of the Cd-like sequence. This provides an unexpected gift of optical transitions for metrology applications. Extensive theoretical effort during the past 5 years resulted in the identification of many such candidate systems in highly charged ions (HCIs), predictions of their properties, and assessments of their potential for tests of α variation (Berengut, Dzuba, and Flambaum, 2011; Berengut, Dzuba, Flambaum, and Ong, 2011; Berengut *et al.*, 2012a, 2012b; Derevianko, Dzuba, and Flambaum, 2012; Dzuba, Derevianko, and Flambaum, 2012a, 2012b; Kozlov, Dzuba, and Flambaum, 2013; Yudin, Taichenachev, and Derevianko, 2014; Dzuba, Flambaum, and Katori, 2015). The most accurate calculations were done using a state-of-the-art hybrid approach that combines coupled-cluster and configuration interaction methods (Safronova *et al.*, 2014a, 2014b, 2014c; Dzuba *et al.*, 2015). Proposals for α-variation searches in HCIs were reviewed by Berengut, Flambaum, and Ong (2013), Ong, Berengut, and Flambaum (2014), and Kozlov *et al.* (2018).

A particular attraction of the HCIs for constructing highly accurate clocks is the suppression of the clock-frequency shifts due to external electric fields which can lead to systematic errors, due to the contraction of the electron cloud with increasing ionization stage. Stronger relativistic effects resulting from localization of the electron cloud also provide enhanced sensitivity to α variation. Assessments of systematic effects in optical clocks based on HCIs concluded that an uncertainty of 10^{-19} is achievable (Derevianko, Dzuba, and Flambaum, 2012; Dzuba, Derevianko, and Flambaum, 2012a, 2012b; Dzuba, Flambaum, and Katori, 2015).

Up to this point we have not discussed the technical feasibility of using HCIs to build clocks. Until very recently, the realm of HCI research had little overlap with the field of ultracold precision metrology. In 2015, a breakthrough experiment (Schmöger *et al.*, 2015) demonstrated sympathetic cooling of Ar^{13+} (argon, $Z = 18$) ions with laser-cooled Be^+ (beryllium, $Z = 4$) ions in a cryogenic Paul trap. This result removes a major obstacle for HCI investigations with high-precision laser spectroscopy, paving the way toward future experiments with cold and precisely controlled HCIs. Experimental work toward this goal is underway, starting with the identification of the HCI spectra of interest to α-variation studies (Windberger *et al.*, 2015). Optical transitions in HCIs and their applications will be reviewed in detail in a separate Reviews of Modern Physics article.

Hyperfine transitions of hydrogenlike HCIs, such as $^{207}\mathrm{Pb}^{81+}$ (lead, $Z = 82$), have also been proposed for tests of fundamental constant variation (Schiller, 2007; Yudin, Taichenachev, and Derevianko, 2014). Because of a high degree of ionization, the ground-state hyperfine transition wavelength is in the infrared, with a Q factor of about 10^{14}. The importance of such HCI transitions is their sensitivity to the variation of μ and g factors, and Q factors that are much larger than those of Cs and Rb hyperfine transitions.

3. A candidate nuclear clock

With atoms and ions of the periodic table now considered, we turn our attention to nuclei. Can we build clocks based on transitions between different states of a nucleus? A great attraction of such an idea is the suppression of the field-induced frequency shifts since the nucleus is highly isolated from the environment due to the electron cloud and interacts only via the relatively small nuclear moments (Yamaguchi *et al.*, 2015). There is a vast catalog of nuclear energy levels (Firestone and Shirley, 1998), but their transition frequencies are higher by factors of 10^4–10^6 than those accessible by modern laser technologies. Only one sufficiently long-lived nuclear transition, between the ground state of $^{229}\mathrm{Th}$ (thorium, $Z = 90$) and a low-lying isomer (i.e., long-lived excited nuclear state), has a suitable wavelength, predicted to be 160(10) nm (Beck *et al.*, 2007, 2009). This transition was proposed for the application in a nuclear clock (Peik and Tamm, 2003; Campbell *et al.*, 2012), but a decade of searches did not result in its detection (Jeet *et al.*, 2015; Peik and Okhapkin, 2015; Yamaguchi *et al.*, 2015). Finally, in 2016, the existence of the isomer was confirmed (von der Wense *et al.*, 2016), although there remains a significant uncertainty in its energy, motivating continued searches. The measurement of the internal-conversion decay half-life of neutral $^{229\mathrm{m}}\mathrm{Th}$ was reported by Seiferle, von der Wense, and Thirolf (2017). The hyperfine structure of $^{229\mathrm{m}}\mathrm{Th}^{2+}$ was investigated by Thielking *et al.* (2018) using the laser spectroscopy, yielding values of the magnetic dipole and electric quadrupole moments as well as the nuclear charge radius.

Flambaum (2006a) estimated that the relative effects of the variation of α and $m_q/\Lambda_{\mathrm{QCD}}$ in this $^{229}\mathrm{Th}$ nuclear transition are enhanced by 5–6 orders of magnitude using the Walecka model of nuclear forces and other assumptions. Other nuclear calculations predicted no enhancement (Hayes, Friar, and Möller, 2008), but their uncertainly was also very large, with a

4×10^3 enhancement factor still being within their uncertainty limit [see Berengut *et al.* (2009) for a discussion]. With nuclear calculations currently unable to determine the sensitivity factor, an alternative method for extracting sensitivity to α variation using laboratory measurements of the change in nuclear mean-square charge radius and electric quadrupole moment between the isomer and the ground-state nucleus was proposed by Berengut *et al.* (2009). The first experimental results were reported by Thielking *et al.* (2018) but the precision of the electric quadrupole moment was not sufficient to extract the sensitivity of the nuclear clock to α variation.

G. Laboratory searches for variation of fundamental constants with molecules

Molecular spectroscopy provides further possibilities for testing the stability of fundamental constants owing to rich spectra with many different transition types. The proton-to-electron mass ratio μ defines the scales of electronic, vibrational, and rotational intervals in molecular spectra:

$$E_{el} : E_{vib} : E_{rot} \sim 1 : \mu^{-1/2} : \mu^{-1}. \qquad (17)$$

Purely vibrational and rotational transitions will have the $K_\mu = -1/2$ and -1 sensitivity factors to the variation of μ, respectively. Moreover, molecules have fine and hyperfine structures, Λ doubling, hindered rotation, etc., which adds a variety of dependences on the fundamental constants (Chin, Flambaum, and Kozlov, 2009).

The first experimental comparison of a molecular clock to an atomic clock (Shelkovnikov *et al.*, 2008) was obtained by comparing the frequency of a rovibrational transition in SF_6 with the hyperfine transition of the Cs clock. The measured rovibrational transition frequency in SF_6 depends only on μ (the Rydberg constant cancels out when comparing to any other transition):

$$\nu_{SF_6} = A \left(\frac{m_e}{m_p} \right)^{1/2} R_\infty,$$

where A is a numerical factor. The resulting constraint on the fractional temporal variation of the proton-to-electron mass ratio was reported as $\dot\mu/\mu = (-3.8 \pm 5.6) \times 10^{-14}$ yr^{-1}. While this limit is less stringent than that set by optical clocks (Godun *et al.*, 2014; Huntemann *et al.*, 2014), this study offers a clean separation of μ variation from α variation.

Proposals for future tests of the variation of fundamental constants with ultracold molecules were reviewed by Chin, Flambaum, and Kozlov (2009) and we provide only a brief summary here. These proposals are based on the enhanced sensitivities to α, μ, and m_q/Λ_{QCD} for accidentally closely spaced levels. We note that there is a difference between proposals with enhanced relative sensitivities and those with enhanced absolute sensitivities. The relative-sensitivity proposals (Flambaum, 2006b) are practical for cases where the frequency uncertainty scales with the frequency, such as Doppler shifts in astrophysical measurements. Most of the laboratory measurements are limited by absolute frequency uncertainties, so transitions with large overall shifts may be

better candidates; see, for example, DeMille, Sainis *et al.* (2008), Zelevinsky, Kotochigova, and Ye (2008), Kajita, Gopakumar, Abe, and Hada (2014), and Hanneke, Carollo, and Lane (2016). In special cases, there are both absolute and relative enhancements to μ variation (DeMille, Sainis *et al.*, 2008; Hanneke, Carollo, and Lane, 2016).

The relative effect of α variation in microwave transitions between very close and narrow rotational-hyperfine levels may be enhanced by 2–3 orders of magnitude in diatomic molecules with unpaired electrons such as LaS, LaO, LuS, LuO, YbF, and similar molecular ions due to accidental degeneracies of hyperfine and rotational structures (Flambaum, 2006b). Degeneracies between the fine and vibrational structures within the electronic ground states of diatomic molecules, such as Cl_2^+, CuS, IrC, SiBr, and HfF^+, lead to enhanced sensitivities to the variation of both α and μ (Flambaum and Kozlov, 2007; Beloy *et al.*, 2010). Strong enhancements of α- and μ-variation effects in dihalogens and hydrogen halides, HBr^+, HI^+, Br_2^+, I_2^+, IBr^+, ICl^+, and IF^+, were reported by Pašteka *et al.* (2015). The calculation of Flambaum *et al.* (2013) demonstrated enhanced sensitivity to the variation of α and m_q/Λ_{QCD} in opposite-parity closely spaced levels of the ^{207}Pb^{19}F molecule due to a near cancellation of the omega-type doubling and magnetic hyperfine-interaction-energy shifts.

Experiments with cold diatomic molecules Cs_2 (DeMille, Sainis *et al.*, 2008) and Sr_2 (Zelevinsky, Kotochigova, and Ye, 2008) have also been proposed. DeMille, Sainis *et al.* (2008) predicted that the splitting between pairs of Cs_2 nearly degenerate vibrational levels, where each state is associated with a different electronic potential, could be measured precisely enough to sense a fractional change of $\delta\mu/\mu \lesssim 10^{-17}$. Detailed spectroscopy of the Cs_2 $a^3\Sigma_u^+$ state was performed by Sainis *et al.* (2012), who further discussed the prospects for μ-variation measurements. Coherent control of molecular quantum states, which is a prerequisite for a "molecular lattice clock," was achieved for Sr_2 (McGuyer *et al.*, 2015). Searches for μ variation might be made using vibrational transitions in diatomic alkali-alkaline-earth molecules and alkaline-earth hydride molecular ions (Kajita, Gopakumar, Abe, and Hada, 2014).

Several high-sensitivity transitions with narrow linewidths were identified in the deeply bound O_2^+ molecular ion by Hanneke, Carollo, and Lane (2016). They suggested the experimentally feasible routes toward the μ-variation measurements in this system. Another method to search for the μ variation using vibrational transitions in O_2^+ with high accuracy was proposed by Kajita (2017a, 2017b). Kajita, Gopakumar, Abe, Hada, and Keller (2014) proposed the search for μ variation using vibrational transitions in N_2^+.

The leading systematic effects for the realization of optical clocks with rovibrational levels of the molecular ions H_2^+ and HD^+ were assessed by Karr (2014) and Schiller, Bakalov, and Korobov (2014), who also discussed their potential sensitivity to μ variation. The principle issues limiting the accuracy of such clocks involved effects due to light shifts, although it is possible these could be suppressed with appropriate pulse sequences (Yudin *et al.*, 2010; Huntemann *et al.*, 2014). Ramsey-type spectroscopy in a beam of metastable

CO molecules was reported by de Nijs, Ubachs, and Bethlem (2014) for further tests of the variation of μ.

Santamaria *et al.* (2014) discussed the design of an experiment aimed to constrain the fractional temporal variation of μ at a level of 10^{-15}/yr using spectroscopic frequency measurements on a beam of cold CF_3H molecules. Progress toward precision spectroscopic measurement with ultracold deuterated ammonia ND_3 for future laboratory tests for variations of μ was reported by Quintero-Pérez *et al.* (2014). Prospects for high-resolution microwave spectroscopy of methanol CH_3OH and CD_3OH molecules in a Stark-deflected molecular beam were discussed by Jansen *et al.* (2013), but the precision must be significantly enhanced for laboratory tests. The current goal of methanol studies is to improve precision to reference the astrophysical searches of μ variation described in Sec. II.H.2.

An alternative proposal to test the variation of fundamental constants with atoms and molecules involves precise measurements of the scattering lengths in Bose-Einstein condensate and Feshbach molecular experiments (Chin and Flambaum, 2006; Gacesa and Côté, 2014). A measurement of the scattering length accurate to 10^{-6} performed near narrow Feshbach resonances in 2 consecutive years was estimated to probe the variation of μ at the level of 10^{-15}–10^{-18} yr^{-1} depending on the choice of atomic species (Chin, Flambaum, and Kozlov, 2009).

Recent advances in cooling and control of molecules (Hutzler, Lu, and Doyle, 2012; Germann, Tong, and Willitsch, 2014; Kobayashi, Ogino, and Inouye, 2015; Cheng *et al.*, 2016; Norrgard *et al.*, 2016; Prehn *et al.*, 2016; Wolf *et al.*, 2016; Kozyryev *et al.*, 2017; Park *et al.*, 2017; Truppe *et al.*, 2017; Wu *et al.*, 2017; wen Chou *et al.*, 2017) promise future progress in laboratory tests of variation of fundamental constants with molecules.

H. Limits on variation of α and μ from quasar-absorption spectra

The discussion of Secs. II.D–II.G concerns a question: Do fundamental constants vary now? The dependence of atomic and molecular spectra on fundamental constants may also be used to probe for their variation in a distant past, as far back as $\approx 10^{10}$ years ago, the scale given by the age of the Universe. The basic idea is the same: to compare the spectra from two different times, but to increase the time separation δt from $\delta t = 1$–15 yr of the laboratory tests to $\delta t = (3$–$13) \times 10^9$ yr. In practice, we need a particularly bright, distant astrophysical light source, such as a quasar, to serve as a backlight of high-redshift gas clouds in which atomic or molecular absorption spectra can be observed. Emission spectra are also used in some studies. The sensitivities of those spectra to the variations of α and μ are defined and calculated in the same way as for the terrestrial experiments.

Because of the expansion of the Universe, all wavelengths of light λ from the Universe's past are redshifted. A cosmological redshift z is defined as the ratio

$$z = \frac{\lambda_{\text{lab}} - \lambda}{\lambda}, \qquad (18)$$

where λ is the wavelength of the absorbed and emitted light and λ_{lab} is the wavelength of the light which is observed on Earth. A redshift of $z = 1$ means that a 500 nm absorption wavelength is observed on Earth as 1000 nm instead. This corresponds to a "look back" time of $\approx 8 \times 10^9$ yr (Pilipenko, 2013).

To separate the redshift, one needs to compare "ancient" and present wavelengths of at least two spectral lines that have different sensitivities to the constants of interest.

Uzan (2011) provided a detailed review of atomic and molecular quasar-absorption studies, so we will provide only key points and more recent results here.

1. Limits on variation of α from quasar-absorption studies of atomic spectra

Quasar-absorption studies of α variation use alkali-doublet (Murphy *et al.*, 2001b), many-multiplet (Webb *et al.*, 1999), and single-ion differential α-measurement (Levshakov *et al.*, 2006) methods. The alkali-doublet method uses the $ns - np_{1/2}$, $ns - np_{3/2}$ fine-structure intervals of alkali-metal atoms as a probe of α variation. The many-multiplet method is a generalization of this approach which uses many atomic transitions with different dependences on α, and yields more accurate results than the alkali-doublet method. The single-ion differential α-measurement (SIDAM) method uses different transitions of one ionic species in an individual exposure, in an attempt to reduce some of the systematics of the many-multiplet method. It is mainly used with Fe^+ (iron, $Z = 26$) which has several transitions with both positive and negative K, allowing one to compare lines within a single spectrum. Most of the quasar-absorption studies with atoms are based on strong UV lines redshifted into the visible spectrum range. Unfortunately, these transitions depend weakly on α for most atoms visible from these sources, since the atoms are relatively light, $Z \leq 30$, which generally leads to smaller values of K. For example, the maximum ΔK difference for any two lines of Fe^+ is $\Delta K = 0.11$ with an estimated 30% uncertainty (Porsev *et al.*, 2007). Another difficulty of the many-multiplet method is ensuring that one compares transition lines from the same object, i.e., at the same redshift z. The advantage of SIDAM is using lines of the same element, eliminating or simplifying this issue. Another significant systematic arises from the assumption of the isotopic-abundance ratios for each atom or ion used for the analysis in the distant past, in particular, the $^{25,26}Mg/^{24}Mg$ (magnesium, $Z = 12$) ratios, and their possible deviations from the terrestrial values. This issue, discussed by Kozlov *et al.* (2004), is further complicated by the lack of isotope-shift measurements for a number for transitions that are used in the quasar-absorption studies (Berengut *et al.*, 2011).

A large-scale many-multiplet analysis of the Keck telescope high-resolution Echelle-spectrometer (HIRES) data from 143 absorption systems at $0.2 < z < 4.2$ indicated a variation of α (Murphy *et al.*, 2004):

$$\frac{\Delta\alpha}{\alpha} = \frac{\alpha_{\text{obs}} - \alpha_{\text{lab}}}{\alpha_{\text{lab}}} = (-0.57 \pm 0.11) \times 10^{-5}, \qquad (19)$$

where α_{obs} corresponds to a value of α in the distant past, between 2 and 12.4 Gyr here, and α_{lab} is the current terrestrial value.

However, the analysis of data from 23 absorption systems taken by the Very Large Telescope (VLT) ultraviolet and visual Echelle spectrograph (UVES) yielded a null result

$$\frac{\Delta\alpha}{\alpha} = (-0.06 \pm 0.06) \times 10^{-5}, \qquad (20)$$

for $0.4 < z < 2.3$ (Chand *et al.*, 2004; Srianand *et al.*, 2004). This analysis was disputed by Murphy, Webb, and Flambaum (2007, 2008b, 2008c), who obtained different results from an analysis of the same data; this was followed by the reply of Srianand *et al.* (2007).

An intriguing solution to this discrepancy was suggested by Webb *et al.* (2011): since Keck and VLT data come from different hemispheres, both results can be made consistent by introducing a dipole spatial variation of α; this topic is discussed further in Sec. II.I. The VLT data were reanalyzed in the more recent work by Wilczynska *et al.* (2015). Considering both statistical and systematic error contributions, Wilczynska *et al.* (2015) obtained $\delta\alpha/\alpha = (0.22 \pm 0.23) \times 10^{-5}$, consistent with the dipole spatial variation limits introduced by Webb *et al.* (2011).

An impact of instrumental systematic errors on α-variation results obtained from atomic quasar-absorption data was recently studied by Whitmore and Murphy (2015) using 20 years of archival spectra from VLT and Keck spectrographs. Whitmore and Murphy (2015) concluded that systematic errors in their wavelength scales were substantial and capable of significantly weakening the evidence for variations of α from quasar-absorption lines. However, they still cannot entirely explain the Keck-HIRES result (19).

To summarize, atomic quasar-absorption data remain a subject of open controversy which requires further study and future deployment of high-resolution ultrastable spectrographs such as ESPRESSO (for the VLT) and ELT-HIRES (Martins, 2015) for improved astrophysical measurements. Laser frequency-comb techniques for precise astronomical spectroscopy were described by Murphy *et al.* (2012).

2. Limits on variation of μ from quasar-absorption studies of molecular spectra

Molecular spectra provide clean constraints on μ variation since rotational and vibration transitions have different μ dependences given by Eq. (17). There are two main considerations when selecting molecules for astrophysical studies of μ variation:

- How sensitive are the molecular transitions to the variation of μ? This is quantified with a dimensionless sensitivity factor K_μ, analogous to the K factor for sensitivity to α variation.
- How abundant is this molecule in the Universe? A high-sensitivity factor would be good for the laboratory tests of Sec. II.G, but useless for astrophysical studies if it is impossible to observe the corresponding transitions.

It is particularly advantageous if a molecule has several transitions with different K_μ, preferably of opposite sign. Then transitions in the same molecule can be used for the astrophysical search for μ variation, reducing important systematic effects.

Until recently, the most accurate astrophysical limits on the variation of μ came from H_2 studies, reviewed by Ubachs *et al.* (2016), since H_2 is the most abundant molecule observed, with 56 absorption systems known at the present time. A combined H_2 result from ten systems with $2.0 < z < 4.2$ sets the limit on the variation of μ at

$$\left| \frac{\Delta\mu}{\mu} \right| = \left| \frac{\mu_{\mathrm{obs}} - \mu_{\mathrm{lab}}}{\mu_{\mathrm{lab}}} \right| \leq 5 \times 10^{-6} \quad (3\sigma), \qquad (21)$$

where μ_{obs} corresponds to the value of μ in the distant past, from 10 to 12.4 Gyr in this study, and μ_{lab} is the current terrestrial value (Ubachs *et al.*, 2016). These molecular-hydrogen studies use the UV transitions in Lyman and Werner bands that are redshifted into the visible spectrum. The $B^1\Sigma_u^+ - X^1\Sigma_g^+$ Lyman and $C^1\Pi_u^+ - X^1\Sigma_g^+$ Werner band lines are strong dipole-allowed absorption lines of the H_2 molecule with $\lambda = 910$–1140 Å. All of these transitions have a weak dependence on μ, with a maximum sensitivity coefficient $\Delta K_\mu \approx 0.06$ (Kozlov and Levshakov, 2013).

Improved limits on the variation of μ are obtained by going from optical to microwave frequencies, where a number of molecular transitions are available with values of K_μ greater by factors of 100–1000. The dependence of microwave and submillimeter molecular transitions on fundamental constants was reviewed by Kozlov and Levshakov (2013). The following molecules were considered: CH, OH, NH^+, C_3H, H_3O^+, NH_3 (ammonia), H_2O_2 (hydrogen peroxide), CH_3OH (methanol), and CH_3NH_2 (methylamine). Nine diatomic and 16 polyatomic molecular candidates for μ-variation studies were reviewed by Jansen, Bethlem, and Ubachs (2014).

In 2011, a number of polyatomic molecules including methanol and methylamine were observed for the first time at high redshift $z = 0.89$ corresponding to a look-back time of 7.5×10^9 yr. The K_μ coefficient for ammonia is -4.5 (Kozlov and Levshakov, 2013), which represents a 2 orders of magnitude enhancement in comparison with H_2. However, all of the ammonia lines exhibit the same sensitivity, so comparison with other systems is required. Two absorption systems are known with NH_3 lines at $z = 0.69$ and 0.89. Studies of μ variation in these systems resulted in a 2σ limit $|\Delta\mu/\mu| < 1.8 \times 10^{-6}$ (Murphy, Flambaum *et al.*, 2008) and 3σ limit of $|\Delta\mu/\mu| < 1.4 \times 10^{-6}$ (Henkel *et al.*, 2009), respectively. A joint three-component fit to the NH_3, CS, and H_2CO lines yielded $|\Delta\mu/\mu| < 3.6 \times 10^{-6}$ for $z = 0.69$ (Kanekar, 2011).

The sensitivity coefficients in methanol transitions range from 17 to -43, potentially allowing for the maximum enhancement of $|\Delta K_\mu| \approx 60$ (Kozlov and Levshakov, 2013).[1] Bagdonaite, Jansen *et al.* (2013) set the most stringent limits of the past variation of μ, $|\Delta\mu/\mu| < 1 \times 10^{-7}$ at 1σ, using four methanol lines at $z = 0.89$. An extended study of μ-variation based on 17 measurements of ten different absorption lines of methanol was carried out by

---

[1]We caution the reader that here $\mu = m_{\mathrm{p}}/m_{\mathrm{e}}$ but $\mu = m_{\mathrm{e}}/m_{\mathrm{p}}$ is frequently used in the literature, leading to opposite signs of the K_μ coefficients in different sources.

Bagdonaite, Daprà *et al.* (2013), allowing for a quantitative analysis of previously unaddressed underlying systematic effects yielding $\Delta\mu/\mu = (-1.0 \pm 0.8_{\text{stat}} \pm 1.0_{\text{sys}}) \times 10^{-7}$. Assuming a linear variation of μ with time, this limit translates into $\dot{\mu}/\mu < 2 \times 10^{-17}$ yr^{-1} which is more constraining than the atomic clock limit (Godun *et al.*, 2014; Huntemann *et al.*, 2014) associated with the same linear model of the fundamental constant variation. We note that there is no theoretical basis to assume the linear variation of fundamental constants. We make such a comparison only as an illustration of the accuracies reached by the astrophysical and laboratory studies.

In 2015, one of the four methanol lines observed at $z = 0.89$ and used in the analysis of this absorption system was noted to have a different line profile: the line full widths at half maximum was larger, at 4.3σ significance, suggesting that the sight line in this transition traces different absorbing gas from that detected in the other three lines (Kanekar *et al.*, 2015). Therefore, it was recommended to exclude this line from the analysis, resulting in a 2σ constraint of $|\Delta\mu/\mu| < 4 \times 10^{-7}$.

Using combinations of atomic and molecular lines allows one to probe the variation of various combinations of fundamental constants. A comparison of the atomic hydrogen 21 cm hyperfine ground-state transition with atomic UV spectral lines (Tzanavaris *et al.*, 2005, 2007; Rahmani *et al.*, 2012) or OH molecular transitions (Chengalur and Kanekar, 2003) constrains combinations of α, μ, and the proton g factor.

Comparing the 21 cm line to molecular rotational transitions in CO, HCO$^+$, and HCN eliminates the dependence on μ, which is $1/\mu$ for both types of transition (Murphy *et al.*, 2001a).

The combination $F = \alpha^2\mu$ was probed with a C$^+$ and CO transitions (Levshakov *et al.*, 2008, 2012), thus eliminating the dependence on g_{p} and yielding a constraint $\Delta F/F < 2 \times 10^{-5}$ at $z = 5.2$.

In summary, currently the best astrophysical constraint on the μ variation for high redshifts, up to $z = 4.2$ (12.4 Gyr), come from the H$_2$ data (Ubachs *et al.*, 2016), while the strictest constraints for lower redshifts $z = 0.89$ are obtained from the methanol data (Bagdonaite, Daprà *et al.*, 2013; Kanekar *et al.*, 2015). Further improvement may come from the observation of ammonia, methanol, and other more complicated molecules with high sensitivities to μ variation at higher redshifts, increased sensitivity, and spectral resolution of astronomical observations and increased precision of the laboratory measurements for the most sensitive molecular transitions (Kozlov and Levshakov, 2013).

I. Spatial variation of fundamental constants

As discussed in Sec. II.C, if the fundamental constants depend on some dynamical scalar field ϕ they become dynamical. A coupling of such scalar field ϕ to electromagnetic fields induces a coupling to matter which may depend on the local matter density. Such density-dependent couplings may lead to a spatial variation of fundamental constants: fundamental constants will be different in the regions of high density of matter in comparison to regions of low density. However, such spatial variation at the cosmological scales is

expected to be much smaller in most theories than a temporal variation unless under extreme densities, such as in the vicinity of a neutron star (Uzan, 2011). Therefore, the Webb *et al.* (2011) hypothesis of a dipole spatial variation of α introduced to explain the discrepancy between Keck and VLT data discussed in Sec. II.H.1 was quite extraordinary.

The spatial variation idea arises from the geographical positions of Keck and VLT telescopes in northern (Hawaii) and southern (Chile) hemispheres, respectively, separated by $45°$ in latitude. These two telescopes, on average, observe different directions in the sky and Keck and VLT α-variation results can be made consistent by introducing a spatial variation of α. The result of Webb *et al.* (2011) would mean that α was larger in the past in one direction and smaller in the past in the opposite direction according to

$$\frac{\Delta\alpha}{\alpha} = \frac{\alpha(\mathbf{r}) - \alpha_0}{\alpha_0} = (1.10 \pm 0.25) \times 10^{-6} r\cos\psi \, \text{Gly}^{-1}, \quad (22)$$

where $[\alpha(\mathbf{r}) - \alpha_0]/\alpha_0$ is a variation of α at a particular place $\mathbf{r}$ in the Universe relative to α_0 on Earth at $\mathbf{r} = 0$. The function $r\cos\psi$ describes the geometry of the spatial variation, where ψ is the angle between the direction of the measurement and the axis of the dipolar variation. The distance function r is the light-travel distance $r = ct$ measured in giga-light years. The Keck and VLT data were further analyzed in terms of spatial variation of α by Berengut, Flambaum, King, Curran, and Webb (2011), Berengut, Kava, and Flambaum (2012), and King *et al.* (2012).

A subsequent analysis of the Keck and VLT systematic instrumental errors by Whitmore and Murphy (2015) weakened but not completely eliminated such a scenario. The extraordinary claim of the spatial variation of α will require future extraordinary evidence obtained with next-generation ultrastable high-resolution spectrographs and a higher level of control of systematic errors.

Nevertheless, the subject of the spatial variation of fundamental constants is an interesting subject and various scenarios for new physics could exist that may be tested with astrophysics and laboratory studies. Regardless of validity of the Webb *et al.* (2011) result, we invite the interested reader to use it as an example to consider the following question: What type of new physics can induce a spatial cosmological variation of fundamental constants and how can we test for it? Berengut and Flambaum (2012), Berengut, Kava, and Flambaum (2012), Olive, Peloso, and Uzan (2011), and Olive, Peloso, and Peterson (2012) considered three scenarios, described as follows:

(I) Fundamental constants may fluctuate on a cosmological scale involving regions not in causal contact due to super-Hubble quantum fluctuations of a light field during inflation; further constraints from CMB are described by Sigurdson, Kurylov, and Kamionkowski (2003).

(II) A background value of ϕ depends on position and time, i.e., there is a nonzero spatial gradient of the field $\nabla\phi \neq 0$. Olive, Peloso, and Uzan (2011) pointed out that the generalization of the Copernican principle that assumes a homogeneous universe at

large scales is not fully satisfied in such a model and its theoretical foundation is unclear. Such a model will result in a dipole variation of the fundamental constants in the general form of Eq. (22) with the axis of the dipole being in the direction of the gradient $\nabla\phi$. The spatial variation of fundamental constant X is described by

$$\delta X/X = k_X \delta\phi, \qquad (23)$$

where k_X is a dimensionless factor quantifying the spatial variation of the fundamental constant X. Assuming that the same field is responsible for the variation of all fundamental constants, the direction of the dipole is the same for all fundamental constants.

Berengut and Flambaum (2012) proposed that such a dipole variation can be tested using atomic clocks, quasar atomic and molecular spectra, the Oklo natural nuclear reactor, meteorite dating, and cosmic microwave background. The Earth is moving along with the Sun with respect to the rest frame of the CMB and this motion has a component along the direction of the ϕ gradient. This model results in a small spatial variation as well as annual modulation of fundamental constants with Earth motion around the Sun. The result of Webb *et al.* (2011) roughly translates into a $\dot\alpha/\alpha \approx 10^{-19}$ yr^{-1} variation with a $\Delta\alpha/\alpha \approx 10^{-20}$ annual modulation. Therefore, atomic clocks with high sensitivities to α variation described in Sec. II.F.2 are particularly desirable for such tests. The present CMB constraint on the dipolar modulation of α (corresponding to a gradient across the observable Universe) from 2015 Planck data is $(-2.7 \pm 3.7) \times 10^{-2}$ at the 68% confidence level (Adam *et al.*, 2016).

(III) Olive, Peloso, and Uzan (2011) theorized that such spatial variations of α may be a signature of a domain wall produced in the spontaneous symmetry breaking in the early Universe, involving a scalar field coupled to electromagnetism. In this scenario, there is no spatial gradient but a discontinuity in the values of fundamental constants at the domain wall (or walls) in our Hubble volume. The fundamental constants on either side of the wall differ, and the quasar-absorption spectra may not be actually testing a deviation of α from the current Earth value, but probe locations of the domain walls in our Hubble volume. Attempts to fit Keck and VLT quasar-absorption data into the one- or two-wall models faced difficulties (Berengut, Kava, and Flambaum, 2012; Olive, Peloso, and Peterson, 2012).

Atomic clocks are sensitive only to such a scenario of spatial α- variation if the Earth actually passes thorough a domain wall at the present time. Precision magnetometery and atomic clock experiments aimed at detection of domain walls are discussed in Sec. IX.

In a different type of experiment, Wiens, Nevsky, and Schiller (2016) used an optical resonator fabricated from crystalline silicon at 1.5 K continuously for over 1 yr, repeatedly comparing its resonance frequency with the frequency of a Global Positioning System (GPS) monitored hydrogen maser. The resonator frequency is determined by the physical length and the speed of light and Wiens, Nevsky, and Schiller (2016) measured it with respect to the atomic unit of time, ruling out to first order a hypothetical differential effect of the Universe's expansion on rulers and atomic clocks. Wiens, Nevsky, and Schiller (2016) also constrained a hypothetical violation of the principle of local position invariance for resonator-based clocks and derived bounds for the strength of spacetime fluctuations.

Analysis of H_2 molecular spectra in terms of spatial dependence of μ on cosmological scales is presented by Ubachs *et al.* (2016). Spatial variation of fundamental constants may also manifest itself at local scales (Milky Way and the Solar System). Two types of tests are being pursued with atoms and molecules described next.

1. Search for coupling of fundamental constants to a changing gravitational potential

First, a spatial change in fundamental constants may be induced by light scalar fields that change linearly with changes in the local gravitational potential. This may be tested by searching for a dependence of fundamental constants on a varying gravitational potential.

Variations in fundamental constant X with the change in the gravitational potential are modeled as

$$\frac{\Delta X}{X} = k_X \frac{\Delta U(t)}{c^2}, \qquad (24)$$

where $\Delta U(t)$ is the variation in the gravitational potential. The goal of experiments is to measure or set constraints on the quantities k_X which quantify the couplings of various fundamental constants to the changing gravitational potential. Because of the eccentricity of the Earth's orbit around the Sun, the gravitational potential has a seasonal 3% variation and a corresponding modulation of the constants may be studied with atomic clocks and other precision instruments.

The idea for such experiment is illustrated in Fig. 4. Blatt *et al.* (2008) searched for such change in fundamental constants by monitoring the ratio of Sr and Cs clock frequencies. They combined their result with Hg^+/Cs (Fortier *et al.*, 2007) and H-maser and Cs (Ashby *et al.*, 2007) clock experiments to set constraints on the couplings of fundamental constants α, $1/\mu = m_e/m_p$ (designated by the subscript μ in this section), and $X_q = m_q/\Lambda_{QCD}$ (designated by the subscript q) to the changing gravitational potential defined by Eq. (24):

$$k_\alpha = (2.5 \pm 3.1) \times 10^{-6},$$
$$k_\mu = (-1.3 \pm 1.7) \times 10^{-5},$$
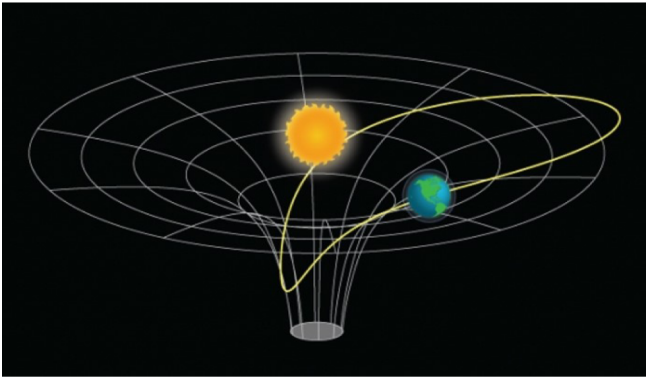$$k_q = (-1.9 \pm 2.7) \times 10^{-5},$$

FIG. 4. Earth orbiting the Sun (mass $m_\odot$) in gravitational potential; the orbit eccentricity is exaggerated. Image credit: Jun Ye's group and Greg Kuebler.

We note that decoupling of k_q is not straightforward and is dependent on the nuclear model (Flambaum and Tedesco, 2006; Jackson Kimball, 2015). Only the dependence of the H-maser frequency on the light quark mass was taken into account, but not of the Cs clock.

A limit on k_α was obtained with a measurement of frequencies in atomic dysprosium, which is only sensitive to α variation (Ferrell *et al.*, 2007).

Guéna, Abgrall *et al.* (2012) reported a limit on a fractional variation of the Rb/Cs frequency ratio with gravitational potential at the level of $(0.11 \pm 1.04) \times 10^{-6}$. A global fit to available clock data yielded constraints similar to the analysis of Blatt *et al.* (2008). Tobar *et al.* (2013) constrained a fractional variation of the Cs/H and Rb/H frequency ratios with gravitational potential at the level of $3.6(4.8) \times 10^{-6}$ and $6.3(10) \times 10^{-6}$, respectively, over 8 yr of measurements.

Peil *et al.* (2013) reported a limit on the fractional variation of the Rb/Cs, Rb/H, and Cs/H frequency ratios with the gravitational potential at the level of $(-1.6 \pm 1.3) \times 10^{-6}$, $(-2.7 \pm 4.9) \times 10^{-6}$, and $(-0.7 \pm 1.1) \times 10^{-6}$, respectively, over 1.5 yr of measurements. Peil *et al.* (2013) performed a global fit of constraints which included clock data from Ashby *et al.* (2007), Fortier *et al.* (2007), Blatt *et al.* (2008), and Guéna, Abgrall *et al.* (2012) which gave improved values:

$$k_\alpha = (1.7 \pm 7.5) \times 10^{-7},$$
$$k_\mu = (-2.5 \pm 5.4) \times 10^{-6},$$
$$k_q = (3.8 \pm 4.9) \times 10^{-6}.$$

In 2013, a new Dy frequency measurement set an improved limit on k_α (Leefer *et al.*, 2013):

$$k_\alpha = (-5.5 \pm 5.2) \times 10^{-7}.$$

Clock experiments intended for the Atomic Clock Ensemble in Space (ACES) space mission on the International Space Station (ISS) (Cacciapuoti *et al.*, 2007) could improve upon the precision of absolute redshift measurements. However, this does not help differential measurements since the annual modulation of the gravitational potential due to the Sun is the same for a clock on Earth and ISS, and the orbit around the Earth is circular.

Further improvements may come from further optical clock tests and proposed space missions that would put clocks in a highly eccentric Earth orbit (Schiller *et al.*, 2009) or a Solar System escape trajectory (Wolf *et al.*, 2009). The use of optical clocks based on the Yb$^+$ octupole transition (Huntemann *et al.*, 2016) as well as new clock schemes with high sensitivity to α variation described in Sec. II.F.2 may significantly improve the constraints.

Berengut *et al.* (2013) proposed a new test of α variation in a strong gravitational field using metal lines in the spectra of white dwarf stars. A goal of such studies is to probe α variation with gravitational potential mediated by a light scalar field at a much stronger, by 5 orders of magnitude, gravitational potential than probed by clock experiments. Laboratory measurements of relevant metal lines, such as the Fe^{4+} and Ni^{4+} (nickel, $Z = 28$) spectra, are needed to improve on the results of Berengut *et al.* (2013). Limits on a gravitational field dependence of μ from H$_2$ spectra in white dwarfs were reported by Bagdonaite *et al.* (2014).

2. Search for chameleons: Testing the dependence of fundamental constants on the mass density of the environment

Second, a spatial variation of fundamental constants may result from a shift in the expectation value of ϕ between dense and rarefied environments (Olive and Pospelov, 2008), when coupling of field to matter depends on its density via, for example, chameleon mechanism. Such tests also probe local position invariance.

In chameleon models, the scalar fields which are dark energy candidates are ultralight in a cosmic vacuum but possess an effectively large mass when coupled to normal matter (Olive and Pospelov, 2008; Joyce *et al.*, 2015) as discussed in Sec. IX, hence the "chameleon" name. Chameleon dark matter models and relevant experimental tests were recently reviewed by Joyce *et al.* (2015). The chameleon mechanism can potentially significantly affect quasar-absorption spectra used to search for variations of fundamental constants as well as comparison of laboratory and astrophysics limits.

Here we describe testing a class of chameleon models with scalar-field couplings to matter that are much stronger than the gravitational coupling (Olive and Pospelov, 2008). In such a scenario, fundamental constants depend on the local matter density ρ and one expects $\delta\alpha/\alpha \neq 0$ and $\delta\mu/\mu \neq 0$ for all interstellar clouds, when compared to terrestrial laboratory values. This change is due to differences in densities of the interstellar clouds and Earth environments $\rho_\oplus/\rho_{cloud} > 10^{10}$ (Levshakov *et al.*, 2011). The large matter density on Earth results in a screening of the cosmological chameleon field for terrestrial frequency measurements.

Molecular studies with CO, CH, ammonia (NH$_3$), and methanol CH$_3$OH have provided the most accurate limits on matter-density couplings of fundamental constants because of high sensitivity of some molecular absorption spectra in our Galaxy to μ variation. Variation of the quantity $F = \alpha^2 \mu$ with matter density was probed using a combination of C$^+$ and CO transitions (Levshakov, Molaro, and Reimers, 2010), yielding a constraint $|\Delta F/F| < 3.7 \times 10^{-7}$. The best-quality radio astronomical data for methanol lines were used to constrain

the variability of $\bar{\mu} = 1/\mu$ in the Milky Way at the level of $|\Delta\bar{\mu}/\bar{\mu}| < 2.8 \times 10^{-8}$ (Levshakov, Kozlov, and Reimers, 2011). This result can be further improved with better laboratory spectroscopy of the CH_3OH microwave lines.

In 2010, Levshakov, Lapinov *et al.* (2010) and Levshakov, Molaro *et al.* (2010) reported a surprising nonzero $\Delta\bar{\mu}/\bar{\mu} = (26 \pm 1_{\text{stat}} \pm 3_{\text{sys}}) \times 10^{-9}$ result for μ variation using the ammonia method. This approach involves observations of the NH_3 inversion lines complemented by rotational lines of other molecules in the Milky Way and comparing these frequencies with terrestrial values. In 2010–2013, Levshakov *et al.* (2013) carried out additional observations in the Milky Way to test for hidden errors and found a systematic error in the radial velocities of earlier studies. A revised value of $\Delta\bar{\mu}/\bar{\mu} < 2 \times 10^{-8}$ at the 3σ confidence level obtained using the ammonia method was reported by Levshakov *et al.* (2013), resolving the discrepancy.

A spectroscopic method for pulsed beams of cold molecules was developed by Truppe *et al.* (2013) and applied to measure the frequencies of microwave transitions in CH. Comparing new CH values and OH laboratory results (Hudson *et al.*, 2006) with those measured from Milky Way sources of CH and OH, Truppe *et al.* (2013) constrained the variation of α and μ between the high- and low-density environments of the Earth and the interstellar medium at the levels of $\Delta\alpha/\alpha = (0.3 \pm 1.1) \times 10^{-7}$ and $\Delta\bar{\mu}/\bar{\mu} = (-0.7 \pm 2.2) \times 10^{-7}$. Sensitivities for relevant transitions were calculated by Kozlov (2009).

III. PRECISION TESTS OF QUANTUM ELECTRODYNAMICS

A. Introduction

In this section, we give an overview of low-energy precision tests of quantum electrodynamics (QED) with tools of atomic physics. Historically, QED is the first relativistic quantum field theory, which laid the foundation of the modern formalism of the standard model. It is arguably the most stringently tested sector of the standard model.

We focus on recent results and existing inconsistencies. The interested reader is referred to textbooks [see, e.g., Bjorken and Drell (1964) and Peskin and Schroeder (1995)] for a general introduction to QED and recent reviews by Eides, Grotch, and Shelyuto (2001), Drake and Yan (2008), Beiersdorfer (2010), and Karshenboim (2005) for a more detailed exposure.

Precision tests of QED are carried out by comparing experimental results with theoretical predictions. For example, QED predictions depend on the value of the electromagnetic fine-structure constant α. QED is then validated to the extent that the deduced values of α from different methods, one of which incorporates QED calculations, agree with each other, as described in Sec. III.B. The comparisons are affected by the uncertainties in the values of fundamental constants (such as masses, Rydberg constant, etc.) and by the uncertainties in the strong-force (hadronic) contributions beyond QED.

In general, one distinguishes between free-particle properties, such as the anomalous magnetic moment of the electron,

and bound-state QED (Lamb shift being the most prominent example).

Bound-state QED can be tested in a number of systems and we highlight the advantages of various approaches. Such tests are expected to be more accurate in light systems such as H, D, $^3He^+$, He, positronium (Ps), and muonium (Mu), where the contribution of interelectron interaction is either absent or can be evaluated to high accuracy. QED tests with these systems were reviewed by Karshenboim (2005). The relative importance of interelectron interactions is also reduced in HCIs. However, in HCIs the nuclear structure uncertainty is the limiting factor and QED calculation in heavy ions requires a development of nonperturbative methods. Interesting intermediate cases are few-electron systems, where the electron-electron correlations must be taken into account on par with the nominally field-theoretic (QED) contributions. High-precision QED atomic calculations for Li and Be^+ were carried out by Yan, Nörtershäuser, and Drake (2008) and resulting energies were found to be in good agreement with experiment, with the exception of the Be^+ ionization potential. QED corrections to the $2p$ fine structure in Li were calculated by Puchalski and Pachucki (2014), yielding the splitting value with 6×10^{-6} uncertainty, in agreement with recent high-precision experiment (Brown *et al.*, 2013). Precision test of many-body QED was reported by Nörtershäuser *et al.* (2015) using the Be^+ $2p$ fine-structure doublets measured in short-lived isotopes. Simple molecules H_2, HD, and D_2 as well as H^{2+} and HD^+ molecular ions (Salumbides *et al.*, 2011; Dickenson *et al.*, 2013; Biesheuvel *et al.*, 2016) offer additional QED tests.

Next we highlight a few recent examples of precision QED tests and review the recent progress in QED tests with HCIs.

B. Anomalous magnetic moment of the electron

At present, the most accurate contributions to the determination of α come from the comparison of theory and experiment for the electron magnetic-moment anomaly a_e (Mohr, Taylor, and Newell, 2012; Mohr, Newell, and Taylor, 2016). This quantity is defined as follows. The magnetic moment of the electron is

$$\boldsymbol{\mu}_e = g_e \frac{e}{2m_e} \boldsymbol{s}, \qquad (25)$$

where g_e is the (dimensionless) electron g factor, m_e is its mass, and $\boldsymbol{s}$ is its spin. The magnetic-moment anomaly a_e is defined by

$$|g_e| = 2(1 + a_e).$$

The solution of the Dirac equation for a free electron gives $g_e = -2$ and thus $a_e = 0$. In the standard model, $a_e \neq 0$, it is given by

$$a_{e(\text{th})} = a_e(\text{QED}) + a_e(\text{weak}) + a_e(\text{hadronic}),$$

where the three terms account, respectively, for the purely quantum electrodynamic, predominantly electroweak, and predominantly hadronic contributions [using the notation of Mohr, Newell, and Taylor (2016)]. The $a_e(\text{QED})$ contribution

depends on α and can be expressed as a powers series of α/π whose coefficients are calculated from QED. The dependence of a_e on α for the other two contributions is negligible.

The most accurate measurement of a_e was carried out with a single electron that was suspended for months at a time in a cylindrical Penning trap (Hanneke, Fogwell, and Gabrielse, 2008). The ratio of electron spin-flip frequency to the cyclotron frequency in the trap determines a_e. The resulting value of α extracted by combining the 2008 measurement (Hanneke, Fogwell, and Gabrielse, 2008) and theoretical result for a_e is

$$1/\alpha = 137.035\,999\,084(51), \qquad (26)$$

which has a relative uncertainty of 3.7×10^{-10}. The theoretical uncertainty contribution is 2.8×10^{-10}.

Alternatively, the value of α can be obtained from (Wicht *et al.*, 2002)

$$\alpha^2 = \frac{2R_\infty}{c} \frac{M}{m_e} \frac{h}{M}, \qquad (27)$$

where M is the mass of any atom. The relative standard uncertainties of the R_∞ and M/m_e are about 6×10^{-12} and a few times 10^{-10} or less (Mohr, Newell, and Taylor, 2016). Therefore, a precision measurement of the ratio h/M for a particular atom can provide a value of α with a precision competitive to that of the determination of α from a_e described previously.

Wicht *et al.* (2002) used atom interferometry to measure the recoil velocity $v_r = \hbar k/M$ of a ^{133}Cs atom when it absorbs a photon with momentum $\hbar k$. The resulting value of $h/M(^{133}$Cs$)$ yielded a value of α with a relative uncertainty of 7×10^{-9}.

Cadoret *et al.* (2008) used Bloch oscillations[2] of ^{87}Rb atoms in an optical lattice to impart to the atoms up to 1600 recoil momenta and a Ramsey-Bordé interferometer to precisely measure the induced atomic velocity variation. Bouchendira *et al.* (2011) improved this method further and measured the ratio of the Planck constant to the mass of the ^{87}Rb atom to obtain a value of α, accurate to 6.6×10^{-10}:

$$1/\alpha = 137.035\,999\,037(91), \qquad (28)$$

improving the result of Cadoret *et al.* (2008) by a factor of 7. Terranova and Tino (2014) discussed the potential for further improvement of h/M measurements, demonstrating that it may be possible to attain the level of precision needed to test the anomaly for the magnetic moment of the muon (Bennett *et al.*, 2006).

The agreement of two determinations of α, from the measurements of a_e and of $h/M(^{87}$Rb$)$, validates the theoretical QED calculation of a_e (Aoyama *et al.*, 2008). This, in turn, provides the most accurate test of quantum electrodynamics and the SM to date. We emphasize that a_e is calculated in terms

of the fundamental constant α, but α is a SM parameter as it cannot be calculated from the first principles.

C. Quantum electrodynamics tests with polyelectrons

In 1946, Wheeler denoted as "polyelectrons" all bound complexes consisting of only electrons and positrons (Wheeler, 1946). Although all such complexes are likely unstable with respect to electron-positron annihilation into gamma rays, there are some that are stable with respect to dissociation into simpler complexes, and thus may live sufficiently long to have physical and even chemical significance. Positronium (Ps), the atom consisting of one electron and one positron, is the simplest example: it has the same discrete spectrum as the hydrogen atom in nonrelativistic quantum mechanics, up to a multiplicative factor of $(m_p + m_e)/2m_p$. Wheeler (1946) used a simple variational calculation to show that Ps$^-$ should also be stable, and Hylleraas and Ore (1947) determined that Ps$_2$ should be stable. These three species were subsequently found experimentally. Reviews of developments in this field up to 2012 were given by Karshenboim (2005) and Namba (2012), and of more recent work by Mills (2014) and Nagashima (2014).

As purely leptonic systems, polyelectrons offer a test bed for precision comparison of QED theory with experiment, particularly for bound-state systems. We review recent results and future prospects later. There is no experimental evidence for more complex polyelectrons. Frolov and Wardlaw (2008) suggested that Ps$_2^-$ and Ps$_3$ should be stable, but Bubin, Prezhdo, and Varga (2013) and Varga (2014), respectively, considered these two species to be unstable.

1. Positronium

Ps, the atom consisting of one electron and one positron, was first identified in the laboratory by Deutsch (1951). It is a system in which bound-state QED has been studied with precision. Most recently, the structure of the lowest triplet term of Ps was measured by optical spectroscopy (Cassidy *et al.*, 2012c), and the transition between the triplet and singlet terms of the Ps ground state has been observed directly (Yamazaki *et al.*, 2012; Miyazaki *et al.*, 2015). This energy splitting is a benchmark for first-principles QED calculations of two-particle systems. It has been calculated by QED theory up to the order of α^6 to an accuracy of 1 ppm. The result differs by 4σ from the experimental determination, which presently has an uncertainty of around 3 ppm (Cassidy *et al.*, 2012c). Improvements in precision are required to resolve this discrepancy. [A more recent experiment does claim to have a result closer to theory (Ishida *et al.*, 2014; Ishida, 2015)]. There are suggestions about beyond SM physics mechanisms to which positronium might be particularly susceptible (Lamm, 2017), and there are substantial efforts to extend QED theory to the order of α^7 in order to sharpen the comparison with experiment (Adkins *et al.*, 2015; Eides and Shelyuto, 2017).

Another noteworthy recent development is the advent of Ps Rydberg spectroscopy, in which states have been resolved with principal quantum numbers n as large as 50 (Cassidy *et al.*, 2012a; Jones *et al.*, 2014; Alonso *et al.*, 2015; Wall *et al.*, 2015). Such states may be of fundamental interest for

---

[2]The atoms in an optical lattice created by two counterpropagating laser beams whose frequency difference is swept linearly undergo a succession of Raman transitions which correspond to the absorption of one photon from a beam and a stimulated emission of a photon to the other beam. The internal state is unchanged while the atomic velocity increases by $2v_r$ per oscillation (Cadoret *et al.*, 2008).

testing QED, as some QED corrections appear at lower orders of α than they do for the ground state (Lamm, 2017). Ps Rydberg states can also have longer lifetimes than the $n = 1$ ground state, since the electron-positron annihilation rate is proportional to the probability density at the point of contact, which scales as n^{-3} for *s* states and can be further reduced by using states with higher values of *l*. This could be advantageous for a precision spectroscopic study or for the use of Rydberg Ps states as reservoirs for positrons used to produce the antihydrogen required for the studies described in Sec. VI. If Ps could be placed in highly "circular" Rydberg states, it could be a candidate for studies of the Einstein equivalence principle for a mixed matter-antimatter system, via either free-fall measurements or gravitational quantum state spectroscopy (Dufour *et al.*, 2015). A recent review of laser spectroscopy of Ps is given by Cassidy (2018).

2. Positronium anion Ps$^-$

In the laboratory, the positron that ends up in Ps is typically born at energies around 0.5 MeV by beta decay of a radionuclide such as ^{22}Na. The positron is moderated down to ≈ 10 meV energies by passage through matter, at which stage it can be controlled by conventional electron-optical techniques for use in scattering experiments, or produce Ps by electron capture from solids (Charlton and Humberston, 2000; Mills, 2014). The positronium anion Ps$^-$ was first obtained in the laboratory by Mills (1981). An experimental breakthrough in 2008 made it possible to generate Ps$^-$ with efficiencies above 1%, i.e., for every 100 positrons entering the moderator, one Ps$^-$ emerges (Nagashima, 2014). This development transformed the study of Ps$^-$, for example, making possible the observation of a shape resonance in its photodetachment (Michishio *et al.*, 2016). It also provides a means for producing energy-tunable beams of Ps, by applying standard acceleration procedures to Ps$^-$ and then neutralizing it by photodetachment. There is a considerable body of theory on the structure of Ps$^-$, including treatment of QED corrections (Drake, Cassar, and Nistor, 2002; Frolov, 2005). In time, the postronium anion may become a benchmark for testing QED in three-particle systems.

3. Diatomic positronium Ps$_2$

The Ps$_2$ molecule was also observed, both in its ground state (Cassidy and Mills, 2007) and in an $L = 1$ bound excited state that was predicted by Usukura, Varga, and Suzuki (1998) and Varga, Usukura, and Suzuki (1998) and subsequently observed by Cassidy *et al.* (2012b). The wavelength of the ground to excited state transition in Ps$_2$ was predicted to be 250.9179(11) nm. The observed wavelength reported by Cassidy *et al.* (2012b) is 250.979(6) nm. At present, the reason for the difference is not understood in detail. The Ps$_2$ is thought to be located in a porous silica matrix, which has been found to produce shifts in Ps transition wavelengths that are comparable to the difference between the theoretical and observed values for Ps$_2$.

D. Tests of QED in highly charged ions

QED tests in highly charged ions were recently reviewed by Beiersdorfer (2010), Sturm, Werth, and Blaum (2013),

Volotka *et al.* (2013), Shabaev *et al.* (2015), and Sturm *et al.* (2017) and we focus on key results and new developments. The spectroscopic properties involved in the HCI QED tests are atomic transition energies, hyperfine splittings, and *g* factors.

1. Energies

The ground-state Lamb shift in H-like uranium (U, $Z = 92$) was measured by Gumberidze *et al.* (2005) with 1% uncertainty, 460.2 ± 4.6 eV. The theory prediction is 463.99(39) eV, with QED contributing 265.2 eV [of which $-1.26(33)$ eV is due to second order QED] (Yerokhin, Indelicato, and Shabaev, 2003) and finite nuclear size contributing 198.54(19) eV (Kozhedub *et al.*, 2008). Combining theory and experiment provided a test of QED at the 2% level.

The $2s - 2p_{1/2}$ transition energy in Li-like U^{89+}, 280.645(15) eV, was measured with much higher, 0.005% precision, in agreement with theoretical value of 280.71(10) eV (Kozhedub *et al.*, 2008). The Li-like uranium study tested second-order (in α) QED effects to 6% (Volotka *et al.*, 2013). Theoretical accuracy of HCI QED tests is limited by the nuclear polarization correction.

The experimental accuracy is much higher for lighter ions. The $1s2p\ ^1P_1 - 1s^2\ ^1S_0$ resonance line in He-like Ar^{16+} was measured with a relative uncertainty of 2×10^{-6} for a test of two-electron and two-photon QED radiative corrections (Bruhns *et al.*, 2007). The experimental value was in perfect agreement with theoretical prediction (Artemyev *et al.*, 2005), as well as with a later 1.5 ppm measurement of 3139.581(5) eV (Kubiček *et al.*, 2012). However, a measurement of the He-like Ti (titanium, $Z = 22$) resonant line, 4749.85(7) eV, by Chantler *et al.* (2012) differed by 3σ from the theoretical prediction (Artemyev *et al.*, 2005). Chantler *et al.* (2012) noted that there appeared to be an evidence for a Z-dependent divergence between experiment and calculation in He-like isoelectronic sequence with $Z > 20$. This analysis was disputed by Epp (2013), in particular, the omission of the Kubiček *et al.* (2012) value from the fit. This issue was addressed by Chantler *et al.* (2013) and further discussed by Gillaspy (2014), indicating need for further experimental and theoretical work. Measurement of the resonant line in He-like Fe^{24+} (Kubiček *et al.*, 2014) was found to be in agreement with theory (Artemyev *et al.*, 2005) and inconsistent with a claim of systematic divergence between theory and experiment (Chantler *et al.*, 2012) at a 3σ level. The other Fe^{24+} spectroscopy data (Rudolph *et al.*, 2013) are also consistent with QED theory values.

The energy of the $1s2s\ ^3S_1 - 1s^2\ ^1S_0$ magnetic dipole transition in heliumlike argon was measured to 2.5 ppm accuracy by Amaro *et al.* (2012), differing by 1.6σ from the theoretical prediction of Artemyev *et al.* (2005). Even higher precision of 0.6 ppm was achieved for $1s^2 2s^2 2p\ ^2P_{3/2} - ^2P_{1/2}$ transition in boronlike Ar^{13+} ions, 441.25568(26) nm (Mäckel *et al.*, 2011). The theoretical value (Artemyev *et al.*, 2007) is in agreement with the experiment, but 2 orders of magnitude less accurate. Since nonrelativistic energies of $p_{1/2}$ and $p_{3/2}$ states are the same, this transition energy is determined by the

relativistic and QED effects, making it an excellent candidate for precision QED tests. Experimental accuracy can be significantly increased by recent demonstration of sympathetic cooling of HCIs (Schmöger *et al.*, 2015), and theory accuracy urgently needs to improve.

A high-precision nonperturbative (in $Z\alpha$) calculation of the nuclear-recoil effect on the Lamb shift of light hydrogenic atoms was carried out by Yerokhin and Shabaev (2015). These resolved previously reported disagreements between the numerical all-order and analytical $Z\alpha$-expansion approaches, which were caused by unusually large higher-order terms omitted in the $Z\alpha$-expansion calculations. This work eliminated the second-largest theoretical uncertainty in the $1S$ and $2S$ Lamb shifts of H.

2. Hyperfine splittings

Klaft *et al.* (1994) reported the first direct observation of a hyperfine splitting in the optical regime and measured the wavelength of the $M1$ transition between the hyperfine levels of the ground state of hydrogenlike ^{209}Bi^{82+}. A number of measurements of the hyperfine splitting in H-like HCIs with about 1×10^{-4} uncertainty [for example, measurements in ^{203}Tl^{80+} and ^{205}Tl^{80+} (thallium, $Z = 81$) by Beiersdorfer *et al.* (2001)] motivated corresponding theoretical efforts. Since the theoretical uncertainty is dominated by the correction due to nuclear magnetization distribution [the Bohr-Weisskopf (BW) effect], Shabaev *et al.* (2001) proposed to consider a specific difference of the ground-state hyperfine splitting in the Li-like ion $\Delta E(2s)$ and the H-like ion $\Delta E(1s)$ for the same nucleus:

$$\Delta'E = \Delta E(2s) - \xi \Delta E(1s). \tag{29}$$

The parameter ξ introduced to cancel the Bohr-Weisskopf effect can be calculated with high precision. In 2012, the theoretical accuracy of the specific difference between the hyperfine splitting values of H- and Li-like Bi (bismuth, $Z = 83$) ions was significantly improved (to a relative uncertainty of $\approx 10^{-4}$) due to a new evaluation (Volotka *et al.*, 2012) of the two-photon exchange corrections to the hyperfine structure in the Li-like ion. Measurements of the H-like and Li-like Bi hyperfine splittings at the 10^{-6} level will allow probing the many-body QED effects at a few percent level (Volotka *et al.*, 2013).

Hyperfine splitting of the $2s$ and $2p_{1/2}$ levels in Li-like and Be-like ions of ^{141}Pr were measured by Beiersdorfer *et al.* (2014) using high-resolution spectroscopy of the $2s - 2p_{1/2}$ transition in the extreme ultraviolet region (EUV). This work demonstrated that EUV spectroscopy can be used to measure the hyperfine structure in high-Z ions with a few valence electrons at the meV level.

Ullmann *et al.* (2017) measured the specific difference given by Eq. (29) between the hyperfine splittings in hydrogenlike ^{209}Bi^{82+} and lithiumlike ^{209}Bi^{80+} with more than an order of magnitude improvement in precision. The parameter $\xi = 0.168\,86$ was chosen from theory to cancel the BW correction for ^{209}Bi (Shabaev *et al.*, 2001). While it was expected that the specific difference is largely insensitive to nuclear structure, the experimental result

$-61.012(5)(21)$ meV differs by 7σ with the theoretical prediction $-61.320(4)(5)$ meV (Volotka *et al.*, 2012). For the experimental value, the parentheses list the statistical and systematic uncertainties. The first and second uncertainties in the theory value arise from uncalculated higher-order terms and the uncertainty of the complete cancellation of all nuclear effects. This is the largest deviation reported in strong-field QED up to now.

3. QED tests for g factors

The experimental determination of the electron g factor in Penning traps was reviewed by Sturm, Werth, and Blaum (2013) and Sturm *et al.* (2017) while the theory of bound-electron g factors in HCIs was reviewed by Shabaev *et al.* (2015). Here we highlight the most recent results.

The g factor of the electron bound in H-like ^{28}Si^{13+} was measured to ten significant digits by Sturm *et al.* (2011) using a single ion confined in a cylindrical Penning trap. The experimental g factor is determined via

$$g = 2\frac{\nu_L}{\nu_c}\frac{q}{|e|}\frac{m_e}{M}, \tag{30}$$

where ν_c is the cyclotron frequency, ν_L is the Larmor precession frequency, M is the ion mass, and q is the ion charge. The experimentally determined quantity is the frequency ratio $\Gamma = \nu_L/\nu_c$. The details of the setup, the experimental procedure, and the data evaluation were given by Schabinger *et al.* (2012). An improved result was reported by Sturm *et al.* (2013), where the electron g factor in ^{28}Si^{13+} was measured with a 4×10^{-11} fractional uncertainty using a phase-detection method to determine the cyclotron frequency. This measurement presented a challenge for theory as the theoretical uncertainty, mostly determined by uncalculated two-loop QED corrections of the order of $\alpha^2(\alpha Z)^5$ and higher (Pachucki *et al.*, 2005), became a factor of 2 larger than the experimental one. This uncertainty can be reduced by combining theoretical and experimental values for two different H-like ions as demonstrated by Sturm *et al.* (2014).

Following Eq. (30), the combination of the precision g-factor measurement and the state-of-the-art QED calculation may be used to determine the electron mass. In 2014, a very precise measurement of the magnetic moment of a single electron in H-like ^{12}C^{5+} combined with QED theory and previous measurement of the electron g factor with ^{28}Si^{13+} (Sturm *et al.*, 2013) were used to extract a new value of the electron mass (Sturm *et al.*, 2014), improving its accuracy by a factor of 13. Carbon ions were used since the ^{12}C atom defines the atomic mass unit, and the mass of the ion is known to high precision. The measurement details including a comprehensive discussion of the systematic shifts and their uncertainties are presented by Köhler *et al.* (2015). Zatorski *et al.* (2017) reevaluated the extraction of the electron mass taking into account recently calculated additional QED contributions (Yerokhin and Harman, 2013; Czarnecki and Szafron, 2016). The resulting value for the electron mass,

$$m_e = 0.000\,548\,579\,909\,065(16)\ \text{u}, \tag{31}$$

is shifted by 0.3σ with respect to earlier evaluations of the same experimental data (Köhler *et al.*, 2015) due to the inclusion of light-by-light scattering terms of the order of $\alpha^2(Z\alpha)^4$ calculated by Czarnecki and Szafron (2016). The theoretical uncertainty of the g factor is now an order of magnitude less than that of the uncertainty in the measurement of the frequency ratio Γ for $^{12}C^{5+}$. Zatorski *et al.* (2017) discussed the prospects for improved determination of m_e, $M(^4\text{He})$, and α.

A recent comparison of the cyclotron frequencies of the protons and $^{12}C^{6+}$ ions yielded a value of the proton mass in atomic mass units with a precision of 32 parts per trillion (Heiße *et al.*, 2017). The resulting value is more precise than the current CODATA recommended value by a factor of 3, but disagrees with it by about 3 standard deviations (Mohr, Newell, and Taylor, 2016).

The most stringent bound-state QED test of the ground state g factor for three-electron systems was carried out for Li-like $^{28}Si^{11+}$ by Wagner *et al.* (2013) and Volotka *et al.* (2014). In the g-factor measurement carried out in a Penning trap, 2.000 889 889 9(21) was found to be in excellent agreement with the theoretical value. The theory precision was further improved by Volotka *et al.* (2014) due to rigorous QED evaluation of the two-photon exchange corrections to the g factor, yielding 2.000 889 892(8). A comparison of this new theoretical value with the experimental result (Wagner *et al.*, 2013) provides tests of relativistic interelectronic interaction at the 10^{-5} level of precision, the one-electron bound-state QED in the presence of a magnetic field at the 0.7% level, and the screened bound-state QED at the 3% level.

By comparing the g factors of two isotopes, it is also possible to cancel most of the bound-state QED contributions and probe nuclear effects. Köhler *et al.* (2016) presented calculations and experiments on the isotope dependence of the Zeeman effect by studying g factors of Li-like $^{40}Ca^{17+}$ and $^{48}Ca^{17+}$ ions.

For heavy ions, a specific difference scheme similar to Eq. (29) can be employed to largely cancel the nuclear effects in the g-factor HCI calculations (Shabaev *et al.*, 2002). Volotka and Plunien (2014) performed a systematic study of the nuclear polarization effects in one-electron and few-electron heavy ions, which included the calculation of the nuclear polarization corrections to the binding energies, the hyperfine splitting, and the bound-electron g factor in the zeroth and first orders in $1/Z$. Strong cancellation of nuclear polarization effects determining the ultimate accuracy of the QED tests was observed in all cases for the specific differences described. A possibility for a determination of α in bound-electron g factor experiments via the study of a specific difference of the g factors of B-like and H-like ions, for the same isotope with zero nuclear spin in the Pb region, was discussed by Shabaev *et al.* (2006).

Further improvement of the experimental accuracy of Γ is expected for any ion from the currently commissioned ALPHATRAP, a Penning-trap setup at the Max Planck Institute for Nuclear Physics (Sturm, Werth, and Blaum, 2013; Sturm *et al.*, 2017). ALPHATRAP receives ions from an external electron beam ion trap that can produce charge states of up to Pb^{81+} for QED tests and a determination of α.

Another experiment currently under commissioning, ARTEMIS (von Lindenfels *et al.*, 2013), located at the HITRAP (Kluge *et al.*, 2008) facility at GSI, Darmstadt will employ a spectroscopic technique for ions with nonzero nuclear spin and is designed to work with ions up to the highest charge states.

E. Proton radius puzzle

The proton radius puzzle, as it is known colloquially, has perplexed the physics community for over half a decade (Jentschura, 2011; Pohl *et al.*, 2013; Carlson, 2015; Pohl, 2016; Hill, 2017). The highly precise root mean square (rms) charge radius $r_p = 0.84087(39)$ fm extracted from the $2S - 2P$ Lamb shift in muonic hydrogen (Pohl *et al.*, 2010; Antognini *et al.*, 2013) is in significant disagreement with the result $r_p = 0.8758(77)$ fm deduced from spectroscopy with ordinary hydrogen (Mohr, Taylor, and Newell, 2012). The latter value is also supported by electron scattering experiments, further exacerbating the problem (Bernauer *et al.*, 2010; Mohr, Taylor, and Newell, 2012; Arrington and Sick, 2015). This outstanding discrepancy has prompted speculation that the discrepancy may hint at physics beyond the standard mModel [see, e.g., Onofrio (2013), Dahia and Lemos (2016b), and Liu, McKeen, and Miller (2016)]. Resolution may be more mundane, such as missing systematic corrections in both theory and experiment or incorrect value of the Rydberg constant (Pohl *et al.*, 2013). In fact, Czarnecki and Szafron (2016) recently pointed out that light-by-light scattering diagrams have been erroneously neglected in the computations of the Lamb shift; they estimated that such contributions decrease the theoretical prediction for the $1S - 2S$ splitting in hydrogen by an amount 28 times larger than the experimental error (Parthey *et al.*, 2011). Interestingly, the same muonic-hydrogen collaboration (CREMA) reported (Pohl *et al.*, 2016) the value of deuteron radius that shows a similar discrepancy with results of deuterium spectroscopy.

Two spectroscopic experiments on hydrogen were reported as this paper was being prepared for publication. Beyer *et al.* (2017) measured the $2S - 4P$ transition frequency in H using a cryogenic beam. The extracted value of the proton radius $r_p = 0.8335(95)$ fm is 3.3 combined standard deviations smaller than the previous "H world data," which is the consensus of previous experiments on the spectroscopy of atomic hydrogen. However, this radius is in good agreement with that inferred from the spectroscopy of muonic hydrogen. On the other hand, Fleurbaey *et al.* (2018) measured the $1S - 3S$ two-photon transition frequency of hydrogen, realized with 205 nm continuous-wave laser excitation of a room-temperature atomic beam. They extracted the value $r_p = 0.877(13)$ fm, which is in good agreement with the current CODATA value. Thus, new hydrogen spectroscopy experiments that were intended to unravel this mystery have only deepened it further.

F. Conclusion

Finally, we emphasize that the detailed understanding of atomic structure and, in particular, QED contributions is

crucial for a number of precision tests of physics beyond the SM. QED contributions are needed for determining fundamental constants. While the stark discrepancies in proton and deuteron radii determinations from various methods have spurred reexaminations of both theory and experiment, the puzzle still remains unresolved. A number of technological advances, such as high-precision Ramsey-comb spectroscopy at deep ultraviolet wavelengths (Altmann *et al.*, 2016) and HCI trapping (Schmöger *et al.*, 2015), are anticipated to extend the QED tests to new regimes.

IV. ATOMIC PARITY VIOLATION

A. Introduction

In this section, we give an overview of parity violation in atomic and molecular physics. This field is generally referred to as parity nonconservation (PNC) or atomic parity violation in the literature. The field of parity violation started with the seminal paper by Lee and Yang (1956) and discovery of PNC in nuclear β decay (Wu *et al.*, 1957), followed by the Nobel Prize in physics awarded to Yang and Lee in 1957. Soon after this discovery, Zeldovich (1959) contemplated a possibility of observing PNC in atoms. He concluded that the effect was too small to be of experimental significance. However, Bouchiat and Bouchiat (1974) realized that PNC is amplified in *heavy* atoms. They showed that the relevant PNC amplitude scales steeply with the nuclear charge Z, roughly as Z^3. PNC amplitudes in heavy atoms, such as Cs, are enhanced over those in hydrogen by a factor of 10^5–10^6. This crucial observation enabled experiments on APV. In atomic physics, the first *P*-violating signal was observed by Barkov and Zolotorev (1978) in Bi, followed closely by a measurement of *P* violation in Tl (Conti *et al.*, 1979; Bucksbaum, Commins, and Hunter, 1981). In the same year, parity violation was reported in inelastic electron-deuterium scattering (Prescott *et al.*, 1978). Direct observations of the charged $W^{\pm}$ boson and neutral Z boson (responsible for APV) were not made until 1983 when they were observed at CERN's proton-antiproton collider (Arnison *et al.*, 1983a, 1983b).

Over the following decades, AMO experiments were refined, with PNC effects observed in several atoms. The most accurate measurement to date was performed in Cs (Wood *et al.*, 1997) and the most recent reported measurement is in ytterbium (Yb, $Z = 70$) (Tsigutkin *et al.*, 2009). New experiments on atomic and molecular PNC are underway or in planning stages as described in Sec. IV.D. There are a number of extensive review articles on APV (Bouchiat and Bouchiat, 1997; Budker, 1999; Ginges and Flambaum, 2004; Derevianko and Porsev, 2007; Roberts, Dzuba, and Flambaum, 2015) as well as a monograph (Khriplovich, 1991). Basics of electroweak theory can be found in a number of textbooks; see, e.g., Commins and Bucksbaum (1983) which has a discussion on APV.

The parity transformation *P*, or spatial inversion, is equivalent to mirror reflection and rotation by 180°. The eigenvalues of *P* are ±1, referred to as even and odd, respectively. Under this transformation, all position vectors **r** change sign: $\mathbf{r} \rightarrow -\mathbf{r}$, while spin and orbital angular momenta remain

unaffected. Electric and magnetic fields are transformed as $\mathcal{E} \rightarrow -\mathcal{E}$ and $\mathcal{B} \rightarrow \mathcal{B}$.

The QED Lagrangian governing AMO physics commutes with *P*, leading to distinct selection rules in atomic physics. For the electronic configuration $n_1 \ell_1 \cdots n_{N_e} \ell_{N_e}$ of N_e-electron atom, the parity eigenvalue is given by $\Pi = (-1)^{\sum_{i=1}^{N_e} \ell_i}$. The parity of a given configuration is determined by the parity of the open electron shell, e.g., the parity of the $[\text{Hg}]6p^3 \; {}^4S^{\circ}_{3/2}$ ground state of Bi is odd. The conventional spectroscopic notation of electronic terms arising from a given electronic configuration includes the label "∘" for odd parity states.

Laporte (1924) discovered parity conservation in atoms from analysis of the iron spectrum and formulated a rule: electric dipole transitions between states of like parity are strictly forbidden. To see this, consider the electric dipole (*E*1) transition amplitude $\mathbf{T}^{(E1)}_{fi} = \langle \Psi_f | \mathbf{D} | \Psi_i \rangle$, where the atomic states $\Psi_{i,f}$ are parity eigenstates and **D** is the electric dipole moment operator. Inserting the identity $1 = P^{\dagger}P$,

$$\mathbf{T}^{(E1)}_{fi} = \langle \Psi_f | P^{\dagger} P \mathbf{D} | \Psi_i \rangle = \langle P\Psi_f | P(\mathbf{D} | \Psi_i \rangle) = -\Pi_f \Pi_i \mathbf{T}^{(E1)}_{fi}.$$

Now if the two states have the same parities, $\mathbf{T}^{(E1)}_{fi} = -\mathbf{T}^{(E1)}_{fi}$ and thereby $\mathbf{T}^{(E1)}_{fi} = 0$. If parity is not conserved, the eigenstates of the full atomic Hamiltonian no longer possess a well-defined parity. In other words, PNC leads to (usually small) mixing of opposite-parity states leading to nonvanishing values of $\mathbf{T}^{(E1)}_{fi}$. The theory and experiments described next show how Laporte's rule is violated in atoms and molecules.

Microscopically, APV is caused by the weak interaction mediated by the exchange of a Z boson. Since the range of this interaction is $\sim \hbar/m_Z c \approx 2 \times 10^{-3}$ fm ($m_Z \approx 91$ GeV/c^2 is the mass of the Z boson), it is essentially a contact interaction on the scale of atomic distances. The relevant contact contribution to the SM Hamiltonian density reads (Marciano, 1995)

$$H_{\text{PV}} = \frac{G_{\text{F}}}{\sqrt{2}} \sum_q (C^{(1)}_q \bar{e}\gamma_{\mu}\gamma_5 e \bar{q}\gamma^{\mu}q + C^{(2)}_q \bar{e}\gamma_{\mu} e \bar{q}\gamma^{\mu}\gamma_5 q), \qquad (32)$$

where the Fermi constant

$$G_{\text{F}} \approx 1.17 \times 10^{-5}(\hbar c)^3 \; \text{GeV}^{-2} = 2.22 \times 10^{-14} \; \text{a.u.}$$

determines the overall strength of the weak interaction, the summation is over quark flavors, $q = \{u, d, s, \ldots\}$, e and q are field operators for electrons and quarks, respectively, γ_{μ} are Dirac matrices, and γ_5 is the Dirac matrix associated with pseudoscalars.

The coupling of the electron axial-vector currents to the quark-vector currents is parametrized by the constants $C^{(1)}_q$; the constants $C^{(2)}_q$ describe the coupling of the electron-vector currents to quark axial-vector currents. These interactions and constants could be further combined into couplings to protons and neutrons of atomic nuclei (Marciano and Sanda, 1978), e.g.,
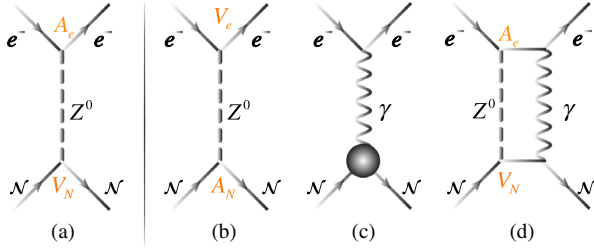
FIG. 5. Major diagrams contributing to the parity violation in atoms. $\mathcal{N}$ and e^- label nucleons and atomic electrons. $A_{e,N}$ and $V_{e,N}$ denote axial-vector and vector currents. (a) Z-boson exchange between electron axial-vector and nucleon-vector currents ($A_n V_e$); (b) Z-boson exchange between nucleon axial-vector and electron-vector currents ($V_n A_e$); (c) electromagnetic interaction of atomic electrons with the nuclear anapole moment (shown as a blob); (d) combined effect of the (a) $A_n V_e$ and hyperfine interaction. The vertical line separates nuclear (a) spin-independent and (b)–(d) spin-dependent diagrams.

$$C_p^{(1)} = 2C_u^{(1)} + C_d^{(1)}, \qquad C_n^{(1)} = C_u^{(1)} + 2C_d^{(1)},$$

reflecting the quark composition of nucleons. Explicitly in terms of the Weinberg angle θ_W:

$$C_p^{(1)} = \tfrac{1}{2}(1 - 4\sin^2\theta_W),$$
$$C_n^{(1)} = -\tfrac{1}{2},$$
$$C_p^{(2)} = -C_n^{(2)} = g_A C_p^{(1)},$$

where $g_A \approx 1.26$ is the scale factor accounting for the partially conserved axial-vector current and $\sin^2\theta_W = 0.231\,26(5)$ (Patrignani *et al.*, 2016). Since $\sin^2\theta_W \approx 1/4$, the $C_n^{(1)}$ contribution dominates H_{PV} except for the ^{1}H atom.

The main diagrams contributing to PNC processes in atoms are shown in Fig. 5. The H_{PV} terms discussed are illustrated by Figs. 5(a) and 5(b). In addition, there is also a contribution from the nuclear anapole moment [Fig. 5(c)] and a combined effect of Z-boson exchange and hyperfine interaction [Fig. 5(d)]. The effective weak Hamiltonian arising from Fig. 5(a) does not depend on the nuclear spin, while that from the set of Figs. 5(b)–5(d) does. We consider the former in Sec. IV.B and the latter in Sec. IV.C.

B. Nuclear-spin-independent effects

1. Overview

The dominant contribution to parity violation in atoms arises from the electron axial-vector–nucleon-vector term in H_{PV}, Fig. 5(a). If we treat the nucleon motion nonrelativistically, average over the nucleon distribution, and neglect the difference between proton and neutron distributions, we reduce the corresponding part of H_{PV} to an effective weak Hamiltonian in the electron sector

$$H_W = Q_W \frac{G_F}{\sqrt{8}} \gamma_5 \rho(r), \qquad (33)$$

where $\rho(r)$ is the nuclear density and Q_W is a nuclear weak charge. The nonrelativistic limit of the operator $\gamma_5 \rho(r)$ is

$$\frac{1}{2c}[2\rho(r)(\boldsymbol{\sigma} \cdot \mathbf{p}) - i(\boldsymbol{\sigma} \cdot \nabla\rho)],$$

where $\mathbf{p}$ is the linear momentum operator and $\boldsymbol{\sigma}$ are electron Pauli matrices.

The nuclear weak charge Q_W entering the effective weak Hamiltonian is

$$Q_W \equiv 2ZC_p^{(1)} + 2NC_n^{(1)},$$

where Z and N are the numbers of protons and neutrons in the nucleus. Electrons predominantly couple to neutrons and $Q_W \approx -N$. This is a "tree-level" (or the lowest-order) value of Q_W; more accurate values include SM radiative corrections (Marciano, 1995), which are typically a few percent and can be computed to high accuracy. A major theme in APV is a comparison of the extracted Q_W with its SM calculated value: a difference between the two values can indicate physics beyond the SM.

H_W is a pseudoscalar operator with its matrix element accumulated inside the nucleus. Its largest matrix element is between $s_{1/2}$ and $p_{1/2}$ atomic orbitals. Since parity is no longer a good quantum number, yet the total angular momentum J is conserved, atomic states of nominal parity acquire admixtures of states of opposite parity with the same J. The relative size of the admixture is governed by the ratio of the matrix element of H_W (typically $\propto Z^3$) to the energy splitting between the nearby states of opposite parity (typically ≈ 1 a.u.).

Since $G_F \approx 10^{-14}$ a.u., matrix elements of H_W are exceptionally small ($\approx 10^{-11}$ a.u. for Cs) compared to the typical 1 a.u. transition amplitudes in atomic physics. To amplify the PNC signal, all experiments rely on an interference technique, where the H_W-induced amplitude T_{PV} is amplified by beating it against an allowed amplitude T_0. Indeed, if the total transition amplitude is $T_{\text{tot}} = T_0 + T_{PV}$, then the transition probability (amplitude squared) acquires an interference term $T_0^* T_{PV} + \text{c.c.}$ and the experiments extract T_{PV} by measuring this interference term.

The first APV signal was observed by the Novosibirsk group in 1978 using the "optical rotation" technique in Bi (Barkov and Zolotorev, 1978). This technique is based on the interference between the APV and the allowed magnetic dipole ($M1$) transition amplitudes. Parity violation leads to optical activity, i.e., atoms interacting differently with left- and right-circularly polarized light. Thereby the polarization vector of linearly polarized light is rotated as the light passes through an atomic vapor. The measured quantity, the rotation angle, is proportional to the ratio of APV and $M1$ amplitudes. APV was measured in optical rotation experiments with ^{209}Bi, ^{209}Pb, and ^{205}Tl (Macpherson *et al.*, 1991; Meekhof *et al.*, 1993; Warrington, Thompson, and Stacey, 1993; Edwards *et al.*, 1995; Vetter *et al.*, 1995; Phipp *et al.*, 1996).

An alternative to the optical rotation scheme is the Stark interference technique (Bouchiat and Bouchiat, 1975), which we illustrate next using a ^{133}Cs experiment (Wood *et al.*, 1997)

as an example. This technique was used in Cs (Wood *et al.*, 1997; Lintz, Guena, and Bouchiat, 2007), Tl (Conti *et al.*, 1979), and Yb (Tsigutkin *et al.*, 2009) APV experiments. Additional interference techniques are described in Sec. IV.D.

2. Parity violation in cesium

The measurement of APV in ^{133}Cs (Wood *et al.*, 1997) is the most accurate to date, and supplemented with sophisticated atomic theory, it probes the SM low-energy electroweak sector with exquisite precision.

An alkali-metal atom with 55 electrons, Cs has a single valence electron outside a tightly bound Xe-like core: its ground electronic level is designated [Xe]$6s$ $^2S_{1/2}$, sometimes called $6S_{1/2}$. We focus on the optical transition between a $6S_{1/2}$ ground state and an excited state of the same parity $7S_{1/2}$. This transition is $E1$ forbidden due to the parity selection rule $\langle 6S_{1/2}|D|7S_{1/2}\rangle = 0$. The weak interaction leads to an admixture of states of opposite parity: $P_{1/2}$ states mix with the $S_{1/2}$ states, leading to a small $E1$ transition amplitude[3] E_{PV} of magnitude $E_{PV} \approx 10^{-11}$ a.u.

The Stark interference technique mentioned in Sec. IV.B.1 is used to amplify the parity-violating signal. Application of an external electric field $\mathcal{E}$ induces an additional admixture of P states. This provides a strong $E1$ pathway with a transition amplitude $\beta\mathcal{E}$, where β is the vector transition polarizability. The optical excitation rate for the $6S_{1/2} - 7S_{1/2}$ transition is proportional to the square of the transition amplitude $\beta^2\mathcal{E}^2 + (\beta\mathcal{E}E_{PV} + \text{c.c.})$, where the term quadratic in E_{PV} is negligible. By changing direction of the electric field, the excitation rate can be modulated, and the PNC amplitude E_{PV} can be isolated.

The nuclear spin of ^{133}Cs is $I = 7/2$, so each of the $S_{1/2}$ electronic states is split into $F = 3$ and 4 hyperfine components. Measuring the transition amplitudes between the different hyperfine states enables one to separate nuclear-spin-dependent and spin-independent effects. Multiple reversals of the electric field, magnetic substates, and laser polarization are used to further isolate the APV effect. The measured quantity is the ratio $R_{\text{Stark}} = \text{Im}(E_{PV})/\beta$ for $F = 3 \rightarrow F = 4$ and $F = 4 \rightarrow F = 3$ transitions between hyperfine states.

A first measurement of R_{Stark}, accurate to 10%, was performed by the Paris group (Bouchiat *et al.*, 1984), who ultimately reached an accuracy of 2.6% (Lintz, Guena, and Bouchiat, 2007). A series of measurements by the JILA group culminated in a determination of R_{Stark} with an accuracy of 0.35% (Wood *et al.*, 1997). The JILA measurements also resolved the difference between $R_{\text{Stark}}(6S_{F=3} \rightarrow 7S_{F=4})$ and $R_{\text{Stark}}(6S_{F=4} \rightarrow 7S_{F=3})$, providing the first signature of a nuclear anapole moment. This is discussed further in Sec. IV.C.

The nuclear-spin-independent parity-violating amplitude is extracted from the measured R_{Stark} and β (Bennett and Wieman, 1999):

---

[3]It is conventional to define E_{PV} parity-violating amplitude as the transition matrix element $\langle\Psi_f|\mathbf{D}|\Psi_i\rangle$ between the states with the maximum values of the magnetic quantum numbers m.

$$\text{Im}(E_{PV}) = -0.8374(31)_{\text{exp}}(21)_{\text{th}} \times 10^{-11} \text{ a.u.}$$

Extraction of the weak charge Q_W requires calculating an atomic-structure factor k_{PV}, defined as

$$E_{PV} = k_{PV}Q_W. \tag{34}$$

Reaching theoretical accuracy in k_{PV} equal to or better than the experimental accuracy of 0.35% has been a challenging task. In fact, theoretical calculations of k_{PV} and extraction of the weak charge from the Cs APV experiment (Wood *et al.*, 1997) has been a subject of controversy and lively activity over the past 15 years. At the time of the 1997 APV measurement, the accuracy of the theoretical calculations (Dzuba, Flambaum, and Sushkov, 1989; Blundell, Johnson, and Sapirstein, 1990) was estimated to be 1%. New atomic lifetime and polarizability data reported by 1999 improved the agreement of theory and experiment and the theoretical uncertainty was reduced to 0.4% (Bennett and Wieman, 1999). The resulting value of Q_W differed by 2.5σ from the prediction of the SM (Bennett and Wieman, 1999). That discrepancy prompted substantial interest in the particle physics community (Casalbuoni *et al.*, 1999; Ramsey-Musolf, 1999; Rosner, 1999, 2002). At the same time, the reduced theoretical uncertainty raised the question of whether some "small" sub-1% atomic-structure effects could be the reason for the discrepancy. Several groups contributed to understanding such small corrections (Derevianko, 2000; Dzuba *et al.*, 2001; Johnson, Bednyakov, and Soff, 2001; Kozlov, Porsev, and Tupitsyn, 2001; Sushkov, 2001; Derevianko and Porsev, 2002; Kuchiev and Flambaum, 2002; Milstein, Sushkov, and Terekhov, 2002, 2003; Sapirstein *et al.*, 2003; Shabaev *et al.*, 2005) [reviewed by Derevianko and Porsev (2007)]. The dominant corrections were found to be due to the Breit interaction, radiative QED effects, and the neutron skin correction, which is the difference between the well-known proton nuclear distribution and the relatively poorly known neutron distribution that dominates H_W. This issue is described in Sec. IV.B.4. In 2005, these corrections essentially reconciled APV in Cs with the SM, with theoretical uncertainty standing at 0.5%, still larger than the experimental error bar.

With the small corrections sorted out, major theoretical effort turned to more accurate calculation of the dominant many-body Coulomb correlation contribution to the structure factor k_{PV} (Porsev, Beloy, and Derevianko, 2009, 2010). State-of-the-art calculations built upon the *ab initio* relativistic coupled-cluster scheme of Blundell, Johnson, and Sapirstein (1990) included a large class of higher-order many-body effects. All relevant atomic properties were reproduced at a level better than 0.3%, leading to an overall 0.27% theoretical uncertainty in the structure factor k_{PV} (Porsev, Beloy, and Derevianko, 2009, 2010). The final value of the extracted Q_W was in essential agreement with the SM value.

Recent reevaluation of some subleading correlation contributions to k_{PV} by Dzuba *et al.* (2012) (contributions of the core and highly excited states) raised the theoretical uncertainty back to 0.5%, slightly shifting the value of k_{PV} from that of Porsev, Beloy, and Derevianko (2009, 2010), but

maintaining agreement with the SM. The difference in the core contribution [$0.0038 \times 10^{-11} i(-Q_W/N)$ a.u.] came from the inclusion of the core polarization (i.e., the change in the self-consistent Hartree-Fock potential due to an electric dipole field of the external photon and the weak interaction of atomic electrons with the nucleus) and Brueckner-type correlations which describe the correlation interaction of the external electron with the atomic core (Dzuba *et al.*, 2012). One of us, A.D., thinks that the correction to the contribution of highly excited states (Dzuba *et al.*, 2012) may have come from the use of many-body intermediate states by Dzuba *et al.* (2012) that is inconsistent with the one employed by Porsev, Beloy, and Derevianko (2009), as the summation over intermediate states while evaluating k_{PV} must be carried out over a complete set and thereby the results of Dzuba *et al.* (2012) require revision. This matter remains unresolved at present but new methods are being developed to address it. The ever-increasing power of computation is anticipated to bring further improvements in the atomic-structure analysis.

3. Implications for particle physics and the dark sector

Atomic parity violation yields the most accurate up-to-date probe of the low-energy electroweak sector of the SM, playing a unique role complementary to that of high-energy physics experiments. Figure 6 illustrates the energy dependence (or running) of the electroweak interaction and places APV in the context of other precision electroweak measurements. The solid curve is the SM prediction for the dependence of $\sin^2 \theta_W$ on the four-momentum transfer Q. At low Q, it describes the evolution primarily through quark loops with small leptonic corrections; the minimum at 100 GeV/c occurs when the W^+W^- loop starts contributing substantially at $Q \sim 2m_W$, m_W being the mass of W bosons. The Cs APV result is placed at
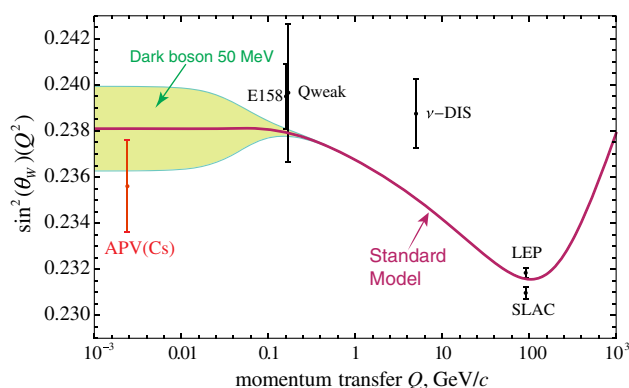

FIG. 6. Running of the weak mixing angle with momentum transfer Q. The solid red curve is the SM prediction. The Cs APV result is supplemented with data from particle physics experiments: $E158$, Møller (electron-electron) scattering; Q-weak, PNC electron-proton scattering, ν-DIS, deep inelastic scattering; LEP, and SLAC results. The area colored in yellow comes from one of the "new physics" scenarios (Davoudiasl, Lee, and Marciano, 2014): a dark boson of mass 50 MeV. The colored area is limited by constraints on model parameters that would explain the discrepancy (Bennett *et al.*, 2006) between the muon's experimental anomalous magnetic moment and the SM prediction. Adapted from Davoudiasl, Lee, and Marciano, 2014.

$Q = 2.4$ MeV/c (Bouchiat and Piketty, 1983), which is roughly $\hbar/(a_0/Z)$, where a_0 is the Bohr radius. This relates the momentum to the radius of the innermost electron shell of the Cs atom. Together with the results of high-energy collider experiments, APV demonstrates the validity of the running of the electroweak interaction over an energy range spanning 5 orders of magnitude. An alternative and more detailed plot in a different renormalization scheme can be found in Patrignani *et al.* (2016); this Particle Data Group review also provides further discussion of relevant particle physics experiments.

The transitions measured in APV studies are typically on a 1 eV energy scale, yet the accuracy of those measurements and calculations probes minute contributions of the sea of virtual particles at a much higher mass scale, including candidates beyond the SM. For example, APV is uniquely sensitive to extra Z (Z') bosons predicted in grand unified theories, technicolor models, supersymmetry (SUSY), and string theories (Langacker, 2009). Limits on their masses set by APV are at the TeV scale (Porsev, Beloy, and Derevianko, 2009), and these were only recently improved upon by direct searches at the Large Hadron Collider (Patrignani *et al.*, 2016). Such Z' bosons can also mediate new spin-dependent interactions; see Sec. VII.B.5.

Low-energy precision measurements are also uniquely sensitive to possible "dark forces" which are motivated by the intriguing possibility of a "dark sector" extension to the SM (Andreas, 2012). The dark sector is understood broadly as new physics constituents and forces that couple to SM fields weakly or do not couple at all, so that the current experiments are blind to their existence. Dark matter may be a small part of the dark sector, or many dark sectors could exist, each with their own forces and constituent particles. Dark matter may be accompanied by heretofore unknown gauge bosons (dark force carriers) which can couple dark matter particles and ordinary particles with exceptionally weak couplings. Modern colliders can be blind to such new forces, even though the mass of the dark force carriers can be quite small. This is because the cross sections of relevant processes for ordinary matter are so small that the dark force events are statistically insignificant and are discarded in high-energy experiments.

Light-mass, weakly coupled dark sector particles that interact with ordinary matter have been proposed as explanations of astronomical anomalies (Fayet, 2004; Arkani-Hamed *et al.*, 2009) as well as discrepancies between the calculated and measured magnetic moment of the muon (Fayet, 2007; Pospelov, 2009). There are several proposed inroads into the detection of weakly coupled particles and their associated dark forces (Rouven *et al.*, 2013). One such example is the dark photon (Holdom, 1986), discussed in Sec. IX, that is hypothesized to be a massive particle that couples to electromagnetic currents just as the photon does. In addition, dark Z bosons have been proposed (Davoudiasl, Lee, and Marciano, 2014) that couple to the weak neutral currents, i.e., their interactions are parity violating. In a sense, dark photons are massive photons, while dark Z bosons are light versions of Z bosons. In Fig. 6, the yellow-colored area represents the limits on dark Z bosons in the model by Davoudiasl, Lee, and Marciano (2014); the unique sensitivity and discovery potential of APV are apparent. We also point the interested reader to Bouchiat

and Piketty (1983), who considered APV mediated by a light gauge boson.

Another novel possibility for probing the dark sector with APV experiments is associated with the search for axions and axionlike particles (Roberts *et al.*, 2014a, 2014b; Stadnik and Flambaum, 2014c). The axion (see also Secs. VII and IX) is a pseudoscalar particle introduced by Peccei and Quinn (1977b) to solve the strong *CP* problem, which is the "unnatural" smallness of the $\bar{\theta}_{\text{QCD}}$ parameter in the QCD Lagrangian that quantifies the amount of *CP* violation (Weinberg, 1976); see Sec. V for more detail. Axions are also viable dark matter candidates (Bertone, 2013). The relevant pseudoscalar coupling is

$$\mathcal{L}' = i\zeta_1 m_e \phi \bar{e} \gamma_5 e + \zeta_2 (\partial_\mu \phi) \bar{e} \gamma^\mu \gamma_5 e,$$

where ζ_1 and ζ_2 are the coupling strengths. The spin-0 bosonic field

$$\phi(r, t) = \phi_0 \cos(\omega_\phi t - \mathbf{k} \cdot \mathbf{r} + \cdots) \qquad (35)$$

has an amplitude ϕ_0 related to the DM energy density and it oscillates at the particle Compton frequency. $\omega_\phi = m_\phi c^2 / \hbar$ for a particle of mass m_ϕ and $\cdots$ in Eq. (35) stands for an unknown phase. The k vectors follow the virial distribution of DM velocities. This interaction induces small oscillations in the APV amplitude at the Compton frequency. A power spectral density of the measured time series of the APV amplitude would exhibit a characteristic peak at the Compton frequency with a characteristic strongly asymmetric profile derived by Derevianko (2016). Such proposals are complementary to searches for axion-induced *P*-conserving *M*1 transitions (Sikivie, 2014).

4. Isotopic chains and neutron skin

All APV studies to date have been conducted with a single isotope and required the theoretical calculation of a k_{PV} factor in Eq. (34). Considering challenges faced by such calculations, an alternative approach was proposed by Dzuba, Flambaum, and Khriplovich (1986). The idea was to form a ratio $\mathcal{R}$ of the PNC amplitudes for two isotopes of the same element. Since the factor k_{PV} remains the same, it cancels out in the ratio. However, Fortson, Pang, and Wilets (1990) pointed out a conceptual limitation to this approach—an enhanced sensitivity of possible constraints on new physics to uncertainties in the *neutron* distributions. This problem is usually referred to as that of "neutron skin." The neutron skin is defined as the difference between the root-mean-square radii R_n and R_p of neutron and proton distributions. While nuclear charge densities (i.e., proton distributions) have been accurately measured with electron scattering, and the mean-square charge radii are well determined from isotope-shift measurements, neutron distributions, while expected to largely follow the proton distributions, are poorly known (Brown, Derevianko, and Flambaum, 2009).

Even in the interpretation of the most accurate to date single isotope measurement in Cs (Wood *et al.*, 1997), neutron skin was a point of concern, as the induced uncertainty was comparable to the experimental uncertainty in the APV

amplitude (Pollock and Welliver, 1999; Vretenar, Lalazissis, and Ring, 2000). The question was addressed by Derevianko and Porsev (2002), where empirical antiprotonic-atom data fit for the neutron skin was used (Trzcinska *et al.*, 2001), and the associated uncertainty in the neutron skin contribution to k_{PV} was substantially reduced. An analysis for multiple isotopes (Brown, Derevianko, and Flambaum, 2009) shows that in Fr and Ra$^+$ the present uncertainty in the neutron skin would limit extraction of weak charge to 0.2% accuracy.

The question of determining neutron skin is of interest in its own right, for example, as it relates to the equation of state for neutron stars. The ^{208}Pb Radius Experiment (PREX) at Jefferson Lab (JLAB) (Abrahamyan *et al.*, 2012) used PNC asymmetry in elastic scattering of electrons from ^{208}Pb with the goal of measuring R_n to 1% accuracy. Brown, Derevianko, and Flambaum (2009) examined the question of whether neutron skin can be probed with APV. The neutron skin correction is about 0.2% for Cs APV and 0.6% for Fr and Ra$^+$. Yb, francium (Fr, $Z = 87$), and radium (Ra, $Z = 88$) have a number of isotopes available for the APV experiment and highly accurate measurements of APV in two isotopes may, in principle, be used to extract the neutron skin data. In isotopic chain experiments the largest effect is attained for a pair of isotopes comprised of the lightest (neutron-depleted) and the heaviest (neutron-rich) isotopes of the chain. For Yb the accuracy in the ratio determination should be smaller than 0.2% (0.3% for Fr and Ra$^+$) just to detect the effects of having different rms neutron radii for two isotopes. This may prove more challenging than the single isotope approach, unless common systematics in measuring APV amplitudes in individual isotopes cancel out in the ratio. APV measurements on Yb (Leefer *et al.*, 2014) also benefit from a 100-fold enhancement in E_{PV} compared to Cs; the enhancement is due to the presence of closely spaced opposite parity levels (DeMille, 1995).

While the single isotope measurements are sensitive to new physics associated with electron-neutron couplings, the isotopic ratios predominantly probe electron-proton (*e*-*p*) couplings (Ramsey-Musolf, 1999). Bounds on the *e*-*p* new physics can also be directly established from PNC electron scattering off protons in the *Q*-weak experiment at JLAB (Androic *et al.*, 2013). While it was previously argued (Fortson, Pang, and Wilets, 1990; Ramsey-Musolf, 1999; Derevianko and Porsev, 2002) that APV ratios, due to neutron skin uncertainties, are not competitive to such direct experiments, Brown, Derevianko, and Flambaum (2009) showed that the induced neutron skin uncertainties for isotopes are highly correlated and tend to strongly cancel while forming $\mathcal{R}$. This observation makes APV isotopic ratio experiments a competitive tool in probing new physics *e*-*p* couplings, provided the experiments can reach the required level of accuracy.

C. Nuclear-spin-dependent effects and the nuclear anapole moment

1. Overview

The three nuclear-spin-dependent diagrams, Figs. 5(b)–5(d), can be reduced to the effective interaction in the electron sector

$$H_{\mathrm{NSD}} = \frac{G_{\mathrm{F}}}{\sqrt{2}} (\eta_{\mathrm{axial}} + \eta_{\mathrm{NAM}} + \eta_{\mathrm{hf}})(\boldsymbol{\alpha} \cdot \mathbf{I})\rho(r), \qquad (36)$$

where $\boldsymbol{\alpha}$ is the velocity operator ($\alpha_i = \gamma_0 \gamma^i$) for atomic electrons, ρ is the nuclear density, and I is the nuclear spin. This contribution is present only for $I \neq 0$ isotopes and open-shell atoms. The dimensionless parameters η primarily come from nuclear physics. In the ideal nuclear shell-model limit these coefficients are associated with the properties of the valence nucleon $\mathcal{N}$: $\mathcal{N} = p$ or n depending on a specific nucleus. The nonrelativistic reduction of the operator $(\boldsymbol{\alpha} \cdot \mathbf{I})\rho(r)$ in H_{NSD} reads

$$\frac{1}{2c}[2\rho(r)(\mathbf{I} \cdot \mathbf{p}) - i(\mathbf{I} \cdot \nabla\rho) + \boldsymbol{\sigma} \cdot (\nabla\rho \times \mathbf{I})].$$

The coefficient η_{axial} is associated with the Z exchange interaction from nucleon axial-vector ($A_n V_e$) currents, Fig. 5(b), and its nuclear shell-model value is (Flambaum and Khriplovich, 1980)

$$\eta_{\mathrm{axial}} = -C_{\mathcal{N}}^{(2)} \frac{\kappa_{\mathcal{N}} - 1/2}{I(I+1)}, \qquad (37)$$

where the weak-interaction constants $C_{n,p}^{(2)}$ were introduced in Sec. IV.A and

$$\kappa_{\mathcal{N}} = (I + 1/2)(-1)^{I+\ell_{\mathcal{N}}+1/2}$$

is the relativistic angular quantum number for the unpaired nucleon in a state with orbital angular momentum $\ell_{\mathcal{N}}$. Notice that this contribution is substantially suppressed compared to the $V_n A_e$ diagram Fig. 5(a) because

$$|C_{\mathcal{N}}^{(2)}/C_n^{(1)}| = g_A(1 - 4\sin^2\theta_{\mathrm{W}}) \approx 0.1$$

and only the unpaired nucleon contributes to Fig. 5(b), whereas all nucleons coherently contribute to Fig. 5(a).

The η_{NAM} coefficient parametrizes the nuclear anapole moment (NAM) contribution to atomic parity violation. It is illustrated in Fig. 5(c) and discussed in Sec. IV.C.2. Parity violation in the nucleus leads to toroidal currents that in turn generate a parity-odd, time-reversal-even (P-odd, T-even) moment, known as the nuclear anapole moment, that couples electromagnetically to atomic electrons. The nuclear shell-model expression for the anapole moment (Flambaum, Khriplovich, and Sushkov, 1984),

$$\eta_{\mathrm{NAM}} = 1.15 \times 10^{-3} \frac{\kappa_{\mathcal{N}}}{I(I+1)} \mu_{\mathcal{N}} g_{\mathcal{N}} A^{2/3}, \qquad (38)$$

depends on the atomic number A, the magnetic moment $\mu_{\mathcal{N}}$ of the unpaired nucleon expressed in units of the nuclear magneton, and the weak coupling constant $g_{\mathcal{N}}$. Their values are $\mu_p \approx 2.8$, $\mu_n \approx -1.9$, $g_p \approx 5$, and $g_n \approx -1$.

The combined action of the hyperfine interaction and the spin-independent Z-exchange interaction from nucleon-vector ($V_n A_e$) currents leads to the third nuclear-spin-dependent parity-violating effect, Fig. 5(d). This contribution is

quantified by a parameter η_{hf}. An analytical approximation for η_{hf} was derived by Flambaum and Khriplovich (1985b) and values of η_{hf} were determined for various cases of experimental interest by Bouchiat and Piketty (1991) and Johnson, Safronova, and Safronova (2003). Johnson, Safronova, and Safronova (2003) also tabulated the values of η_{hf} for microwave transitions between ground-state hyperfine levels in atoms of potential experimental interest.

Recently, Flambaum (2016) pointed out a novel nuclear-spin-dependent effect: the quadrupole moment of the neutron distribution leads to a tensor weak interaction that mixes opposite parity states in atoms with total angular momentum difference ≤ 2. This effect should be carefully investigated in future work to see if it influences determination of the anapole moments from APV measurements. The effect is of interest on its own as a probe of the neutron distributions in nuclei (Flambaum, Dzuba, and Harabati, 2017). The atom or molecule should contain a nucleus with $I > 1/2$, and there is an enhancement for heavy and deformed nuclei.

An outstanding question is the relative importance of the nuclear-spin-dependent contributions. The η_{hf} coefficient can be carefully evaluated and it is usually suppressed compared to η_{NAM} and η_{axial}. Generically, because of the $A^{2/3}$ scaling, the anapole contribution dominates for heavier nuclei. For lighter nuclei, the axial contribution is more important and APV experiments can be a sensitive probe of $C_{n,p}^{(2)}$ electroweak parameters, providing a window on the $A_n V_e$ interactions that are typically studied with deep inelastic scattering (The Jefferson Lab PVDIS Collaboration, 2014). The boundary between the axial- and anapole-dominated regimes depends on quantum numbers of the valence and type of the valence nucleon (DeMille, Cahn *et al.*, 2008). Values of $C_{n,p}^{(2)}$ can set constraints on exotic new physics such as leptophobic Z' bosons (Buckley and Ramsey-Musolf, 2012), while NAMs probe hadronic PNC.

2. Nuclear anapole moments as a probe of hadronic parity violation

The traditional multipolar expansion of electromagnetic potentials generated by a finite distribution of currents and charges leads to the identification of magnetic (MJ) and electric (EJ) multipolar moments (Jackson, 1999). Nonvanishing nuclear multipolar moments (charge $E0$, magnetic dipole $M1$, electric quadrupole $E2$, etc.) respect parity and time reversal, i.e., they are P even and T even, and describe multipolar fields outside the finite distribution. Weak interactions inside the nucleus lead to additional P-odd moments (Gray, Karl, and Novikov, 2010); the leading moment is referred to as the anapole moment. Zel'dovich and Vaks were the first to point out the possibility of such a moment (Zel'dovich, 1957).

The anapole moment $\boldsymbol{a}$ of a current density distribution $\boldsymbol{j}(\boldsymbol{r})$ is defined as

$$\boldsymbol{a} = -\pi \int d^3 r\, r^2 \boldsymbol{j}(\boldsymbol{r}), \qquad (39)$$

with magnetic vector potential $\boldsymbol{A} = \boldsymbol{a}\delta(\boldsymbol{r})$ leading to the electromagnetic coupling of electrons to the nuclear anapole
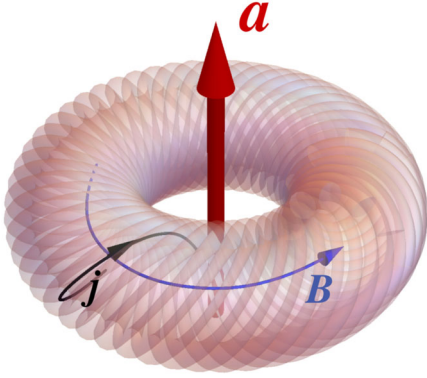
FIG. 7. The toroidal component of current density j produces anapole moment a, with magnetic field $\mathcal{B}$ that is entirely confined inside the "doughnut." The azimuthal component of current density generates the magnetic dipole moment aligned with a with its associated conventional dipolar magnetic field not shown.
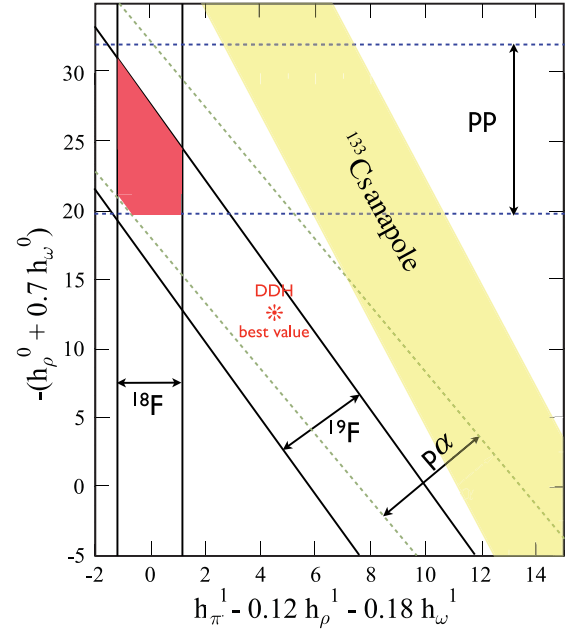

FIG. 8. Constraints on combinations of parity-violating meson couplings ($\times 10^7$) derived from the Cs anapole moment (yellow band) and nuclear experiments. Bands have a width of 1 standard deviation. The best value predicted by the DDH analysis is also shown. This figure combines the Cs NAM band from Haxton and Wieman (2001) with more recent nuclear physics constraints. From Haxton and Holstein, 2013.

moment $(\boldsymbol{\alpha} \cdot \boldsymbol{A})$. A classical analog of the anapole moment is a tokamak like configuration shown in Fig. 7. The inner and outer parts of the toroidal currents are weighted differently by r^2 in Eq. (39), leading to a nonvanishing value of the anapole moment. Microscopically, a nuclear anapole moment can be related to a chiral distribution of nuclear magnetization caused by parity-violating nuclear forces (Bouchiat and Piketty, 1991). Because of the Wigner-Eckart theorem, the NAM (just as the nuclear magnetic moment) is proportional to the nuclear spin I so that

$$a = \frac{G_{\mathrm{F}}}{|e|\sqrt{2}} \eta_{\mathrm{NAM}} I,$$

defining the constant η_{NAM} in Eq. (36). Atomic electrons interact with NAM only inside the nucleus, as is apparent from the classical analog, since the magnetic field is entirely confined inside the "doughnut." Another important observation is that the NAM is proportional to the area of the toroidal winding, i.e., $\propto$ (nuclear radius)$^2 \propto A^{2/3}$, where A is the atomic number, illustrating the trend in Eq. (38).

Microscopically, the nuclear anapole arises due to the nucleon-nucleon interaction, mediated by meson exchange, where one of the nucleon-meson vertices is strong and another is weak and P violating. Thus, determination of anapole moments from atomic parity violation provides an important window into hadronic PNC (Haxton and Wieman, 2001). The innards of the anapole bubble in Fig. 5(c) are shown in Fig. 7 of the review by Haxton and Wieman (2001). The nuclear physics approach is to characterize weak meson-nucleon couplings in terms of parameters of Desplanques, Donoghue, and Holstein (1980) (DDH), who deduced SM estimates of their values. These six hadronic PNC parameters are f_π, $h_\rho^{0,1,2}$, $h_\omega^{0,1}$, where the subscript (π, ρ, ω) indicates meson type and the superscript stands for isoscalar (0), isovector (1), or isotensor (2). We refer the interested reader to Haxton and Wieman (2001) for a detailed review of nuclear structure calculations of NAMs within the DDH parametrization. The effective field theory parametrizations of hadronic

PNC, an alternative to DDH, are also discussed (Ramsey-Musolf and Page, 2006), although NAM analysis in this framework remains to be carried out. It should be pointed out that a more recent review (Haxton and Holstein, 2013) omits the Cs result. They explained the omission by the fact that the accuracy of the constraints on the nucleon-nucleon PNC interaction derived from the NAM experiments is somewhat difficult to assess due to complex nuclear polarizability issues.

The derived bounds (Haxton and Wieman, 2001; Haxton and Holstein, 2013) on PNC meson couplings are shown in Fig. 8. The ^{133}Cs APV result is shown in addition to constraints from scattering of polarized protons on unpolarized proton and ^{4}He targets and emission of circularly polarized photons from ^{18}F and ^{19}F nuclei. The area colored red lies at the intersection of nuclear experimental bands. There is some tension with the Cs anapole moment result, although the Cs result is consistent with "reasonable ranges" of the DDH parameters. Haxton and Wieman (2001) pointed out that additional APV experiments with unpaired-neutron nuclei would produce a band perpendicular to the Cs band (the ^{133}Cs anapole moment is primarily due to a valence proton). This provides strong motivation for the ongoing experiments to measure nuclear-spin-dependent APV effects in nuclei with unpaired neutrons such as ^{171}Yb (Leefer *et al.*, 2014), ^{212}Fr (Aubin *et al.*, 2013), and ^{137}Ba (DeMille, Cahn *et al.*, 2008).

D. New and ongoing APV experiments

We limit our discussion to APV experiments that are now being actively pursued. We refer the interested reader to the

earlier reviews (Bouchiat and Bouchiat, 1997; Budker, 1999; Ginges and Flambaum, 2004; Roberts, Dzuba, and Flambaum, 2015) for a discussion of various proposals.

Experimental efforts to improve the accuracy of PNC measurements in Cs are underway at Purdue University (Antypas and Elliott, 2014). This group is exploring a new two-pathway coherent control technique. Here two optical excitations, starting from the same initial state ($6S_{1/2}$) and leading to the same final ($7S_{1/2}$) state, are driven by two different mutually coherent fields. One of the lasers is resonant with the $6S_{1/2} - 7S_{1/2}$ transition and the other operates at half the resonant frequency driving an allowed two-photon $E1$ amplitude. The absorption rate contains an interference term between the two-photon amplitude and a sum of Stark-induced and PNC amplitudes, and it depends on the relative phase of the applied laser fields. By experimentally varying the relative phase one would observe oscillating modulation of the transition rate. As a demonstration, the Purdue group has measured several atomic properties of Cs (Antypas and Elliott, 2011, 2013a, 2013b).

Francium and the Ra$^+$ ion have an electronic atomic structure similar to Cs, but larger nuclear charge Z and thereby larger PNC amplitude due to the Z^3 enhancement. Both atoms are amenable to the application of the same theoretical techniques as Cs (Dzuba, Flambaum, and Sushkov, 1995; Safronova and Johnson, 2000; Dzuba, Flambaum, and Ginges, 2001; Wansbeek *et al.*, 2008; Pal *et al.*, 2009; Sahoo, 2010) and potentially offer improved probes of the low-energy electroweak sector. The experimental challenge with these systems lies in their radioactivity which requires special experimental facilities. A Fr experiment is in preparatory stages at the TRIUMF facility in Vancouver (Aubin *et al.*, 2013), while Ra$^+$ ion is investigated in Groningen (Gomez, Orozco, and Sprouse, 2006; Nuñez Portela *et al.*, 2013). Ra$^+$ is an ion and requires application of novel experimental techniques (Fortson, 1993).

Since the accuracy of atomic calculations for multivalent systems is unlikely to approach that achieved for atoms with a single valence electron (Cs, Fr, Ra$^+$), the strategy for ongoing experiments in Yb is to pursue isotopic ratios, as discussed in Sec. IV.B.4. One of the most immediate goals of Yb APV experiments (Leefer *et al.*, 2014) is verification of the isotopic dependence of the weak charge, with the Yb experiment (recently moved from Berkeley to Mainz) currently taking data. Experiments with Dy, where there are nearly degenerate states of opposite parity, have not yet detected APV (Nguyen *et al.*, 1997); however, this is expected in the new generation of the apparatus (Leefer *et al.*, 2014).

While Cs is the only experiment to date that has measured NAM (Wood *et al.*, 1997), there are several proposals on NAM detection in atomic and molecular experiments. Bouchiat (2007) discussed a NAM-induced linear dc Stark shift of the individual substates of an alkali atom in its ground state, dressed by a circularly polarized laser field. Choi and Elliott (2016) proposed an application of the two-pathway coherent control technique for direct measurement of the anapole moment using the ground-state hyperfine splitting of Cs. Measurements in a chain of Fr isotopes (Gomez *et al.*, 2007; Aubin *et al.*, 2013) are being actively explored, with

future plans for APV measurements using both $7S_{1/2} - 8S_{1/2}$ and $7S_{1/2}$ hyperfine transitions. DeMille, Cahn *et al.* (2008) outlined a Stark-interference technique to measure spin-dependent APV effects to determine the mixing between opposite-parity rotational and hyperfine levels of ground-state molecules. By using a magnetic field to tune these levels to near degeneracy, the usual PNC-induced mixing is dramatically amplified (Kozlov, Labzovskii, and Mitruschenkov, 1991). This method can in principle give a large enhancement in sensitivity relative to traditional experiments with atoms. The technique is applicable to nuclei over a wide range of atomic numbers in diatomic species that are theoretically tractable. Both NAMs and $C_{n,p}^{(2)}$ electroweak parameters, discussed in Sec. IV.C, can be probed. Such experiments are underway at Yale (Cahn *et al.*, 2014; Altuntas *et al.*, 2017, 2018).

While PNC interactions do not normally cause first-order energy shifts because they mix states of opposite parity, such energy shifts do occur in chiral systems. This fact has been recognized since the 1970s (Letokhov, 1975), and searches for minute PNC energy shifts between states of chiral enantiomers (molecules that are mirror images of one another) via high-resolution spectroscopy have been ongoing ever since then [see, for example, Tokunaga *et al.* (2013) and references therein]. So far there have been no conclusive observations of a parity-violating effect in chiral molecules. Eills *et al.* (2017) proposed a new experiment to search for PNC in chemical shifts of chiral molecules using nuclear magnetic resonance (NMR) spectroscopy. A proof-of-principle experiment with ^{13}C-containing molecules was presented, with molecules containing heavier nuclei with enhanced PNC effects to be used next. Precision measurements of this kind may be useful for studying nuclear PNC and testing exotic physics models that predict the presence of parity-violating cosmic fields (Roberts *et al.*, 2014a, 2014b).

V. TIME-REVERSAL VIOLATION: ELECTRIC DIPOLE MOMENTS AND RELATED PHENOMENA

A. Introduction

In this section, we review phenomena related to simultaneous time-reversal (T) and parity (P) violation in atomic and molecular physics. As we will describe, recent searches for T-, P-violating (T,PV) effects in these systems are probing energy scales well above 1 TeV in particle theory models widely considered as natural extensions to the SM. Clear prospects for future improvements make it likely that work in this area will remain at the forefront of particle physics for some time. This topic has been reviewed frequently, with emphasis on different aspects of the related physics: see, for example, Barr (1993), Khriplovich and Lamoureaux (1997), Ginges and Flambaum (2004), Pospelov and Ritz (2005), Commins and DeMille (2009), Chupp (2010), Fukuyama (2012), Engel, Ramsey-Musolf, and van Kolck (2013), Jungmann (2013), Yamanaka *et al.* (2017), and Chupp *et al.* (2017). Here we focus on the connection between underlying physics and observable signals in atomic and molecular systems and the resulting impact on particle physics.
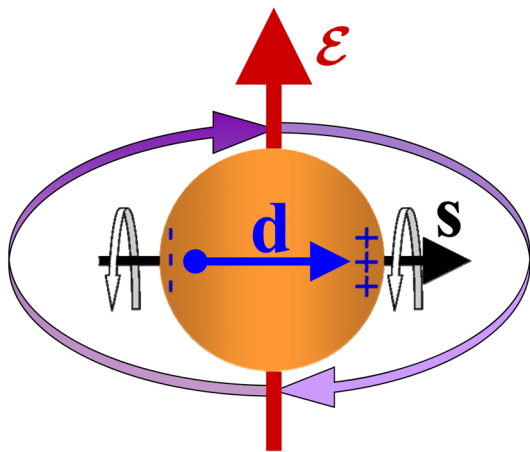
FIG. 9.   Basic concept of EDM measurements. When a particle has an EDM **d** along its spin axis **s**, an electric field $\mathcal{E}$ causes **s** to precess about $\mathcal{E}$.

A particularly relevant example of a T,PV effect is when a particle has an EDM **d**, along its spin **s**, i.e., $\mathbf{d} = d\mathbf{s}/s$ (Fig. 9). The idea that elementary particles might possess a permanent EDM in addition to a magnetic dipole moment was proposed by Purcell and Ramsey (1950). This leads to an interaction with an electric field $\mathcal{E}$ described by the Hamiltonian

$$H_{\mathrm{EDM}} = -\mathbf{d} \cdot \mathcal{E} \propto d\mathbf{s} \cdot \mathcal{E}.$$

H_{EDM} is odd under both T and P: **s** changes sign under T but $\mathcal{E}$ does not, while under P, $\mathcal{E}$ changes sign but the axial vector **s** does not. Most T,PV effects in atomic and molecular systems result in an EDM or some closely related quantity (for example, an interaction between a spin and the internuclear axis in a molecule).[4]

In relativistic quantum field theories, the combined symmetry CPT (where C is charge conjugation) is always conserved (Streater and Wightman, 2000). Moreover, CPT conservation has been experimentally confirmed to extraordinary precision (see Sec. V). Hence, in typical theoretical extensions to the SM, it is assumed that T violation is equivalent to CP violation (CPV), and for the remainder of this section we do so as well. Based on very general considerations in quantum field theory at low energies the largest effects of CPV are expected to appear as T,PV interactions rather than T-violating but P-conserving (TV) signals (Khriplovich and Lamoureaux, 1997). In fact, limits on T,PV effects in combination with established principles of field theory rule out TV effects (Conti and Khriplovich, 1992) far below the level of any conceived experiment to detect them (Kozlov and Porsev, 1989; Hopkinson and Baird, 2002). Hence for the remainder of this section we use the terms CPV and T,PV interchangeably.

---

[4]In this section, expressions related to electromagnetism will use the cgs system of units so that electric and magnetic fields, as well as electric and magnetic dipole moments, have the same dimensions. For many expressions we use mixed units that are standard for the field, such as electric fields in units V/cm and electric dipole moments in units e cm.

The time-reversal operator T is antiunitary: it can be represented as the product of a unitary operator and the complex conjugation operator (Sakurai and Napolitano, 2011). Hence while quantum wave equations with real-valued potentials are T invariant [i.e., if some wave function $\Psi(t)$ is a solution, then $\Psi^*(-t)$ is also a solution], T-violating effects arise for complex-valued potentials. Thus, T (and CP) violation is associated with the irreducible presence of complex numbers in the underlying theory. The strength of CPV interactions is proportional to $\sin\phi_{CP}$, where ϕ_{CP} is the phase of such a complex number (Fortson, Sandars, and Barr, 2003). It is known that CPV occurs in nature, from observations of CPV in decays of K^0 and B^0 mesons (Patrignani *et al.*, 2016). These observations are all consistent with a single source of CPV in the SM: a complex phase in the Cabibbo-Kobayashi-Maskawa (CKM) matrix that describes the mixing between quark flavors to form mass eigenstates. The measured value of this phase is large: $\delta_{\mathrm{CKM}} \sim 1$ rad. However, the linkage with flavor mixing causes the observable effects of CPV to be systematically small in the SM (Khriplovich and Zhitnitsky, 1982; McKellar *et al.*, 1987; Pospelov and Ritz, 2014; Yamanaka and Hiyama, 2016; Bernreuther and Suzuki, 1991). In particular, EDMs within the SM are exceptionally small, despite the large value of δ_{CKM}. By contrast, theories that extend the SM naturally can, and frequently do, include new CPV phases that contribute to EDMs and related phenomena in a more direct way, with no obvious mechanisms for suppression (Barr, 1993). This makes EDMs a nearly background-free signal for detecting new physics associated with CPV (Pospelov and Ritz, 2005; Engel, Ramsey-Musolf, and van Kolck, 2013).

Moreover, there must be new sources of CPV in nature. This conclusion arises from the observation of a baryon asymmetry—a cosmological imbalance between matter and antimatter (Dine and Kusenko, 2003). Since matter-antimatter annihilations in the aftermath of the big bang produce photons, this asymmetry is typically parametrized by the cosmological baryon-to-photon ratio $\eta \sim 10^{-10}$. Sakharov (1967) showed that, among other conditions, CPV is necessary to generate this asymmetry. While the SM in principle incorporates all the Sakharov conditions, the size of CPV effects in the SM is far too small to account for the observed value of η (Gavela *et al.*, 1994). By contrast, theoretical models containing new particles with masses near the electroweak scale $M_Z \sim 100$ GeV, together with new CPV phases, could explain the experimentally observed value of η. In these scenarios known as electroweak baryogenesis, CPV (or, equivalently, T,PV) signals typically are predicted to appear at a level near current experimental sensitivities (Engel, Ramsey-Musolf, and van Kolck, 2013).

B. Observable effects in atoms and molecules

Atomic and molecular experiments searching for T,PV can be broadly classified into two categories, based on whether the system is paramagnetic, with unpaired electron spins, or diamagnetic, with closed electron shells but nonzero nuclear spin (Barr, 1993; Khriplovich and Lamoureaux, 1997). Paramagnetic systems are most sensitive to effects that depend explicitly on electron spin: the electron EDM (eEDM)

and one type of semileptonic (electron-nucleus) interaction. Diamagnetic systems are most sensitive to effects that depend explicitly on nuclear spin: purely hadronic T,PV interactions, EDMs of nucleons, and other types of semileptonic interactions.

To understand how T,PV effects are related to EDMs in atoms and molecules, consider a toy system consisting of two states with opposite-parity eigenvalues $\Pi = \pm 1$, each with angular momentum j, split in energy by Δ, and, in particular, a pair of substates $|j, m, \Pi\rangle$ with the same projection m. These states can be mixed by a T-,P-odd Hamiltonian H_{TP}; since this is a rank-0 tensor, its matrix elements δ_{TP} are independent of m. The levels can also be mixed by the Stark Hamiltonian

$$H_{\mathrm{St}} = -\mathbf{D} \cdot \mathcal{E}\hat{z},$$

with electric dipole matrix element

$$\langle j, m, +|D_z|j, m, -\rangle \equiv D\mathrm{sgn}(m),$$

where the m dependence follows from the Wigner-Eckart theorem. This system is described by the Hamiltonian

$$H_{\mathrm{toy}} = \begin{pmatrix} -\Delta/2 & -D\mathcal{E}\mathrm{sgn}(m) + \delta_{TP} \\ -D\mathcal{E}\mathrm{sgn}(m) + \delta_{TP} & \Delta/2 \end{pmatrix}. \quad (40)$$

In addition to the usual Stark shifts there are T,PV shifts, given to first order in δ_{TP} by

$$\Delta E_{TP}^{\pm} = \mp \, \mathcal{P}\delta_{TP}\mathrm{sgn}(m).$$

Here the dimensionless quantity

$$\mathcal{P} \equiv \frac{D\mathcal{E}}{\sqrt{(\Delta/2)^2 + D^2\mathcal{E}^2}}$$

(with values $0 \leq \mathcal{P} < 1$) quantifies the polarization of the system. The superscript $\pm$ refers to the upper or lower state of the system.

This has simple behavior in the limiting cases where $D\mathcal{E} \ll \Delta$ or $\gg \Delta$. Consider the weak-field limit, where $\mathcal{P} \ll 1$; then

$$\Delta E_{TP}^{\pm} \approx \mp \, (2D\mathcal{E}/\Delta)\delta_{TP}\mathrm{sgn}(m).$$

This is exactly the shift that would be found for a system with permanent dipole moment $\mathbf{d}^{\pm} = \pm d\mathbf{j}/j$, where

$$d = 2D\delta_{TP}/\Delta.$$

Hence, in this weakly polarized regime it is sensible to say that H_{TP} induces a dipole moment (of opposite sign in the upper or lower states of the system), and the energy shifts of interest are proportional to the strength of the applied field $\mathcal{E}$. Next, consider the strong-field case, where $1 - \mathcal{P} \ll 1$. In this regime, $\Delta E_{TP}^{\pm} \approx \mp \delta_{TP}\mathrm{sgn}(m)$. Here the T,PV energy shifts are independent of $\mathcal{E}$, and it is no longer sensible to speak of a T,PV dipole moment of the system. The shifts are also maximal in this regime.

It is infeasible to reach the strong-field regime in the ground states of atoms: for typical splittings between opposite-parity levels $\Delta \sim E_{\mathrm{h}}$ (the atomic unit of energy e^2/a_0) and dipole matrix elements $D \sim ea_0$, the required field strength $\mathcal{E} \gtrsim \mathcal{E}_{\mathrm{at}}$, where $\mathcal{E}_{\mathrm{at}} = e/a_0^2 \sim 5 \times 10^9$ V/cm is the atomic unit of electric field. This is far too large to apply in the lab. However, in polar molecules there are levels of opposite parity with much smaller energy splittings but similar dipole matrix elements, making it far easier to polarize these systems. Such pairs of levels, associated with rotational structure (where $\Delta \sim [m_{\mathrm{e}}/m_{\mathrm{p}}]E_{\mathrm{h}}$) or Ω-doublet structure (where $\Delta \sim [m_{\mathrm{e}}/m_{\mathrm{p}}]^n E_{\mathrm{h}}$, with $n = 1$ or 2 depending on the type of electronic state), make it routine to reach the regime of nearly full polarization in these systems (Sandars, 1967; Sushkov and Flambaum, 1978). The increase in observable T,PV energy shifts, relative to the case of atoms in lab-scale $\mathcal{E}$ fields, is typically 3–5 orders of magnitude. Hence, experiments with molecules play an important role in this field (Kozlov and Labzowsky, 1995).

C. Underlying physical mechanisms for T,PV

1. Semileptonic interactions

Semileptonic interactions (SLIs) arise in several particle theory models. They can be described as a four-fermion interaction, related to the exchange of a heavy force-carrying boson between electrons and the nucleus. Effects due to exchange of lighter force carriers are discussed in Sec. VII.C. A few distinct forms of interaction give nonzero effects (Khriplovich and Lamoureaux, 1997). The first is the coupling of a scalar current from nucleons n in the nucleus to a pseudoscalar electron current, described by the relativistic Lagrangian density

$$\mathcal{L}_{\mathrm{SP}} \propto \sum_n \bar{\psi}_{\mathrm{e}} i\gamma^5 \psi_{\mathrm{e}} \bar{\psi}_n \psi_n.$$

This yields a relativistic Hamiltonian for the interaction of a single electron with a pointlike nucleus,

$$H_{\mathrm{SP}}^{\mathrm{rel}} = i\frac{G_{\mathrm{F}}}{\sqrt{2}} \frac{1}{2m_{\mathrm{e}}c} Q_{\mathrm{SP}}\delta^3(\mathbf{r})\gamma^0\gamma^5.$$

Here Q_{SP} is the effective charge of the nucleus for the scalar-pseudoscalar interaction, analogous to the weak charge Q_{W} for the PV weak interaction. This is frequently written in the form $Q_{\mathrm{SP}} = AC_{\mathrm{S}}$, where A is the mass number and C_{S} is the average effective charge per nucleon. In the nonrelativistic (nr) limit, this Hamiltonian takes the form

$$H_{\mathrm{SP}}^{\mathrm{nr}} = i\frac{G_{\mathrm{F}}}{\sqrt{2}} \frac{1}{2m_{\mathrm{e}}c\hbar} AC_{\mathrm{S}}\{\mathbf{s} \cdot \mathbf{p}, \delta^3(\mathbf{r})\},$$

where $\{\}$ denotes the anticommutator. This has the same form as the P-odd (but T-even) Hamiltonian arising from Z^0-boson exchange, aside from the factor of i. Because of the contact nature of the interaction, H^{SP} mixes only $s_{1/2}$ and $p_{1/2}$ orbitals in atoms, with typical matrix element

$$\delta_{\mathrm{SP}} = \langle s_{1/2}|H_{\mathrm{SP}}|p_{1/2}\rangle$$
$$\sim C_{\mathrm{S}} A Z^2 G_{\mathrm{F}} \frac{\hbar}{m_e c a_0^4} \sim 10^{-16} \times C_{\mathrm{S}} A Z^2 E_{\mathrm{h}}.$$

The explicit dependence of $H_{\mathrm{SP}}^{\mathrm{nr}}$ on **s** shows that, to lowest order, the effect of H_{SP} is nonzero only for paramagnetic systems; in diamagnetic systems, hyperfine-induced mixing leads to a nonzero effect at higher order (Flambaum and Khriplovich, 1985a).

Other forms of SLIs lead to Lagrangian densities with the form of a pseudoscalar nucleon-scalar electron current or a tensor-tensor interaction, which give rise to Hamiltonians that depend on the nuclear spin **I** in the system. However, the effects of these interactions are usually strongly suppressed, either in the underlying particle theory models or at the atomic or nuclear level. We refer the interested reader to Khriplovich and Lamoureaux (1997) for more details.

2. EDMs of constituent particles: Schiff's theorem

We next turn to the question of how EDMs of constituent particles in an atom or molecule, electrons or nuclei, can lead to observable T,PV. The answer is subtle. Schiff (1963) showed that under reasonable first-order assumptions, i.e., nonrelativistic point particles moving in a purely electrostatic potential, there is no energy shift when an $\mathcal{E}$ field is applied to a neutral system built from such constituents. The proof is simple. The total electric field $\mathcal{E}^{\mathrm{tot}}$ experienced by the particle of interest, which is the sum of an externally applied field $\mathcal{E}$ and the internal field $\mathcal{E}^{\mathrm{int}}$ due to other particles in the system, can be expressed as $\mathcal{E}^{\mathrm{tot}} = -\nabla\Phi$, where Φ is an electrostatic potential. The Hamiltonian for the particle of charge q and mass m, neglecting the EDM, is

$$H_0 = p^2/(2m) + q\Phi.$$

Since $\mathbf{p} = -i\hbar\nabla$, $\mathcal{E}^{\mathrm{tot}} \propto [p, H_0]$. Thus, for any eigenstate $|\psi\rangle$ of H_0, the expectation value of the total $\mathcal{E}$ field vanishes: $\langle\mathcal{E}^{\mathrm{tot}}\rangle = 0$. Hence, the energy shift due to the constituent particle's EDM **d** also vanishes: $\langle H_{\mathrm{EDM}}\rangle = -\mathbf{d}\cdot\langle\mathcal{E}^{\mathrm{tot}}\rangle = 0$. The physical meaning of this result, known as Schiff's theorem, is that other parts of the system rearrange so as to completely screen the external $\mathcal{E}$ field felt by the charged particle; otherwise, it would undergo a net acceleration. Mechanisms for evading Schiff's theorem are thus central to experiments searching for constituent particle EDMs in atoms and molecules.

3. Electron EDM

First we consider the eEDM in a paramagnetic atom. Remarkably, the relativistic motion of the bound electron can lead to energy shifts orders of magnitude larger than the shift for a free electron, $\Delta E_{TP} = -\mathbf{d}_e \cdot \mathcal{E}$, where $\mathbf{d}_e$ is the eEDM. This enhancement, first recognized by Sandars (1965), makes atomic and molecular experiments particularly sensitive to the eEDM. We discuss the underlying mechanism here.

The relativistic Lagrangian density associated with the interaction between the eEDM d_e and an electromagnetic field, described by the field tensor $F^{\mu\nu}$, is

$$\mathcal{L}_{\mathrm{eEDM}} = -i\frac{d_e}{2}\bar{\Psi}\sigma^{\mu\nu}\gamma^5\Psi F_{\mu\nu}, \tag{41}$$

where Ψ is the Dirac bispinor for the electron and $\sigma^{\mu\nu} = (i/2)(\gamma^\mu\gamma^\nu - \gamma^\nu\gamma^\mu)$. This yields the following single-electron relativistic Hamiltonian $H_{\mathrm{eEDM}}^{\mathrm{rel}}$:

$$H_{\mathrm{eEDM}}^{\mathrm{rel}} = -d_e\gamma^0\mathbf{\Sigma}\cdot\mathcal{E}, \tag{42}$$

where $\mathbf{\Sigma}$ is a Dirac spin operator. From Schiff's theorem, on application of an external field $\mathcal{E}$ the nr version of this Hamiltonian (still expressed in terms of bispinors), $-d_e\mathbf{\Sigma}\cdot\mathcal{E}^{\mathrm{tot}}$, will yield a vanishing energy shift. Hence, we may subtract this term to find an *effective* Hamiltonian that will account for any observable energy shift due to the eEDM:

$$H_{\mathrm{eEDM}}^{\mathrm{rel,eff}} = -d_e(\gamma^0 - 1)\mathbf{\Sigma}\cdot\mathcal{E}^{\mathrm{tot}}. \tag{43}$$

In the nr limit, this takes the form

$$H_{\mathrm{eEDM}}^{\mathrm{nr,eff}} = 4\frac{d_e}{m_e^2 c^2 \hbar^3}[(\mathbf{s}\cdot\mathbf{p})(\mathbf{s}\cdot\mathcal{E}^{\mathrm{tot}})(\mathbf{s}\cdot\mathbf{p})]. \tag{44}$$

The matrix elements of $H_{\mathrm{eEDM}}^{\mathrm{nr,eff}}$ between atomic s and p orbitals are

$$\delta_{\mathrm{eEDM}} \sim d_e(Z^3\alpha^2)\mathcal{E}_{\mathrm{at}}$$

(Sandars, 1966; Khriplovich and Lamoureaux, 1997). On application of a polarizing external field $\mathcal{E}$, this gives rise to energy shifts

$$\Delta E_{\mathrm{eEDM}}^{\pm} = \mp \mathcal{P}\delta_{\mathrm{eEDM}}.$$

For a fully polarized system, we can write

$$\Delta E_{\mathrm{eEDM}}^{\pm} = -d_e\mathcal{E}^{\mathrm{eff}},$$

where

$$\mathcal{E}^{\mathrm{eff}} \sim \pm(Z^3\alpha^2)\mathcal{E}_{\mathrm{at}}.$$

This effective electric field can be orders of magnitude larger than the applied field $\mathcal{E}$: for $Z \approx 90$, typically $\mathcal{E}^{\mathrm{eff}} \sim 100$ GV/cm. For a weakly polarized system, $\Delta E_{\mathrm{eEDM}}^{\pm} = \mp 2D\mathcal{E}\delta_{\mathrm{eEDM}}/\Delta$ can be written as

$$\Delta E_{\mathrm{eEDM}}^{\pm} = \mp d_e F_e(Z)\mathcal{E},$$

where the quantity $F_e(Z)$ is referred to as the eEDM enhancement factor for atoms: it describes the factor by which, in the limit of weak polarization, ΔE_{eEDM} exceeds the shift for a free electron. With $D \sim ea_0$ and $\Delta \sim E_{\mathrm{h}}$, $F_e(Z) \sim 2Z^3\alpha^2$, with the typical values $F_e \approx 100$–600 for $Z \approx 55$–80.

The evasion of Schiff's theorem here is remarkable, since even in the relativistic case the expectation value of $\mathcal{E}^{\mathrm{tot}}$ vanishes. The nonzero effect can be understood heuristically as arising from the relativistic length contraction of the eEDM, acting in concert with the spatial variation of the Coulomb

field $\mathcal{E}^{\text{int}}$ (Commins, Jackson, and DeMille, 2007). Since neither the length-contracted dipole moment $\mathbf{d}_e^{\text{rel}}$ nor the electric field $\mathcal{E}^{\text{tot}} = \mathcal{E} + \mathcal{E}^{\text{int}}$ are constants over the atomic volume, it makes sense that $\langle -\mathbf{d}_e^{\text{rel}} \cdot \mathcal{E}^{\text{tot}} \rangle \neq 0 = \langle \mathbf{d}_e^{\text{rel}} \rangle \cdot \langle \mathcal{E}^{\text{tot}} \rangle$.

4. Hadronic T,PV: Nuclear Schiff moment and related effects

Similar to how T-, P-odd SLIs and/or the eEDM can induce an atomic EDM, the presence of a proton or neutron EDM, or of T-, P-odd hadronic interactions can mix nuclear states to induce a nuclear EDM. However, within an atom the motion of a nucleus is deeply nonrelativistic. Hence, according to Schiff's theorem, any nuclear EDM is effectively screened from external fields and leads to negligible energy shifts. Nevertheless, the same T-, P-odd hadronic effects can induce changes in the nuclear charge and current distributions corresponding to electromagnetic moments other than an EDM. These modified distributions, unlike a nuclear EDM, can give rise to T,PV energy shifts in an electrically polarized atom or molecule.

The primary mechanism for these shifts is associated with the finite size of the nucleus. Penetration of valence electrons into the finite nuclear volume allows them to interact with a local (intranuclear) $\mathcal{E}$ field different from that of a point dipole, which would be completely screened. The charge distribution that leads to the lowest-order observable T,PV energy shift is known as the Schiff moment (SMt) $\boldsymbol{\mathcal{S}} = \mathcal{S}\mathbf{I}/I$ (Schiff, 1963):

$$\boldsymbol{\mathcal{S}} \equiv \frac{Ze}{10} \left[\int \rho_Z(\mathbf{r})\mathbf{r}r^2 d^3\mathbf{r} - \frac{5}{3} \int \rho_Z(\mathbf{r})\mathbf{r}d^3\mathbf{r} \int \rho_Z(\mathbf{r})r^2 d^3\mathbf{r} \right],$$

where ρ_Z is the nuclear charge density normalized as $\int \rho_Z(\mathbf{r})d^3\mathbf{r} = 1$. Physically, $\mathcal{S}$ corresponds to the charge distribution that gives a constant electric field $\mathcal{E}_{\mathcal{S}} \| \mathbf{I}$ within the volume of the nucleus (Flambaum and Ginges, 2002); it has dimensions of [charge × volume].

This yields a term H_{S} in the nr atomic or molecular Hamiltonian that, for a spherical nucleus of radius R_N, has the form

$$H_{\mathrm{S}} = -15e(\mathcal{S}/R_N^5)\mathbf{r} \cdot \mathbf{I}/I(r < R_N). \tag{45}$$

This interaction gives first-order effects in both diamagnetic and paramagnetic systems. The associated T,PV atomic and molecular matrix elements have typical size $\delta_{\mathrm{S}} \equiv \langle p|H_{\mathrm{S}}|s \rangle \sim Z^2\mathcal{S}/(ea_0^3)E_{\mathrm{h}}$ (Khriplovich and Lamoureaux, 1997).

A nuclear SMt can be induced by a variety of microscopic physics effects. An example is when the nucleus contains a valence nucleon n with dipole moment d_n. In a nuclear shell model where n moves around a uniform spherical core of radius $R_N = R_0 A^{1/3}$ (where A is the nuclear mass number and $R_0 \approx 1.2$ fm is the characteristic nuclear size), the SMt has magnitude $\mathcal{S} \sim 0.1 d_n A^{2/3} R_0^2$. In the weak polarization limit, H_S induces an atomic or molecular EDM d_a. Since $\mathcal{S} \propto d_n$, the quantity $F_n = d_a/d_n$ is analogous to the eEDM enhancement factor F_e for the eEDM. However, here there is instead a suppression $F_n \sim Z^2 A^{2/3} R_0^2/a_0^2$, with typical numerical value $F_n \approx 10^{-3}$ for $Z = 80$ (Khriplovich and Lamoureaux, 1997).

In most theoretical models, T-, P-odd intranuclear interactions, rather than the nucleon EDM, give dominant contributions to the nuclear SMt (Sushkov, Flambaum, and Khriplovich, 1984). For example, in many theories quarks acquire a chromo-EDM (cEDM) $\tilde{d}_q$, which is the strong-interaction analog of the ordinary EDM. The color field resulting from the cEDM induces a T-, P-odd strong interaction, typically described as an effective T,PV nucleon-nucleon interaction, between a valence nucleon and the remainder of the nucleus. This mechanism generally leads to a larger nuclear SMt than that from the ordinary nucleon EDM (Fischler, Paban, and Thomas, 1992), by a factor of $\sim$40, for the same size of $\tilde{d}_q$ and d_n (Khriplovich and Lamoureaux, 1997).[5] Hence these experiments are particularly sensitive to new physics at high-energy scales that is related to quark cEDMs (Pospelov and Ritz, 2005; Engel, Ramsey-Musolf, and van Kolck, 2013).

In addition, there is the possibility in QCD of an irreducible CPV interaction [see, for example, the reviews by Peccei (2008), Kim and Carosi (2010), and Sikivie (2012)], described by the Lagrangian density

$$\mathcal{L}_\theta = -\bar{\theta}_{\mathrm{QCD}}(\alpha_s/8\pi)(\epsilon^{\mu\nu\kappa\lambda}/2)G_{\mu\nu}^{\mathrm{a}}G_{\kappa\lambda}^{\mathrm{a}}.$$

Here α_s is the strong-interaction analog of the fine-structure constant α in electromagnetism, $\epsilon_{\mu\nu\kappa\lambda}$ is the completely antisymmetric tensor, G^{a} is the gluon field tensor, and $\bar{\theta}_{\mathrm{QCD}}$ is a dimensionless constant parametrizing the strength of this term relative to the ordinary strong interaction. $\mathcal{L}_\theta$ also leads to an effective T,PV nucleon-nucleon interaction (Crewther *et al.*, 1979; Pospelov and Ritz, 2005; Engel, Ramsey-Musolf, and van Kolck, 2013). Typical calculations in spherical nuclei of the relation between $\bar{\theta}_{\mathrm{QCD}}$ and $\mathcal{S}$ yield $\mathcal{S} \sim 10^{-3}\bar{\theta}_{\mathrm{QCD}}eR_0^3$ (Khriplovich and Lamoureaux, 1997). Searches for nuclear SMts (and the bare neutron's EDM) (Baker *et al.*, 2006; Pendlebury *et al.*, 2015) set a strong bound $\bar{\theta}_{\mathrm{QCD}} \lesssim 10^{-10}$, while naively one expects dimensionless fundamental parameters to have values of order unity. The hypothetical particle known as the axion was first devised as a mechanism to solve this so-called "strong *CP* problem." (Axions are discussed further in Secs. VII.A.3 and IX.)

While the SMt makes the dominant contribution to T,PV energy shifts in diamagnetic systems, in paramagnetic systems with nuclear spin $I \geq 1$, another mechanism typically leads to larger nuclear-spin-dependent T,PV effects (Sushkov, Flambaum, and Khriplovich, 1984; Khriplovich and Lamoureaux, 1997). Here the underlying hadronic T,PV physics leads to a current distribution in the nucleus that corresponds to a magnetic quadrupole moment (MQM). This MQM couples to the gradient of the magnetic field produced by the electron and mixes $s_{1/2}$ and $p_{3/2}$ atomic orbitals. The nuclear-spin-dependent T,PV energy shifts associated with the MQM can exceed those due to the nuclear SMt by a factor of $\sim$10–100.

---

[5]The color field within the nucleon from $\tilde{d}_q$ induces $d_n \sim e\tilde{d}_q$.

D. State-of-the-art experiments

1. General remarks

All recent atomic and molecular experiments that have set stringent limits on T,PV effects rely on the same basic measurement principle. A T-, P-odd Hamiltonian H_{TP}, together with an applied electric field $\mathcal{E} = \mathcal{E}\hat{z}$, results in an energy shift ΔE_{TP} of the state $|j, m_j\rangle$, given by $\Delta E_{TP} = \mathcal{P}\delta_{TP}\text{sgn}(m_j)$. Since δ_{TP} grows rapidly with Z, all experiments use heavy atoms. To measure ΔE_{TP}, an equal superposition of states with $\pm m_j$ is prepared and allowed to freely evolve for time τ. This state is typically prepared with high efficiency by optical pumping, sometimes in combination with radio frequency spin flips. The energy splitting leads to a relative phase accumulated between the states $\phi = 2\Delta E_{TP}\tau/\hbar$. The superposition state corresponds to an orientation or alignment of $\mathbf{j}$ in the x-y plane, and the phase evolution is equivalent to a precession of $\mathbf{j}$ about $\mathcal{E}$ by angle ϕ. For a single particle, ΔE_{TP} can be measured with minimum uncertainty $\hbar/(4\tau)$; hence with N uncorrelated particles, the T,PV energy shift can be measured with uncertainty $\delta(\Delta E_{TP}) = \hbar/(4\tau\sqrt{N})$.

Experiments of this type contend with certain common issues related to the fact that m_j-dependent energy shifts can be easily caused not only by T,PV effects, but also by magnetic fields $\mathcal{B}$ due to their interaction with the magnetic moment $\mu \propto \mathbf{j}$. Random $\mathcal{B}$-field fluctuations can degrade the signal-to-noise ratio. Nearly all experiments minimize this effect by reversing $\mathcal{E}$ in order to reverse the system polarization $\mathcal{P}$ as frequently as possible. It is also common to perform measurements on side-by-side regions with opposing $\mathcal{E}$ fields; common-mode magnetic field shifts cancel in the difference between energy shifts in these regions. In addition, $\mathcal{B}$ fields correlated with $\mathcal{E}$ can lead to systematic errors that mimic ΔE_{TP}. These can arise due to leakage currents associated with the $\mathcal{E}$ field and due to motional effects (since a particle moving in an electric field $\mathcal{E}$ with velocity $\mathbf{v}$ experiences a magnetic field $\mathcal{B}_{\text{mot}} = \mathcal{E} \times \mathbf{v}/c$). Frequently, experiments replicate the measurements on an EDM-insensitive system [e.g., a lighter species as in Regan *et al.* (2002)] or on a state of the same system with opposite sign of $\mathcal{P}$ [e.g., the excited state of the pair in the toy model of Sec. V.B, as first used by DeMille *et al.* (2001) and Eckel *et al.* (2013)] and hence also ΔE_{TP}. These "comagnetometers" act as a useful probe for systematic errors.

2. Experiments on paramagnetic systems

The ACME Collaboration (Yale and Harvard) recently completed the most sensitive experiment using a paramagnetic system (Baron *et al.*, 2014, 2017). In ACME, ThO molecules are prepared in a metastable triplet state with two valence electrons. In this state (labeled $H^3\Delta_1$), one electron is in a $\sigma_{1/2}$ orbital—roughly, a linear combination of $s_{1/2}$ and $p_{1/2}$ atomic Th orbitals—and provides excellent sensitivity to T,PV effects. The second electron, in a $\delta_{3/2}$ orbital, nearly cancels the magnetic moment of the first electron and also gives rise to high polarizability due to a small Ω-doublet splitting (Meyer, Bohn, and Deskevich, 2006; Meyer and Bohn, 2008; Vutha *et al.*, 2010). In the experiment (see Fig. 10), a beam of ThO
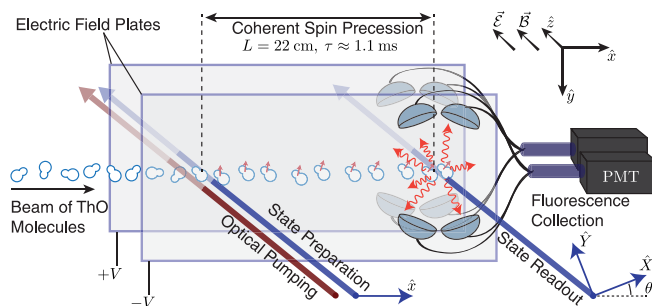

FIG. 10. Schematic of the ACME eEDM experiment. The figure shows only the magnetically shielded region where spin precession takes place. From Baron *et al.*, 2014.

molecules is produced with a cryogenic source that yields, relative to conventional molecular beam sources, a low forward velocity, low internal temperature, and high flux. The sequence of events experienced by molecules in the beam proceeds as follows. First, a set of "rotational cooling" lasers optically pumps ground-state ThO molecules to accumulate population in a single rotational level. Next, they enter a magnetically shielded interaction region where an electric field $\mathcal{E}$ with magnitude $\mathcal{E} \sim 100$ V/cm is applied to achieve polarization $\mathcal{P} \cong 1$. Once in this region, a laser pumps population from the enhanced rotational level into the H state. Next, another laser is used to spin align the H-state molecules in a direction perpendicular to $\mathcal{E}$, after which they fly freely for a distance of ≈ 20 cm. In the slow molecular beam, this corresponds to spin evolution time $\tau \approx 1$ ms, comparable to the metastable level's lifetime $\tau_H \approx 2$ ms. A magnetic field $\mathcal{B}$ is applied parallel to $\mathcal{E}$ to provide a bias (typically $\pi/4$ rad) to the spin precession. After the free-flight region, the final direction of the spin alignment axis is detected by the relative strength of laser-induced fluorescence when molecules are excited by a laser beam with alternating orthogonal polarizations. To suppress a wide range of systematic errors, the measurement is performed in both the positively and negatively polarized states of the Ω doublet and at different magnitudes of the applied field $\mathcal{E}$. With a rate $dN/dt \sim 5 \times 10^4$/s of detected molecules and ~ 2 weeks of data, ACME was sensitive to an energy shift $\Delta E_{TP}/h < 2$ mHz. Given the calculated sensitivity of the ThO H state to the eEDM, from $\mathcal{E}^{\text{eff}} \approx 80$ GV/cm (Meyer, Bohn, and Deskevich, 2006; Skripnikov, Petrov, and Titov, 2013; Denis and Fleig, 2016; Skripnikov, 2016), and to the pseudoscalar electron-scalar nucleon SLI (Denis and Fleig, 2016; Skripnikov, 2016), this corresponds to limits $d_e < 9 \times 10^{-29} e$ cm or $C_S < 6 \times 10^{-9}$ (both at 90% C.L.) (Baron *et al.*, 2017) (in each case assuming only one of the two terms is nonzero).

Recently, results from a new experiment at JILA were reported (Cairncross *et al.*, 2017). Here HfF$^+$ molecular ions in a metastable $^3\Delta_1$ state are exposed to a rotating $\mathcal{E}$ field ($\mathcal{E} \sim 20$ V/cm) that serves both to fully polarize the Ω-doublet levels and to trap the ions (Leanhardt *et al.*, 2011; Loh *et al.*, 2013; Gresh *et al.*, 2016). A small, static quadrupolar magnetic field is applied; since molecules orbit a finite distance from the center of the trap, this lab-frame field

gradient causes them to experience a rotating $\mathcal{B}$ field, parallel to the rotating field $\mathcal{E}$. All state preparation and readout operations are performed in synchrony with the rotating fields. The spin precession frequency is measured relative to this rotating frame, with a Ramsey measurement sequence of two $\pi/2$ pulses to prepare a superposition of $\pm m$ states and then to transfer information on the final direction of the spin to the populations of these states. Metastable state population and spin polarization along $\mathcal{E}$ are achieved with a series of laser pulses. The $\pi/2$ pulses are applied using a rotation-induced third-order coupling between the states, amplified by briefly reducing $\mathcal{E}$. The population in one m state is determined by a series of laser pulses that photodissociates molecules only in that state and detection of resulting Hf^+ ions. A remarkably long spin coherence time $\tau \approx 700$ ms is achieved. However, ion-ion Coulomb interactions in the trap limit the useful molecular density, leading to a low counting rate $dN/dt \sim 10/s$. With ~ 2 weeks of data, this experiment was sensitive to an energy shift $\Delta E_{TP}/h < 0.8$ mHz. With the calculated value $\mathcal{E}^{\text{eff}} \approx 23$ GV/cm for the HfF^+ $^3\Delta_1$ state (Meyer, Bohn, and Deskevich, 2006; Petrov *et al.*, 2007; Fleig and Nayak, 2013; Fleig, 2017; Skripnikov, 2017), this corresponds to $d_e < 13 \times 10^{-29}$ e cm (90% C.L.), only a factor of 1.4 less stringent than the ACME result. This experiment can also be interpreted as a limit on C_S; from the calculated sensitivity of HfF^+ (Fleig, 2017; Skripnikov, 2017), we infer $C_S < 14 \times 10^{-9}$, about 2.3 times less sensitive than ACME. Because of the different relative sensitivity to d_e and C_S in ThO and HfF^+, a combination of the two can be used to set joint limits on both quantities (Jung, 2013; Khriplovich and Lamoureaux, 1997; Chupp and Ramsey-Musolf, 2015). Earlier experiments, one using a beam of YbF molecules (Hudson *et al.*, 2011) and the other using side-by-side beams of both Tl and sodium (Na, $Z = 11$) atoms (Regan *et al.*, 2002), each set limits about $10\times$ less stringent than those of ACME.

3. Experiments on diamagnetic systems

By far the most sensitive experiment using a diamagnetic system is the long-running Hg EDM search at the University of Washington (Swallows *et al.*, 2013; Graner *et al.*, 2016). Here ^{199}Hg atoms (with a $^1S_0$ closed-shell ground state) are contained at high density in vapor cells (see Fig. 11). Their nuclear spins ($I = 1/2$) are polarized by optical pumping with a resonant laser beam, whose intensity is modulated at the precession frequency of the atoms in the nominally uniform and static applied $\mathcal{B}$ field. A stack of four nominally identical cells is used; the inner cells have strong, equal, and opposite $\mathcal{E}$ fields along the $\mathcal{B}$-field axis, while the outer cells have $\mathcal{E} = 0$. This configuration makes it possible to cancel fluctuations not only in the average value of $\mathcal{B}$, but also in its first-order gradient. At the applied field $\mathcal{E} \approx 10$ kV/cm, the atomic Hg reaches a polarization $\mathcal{P} \sim 3 \times 10^{-5}$. The cells are filled with ~ 0.5 atm of CO buffer gas to slow diffusion of the Hg atoms to the walls, which are coated with paraffin to suppress spin relaxation. After initial polarization, the spins freely precess over $\tau = 170$ s, after which nearly all remain polarized. The final spin direction is probed by monitoring the angle by which the linear polarization of a near-resonant probe laser beam is rotated as it passes through the atomic vapor. Decades
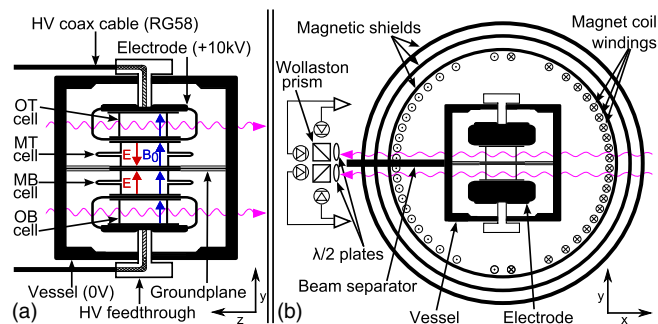

FIG. 11. Schematic of the ^{199}Hg EDM experiment. Purple arrows show probe laser beams, polarization analyzed by the combination of Wollaston prisms and photodiodes. (a) Section through the *y-z* plane of the vessel containing all four vapor cells, showing probe beams through the outer cells (where $\mathcal{E} = 0$). (b) Section through the *x-y* plane showing probe beams through the inner cells. From Graner *et al.*, 2016.

of development led to cells with extremely low leakage currents (< 40 fA). The slow diffusion ensures small motional field effects. The primary systematic errors were associated with nm-scale voltage-induced movements of the vapor cells together with uncontrolled $\mathcal{B}$-field gradients. With $N \sim 10^{14}$ atoms detected in each measurement cycle and ~ 250 days of data, the experiment was sensitive to an energy shift $\Delta E_{TP}/h < 20$ pHz. From the calculated sensitivity of the atomic EDM to the nuclear SMt $\mathcal{S}_{\text{Hg}}$ (Dzuba *et al.*, 2002; Dzuba, Flambaum, and Porsev, 2009; Radžiūtė *et al.*, 2014; Latha *et al.*, 2009; Singh and Sahoo, 2015), this sets a limit $\mathcal{S}_{\text{Hg}} < 3 \times 10^{-13}$ e fm^3 (95% C.L.). This can be interpreted in terms of underlying mechanisms that give rise to $\mathcal{S}$. For example, this yields a limit on the neutron EDM, $d_n < 1.6 \times 10^{-26}$ e cm, that is more stringent than the best limit from direct measurements with free neutrons (Baker *et al.*, 2006; Pendlebury *et al.*, 2015) by a factor of ~ 2. Similarly, the ^{199}Hg experiment sets the best limits on quark cEDMs ($\tilde{d}_u - \tilde{d}_d < 6 \times 10^{-27}$ cm) and on the observable QCD θ parameter $\bar{\theta}_{\text{QCD}} < 1.5 \times 10^{-10}$ as well as on hadronic *T*-, *P*-odd couplings, pseudoscalar-scalar and tensor-tensor SLI couplings, and the proton EDM d_p. Remarkably, despite having no sensitivity to the scalar-pseudoscalar SLI at lowest order, the limit on C_S from ^{199}Hg is only $\sim 2\times$ less strict than that from ACME.

Other experiments with diamagnetic systems also have set limits on nuclear SMts and nuclear-spin-dependent SLI couplings. The most sensitive include searches for an EDM of ^{129}Xe (Rosenberry and Chupp, 2001) and ^{225}Ra atoms (Bishof *et al.*, 2016), and for a T,PV energy shift in ^{205}TlF molecules (Cho, Sangster, and Hinds, 1989, 1991). All of these are several orders of magnitude less sensitive to the underlying physics than is the ^{199}Hg experiment. Nevertheless, their sensitivity to different linear combinations of the large set of parameters needed to describe T,PV in these systems makes them useful for providing global constraints (Chupp and Ramsey-Musolf, 2015).

4. Role of low-energy theory

Interpreting the results of atomic and molecular EDM experiments in terms of underlying physical parameters

requires knowledge of electronic wave functions. Calculations of EDM sensitivity (i.e., the ratio of atomic EDM to eEDM or SLI coupling strength) for paramagnetic atoms are similar to those needed to interpret APV experiments and have accuracy $\lesssim 5\%$ for single valence-electron atoms such as Tl, Cs, and Fr [see, for example, Dzuba and Flambaum (2009a)]. Remarkably, calculations for paramagnetic molecules with one valence electron (YbF, BaF) or even two (ThO, HfF$^+$) now have accuracy of 10% or better [see, for example, Abe *et al.* (2014), Denis and Fleig (2016), and Skripnikov (2016)]. Calculations of electronic structure for diamagnetic systems, both atoms (Hg, Ra, Xe) and molecules (TlF), give the ratio between observable energy shift and nuclear SMt with accuracy $\lesssim 20\%$ [see, for example, Dzuba *et al.* (2002) and Yamanaka *et al.* (2017)]. For the null results from all current EDM experiments, these small uncertainties have negligible impact on the limits that can be set on underlying physics.

By contrast, theoretical uncertainties associated with strongly interacting particles are not negligible for interpretation of underlying hadronic T,PV parameters. There are difficulties with the relations both between quark- and nucleon-level parameters (e.g., what value of the proton EDM d_p results from a given value of $\bar{\theta}_{\mathrm{QCD}}$ or the up-quark chromo-EDM $\tilde{d}_u$) and between nucleon- and nucleus-level parameters (e.g., what value of a nuclear SMt arises from d_p or from a given strength of effective nucleon-nucleon T,PV interaction). In the former case, the uncertainties are estimated to be at the level of $\sim 100\%$; in the latter, they can be as large as $\sim 500\%$, i.e., even the sign of the relation is not reliably known (Pospelov and Ritz, 2005; Engel, Ramsey-Musolf, and van Kolck, 2013). These uncertainties are typically not folded into quoted limits on fundamental parameters from diamagnetic system EDM experiments; if properly included, the corresponding limits would typically be weaker by factors of a few.

E. Impact on particle physics

To discuss the impact of these experiments, it is useful to begin with crude estimates for the size of the underlying effects in models with new T,PV physics at a high-energy scale (Pospelov and Ritz, 2005; Commins and DeMille, 2009). First, consider effects associated with the EDMs (and cEDMs) of the light fundamental fermions that make up atoms: the electron and the up and down quarks. The nonrenormalizable EDM Lagrangian $\mathcal{L}_{\mathrm{EDM}}$ describes the effect of radiative corrections (Feynman loop diagrams) in the underlying theory. If the associated diagram for a fermion with mass m_f has n_ℓ loops that contain heavy new particles with mass up to m_X, a typical size of the associated EDM will be

$$d \sim \mu_f \sin \phi_{CP} (g^2/2\pi)^{n_\ell} m_f^2/m_X^2,$$

where $\mu_f = e\hbar/(2m_f c)$ is the magnetic moment for a Dirac fermion and g is a dimensionless coupling strength (e.g., $g^2 = \alpha$ for electromagnetic interactions). The factor $1/m_X^2$ is associated with the propagator of the heavy particle in the loop.

In the SM, electron and quark EDMs appear only at four- and three-loop levels, respectively (Khriplovich and Lamoureaux, 1997). There is a strong additional suppression of EDMs in the SM due to a near cancellation in the sum over all contributing amplitudes (Shabalin, 1978; Nanopoulos, Yildiz, and Cox, 1979; Hoogeveen, 1990). This mechanism, which arises from the explicit linkage of flavor mixing and CPV via the CKM matrix, makes the SM predictions for EDMs extraordinarily small—for example, some 5–10 orders of magnitude below current limits for d_n and d_e, respectively. By contrast, for an uncanceled one-loop diagram ($n_\ell = 1$) and with $\sin \phi_{CP} \sim 1$, the current limit on the eEDM corresponds to $m_X \gtrsim 10$ TeV; bounds from ^{199}Hg on the quark chromo-EDMs probe a similar scale (Barr, 1993; Pospelov and Ritz, 2005; Engel, Ramsey-Musolf, and van Kolck, 2013).

Detailed calculations of the size of the relevant T,PV parameters have been made in a wide range of theoretical models. Among the most widely explored are models that incorporate SUSY that is broken near the electroweak scale, i.e., which predict superpartner particles with mass $M_{\mathrm{SUSY}} \sim M_Z \sim 0.1$ TeV. Weak-scale SUSY naturally includes many attractive features (Kane, 2002): it stabilizes the Higgs mass against radiative corrections, at around its observed value; includes candidate particles for dark matter; modifies the energy-dependent running of strong, weak, and electromagnetic couplings so that they converge at a sensible scale for grand unification; and includes new CPV phases δ_{SUSY} that could produce the cosmic baryon asymmetry.

The simplest weak-scale SUSY models include one-loop diagrams that lead to EDMs much larger than the experimental limits, unless $\delta_{\mathrm{SUSY}} M_{\mathrm{SUSY}}^{-2} \lesssim (10 \text{ TeV})^{-2}$ (Barr, 1993; Pospelov and Ritz, 2005; Engel, Ramsey-Musolf, and van Kolck, 2013; Feng, 2013). Improved EDM sensitivity by 1–2 orders of magnitude will either yield a discovery or conclusively rule out SUSY models, such as these, that are compatible with electroweak baryogenesis (Balazs, White, and Yue, 2017; Cirigliano *et al.*, 2010; Huber, Pospelov, and Ritz, 2007). There is growing interest in models where only a few of the new particles have $M_{\mathrm{SUSY}} \sim M_Z$ while all other SUSY partners have much higher mass (Arkani-Hamed and Dimopoulos, 2005). Here the primary contribution to EDMs usually comes from two-loop diagrams. Even in these scenarios the eEDM and quark cEDM limits correspond to lower bounds of ~ 2–4 TeV on the masses of the lighter SUSY particles, if $\delta_{\mathrm{SUSY}} \sim 1$ (Giudice and Romanino, 2006; Nakai and Reece, 2016). This is well beyond the direct reach of the LHC for these types of particles (Patrignani *et al.*, 2016). Some typical Feynman diagrams leading to particle EDMs are shown in Fig. 12.

SUSY is a well motivated and thoroughly investigated extension to the SM. However, in nearly every model that predicts new physics near the electroweak scale, new CPV phases appear and T,PV signals in atomic and molecular experiments should arise at values near current experimental bounds. For example, there may be additional scalar fields in nature, analogous to the Higgs boson. In such multi-Higgs models, the relative phase between the fields ϕ_h can lead to CPV (Weinberg, 1976). Exchange of the Higgs bosons between electrons and nucleons can lead to T,PV SLIs (Barr, 1992b), and two-loop diagrams including the Higgs can lead to fermion EDMs and cEDMs (Barr and Zee, 1990).
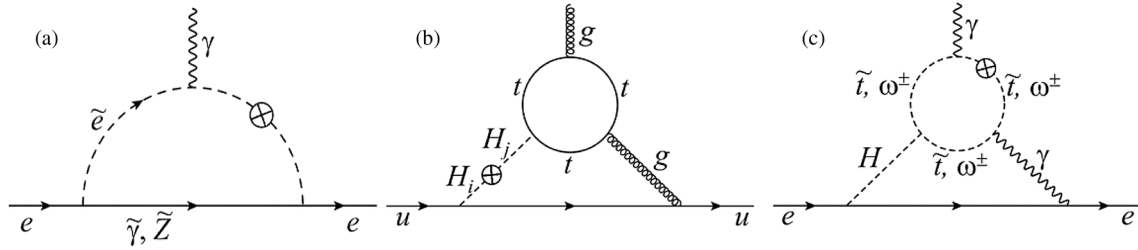
FIG. 12. Example Feynman diagrams leading to particle EDMs. Crosses represent CPV phases and tildes indicate SUSY partners of SM fields. (a) One-loop diagram leading to an eEDM in a SUSY model. The vertical photon represents the coupling of the EDM to an electric field. The CPV phase arises from the mechanism that leads to breaking of SUSY at low energies. (b) Two-loop diagram leading to an up quark cEDM in a multi-Higgs doublet model. $H_{i,j}$ represent different Higgs fields, and the CPV phase arises from mixing between them. The dominant diagram includes t quarks since their large mass indicates a strong coupling to the Higgs field. (c) Dominant two-loop diagrams leading to an eEDM in SUSY models where partners of fermions are heavy. Here $\omega^{\pm}$ are SUSY partners of $W^{\pm}$ bosons.

The relative importance of the SLI and EDM contributions to T,PV signals depends on the details of parameters in the theory. Broadly speaking, however, in these models the ^{199}Hg and ACME experiments set limits of

$$\sin\phi_h M_{h'}^{-2} \lesssim (5 \text{ TeV}/c^2)^{-2},$$

where $M_{h'}$ is the mass of a new Higgs particle (Barr, 1993; Pospelov and Ritz, 2005; Engel, Ramsey-Musolf, and van Kolck, 2013). Again, this substantially exceeds direct LHC bounds on $M_{h'}$, if $\phi_h \sim 1$.

A few authors have also begun to explore the implications of EDM limits on the possible existence of new particles with mass below the electroweak scale, but with very weak couplings to ordinary matter—dark sector particles and their associated dark forces, discussed in Secs. IV and VII.B.5. It was argued (Le Dall, Pospelov, and Ritz, 2015) that within a broad class of models where new particles appear only at low mass scales, EDM limits provide less stringent constraints than other types of experiments (aside from limits on $\bar{\theta}_{\text{QCD}}$, which is not associated with a high mass scale and can appear in such a scenario). However, more generally (e.g., where new particles are present at both low and high mass), EDMs can provide very strict limits on T,PV couplings to dark force carriers with mass below the electroweak scale. The first example of such an analysis (for tensor SLIs) was carried out by Gharibnejad and Derevianko (2015).

F. Future directions

Here we briefly review ongoing or planned T,PV experiments known to us. A few themes are common in new experimental approaches. For example, because of the importance of obtaining long spin precession times, techniques of laser cooling (to obtain lower velocities) and trapping (for the longest hold times) are beginning to be used. Several new and ongoing experiments are also exploiting the high polarizability of polar molecules for enhanced sensitivity. A few groups plan to employ both these concepts, leveraging the recent initial demonstrations of laser cooling and trapping of polar molecules. These methods require optical cycling behavior, which in itself enables both efficient detection (when each molecule emits many fluorescent photons) and

cooling of internal states, such as rotation, via optical pumping.

1. Paramagnetic systems

Improvements in all the recent experiments using paramagnetic molecules are underway. The ACME Collaboration plans several upgrades to improve statistics. In the ongoing second generation of ACME, improved efficiency of state preparation and detection is anticipated to improve the sensitivity to d_e by $\sim 20\times$ (Panda *et al.*, 2016). A third generation with increased molecular beam flux from a new source and electrostatic focusing, enhanced detection efficiency via optical cycling, and longer integration time could yield another $\sim (30-50)\times$ improvement, corresponding to sensitivity at the level $d_e \sim 10^{-31}$ e cm (Vutha *et al.*, 2010). Simultaneously, the YbF experiment at Imperial College is also improving beam flux and velocity by use of a cryogenic beam and rotational cooling, plus optical cycling fluorescence for efficient detection (Rabey *et al.*, 2016). YbF reaches $\mathcal{P} \approx 60\%$ at $\mathcal{E} = 10$ kV/cm, yielding $\mathcal{P}\mathcal{E}_{\text{eff}} \approx 15$ GV/cm, $\approx 5\times$ smaller than $\mathcal{E}_{\text{eff}}$ in ThO (Kara *et al.*, 2012). Future plans call for a dramatic increase in interaction time by use of a laser-cooled molecular fountain similar to that used for atomic Cs clocks (Tarbutt *et al.*, 2013). Kozyryev and Hutzler (2017) recently proposed using certain types of polyatomic paramagnetic molecules that could be laser cooled, and also have a favorable energy level structure for eEDM measurements (similar to the Ω-doublet states used in ACME). Meanwhile, the JILA trapped molecular ion experiment plans a new trap electrode geometry to allow use of much larger ion clouds. An approximately 10 times improved sensitivity to d_e is projected. In the longer term, use of the heavier species ThF$^+$ will improve $\mathcal{E}_{\text{eff}}$ by a factor of $1.5\times$, and possibly also enable longer spin coherence time since here $^3\Delta_1$ is the ground state (Gresh *et al.*, 2016; Cairncross *et al.*, 2017). Kawall (2011) also proposed to perform similar experiments in a storage ring to further increase the trapping volume.

Several other efforts are also under development. A group at Pennsylvania State University is using laser-cooled and optically trapped Cs atoms, with cotrapped Rb as a comagnetometer (Weiss, Fang, and Chen, 2003). Here long coherence times ~ 3 s are anticipated, along with large counting rates to

compensate for the low Z and low $\mathcal{P}$ in Cs atoms, which yield an effective field $F_e\mathcal{E} \sim 10^7$ V/cm with $F_e(\mathrm{Cs}) = 120$ and $\mathcal{E} \sim 10^5$ V/cm. A group at Tohoku University is planning a similar experiment using Fr atoms (Inoue *et al.*, 2015), with $F_e = 900$. Finally, a group at the University of Groningen is constructing an apparatus to electrically decelerate (Mathavan *et al.*, 2016) a beam of BaF molecules (with $\mathcal{P}\mathcal{E}_{\mathrm{eff}} \approx 5$ GV/cm), then apply transverse laser cooling to obtain a very bright and slow molecular beam (Hoekstra, 2016).

2. Diamagnetic systems

A new generation of the ^{199}Hg experiment is planned, with various technical improvements to increase sensitivity by 2–3× (Heckel, 2016). A newer effort at Argonne National Lab uses laser-cooled and optically trapped ^{225}Ra atoms (Bishof *et al.*, 2016). Here there is a large enhancement in the SMt of ^{225}Ra, for the same size of underlying parameters such as quark cEDMs. An octupole deformation of the ^{225}Ra nucleus leads to closely spaced opposite-parity nuclear energy levels, analogous to Ω-doublet levels in polar molecules, and a similar enhancement of the induced SMt due to T,PV effects in the nucleus (Auerbach, Flambaum, and Spevak, 1996). However, the relatively short half-life of ^{225}Ra (~ 15 days) complicates the experimental protocol. Calculations of the SMt for given values of the microscopic T,PV parameters (Ban *et al.*, 2010) generally indicate a 100–1000× larger SMt in ^{225}Ra as compared to ^{199}Hg; the atomic structure of Ra gives another 3× enhancement (Dzuba *et al.*, 2002). In addition, it may be possible to make the uncertainty in the relation between fundamental parameters and nuclear SMt smaller in octupole-deformed nuclei such as ^{225}Ra than in more spherical nuclei such as ^{199}Hg. The Argonne group recently reported a limit on the EDM of atomic ^{225}Ra, $d_{\mathrm{Ra}} < 1.4 \times 10^{23}$ e cm (95% C.L.), corresponding to a limit on the SMt of $S_{\mathrm{Ra}} < 2 \times 10^{-7}$ $e\,\mathrm{fm}^3$ (Bishof *et al.*, 2016). While this is approximately 1000 times less sensitive than the ^{199}Hg experiment at present, dramatic improvements are anticipated in trapped atom number, detection efficiency, and $\mathcal{E}$-field strength (Bishof *et al.*, 2016). Another effort to take advantage of an enhanced SMt due to octupole deformation is underway at TRIUMF using ^{233}Rn, which can be collected in a vapor cell after production at a radioactive beam facility (Tardiff *et al.*, 2014). Groups at Munich (Kuchler *et al.*, 2016), Mainz (Zimmer, 2017), and Tokyo (Sato *et al.*, 2015) are preparing new measurements of the ^{129}Xe EDM. All will use vapor cells, where extraordinarily long spin coherence times can be achieved; all also use ^{3}He as a comagnetometer. However, Xe ($Z = 54$) has lower intrinsic sensitivity than ^{199}Hg; moreover, the inaccessability of optical transitions in Xe forces the use of direct magnetic field sensing of the nuclear spins, with lower signal-to-noise ratio than is routinely achieved with laser-based detection methods.

Finally, groups at Yale, Columbia, and the University of Massachusetts are constructing a new experiment (CeNTREX) to measure the SMt of ^{205}Tl. CeNTREX will use a cryogenic beam of TlF molecules, with rotational cooling and electrostatic focusing for a large useful flux, plus optical cycling for efficient detection of laser-induced fluorescence (Norrgard *et al.*, 2017). The ^{19}F nucleus will be used as a comagnetometer. With near-unit polarization, the sensitivity of TlF to the SMt is $\sim 10^4\times$ larger in TlF than in the ^{199}Hg experiment (Dzuba *et al.*, 2002). This helps to overcome a small spin coherence time of ~ 15 ms in the TlF cryogenic beam. Future generations will employ transverse laser cooling for improved beam flux and eventually optically trapped molecules for long spin coherence time. New experiments also have been proposed to search for a nuclear MQM (Flambaum, DeMille, and Kozlov, 2014). Here two enhancement mechanisms can be employed. First, using a nucleus with large quadrupole deformation enhances the MQM by a factor of ~ 10–20 relative to spherical nuclei (Flambaum *et al.*, 1994). Second, using molecules in a $^3\Delta_1$ state gives the unpaired electron spin needed to couple to the nuclear MQM, high polarization $\mathcal{P}$, and suppressed magnetic moment relative to typical paramagnetic systems, just as in the ThO eEDM experiment. For the same underlying T,PV parameters, the energy shifts in such a system could be $\sim 10^7$ times larger than in the ^{199}Hg experiment.

VI. TESTS OF THE *CPT* THEOREM, MATTER-ANTIMATTER COMPARISONS

Current physical laws are believed to be invariant under the *CPT* transformation (the *CPT* theorem), i.e., combined transformations of charge conjugation, spatial inversion, and time reversal. Within conventional field theory, the *CPT* symmetry is closely related to Lorentz invariance; however, in more general frameworks such as string theory, there is a possibility in principle to violate one symmetry without violating the other (Greenberg, 2002). This topic has been the subject of recent research and lively debates (Dolgov and Novikov, 2012; Tureanu, 2013; Kostelecký and Vargas, 2015).

Since weak interactions are not invariant under charge conjugation and also violate *CP*, a prudent question is whether violation of these symmetries may result in a difference of properties between particles and antiparticles. As it turns out, within the framework of conventional field theory, *CPT* invariance ensures the equality of masses and total lifetimes between particles and antiparticles (Lüders and Zumino, 1957) and the same is true for the magnitude of the magnetic moments (Bluhm, Kostelecký, and Russell, 1997).

Comparison of particle and antiparticle properties, therefore, provides tests of the *CPT* theorem and detection of any discrepancies will be an unambiguous signal of new physics, motivating such experiments which have seen significant progress in recent years. Tests of the *CPT* theorem were recently reviewed by Yamazaki and Ulmer (2013), Gabrielse *et al.* (2014), and Kellerbauer (2015). Here we present only a brief account of recent results and progress toward future *CPT* tests with antiprotons and antihydrogen.

The ALPHA experiment at CERN demonstrated trapping of antihydrogen ($\bar{\mathrm{H}}$) atoms for 1000 s in 2011 (Andresen *et al.*, 2011). With the goals of performing spectroscopy of the $1S - 2S$ and hyperfine transitions for a comparison with their values in hydrogen, the ALPHA team carried out a proof-of-principle experiment using resonant microwave radiation to

flip the spin of the positron in magnetically trapped antihydrogen atoms (Amole *et al.*, 2012). The spin flip caused trapped H̄ to be ejected from the trap and detected via annihilation. While this experiment was not aimed at precision frequency measurement, it bounded the resonance within 100 MHz of the hydrogen hyperfine frequency, corresponding to a relative precision of about 4×10^{-3} (Amole *et al.*, 2012). The ATRAP Collaboration reported accumulation of 4×10^9 electron-cooled positrons in a Penning trap for production and storage of antihydrogen atoms for future tests of *CPT* and antimatter gravity (Fitzakerley *et al.*, 2016).

In 2014, the ASACUSA experiment succeeded for the first time in producing a beam of antihydrogen atoms; detection of 80 antihydrogen atoms 2.7 m downstream of their production was reported (Kuroda *et al.*, 2014). This result represents a milestone toward precision measurements of the ground-state hyperfine splitting of antihydrogen using beam spectroscopy.

An experimental limit on the charge Qe of antihydrogen, in which e is the elementary charge, was reported by the ALPHA Collaboration (Amole *et al.*, 2014). In 2016, they further improved this bound to $|Q| < 0.71$ ppb (1 standard deviation) (Ahmadi *et al.*, 2016). Assuming charge superposition and using the best measured value of the antiproton charge (Patrignani *et al.*, 2016), this measurement placed a new limit on the positron charge anomaly, i.e., the relative difference between the positron and elementary charge, of about 1 ppb.

In December of 2016, ALPHA reported a long awaited breakthrough result (Ahmadi *et al.*, 2017a): they have further improved the efficiency of antihydrogen production (trapping about 14 antiatoms per trial), and employed two-photon laser excitation with 243 nm light to drive the $1S - 2S$ transition. The initial measurements of the transition frequency indicated that it is equal to its hydrogen counterpart at the level of 2×10^{-10} with further significant improvements anticipated in the near future. In 2017, the results of a microwave spectroscopy experiment which probed the response of antihydrogen over a controlled range of frequencies were reported (Ahmadi *et al.*, 2017b) providing a direct, magnetic-field-independent measurement of the hyperfine splitting of 1420.4 ± 0.5 MHz, consistent with expectations from atomic hydrogen at the level of 4 parts in 10^4.

The ATRAP Collaboration (DiSciacca *et al.*, 2013) measured the antiproton magnetic moment with a 4.4 parts per million (ppm) uncertainty with a single particle.

The baryon antibaryon symmetry experiment (BASE) aims at precise comparisons of the fundamental properties of antiprotons and protons for tests of *CPT* (Smorra *et al.*, 2015). The BASE Collaboration observed the first spin flips with a single trapped proton (Ulmer *et al.*, 2011) and performed a direct measurement of the magnetic moment of a single trapped proton with a precision of 3.3 ppb, which is the most precise measurement of g_p to date (Mooser *et al.*, 2014). Nagahama *et al.* (2017) measured the magnetic moment of a single trapped antiproton in a single Penning trap with a superimposed magnetic bottle achieving fractional precision at 0.8 ppm at the 95% confidence level improving the fractional precision by a factor of 6. To avoid the broadening of the resonance lines due to the magnetic bottle, a two-trap method was developed separating

the high-precision frequency measurements to a homogeneous precision trap. The spin-state analysis is performed in a trap with a superimposed magnetic inhomogeneity. Further extension of this method to an advanced cryogenic multi-Penning trap system enabled a ppb measurement of the antiproton magnetic moment (Smorra *et al.*, 2017). This experiment used a particle with an effective temperature of 300 K for magnetic field measurements and a cold particle at 0.12 K for spin transition spectroscopy. Smorra *et al.* (2017) improved the precision of the $\mu_{\bar{p}}$ measurement by a factor of ≈ 350, reporting the value $\mu_{\bar{p}} = 2.792\,847\,344\,1(42)\mu_N$ (at the 68% confidence level). A measurement of the proton magnetic moment at the 0.3 ppb level was reported by Schneider *et al.* (2017); the resulting value is in agreement with the currently accepted CODATA value (Mohr, Newell, and Taylor, 2016) but is an order of magnitude more precise. A comparison of the $\mu_{\bar{p}}$ with the new proton value $\mu_p = 2.792\,847\,344\,62(82)\mu_N$ constrains some *CPT*-violating effects.

The BASE Collaboration proposes to use quantum-logic technologies (Heinzen and Wineland, 1990; Dubielzig *et al.*, 2013) to trap and probe (anti)protons by coupling the (anti)proton to an atomic "qubit" ion trapped in its vicinity via Coulomb interaction. This coupling will be used both for ground-state cooling of single (anti)protons and for the state readout. Such sympathetically cooling the (anti)proton will reduce particle preparation times by more than 2 orders of magnitude, potentially enabling the proton and antiproton magnetic-moment measurements at the parts per trillion level (Schneider *et al.*, 2017).

The BASE Collaboration also performed a comparison of the charge-to-mass ratio for the antiproton $(q/m)_{\bar{p}}$ to that for the proton $(q/m)_p$ using high-precision cyclotron frequency comparisons of a single antiproton and a negatively charged hydrogen ion (H^-) carried out in a Penning-trap system (Ulmer *et al.*, 2015). This experiment established a limit

$$\frac{(q/m)_{\bar{p}}}{(q/m)_p} - 1 = 1(69) \times 10^{-12} \qquad (46)$$

and gave a bound on sidereal variations in the measured ratio of < 720 parts per trillion (Ulmer *et al.*, 2015).

Three-body metastable antiprotonic helium $\bar{p}He^+$ consists of an α particle, an electron, and an antiproton $\bar{p}$. When He captures a slow $\bar{p}$ in an atomic collision, $\bar{p}He^+$ is often formed in a high Rydberg state of $\bar{p}$ orbiting He^+. Such states are amenable to precision laser spectroscopy in order to determine the antiproton-to-electron mass ratio and to test the equality between the magnitudes of antiproton and proton charges and masses. Two-photon spectroscopy of $\bar{p}He^+$ performed by Hori *et al.* (2011) resulted in the determination of the antiproton-to-electron mass ratio $m_{\bar{p}}/m_e = 1836.152\,673\,6(23)$. Recently, Hori *et al.* (2016) employed buffer-gas cooling and performed single-photon spectroscopy of $\bar{p}He^+$. Combining the experimental results and the high-precision calculations of the relevant transition frequencies performed by Korobov (2014) and Korobov, Hilico, and Karr (2014a, 2014b, 2015) yielded a more precise value of $1836.152\,673\,4(15)$ (Hori *et al.*, 2016), which agrees with

the CODATA recommended value of $m_{\rm p}/m_{\rm e}$ at a level of 0.8 ppb. Laser spectroscopy of pionic helium atoms to determine the charged-pion mass was proposed by Hori, Sótér, and Korobov (2014).

The experimental efforts on matter-antimatter comparisons aimed at testing whether antimatter is affected by gravity in the same way as matter are described in Sec. X.D.

Because of the deep intrinsic connection between *CPT* and other symmetries such as Lorentz invariance, testing *CPT* does not always require antimatter (Pospelov and Romalis, 2004). A recent review of "magnetometry" experiments in this area was given by Jackson Kimball, Lamoreaux, and Chupp (2013); see also Sec. XI of this review.

VII. REVIEW OF LABORATORY SEARCHES FOR EXOTIC SPIN-DEPENDENT INTERACTIONS

A. Early work

Ever since the discovery of intrinsic spin [see the historical review by Commins (2012)], a central question in physics has been the role of spin in interactions between elementary particles. Leptons and quarks, the fundamental fermions, are spin-1/2 particles which in principle can possess only two possible multipole moments: monopole moments (such as mass and charge) and dipole moments (such as the magnetic moment). A particle's dipole moment is necessarily proportional to its spin based on the Wigner-Eckart theorem. In fact, the inception of the idea of spin was based on the observation of the anomalous Zeeman effect, a consequence of the interaction of the electron's magnetic dipole moment with an external magnetic field. It is natural to ask what other sorts of spin-dependent interactions might exist between fermions apart from the magnetic dipole interaction.

1. Torsion in gravity

There were a number of hypothetical dipole interactions postulated and searched for soon after the discovery of intrinsic spin. An early theoretical question was how to incorporate the concept of spin into the framework of general relativity. The fact that intrinsic spin possessed all the usual properties of angular momentum but yet could not be understood as arising from the physical rotation of an object posed a deep question for attempts to extend our understanding of gravity to the quantum level. There were indeed general relativistic interactions, such as frame dragging (Lense and Thirring, 1918; Thorne and Hartle, 1985), between macroscopic rotating bodies possessing angular momentum. But it was unclear if analogous effects would exist for particles with spin since general relativity, being a geometrical theory, did not directly include the possibility of intrinsic spin. At the macroscopic scale, mass energy adds up due to its monopole character and leads to observable gravitational effects. On the other hand, spin due to its dipole character tends to average out for astrophysical bodies such as stars and planets. Thus any gravitational effects related to spin would tend to be difficult to detect through astronomical observations, which are the principal vehicles for tests of general relativity to this day. Nonetheless, soon after the invention of general relativity by Einstein (1916), and even before the discovery of electron

spin, Cartan proposed an extension of general relativity that opened the possibility of incorporating spin through its effect on the torsion of spacetime (Cartan, 1922, 1923, 1924, 1925). Significant later work (Costa de Beauregard, 1942, 1964; Weyssenhoff and Raabe, 1947; Stueckelberg, 1948; Papapetrou, 1949; Weyl, 1950) strengthened the theoretical connection between intrinsic spin and spacetime torsion. Torsion quantifies the twisting of a coordinate system as it is transported along a curve. In Einstein's general relativity, mass energy generates curvature of spacetime but the torsion is zero, and so vectors curve along geodesics via parallel transport but do not twist. In Cartan's extension, spin generates nonzero torsion, and so frames transported along geodesics curve due to the effect of mass energy and twist due to the effect of spin [see, for example, the review by Hehl *et al.* (1976)]. The consequence is that gravitational dipole interactions are possible within the framework of Einstein-Cartan theory. From another point of view, assuming there is a way to parametrize gravity in terms of a quantum field theory, in addition to the spin-2 graviton (the hypothetical quantum of the gravitational field associated with Einstein's general relativity), there might exist spin-0 and spin-1 gravitons associated with the torsion field.

2. Electric dipole moments

In 1950, Purcell and Ramsey (1950) proposed another significant idea: elementary particles might possess a permanent EDM in addition to a magnetic dipole moment. As discussed in detail in Sec. V of this review, this hypothetical electric dipole coupling has stimulated intensive experimental and theoretical interest ever since.

3. Axions and axionlike particles (ALPs)

The previous ideas involved new dipole couplings to known fields: gravitational and electric. It was later realized that another possibility existed: there could be heretofore undiscovered fields generating dipole couplings between fermions. Among the earliest and most influential of these proposals was the suggestion that a light spin-0 boson, the axion (Weinberg, 1978; Wilczek, 1978; Kim, 1979; Shifman, Vainshtein, and Zakharov, 1980; Dine, Fischler, and Srednicki, 1981), could possess a coupling to dipoles that might be detectable in laboratory experiments (Moody and Wilczek, 1984). As Moody and Wilczek noted, a spin-0 field φ can couple to fermions in only two possible ways: through a scalar vertex or through a pseudoscalar vertex. In the nonrelativistic limit (small fermion velocity and momentum transfer), a fermion coupling to φ via a scalar vertex acts as a monopole and a fermion coupling to φ via a pseudoscalar vertex acts as a dipole. This can be understood from the fact that in the particle's center-of-mass frame there are only two vectors from which to form a scalar or pseudoscalar quantity: the spin **s** and the momentum **p** (since the field φ is a scalar), so either the vertex does not involve **s** (monopole coupling) or if it does, it depends on $\mathbf{s} \cdot \mathbf{p}$, which is a *P*-odd, pseudoscalar term. Hence it is the pseudoscalar coupling of φ that is the source of new dipole interactions.

The axion emerged from an elegant solution to the strong-*CP* problem (see Sec. V.C.4). The strong-*CP* problem is that

the observable *CP*-violating phase that can appear in the QCD Lagrangian $\bar{\theta}_{\text{QCD}}$ is known from EDM limits to be extremely small: $\bar{\theta}_{\text{QCD}} \lesssim 10^{-10}$. This presents a so-called fine-tuning problem, since naively one would expect $\bar{\theta}_{\text{QCD}} \approx 1$. The solution to the strong-*CP* problem proposed by Peccei and Quinn (1977a, 1977b) was that $\bar{\theta}_{\text{QCD}}$ does not possess a constant value, but rather evolves dynamically. In this model, $\bar{\theta}_{\text{QCD}}$ is replaced in the Lagrangian by a term representing a dynamical field, and the quantum of this field is known as the axion (or, more specifically, the QCD axion). The underlying physics of the Peccei-Quinn solution to the strong-*CP* problem is closely related to the physics behind the Higgs mechanism endowing particles with mass in the standard model: there exists a global continuous symmetry in QCD that is spontaneously broken, and a result of the spontaneous symmetry breaking is the appearance of a new "pseudo–Nambu-Goldstone" boson (in this case the axion). It turns out that the mass of the axion is very small (the upper limits on the axion mass based on astrophysical observations are $\lesssim 10$ meV) (Raffelt, 1999), thus producing long-range dipole forces that can be searched for in laboratory experiments (Moody and Wilczek, 1984). The idea of axions spurred theorists to consider other possibilities for light bosons that could mediate dipole interactions between fermions, such as familons (Wilczek, 1982; Gelmini, Nussinov, and Yanagida, 1983), majorons (Chikashige, Mohapatra, and Peccei, 1981; Gelmini and Roncadelli, 1981), arions (Ansel'm, 1982), and new spin-0 or spin-1 gravitons (Scherk, 1979; Neville, 1980, 1982; Carroll and Field, 1994). Familons are pseudo–Nambu-Goldstone bosons arising from spontaneous breaking of flavor symmetry; majorons were developed to understand neutrino masses and are constrained by searches for neutrinoless double-β decay, and arions are the bosons corresponding to a spontaneous breaking of the chiral lepton symmetry.

4. Early experiments

On the experimental front, early work searching for new dipole interactions focused on EDMs of neutrons, nuclei, and electrons (discussed in Sec. V of this review). Later, some attention turned to the role of spin in gravity. Morgan and Peres (1962) proposed a test of the equivalence principle for a spin-polarized body and Leitner and Okubo (1964) pointed out that a gravitational monopole-dipole interaction would violate *P* and *T* (time-reversal) symmetries. If a gravitational monopole-dipole interaction existed, the energy of a particle would depend upon the orientation of its spin relative to the local gravitational field of the Earth. Since no such dependence had been experimentally observed, Leitner and Okubo were able to derive corresponding constraints on monopole-dipole couplings based on the absence of gravitationally induced splitting of Zeeman sublevels in measurements of the ground-state hyperfine structure of hydrogen. A later experiment searching for such a gravitational dipole moment (GDM) of the proton by Velyukhov (1968) in fact found a nonzero value for the proton GDM, but this result was later proved erroneous by Vasil'ev (1969) and Young (1969). Wineland and Ramsey (1972) searched for a nuclear GDM with orders of magnitude greater sensitivity than previous

experiments by using a deuterium maser. Ramsey (1979) established the first precise constraints on exotic dipole-dipole interactions between protons by comparing the measured magnetic dipole interaction between protons in molecular hydrogen with theoretical calculations.

B. Theoretical motivation

Speculation concerning the possibility of a spin-gravity coupling manifesting as a GDM of elementary fermions (Kobzarev and Okun, 1962; Morgan and Peres, 1962; Leitner and Okubo, 1964; Hari Dass, 1976; Peres, 1978) or a torsion field (Neville, 1980) stood as a principal theoretical impetus encouraging experimental searches for exotic spin-dependent interactions for some time until the appearance of the idea of spin-dependent potentials generated by light spin-0 particles such as the axion (Moody and Wilczek, 1984) and arion (Ansel'm, 1982). The theoretical motivation to search for axions was significantly boosted when it was realized that axions could be the dark matter permeating the Universe [see, for example, Sec. IX and also the reviews by Raffelt (1999), Duffy and Bibber (2009), and Graham *et al.* (2015)].

More recently, the ideas underpinning the concept of the axion have been extended to a diverse array of problems opening new frontiers of research. The numerous light pseudoscalar bosons proposed to address a panoply of theoretical problems in modern physics are known collectively as axionlike particles.

1. Axionlike particles in string theory

ALPs generically arise in string theory as excitations of quantum fields that extend into compactified spacetime dimensions beyond the ordinary four (Bailin and Love, 1987; Svrcek and Witten, 2006). It was further proposed by Arvanitaki *et al.* (2010) that, in fact, because of the topological complexity of the extra-dimensional manifolds of string theory, if string theory is correct and there are indeed spacetime dimensions beyond the known four, there should be many ultralight ALPs, possibly populating each decade of mass down to the Hubble scale of 10^{-33} eV, a so-called axiverse.

2. The hierarchy problem

Another intriguing hypothesis where axions and ALPs appear is a novel proposed solution to the electroweak hierarchy problem (Graham, Kaplan, and Rajendran, 2015). The electroweak hierarchy problem is essentially the question of why the Higgs boson mass is so much lighter than the Planck mass, for one would expect that quantum corrections would cause the effective mass to be closer to the Planck scale. Phrased another way, it is surprising that the electroweak interaction should be so much stronger than gravity. Attempts to solve the hierarchy problem include, for example, supersymmetry (Dimopoulos and Georgi, 1981) and large (sub-mm) extra dimensions (Arkani-Hamed, Dimopoulos, and Dvali, 1998; Randall and Sundrum, 1999b). Graham, Kaplan, and Rajendran (2015) proposed that instead the hierarchy problem is solved by a dynamic relaxation of the effective Higgs mass from the Planck scale to the electroweak

scale in the early Universe that is driven by inflation and a coupling of the Higgs boson to a spin-0 particle dubbed the relaxion, which could be the QCD axion or an ALP. Inflation in the early Universe causes the relaxion field to evolve in time, and because of the coupling between the relaxion and the Higgs, the effective Higgs mass evolves as well. The coupling between the relaxion and the Higgs generates a periodic potential for the relaxion once the Higgs' vacuum expectation value becomes nonzero. When the periodic potential barriers become large enough, the evolution of the relaxion stalls and the effective mass of the Higgs settles at its observed value. A key idea of this scenario is that the electroweak symmetry breaking scale is a special point in the evolution of the Higgs mass, and that is why the Higgs mass eventually settles at the observed value relatively close to the electroweak scale and far from the Planck scale.

3. Dark energy

A further theoretical motivation for ALPs comes from attempts to explain the observed accelerating expansion of the Universe, attributed to a so-called dark energy permeating the Universe (Peebles and Ratra, 2003). Arkani-Hamed *et al.* (2004) proposed an infrared (i.e., at very low-energy scales corresponding to the large distances over which the accelerating expansion of the Universe is observed) modification of gravity that posits dark energy is a ghost condensate, a constant-velocity scalar field permeating the Universe. The ghost condensate acts as a fluid filling the Universe which turns out to behave identically to a cosmological constant by possessing a negative kinetic energy term and thus matches astrophysical observations. The direct coupling of the ghost condensate to matter leads to both apparent Lorentz-violating effects and new long-range spin-dependent interactions (Arkani-Hamed *et al.*, 2004, 2005). Along these same lines, Flambaum, Lambert, and Pospelov (2009) pointed out that if dark energy is a cosmological scalar or pseudoscalar field (which could be considered to be a spin-0 component of gravity) there would be a spin-gravity coupling. This implies that fermions would possess GDMs (as discussed in Sec. VII.A.4), and also predicts spatial and temporal variations of particle masses and couplings.

In general, it should be noted that most other such theories proposing that cosmic acceleration is due to the dynamical evolution of a scalar field (termed quintessence), by virtue of possessing a conventional kinetic energy term, require a certain level of fine-tuning at least at the level of invoking a nonzero cosmological constant; see, for example, the review by Joyce *et al.* (2015). For example, in many quintessence models there must exist a screening mechanism of some kind in order to avoid existing astrophysical and laboratory constraints from tests of gravity (see also Sec. VIII).

4. Unparticles

Yet another theoretical idea that motivates searches for spin-dependent interactions is the unparticle (Georgi, 2007). It is possible in the context of quantum field theory that interactions may be scale invariant (Wilson, 1970; Banks and Zaks, 1982). A scale-invariant interaction's strength is independent of the energy of the interacting particles. This is not the case

for standard model fields: in quantum electrodynamics, for example, the strength of the electromagnetic interaction is energy dependent because of the appearance of virtual particles (i.e., higher-order processes). In fact, unlike standard model fields, quantum excitations of scale-invariant interactions cannot be described in terms of particles (such as the photon): rather they are objects known as unparticles that are unconstrained by any dispersion relation and without definite mass. The coupling of unparticles to fermions results in long-range spin-spin interactions that depend on a nonintegral power of distance between the fermions (Liao and Liu, 2007) that can be searched for in laboratory experiments.

5. Paraphotons, dark photons, hidden photons, and new Z' bosons

An entirely different source of new spin-dependent interactions is exotic spin-1 bosons. There are 12 known gauge bosons in the standard model: the photon, the $W^{\pm}$ and Z bosons, and the eight gluons. Generally speaking, a massless spin-1 boson accompanies any new unbroken $U(1)$ gauge symmetry [such symmetries arise quite naturally, for example, in string theory (Cvetic and Langacker, 1996) and other standard model extensions; $U(1)$ refers to the unitary group of degree 1, the collection of all complex numbers with absolute value 1 under multiplication]. Massless spin-1 bosons are referred to as paraphotons γ' (Holdom, 1986) in analogy with photons, the quanta arising from the $U(1)$ gauge symmetry of electromagnetism. If paraphotons couple directly to standard model particles, in order to generate fermion masses and avoid gauge anomalies (quantum corrections that break the gauge symmetry and lead to theoretical inconsistencies), the gauge symmetry corresponding to the paraphoton must be $U(1)_{B-L}$ (Appelquist, Dobrescu, and Hopper, 2003), where $B-L$ refers to the difference between the baryon (B) and the lepton (L) number: in other words, the "charge" of standard model particles with respect to γ' is given by $B-L$ (so, for example, a proton has $B-L=1$ and an electron has $B-L=-1$). However, if the paraphoton coupling to standard model particles is indirect, i.e., through higher-order processes [so that all standard model particles have zero charge under the new $U(1)$ symmetry], this restriction on the possible charge is removed and the coupling of quarks and leptons to γ' can take on a range of possible values (Dobrescu, 2005). Such couplings generate long-range spin-dependent interactions (Dobrescu and Mocioiu, 2006). A closely related hypothesis is that of the dark photon, which would communicate a "dark" electromagnetic interaction between dark matter particles and could be detectable via mixing with photons (Ackerman *et al.*, 2009). Of course, it is also possible that exotic spin-1 bosons possess nonzero mass, as does the Z boson in the standard model. A nonzero mass for such a hypothetical Z' boson could arise from the breaking of a new $U(1)$ gauge symmetry. There is a plethora of theoretical models predicting new Z' bosons and theoretically motivated masses and couplings to quarks and leptons extend over a broad range [see, for example, the review by Langacker (2009)]. Z' bosons that do not directly interact with standard model particles (and therefore reside in the so-called hidden sector) are commonly referred to as hidden photons (Holdom, 1986).

Hidden photons have some particularly notable features that deserve extra attention. As opposed to generic Z' bosons and some classes of dark photons, the only coupling of hidden photons to standard model fermions is through their mixing into a "real" electromagnetic field. The Lagrangian describing the hidden photon is of the form

$$\mathcal{L} = J^\mu(A_\mu + \kappa X_\mu) + m_{\gamma'}^2 X^2, \qquad (47)$$

where J is the electromagnetic current, A represents the photon field, X represents the hidden-photon field, κ is the mixing parameter, and $m_{\gamma'}$ is the hidden-photon mass. Notice that in the limit where $m_{\gamma'} \to 0$, there is no difference between the photon field and the hidden-photon field. In the $m_{\gamma'} = 0$ limit, one can redefine a linear combination $\mathcal{A} = A + \kappa X$ which couples to electromagnetic current J and a sterile component $\mathcal{X} = X - \kappa A$ which does not interact at all electromagnetically. Essentially this means that all direct hidden-photon interactions are suppressed by powers of $m_{\gamma'}^2$ in the small mass limit. This argument reduces or eliminates many astrophysical bounds on hidden photons (Pospelov, Ritz, and Voloshin, 2008). The nonrelativistic Hamiltonian for the spin-dependent hidden-photon interaction is

$$H_{\gamma'} = \hbar g \mu_B \kappa \mathcal{B}' \cdot \hat{\boldsymbol{\sigma}}, \qquad (48)$$

which describes the interaction of spins $\hat{\boldsymbol{\sigma}}$ with a real magnetic field $\mathcal{B} = \kappa \mathcal{B}'$ always present wherever there is a hidden field $\mathcal{B}'$, g is the Landé factor, and μ_B is the Bohr (or, if relevant, nuclear) magneton. Here the spin coupling occurs via the usual magnetic dipole interaction through the part of $\mathcal{B}'$ that is mixed into a real magnetic field. This means that observable effects of a hidden photon are suppressed within a shielded region (Chaudhuri *et al.*, 2015; Dubovsky and Hernández-Chifflet, 2015): although the hidden-photon field is not blocked by the shield, it does affect charges and spins in the shield via the action of the real magnetic field $\mathcal{B} = \kappa \mathcal{B}'$. The effect of $\mathcal{B}$ in turn generates a "compensating" field $\mathcal{B}_{\text{comp}} \approx -\mathcal{B}$ within the shielded region, canceling the observable effects of the hidden-photon field (Chaudhuri *et al.*, 2015; Jackson Kimball *et al.*, 2016). This shielding suppression is on top of the small mixing parameter κ.

6. Conclusions

Even this brief survey portrays a compelling case for experimental searches for exotic spin-dependent interactions. Such interactions are a ubiquitous feature of theoretical extensions to the standard model and general relativity, and furthermore are intimately connected to the mysteries of dark energy, dark matter, the strong-*CP* problem, and even the hierarchy problem and grand unification.

C. Parametrization

1. Introduction

Considering the vast theoretical jungle filled with hypothetical new particles (and even unparticles) possessing unknown properties outlined in Sec. VII.B, one may ask:

"How are we to systematically search for their effect on atomic systems and quantify their existence or lack thereof?" To set up a general system enabling comparison between different experiments that search for the effects of such new particles and fields, let us consider the related question: if a heretofore undiscovered spin-dependent force exists, how might it affect atoms and their constituents: electrons, protons, and neutrons? It turns out that based on rather general principles, a framework to describe all possible types of interactions between electrons, protons, and neutrons can be quantified by "exotic physics coupling constants" for a range of length scales. Thus experimental goals are clarified: an experiment searches for an exotic interaction and if nothing is found, a limit or constraint is established for coupling constants at the studied length scale for particular forms of interactions. Experimentalists seek to explore regions of parameter space that have not been previously studied to determine if as-yet-undiscovered physics exists with such properties. Then particle theorists can interpret the experimental results in terms of possible new bosons and derive limits on theories introduced in Sec. VII.B.

2. Moody-Wilczek-Dobrescu-Mocioiu formalism

Generally speaking, the most commonly employed framework for the purpose of comparing different experimental searches for exotic spin-dependent interactions is that introduced by Moody and Wilczek (1984) to describe long-range spin-dependent potentials associated with the axion and extended by Dobrescu and Mocioiu (2006) to encompass long-range potentials associated with any generic spin-0 or spin-1 boson exchange; here we denote this framework the Moody-Wilczek-Dobrescu-Mocioiu (MWDM) formalism. Given basic assumptions within the context of quantum field theory (e.g., rotational invariance, energy-momentum conservation, locality), interactions mediated by new bosons can generate 16 independent, long-range potentials between fermions. Most laboratory experiments search for interactions between electrons (e) and nucleons [either protons (p) or neutrons (n)]. In general, because of their different quark content, the couplings of protons and neutrons may be expected to differ [for example, in one of the most widely studied models of the QCD axion, the so-called Kim-Shifman-Vainshtein-Zakharov (KSVZ) model (Kim, 1979; Shifman, Vainshtein, and Zakharov, 1980), the axion coupling to the proton is $\gtrsim 30$ times stronger than that of the neutron (Raffelt, 1999)]. Thus there are six fermion pairs (ee, ep, en, pp, nn, and np) that can couple with 16 different potentials. The potentials are ascribed dimensionless scalar coupling constants f_i^{XY} between different fermions (which in general are momentum dependent, but can be approximated as momentum independent in the nonrelativistic limit). Here XY denotes the possible fermion pairs: $X, Y = e, n, p$ and $i = 1, 2, \ldots, 16$ labels the corresponding potential. The potentials can be written in terms of a dimensionless r-dependent function $y(r)$ that is determined by the exact nature of the propagator describing the exotic boson exchange. Dobrescu and Mocioiu (2006) originally derived the potentials in the so-called "mixed representation" of position **r** and velocity **v** of fermion X, which is useful for analysis of laboratory-scale experiments

where **r** and **v** can be treated as classical variables. However, as noted by Ficek *et al.* (2017), for calculations at the atomic scale it is useful to derive the potentials in position representation, keeping in mind that the momentum **p** should be treated as an operator; this derivation has been recently carried out in detail for all MWDM potentials by Fadeev *et al.* (2018). The potentials enumerated 1–8 by Dobrescu and Mocioiu (2006) encompass all possible *P*-even (scalar) rotational invariants and can be written in the nonrelativistic limit (small fermion velocity and low momentum transfer) as follows:

$$\mathcal{V}_1 = f_1^{XY} \hbar c \frac{y(r)}{r}, \tag{49}$$

$$\mathcal{V}_2 = f_2^{XY} \hbar c (\hat{\boldsymbol{\sigma}}_X \cdot \hat{\boldsymbol{\sigma}}_Y) \frac{y(r)}{r}, \tag{50}$$

$$\mathcal{V}_3 = f_3^{XY} \frac{\hbar^3}{m^2 c} \left[\hat{\boldsymbol{\sigma}}_X \cdot \hat{\boldsymbol{\sigma}}_Y \left(\frac{1}{r^3} - \frac{1}{r^2} \frac{d}{dr} \right) \right. $$
$$\left. - 3(\hat{\boldsymbol{\sigma}}_X \cdot \hat{\mathbf{r}})(\hat{\boldsymbol{\sigma}}_Y \cdot \hat{\mathbf{r}}) \left(\frac{1}{r^3} - \frac{1}{r^2} \frac{d}{dr} + \frac{1}{3r} \frac{d^2}{dr^2} \right) \right] y(r), \tag{51}$$

$$\mathcal{V}_{4+5} = -f_{4+5}^{XY} \frac{\hbar^2}{2m^2 c} \hat{\boldsymbol{\sigma}}_X \cdot \left\{ (\mathbf{p} \times \hat{\mathbf{r}}), \left(\frac{1}{r^2} - \frac{1}{r} \frac{d}{dr} \right) y(r) \right\}, \tag{52}$$

$$\mathcal{V}_{6+7} = -f_{6+7}^{XY} \frac{\hbar^2}{2m^2 c} \left\{ (\hat{\boldsymbol{\sigma}}_X \cdot \mathbf{p}), (\hat{\boldsymbol{\sigma}}_Y \cdot \hat{\mathbf{r}}) \left(\frac{1}{r^2} - \frac{1}{r} \frac{d}{dr} \right) y(r) \right\}, \tag{53}$$

$$\mathcal{V}_8 = f_8^{XY} \frac{\hbar}{4m^2 c} \left\{ (\hat{\boldsymbol{\sigma}}_X \cdot \mathbf{p}), \left\{ (\hat{\boldsymbol{\sigma}}_Y \cdot \mathbf{p}), \frac{y(r)}{r} \right\} \right\}, \tag{54}$$

and those enumerated 9–16 encompass all possible *P*-odd (pseudoscalar) rotational invariants, given in the nonrelativistic limit by

$$\mathcal{V}_{9+10} = -f_{9+10}^{XY} \frac{\hbar^2}{m} \hat{\boldsymbol{\sigma}}_X \cdot \hat{\mathbf{r}} \left(\frac{1}{r^2} - \frac{1}{r} \frac{d}{dr} \right) y(r), \tag{55}$$

$$\mathcal{V}_{11} = -f_{11}^{XY} \frac{\hbar^2}{m} (\hat{\boldsymbol{\sigma}}_X \times \hat{\boldsymbol{\sigma}}_Y) \cdot \hat{\mathbf{r}} \left(\frac{1}{r^2} - \frac{1}{r} \frac{d}{dr} \right) y(r), \tag{56}$$

$$\mathcal{V}_{12+13} = f_{12+13}^{XY} \frac{\hbar}{2m} \hat{\boldsymbol{\sigma}}_X \cdot \left\{ \mathbf{p}, \frac{y(r)}{r} \right\}, \tag{57}$$

$$\mathcal{V}_{15} = f_{15}^{XY} \frac{3\hbar^3}{2m^3 c^2} \left\{ (\hat{\boldsymbol{\sigma}}_X \cdot \hat{\mathbf{r}})[(\hat{\boldsymbol{\sigma}}_Y \times \hat{\mathbf{r}}) \cdot \mathbf{p}], \left(\frac{1}{r^3} - \frac{1}{r^2} \frac{d}{dr} + \frac{1}{3r} \frac{d^2}{dr^2} \right) y(r) \right\} + f_{15}^{XY} \frac{3\hbar^3}{2m^3 c^2} \left\{ (\hat{\boldsymbol{\sigma}}_Y \cdot \hat{\mathbf{r}})[(\hat{\boldsymbol{\sigma}}_X \times \hat{\mathbf{r}}) \cdot \mathbf{p}], \left(\frac{1}{r^3} - \frac{1}{r^2} \frac{d}{dr} + \frac{1}{3r} \frac{d^2}{dr^2} \right) y(r) \right\}, \tag{58}$$

$$\mathcal{V}_{16} = -f_{16}^{XY} \frac{\hbar^2}{8m^3 c^2} \left\{ \hat{\boldsymbol{\sigma}}_Y \cdot \mathbf{p}, \left\{ \hat{\boldsymbol{\sigma}}_X \cdot (\mathbf{p} \times \hat{\mathbf{r}}), \left(\frac{1}{r^2} - \frac{1}{r} \frac{d}{dr} \right) y(r) \right\} \right\} - f_{16}^{XY} \frac{\hbar^2}{8m^3 c^2} \left\{ \hat{\boldsymbol{\sigma}}_X \cdot \mathbf{p}, \left\{ \hat{\boldsymbol{\sigma}}_Y \cdot (\mathbf{p} \times \hat{\mathbf{r}}), \left(\frac{1}{r^2} - \frac{1}{r} \frac{d}{dr} \right) y(r) \right\} \right\}. \tag{59}$$

In Eqs. (49)–(59), $\hbar$ is Planck's constant, c is the speed of light, m is the mass of fermion X, r is the distance between the fermions and $\hat{\mathbf{r}}$ is the unit vector along the line between them, $\hat{\boldsymbol{\sigma}}_i$ is a unit vector in the direction of the spin of fermion i, **p** is the momentum of particle X, and $\{\Box, \Box\}$ denotes the anticommutator. Where sums appear in the potential indices there is dependence on $\hat{\boldsymbol{\sigma}}_X$, the differences of the respective potentials depend on $\hat{\boldsymbol{\sigma}}_Y$. The potential $\mathcal{V}_{14}$ (not listed), proportional to $(\hat{\boldsymbol{\sigma}}_X \times \hat{\boldsymbol{\sigma}}_Y) \cdot \mathbf{p}$, turns out to vanish in the nonrelativistic limit (Fadeev *et al.*, 2018). It is interesting to note that the MWDM formalism applies whether or not the underlying theory obeys Lorentz invariance (so long as rotational invariance is preserved) and also applies in the case of multiboson exchange between the fermions in question. Thus the MWDM formalism is quite general in nature and serves as a useful framework for comparing different experiments.

3. MWDM formalism for Lorentz-invariant, single-boson exchange

A specific form can be obtained for $y(r)$ if some assumptions are made about the propagator. Assuming one-boson exchange within a Lorentz-invariant quantum field theory, $y(r)$ takes on a Yukawa-like form:

$$y(r) = \frac{1}{4\pi} e^{-r/\lambda}, \tag{60}$$

where

$$\lambda = \hbar/Mc \tag{61}$$

is the reduced Compton wavelength of the new boson of mass M, which sets the scale of the new interaction. If there is multiboson exchange or Lorentz invariance is violated, other forms of $y(r)$ can arise, but the spin dependence of the potential functions is preserved. Generally an experimental setup characterized by a distance scale ℓ is sensitive to new bosons of mass $M \lesssim \hbar/(c\ell)$. [Note that the derivative operators with respect to r are understood to act only on $y(r)$ and not on wave functions.]

If particular spin and parity properties of the new boson are specified, correlations between the coupling strengths are found. For example, if the new boson is a spin-0 particle such as an axion or ALP, $f_3^{XY} = -g_p^X g_p^Y/(4\hbar c)$, where $g_p^{X,Y}$

parametrizes the vertex-level pseudoscalar coupling (denoted by the subscript p) of the spin-0 field to the fermions. The quantity $g_p^2/(\hbar c)$ is dimensionless. Under these assumptions, for example, the dipole-dipole potential of Eq. (51) can be written in the form most commonly encountered in the literature,

$$\mathcal{V}_3(r) = -\frac{g_p^X g_p^Y \hbar^2}{16\pi m^2 c^2} \left[\hat{\boldsymbol{\sigma}}_X \cdot \hat{\boldsymbol{\sigma}}_Y \left(\frac{1}{\lambda r^2} + \frac{1}{r^3} \right) \right. \\ \left. - (\hat{\boldsymbol{\sigma}}_X \cdot \hat{\mathbf{r}})(\hat{\boldsymbol{\sigma}}_Y \cdot \hat{\mathbf{r}}) \left(\frac{1}{\lambda^2 r} + \frac{3}{\lambda r^2} + \frac{3}{r^3} \right) \right] e^{-r/\lambda}. \quad (62)$$

If the new interaction possesses both scalar and pseudoscalar couplings, for example, $f_{9+10}^{XY} = g_p^X g_s^Y/\hbar c$ (where the subscript s denotes the scalar coupling), one obtains the following monopole-dipole potential for coupling of polarized fermions X to a monopole source of fermions Y:

$$\mathcal{V}_{9+10}(r) = -\frac{g_p^X g_s^Y \hbar}{4\pi mc} \hat{\boldsymbol{\sigma}}_X \cdot \hat{\mathbf{r}} \left(\frac{1}{r\lambda} + \frac{1}{r^2} \right) e^{-r/\lambda}. \quad (63)$$

Monopole-dipole and dipole-dipole potentials, and indeed the vast majority of the potentials enumerated in Eqs. (49)–(59), can also be generated by the exchange of spin-1 particles, such as a Z' boson (Dobrescu and Mocioiu, 2006; Gomes Ferreiraa *et al.*, 2015). For example, if the new boson is a massive spin-1 boson, $f_3^{XY} = [(1 + m^2/m_Y^2)g_A^X g_A^Y + (2m/m_Y)g_V^X g_V^Y]/(8\hbar c)$, where m_Y is the mass of fermion Y and the subscripts A and V refer to the axial-vector and vector couplings, respectively. An axial-vector coupling also generates the dipole-dipole potential

$$\mathcal{V}_2(r) = -\frac{g_A^X g_A^Y}{4\pi\hbar c} \frac{\hbar c}{r} \hat{\boldsymbol{\sigma}}_X \cdot \hat{\boldsymbol{\sigma}}_Y e^{-r/\lambda}, \quad (64)$$

which has a different scaling with particle separation as compared to the $\mathcal{V}_3(r)$ potential described by Eq. (62). A complete enumeration of the coefficients f_i^{XY} in terms of vertex-level couplings is given by Fadeev *et al.* (2018).

The relative signs of the potentials have recently been analyzed by Daido and Takahashi (2017) and some corrections to the work of Moody and Wilczek (1984) have been noted and incorporated into, for example, Eq. (62). Although these sign errors have to some extent propagated throughout the literature, they do not affect existing constraints since experiments limit the absolute value of the coupling constants.

4. Contact interactions

Another detail to be aware of is that the potentials described in Eqs. (49)–(59) are long-range potentials that assume the fermions under investigation are separated by a finite distance. In searches for exotic spin-dependent interactions in atoms and molecules one must also take into account the possibility of wave function overlap and the contribution of terms in the potentials proportional to Dirac delta functions $\delta^3(\mathbf{r})$. For example, the term

$$-\frac{g_p^X g_p^Y \hbar^2}{12 m_X m_Y c^2} \hat{\boldsymbol{\sigma}}_X \cdot \hat{\boldsymbol{\sigma}}_Y \delta^3(\mathbf{r}) \quad (65)$$

must be added to the expression for the dipole-dipole interaction generated by an ALP given in Eq. (62). Additional contact terms appear in the potentials when higher-order terms in the particles' momenta are included; see Fadeev *et al.* (2018).

Of related interest is the fact that the Higgs boson (Aad *et al.*, 2012; Chatrchyan *et al.*, 2012), a spin-0 particle, is predicted to induce a Yukawa-like interaction between fermions (Haber, Kane, and Sterling, 1979), leading to a delta-function-like potential which could be searched for in precision atomic physics experiments (Delaunay *et al.*, 2016, 2017; Berengut *et al.*, 2018). The Higgs interaction can even produce a P-odd, T-odd electron-nucleon interaction generating EDMs of atoms and molecules (Barr, 1992a, 1992b). Because the mass of the Higgs boson is ≈ 125 GeV, the range of any force mediated by the Higgs is $\approx 10^{-17}$ m (the Higgs Compton wavelength), and thus meaningful constraints on Higgs-mediated interactions have not yet been experimentally obtained.

A closely related point is that measurements of permanent EDMs, discussed in Sec. V, also constrain some exotic spin-dependent forces. This is because a P- and a T-violating interaction between particles will naturally induce a P- and a T-violating atomic EDM, and indeed a number of the potentials $\mathcal{V}_i$ violate P and T symmetries [$\mathcal{V}_{9+10}$, $\mathcal{V}_{14}$, and $\mathcal{V}_{15}$; see Eqs. (55) and (58)]. Gharibnejad and Derevianko (2015) reinterpreted the results of the Hg EDM experiment (Griffith *et al.*, 2009) to constrain a P, T-odd interaction of electrons and nucleons through the exchange of a massive gauge boson and have excluded vector bosons with masses $\gtrsim 1$ MeV with coupling strengths $\gtrsim 10^{-9}$. Stadnik, Dzuba, and Flambaum (2018) analyzed constraints from EDM experiments on spin-0-boson-mediated interactions.

5. Position representation and permutation symmetry

As noted in Sec. VII.C.2, in atomic and molecular calculations for velocity-dependent potentials, it is often useful to convert the momentum $\mathbf{p}$ into the relevant operator in position space. Furthermore, for identical particles care must be taken to account for permutation symmetry. For example, the $\mathcal{V}_8$ potential [Eq. (54)], which can arise from the exchange of axial-vector bosons, can be written for identical particles 1 and 2 as

$$\mathcal{V}_8(r) = \frac{g_A g_A}{4\pi\hbar c} \frac{\hbar^3}{4m^2 c} \left\{ \hat{\boldsymbol{\sigma}}_1 \cdot (\nabla_1 - \nabla_2), \left\{ \hat{\boldsymbol{\sigma}}_2 \cdot (\nabla_1 - \nabla_2), \frac{e^{-r/\lambda}}{r} \right\} \right\}, \quad (66)$$

where ∇_i is the vector differential operator in position space for particle i in the center-of-mass frame. Details concerning this point are addressed by Ficek *et al.* (2017).

6. Quantum field theory details

In order to check whether different experiments are truly measuring the same quantity, it can sometimes be important to

consider further specifics regarding the origin of a spin-dependent coupling within quantum field theory. For example, an ALP field φ can generate the potential $\mathcal{V}_3(r)$ described by Eq. (62) between fermions ψ of mass m in two different ways: either through a Yukawa-like coupling described by the Lagrangian (Moody and Wilczek, 1984; Vasilakis *et al.*, 2009)

$$\mathcal{L}_{\text{Yuk}} = -i\text{g}_p \bar{\psi}\gamma^5\psi\varphi \qquad (67)$$

or through a derivative coupling described by the Lagrangian

$$\mathcal{L}_{\text{Der}} = \frac{\text{g}_p}{2m} \bar{\psi}\gamma_\mu\gamma^5\psi\partial^\mu\varphi, \qquad (68)$$

where in Eqs. (67) and (68) we used the Dirac γ matrices. Although experimental searches for dipole-dipole interactions are sensitive to both Yukawa-like and derivative couplings, various searches for spin-independent interactions and some astrophysical phenomena are sensitive only to one or the other type of coupling (Raffelt and Weiss, 1995; Fischbach and Krause, 1999; Raffelt, 2012). Similarly, Mantry, Pitschmann, and Ramsey-Musolf (2014) showed that by delving deeper into the quantum field theoretic origins of exotic spin-dependent interactions one can distinguish the effects of the QCD axion from generic ALPs by comparing the results of nuclear EDM searches with results of searches for new spin-dependent forces [see also the analysis of Gharibnejad and Derevianko (2015)]. It is also important to note that QCD axion models (Kim, 1979; Shifman, Vainshtein, and Zakharov, 1980; Zhitnitskii, 1980; Dine, Fischler, and Srednicki, 1981) have a definite relationship between the interaction strength and the axion mass, whereas for a generic ALP the mass and the interaction strength are independent parameters.

7. Connection between the MWDM formalism and various fundamental theories

In most cases there is a clear one-to-one correspondence between potentials in the MWDM formalism and the fundamental theories predicting exotic spin-dependent interactions outlined in Sec. VII.B, although there are exceptions such as the predicted potentials generated by unparticles (Sec. VII.B.4).

Consider, for example, the standard QCD axion discussed in Sec. VII.A.3. An axion (or ALP) is characterized by a symmetry breaking scale f_a and an interaction scale Λ, which in the case of the QCD axion is the QCD confinement scale $\Lambda \approx 200$ MeV (ALPs may have different values for Λ). These scales determine, for example, the mass of the axion

$$m_a c^2 = \Lambda^2 / f_a. \qquad (69)$$

The interaction of an axion with a fermion X is determined by a dimensionless coupling constant C_X which can be predicted in the context of a specific theory and related to the coupling constants in the MWDM formalism. For instance, the pseudoscalar coupling

$$\text{g}_p^X / \sqrt{\hbar c} = C_X m c^2 / f_a. \qquad (70)$$

For a particular manifestation of the QCD axion referred to as the KSVZ axion (Kim, 1979; Shifman, Vainshtein, and Zakharov, 1980), $C_p \approx -0.34$ for the proton, $C_n \approx 0.01$ for the neutron, and $C_e = 0$ for the electron (Raffelt, 1999). Note that in this specific theoretical model a single parameter, the symmetry breaking scale f_a, determines both the axion mass and the coupling strength to particular fermions. This formalism connects searches for exotic spin-dependent interactions to the broader context of QCD axion searches: most QCD axion searches exploit the axion-photon coupling, also proportional to $1/f_a$, but with a different coupling constant. For example, the Axion Dark Matter Experiment (ADMX) (Asztalos *et al.*, 2010) searches for axions converted into detectable microwave photons using the inverse Primakoff effect as first outlined by Sikivie (1983). Since experiments such as ADMX probe a different coupling and generally speaking a different axion mass range as compared to searches for spin-dependent interactions, these experimental approaches are largely complementary [see Sec. IX and also the reviews by Kim and Carosi (2010) and Graham *et al.* (2015)].

As another example, a standard propagating gravitational torsion field (see Sec. VII.A.1) can generate a dipole-dipole interaction identical to the $\mathcal{V}_3$ potential in the MWDM formalism (Neville, 1980, 1982; Hammond, 1995; Adelberger *et al.*, 2009) with the relationship

$$\frac{\text{g}_p \text{g}_p}{\hbar c} = \beta^2 \frac{18\pi G m^2}{\hbar c}, \qquad (71)$$

where G is Newton's gravitational constant and the minimal torsion model predicts the torsion constant $\beta = 1$.

In general, there is similar one-to-one correspondence between the MWDM formalism and any model based on a quantum field theory with new force-carrying spin-0 and spin-1 bosons.

8. Relationship between coupling constants for atoms and elementary particles

Furthermore, theoretical knowledge of atomic, molecular, and nuclear structures is critical for interpretation of experiments. In order to meaningfully compare experimental results, the coupling of the exotic field to the atomic spin must be interpreted in terms of the coupling to electron, proton, and neutron spins. The basic scheme of such a parametrization of spin couplings to new physics can be cast in terms of an exotic atomic dipole moment $\boldsymbol{\chi} = \chi_a \mathbf{F}$ related to coupling constants χ_e, χ_p, and χ_n for the electron, proton, and neutron, respectively, where $\mathbf{F}$ is the total atomic angular momentum. It is generally assumed that such couplings do not follow the same scaling as magnetic moments. The coupling constants f_i^{XY} describing the potentials enumerated in Eqs. (49)–(59) can then be written in terms of χ_e, χ_p, and χ_n depending on the specific experiment, where for each different potential $\mathcal{V}_i(r)$ the constants χ_e, χ_p, and χ_n may be different. The nucleon coupling constants χ_p and χ_n can in turn be related to quark and gluon couplings via measurements and calculations based on QCD (Flambaum *et al.*, 2004; Aidala *et al.*, 2013).

It is generally assumed by most theories postulating new interactions (Arkani-Hamed *et al.*, 2005; Dobrescu and

Mocioiu, 2006; Moody and Wilczek, 1984; Georgi, 2007; Liao and Liu, 2007; Flambaum, Lambert, and Pospelov, 2009; Graham and Rajendran, 2013) that there is no coupling of the exotic field to orbital angular momentum $\mathbf{L}$. In the context of quantum field theory, this theoretical bias can be understood as follows. If an exotic field couples to $\mathbf{L}$ then the field couples to particle current. However, the lowest-order coupling to particle current vanishes if the exotic interaction is mediated by a spin-0 particle such as an ALP (Dobrescu and Mocioiu, 2006). On the other hand, a coupling of a generic massive spin-1 boson to particle current is forbidden by gauge invariance (Dobrescu, 2005), and constraints on couplings of massless spin-1 bosons are already quite stringent (Appelquist, Dobrescu, and Hopper, 2003). Thus, generally, couplings of exotic fields to particle current, and thus $\mathbf{L}$, are expected to be suppressed relative to spin couplings. Nonetheless, it should also be noted that there are theories that do postulate exotic couplings to $\mathbf{L}$. For example, hidden photons can mix with ordinary photons and thus can produce real magnetic fields in magnetically shielded regions that would indeed couple to $\mathbf{L}$ (Chaudhuri *et al.*, 2015).

The relationship of the expectation value for total atomic angular momentum $\langle \mathbf{F} \rangle$ to electron spin $\langle \mathbf{S} \rangle$ and nuclear spin $\langle \mathbf{I} \rangle$ can be evaluated for the ground states of most low-to-intermediate mass atoms based on the Russell-Saunders LS-coupling scheme (Budker, Kimball, and DeMille, 2008):

$$\langle \mathbf{F} \rangle = \langle \mathbf{S} \rangle + \langle \mathbf{L} \rangle + \langle \mathbf{I} \rangle,$$
$$= \frac{\langle \mathbf{S} \cdot \mathbf{F} \rangle}{F(F+1)} \langle \mathbf{F} \rangle + \frac{\langle \mathbf{L} \cdot \mathbf{F} \rangle}{F(F+1)} \langle \mathbf{F} \rangle + \frac{\langle \mathbf{I} \cdot \mathbf{F} \rangle}{F(F+1)} \langle \mathbf{F} \rangle, \quad (72)$$

where $\mathbf{L}$ is the orbital angular momentum. It follows that for the exotic atomic dipole moment coupling constant χ_a,

$$\chi_a = \chi_e \frac{\langle \mathbf{S} \cdot \mathbf{F} \rangle}{F(F+1)} + \chi_N \frac{\langle \mathbf{I} \cdot \mathbf{F} \rangle}{F(F+1)}, \quad (73)$$

where χ_N is the exotic nuclear dipole coupling constant which can be expressed in terms of χ_p and χ_n.

The projection of $\mathbf{S}$ on $\mathbf{F}$ can be calculated in terms of eigenvalues of the system according to

$$\langle \mathbf{S} \cdot \mathbf{F} \rangle = \frac{\langle \mathbf{S} \cdot \mathbf{J} \rangle}{J(J+1)} \langle \mathbf{J} \cdot \mathbf{F} \rangle, \quad (74)$$

$$= \frac{[J(J+1) + S(S+1) - L(L+1)][F(F+1) + J(J+1) - I(I+1)]}{4J(J+1)}, \quad (75)$$

where $\mathbf{J} = \mathbf{S} + \mathbf{L}$, and the projection of $\mathbf{I}$ on $\mathbf{F}$ is given by

$$\langle \mathbf{I} \cdot \mathbf{F} \rangle = \tfrac{1}{2}[F(F+1) + I(I+1) - J(J+1)]. \quad (76)$$

The next problem is a more difficult one: what is the relationship between χ_N and the nucleon coupling constants χ_p and χ_n? Traditionally constraints from atomic experiments on exotic couplings to neutron and proton spins have been derived using the single-particle Schmidt model for nuclear spin [see, for example, Venema *et al.* (1992)]. In this model, particular atomic species are sensitive to either neutron or proton spin couplings, but not both. The single-particle Schmidt model assumes that the nuclear spin $\mathbf{I}$ is due to the orbital motion and intrinsic spin of one nucleon only and that the spin and orbital angular momenta of all other nucleons sum to zero (Schmidt, 1937; Klinkenberg, 1952; Blatt and Weisskopf, 1979): in other words, the nuclear spin $\mathbf{I}$ is entirely generated by a combination of the valence nucleon spin ($\mathbf{S}_p$ or $\mathbf{S}_n$) and the valence nucleon orbital angular momentum ℓ, so that we have

$$\chi_N = \frac{\langle \mathbf{S}_{p,n} \cdot \mathbf{I} \rangle}{I(I+1)} \chi_{p,n}, \quad (77)$$

$$= \frac{S_{p,n}(S_{p,n}+1) + I(I+1) - \ell(\ell+1)}{2I(I+1)} \chi_{p,n}, \quad (78)$$

where it is assumed that the valence nucleon is in a well-defined state of ℓ and $S_{p,n}$. However, it is well known that

nuclear magnetic moments are not accurately predicted by the Schmidt model, since in most cases it is a considerable oversimplification of the nucleus. Thus, in general, the nuclear-spin content and magnetic moment cannot be described by a single valence nucleon in a well-defined state of ℓ and $S_{p,n}$. While there have been attempts to apply semiempirical models employing nuclear magnetic-moment data to derive new constraints for nonvalence nucleons (Engel and Vogel, 1989; Flambaum, 2006b; Flambaum, Lambert, and Pospelov, 2009; Stadnik and Flambaum, 2015a), Jackson Kimball (2015) showed that such models cannot reliably be used to predict the spin polarization of nonvalence nucleons by analyzing known physical effects in nuclei and by comparisons with detailed large-scale nuclear shell-model calculations [see, for example, Vietze *et al.* (2015) and Brown *et al.* (2017)]. Thus while the sensitivity of valence nucleons and electrons to exotic physics can be reliably estimated, evaluating the sensitivity of nonvalence nucleons and electrons to exotic physics requires detailed theoretical calculations.

9. Conclusions

Keeping in mind the previous caveats, the MWDM framework introduced by Dobrescu and Mocioiu (2006) and Moody and Wilczek (1984) [Eqs. (49)–(59)] and analyzed in further detail by Fadeev *et al.* (2018) provides a useful tool to compare different experimental searches for exotic spin-dependent effects.

D. Overview of experimental searches

A typical approach in experiments searching for exotic spin-dependent interactions is to develop a sensitive detector of torques or forces on particles (such as a torsion pendulum) and then bring the detector in close proximity to an object that acts as a local source of the exotic field (for example, a large mass or highly polarized spin sample). The object producing the exotic field acts analogously to a charged object producing an electric field. Usually the major difficulty in such measurements is understanding and eliminating systematic errors: in other words, distinguishing exotic torques and forces that would be evidence of new physics from prosaic effects such as magnetic interactions. For this reason, it is advantageous if the source can be manipulated in such a way as to modulate the exotic field in order to distinguish its effects from background processes. In lieu of this, possible sources of systematic errors can be constrained by independent measurements. Another approach, often used to probe exotic spin-dependent interactions at the atomic or molecular length scale, is to compare theory and measurement for some property of a system (such as the energy splitting between different hyperfine states in an atom) that would change if an exotic spin-dependent interaction existed.

As seen in Sec. VII.C, the basic features of an experiment that characterize its particular sensitivity are the identities and properties of the particle constituents of the exotic field source and the detector (determining whether the experiment is searching for neutron-neutron interactions, electron-electron interactions, etc.) and the distance between the source and detector (which determines the range of the interaction to which the experiment is sensitive, or, alternatively, the mass of the exotic boson communicating the interaction). The precision of the experiment determines the strength of the interaction to which it is sensitive. Depending on whether one or both of the source and detector employ polarized particles and if the source and detector are in relative motion, the experiment can be sensitive to different potentials among those enumerated in the MWDM formalism (Sec. VII.C.2). Most experimental searches to date have been for velocity-independent interactions ($\mathcal{V}_1$, $\mathcal{V}_2$, $\mathcal{V}_3$, $\mathcal{V}_{9+10}$, and $\mathcal{V}_{11}$, see Sec. VII.C.2).

While most experiments house a macroscopic source and detector in a single laboratory, thus allowing proximities between source and detector to range from slightly less than a millimeter to a few meters [see, for example, Youdin *et al.* (1996), Vasilakis *et al.* (2009), Tullney *et al.* (2013), and Terrano *et al.* (2015)], the longest-range experiments use the Earth as a source mass [see, for example, Wineland *et al.* (1991), Venema *et al.* (1992), and Jackson Kimball, Dudley *et al.* (2017)] or a source of polarized electrons (Hunter *et al.*, 2013), and the shortest-range experiments probe atomic or molecular structures [see, for example, Ramsey (1979), Ledbetter, Romalis, and Jackson Kimball (2013), and Ficek *et al.* (2017)]. Experiments with the Earth as an exotic field source have the particular challenge of lacking a way to reverse or modulate the interaction. Atomic-range experiments suffer from a similar challenge insofar as they generally must rely on a comparison between calculations of energy levels and spectroscopic measurements.

Experiments searching for exotic spin-dependent interactions typically employ magnetic shielding between the source of the exotic field and the detector. Any such experiment must answer the basic question: what is the effect of the magnetic shield system on the signal detected by the spin-polarized ensemble? This question was considered by Jackson Kimball *et al.* (2016), and the general conclusion is that for common experimental geometries and conditions, magnetic shields do not significantly reduce sensitivity to exotic spin-dependent interactions, especially when the technique of comagnetometry is used (where measurements are simultaneously performed on two or more atomic species) (Lamoreaux, 1989). However, exotic fields that couple to electron spin can induce magnetic fields in the interior of shields made of a soft ferromagnetic or ferrimagnetic material. This induced magnetic field must be taken into account in the interpretation of experiments searching for new spin-dependent interactions.

A particular case, discussed in detail by Chaudhuri *et al.* (2015) and Dubovsky and Hernández-Chifflet (2015) and also in Sec. VII.B.5, where careful consideration of electromagnetic shielding is crucial is that of hidden photons. The photon field and the hidden-photon field couple to standard model particles in essentially the same way: observable effects of the hidden-photon field are nearly entirely through the effects of the mixing of the hidden field into a real electromagnetic field. Thus observable effects of hidden photons can be significantly reduced by electromagnetic shielding (Jackson Kimball *et al.*, 2016). In contrast to hidden photons, generic spin-1 particles such as dark photons or Z' bosons may have no particular relationship with electromagnetism, and thus magnetic shielding generally does not suppress their effects (Jackson Kimball *et al.*, 2016).

In the next sections we review the experiments establishing the best laboratory constraints on various exotic spin-dependent interactions.

E. Experimental constraints on monopole-dipole interactions

Figure 13 shows the most stringent laboratory and astrophysical constraints on exotic monopole-dipole interactions, in particular, the $\mathcal{V}_{9+10}$ potentials as described by the MWDM formalism [Eq. (63)], which can be interpreted as a scalar-pseudoscalar coupling. The horizontal axes show the range of the interaction, inversely proportional to the mass of the boson communicating the interaction [Eq. (61)]. The vertical axes show the dimensionless coupling parameter $|g_p g_s|/\hbar c$ between the studied particles. Typically in experiments, the monopole (scalar) coupling is to an unpolarized sample with roughly equal numbers of protons, neutrons, and electrons, whereas the dipole (pseudoscalar) coupling is to a polarized sample of predominantly one species, so the upper, middle, and lower plots in Fig. 13 can be interpreted as constraints on $|g_p^n g_s^X|/\hbar c$, $|g_p^p g_s^X|/\hbar c$, and $|g_p^e g_s^X|/\hbar c$, where the superscripts n, p, and e refer to neutrons, protons, and electrons, respectively, and $X = n$, p, and e for each case.
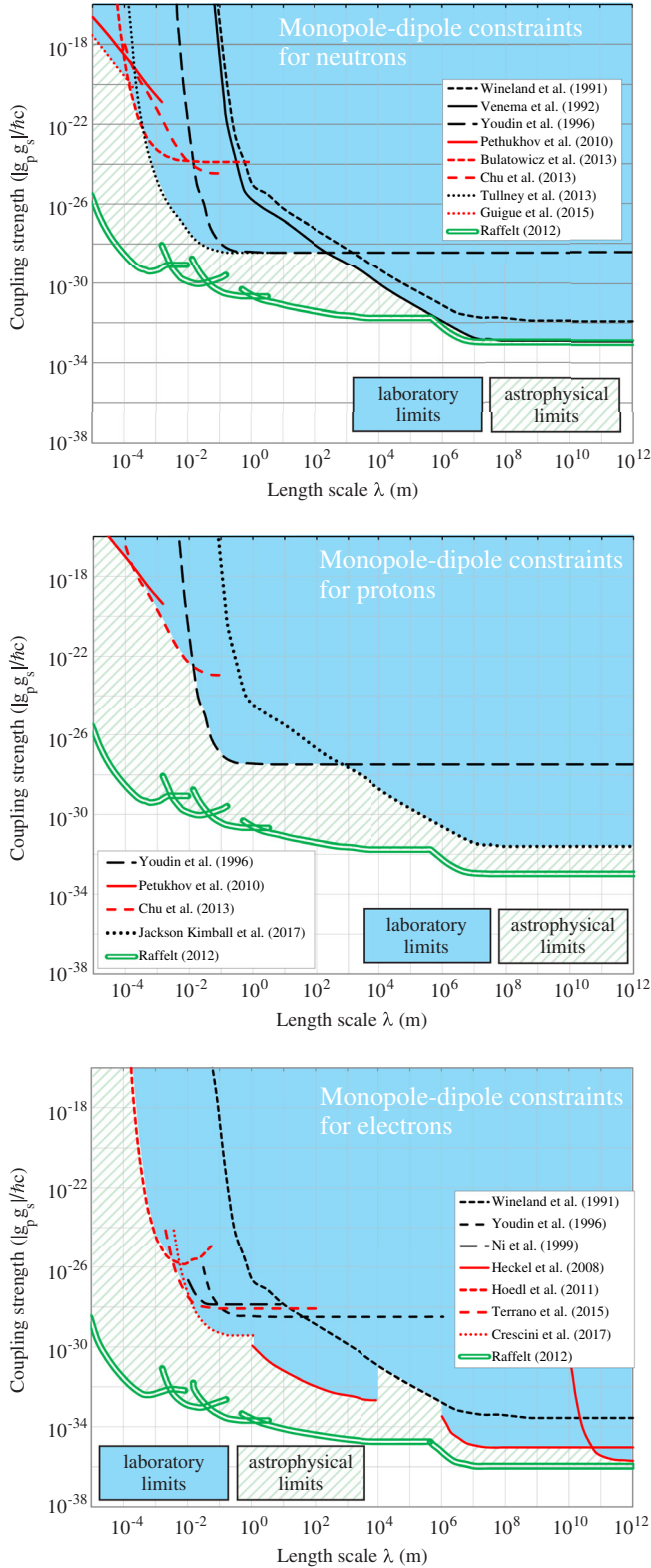
FIG. 13. Laboratory constraints [shaded light blue (gray), see text for discussion of individual experiments] on monopole-dipole (scalar-pseudoscalar) couplings, $|g_p g_s|/\hbar c$ [the $\mathcal{V}_{9+10}$ potentials as described in Eq. (63)], for neutrons, protons, and electrons as a function of the range λ of the interaction (g_p and g_s are the pseudoscalar and scalar coupling constants, respectively). Astrophysical constraints are from the analysis of Raffelt (2012) [excluded parameter space outlined with the solid double green (gray) line, dashed green (gray) shading].

1. Neutrons

At the longest interaction ranges probed by experiments, the most stringent laboratory constraint on monopole-dipole interactions between spin-polarized neutrons and other particles is derived from the experiment of Venema *et al.* (1992), establishing the limit displayed in the upper plot of Fig. 13 with a solid black line. The experiment of Venema *et al.* (1992) illustrates the principles involved in a broad class of experiments that rely on optical measurements of the spin precession of various atomic species in the gas phase [for reviews of these experimental techniques, see Budker *et al.* (2002), Budker and Romalis (2007), and Budker and Jackson Kimball (2013)]. Venema *et al.* (1992) simultaneously measured the spin precession frequencies of two isotopes of Hg (this exemplifies the technique of comagnetometry) as the orientation of a magnetic field $\mathcal{B}$ was changed relative to the Earth's gravitational field g. Since the ground electronic state of Hg is $^1S_0$, the ground-state polarization is entirely due to the nuclear spin I, with ^{199}Hg having $I = 1/2$ and ^{201}Hg having $I = 3/2$. A heretofore undiscovered long-range, monopole-dipole interaction would generate spin precession about an axis directed along the local gravitational field g. In the presence of only $\mathcal{B}$ and g, the spin precession frequencies for the two Hg isotopes are

$$\Omega_{199} = \gamma_{199}\mathcal{B} + \chi_{199}g\cos\phi, \qquad (79)$$

$$\Omega_{201} = \gamma_{201}\mathcal{B} + \chi_{201}g\cos\phi, \qquad (80)$$

where γ_i is the gyromagnetic ratio and χ_i is the so-called "gyrogravitational ratio" parametrizing the new interaction (where the subscripts i denote the respective isotopes), and ϕ is the angle between $\mathcal{B}$ and g. As long as $\chi_{199}/\chi_{201} \neq \gamma_{199}/\gamma_{201}$ (as generally expected), the ratio $\mathcal{R} = \Omega_{199}/\Omega_{201}$ acquires a dependence on $\mathcal{B}$ and ϕ if the χ_i's are nonzero, enabling a search for the long-range monopole-dipole coupling.

The experimental setup is shown in Fig. 14. The Hg atoms were contained in a cylindrical vapor cell situated at the center of a three-layer cylindrical μ-metal shield with internal coils to apply controlled magnetic fields to the atoms. The axes of the concentric cylinders of the shield system (defined to be z) and quadrupole axis of the vapor cell ($\hat{\mathbf{Q}}_c$), as well as the magnetic field during spin precession, were oriented along the Earth's rotation axis ($\hat{\mathbf{\Omega}}_E$). This orientation is designed to make systematic errors related to the Earth's rotation quadratic in the misalignment angle of the apparatus, as discussed next. The experimental procedure consisted of a pump stage and a probe stage. During the pump stage, the atoms were optically pumped in the presence of a small magnetic field along x ($B_x \lesssim 10$ mG) by circularly polarized light propagating along $\hat{\mathbf{x}}$. Optical pumping involves exciting atomic transitions with polarized light in order to generate spin polarization: the angular momentum of the light field is transferred to the atomic sample; see, for example, reviews by Happer (1972) and Happer, Jau, and Walker (2010). In the probe stage, the magnetic field was redirected along $\pm\hat{\mathbf{z}}$ in order to induce
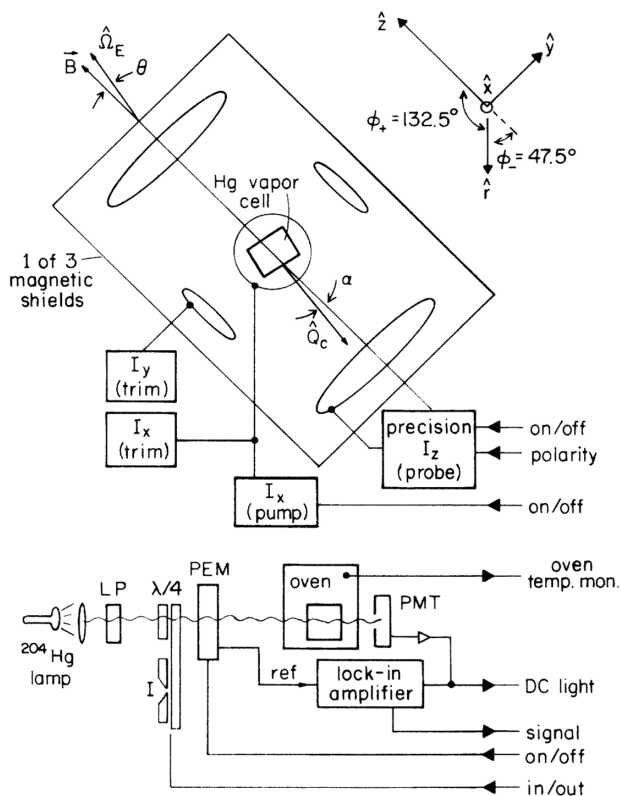
FIG. 14. Experimental setup. LP = linear polarizer, $\lambda/4$ = quarter-wave plate, I = iris, PMT = photomultiplier tube, and PEM = photoelastic modulator. Arrows on the right-hand side indicate computer control and data acquisition. The angles $\phi_\pm$ indicate the projection of $\hat{r}$ (parallel to g) along $\hat{z}$ (parallel to $\mathcal{B}$) for the two magnetic field orientations. From Venema *et al.*, 1992.

spin precession. The light intensity was reduced so as not to significantly perturb the atomic states, and a photoelastic modulator (PEM) rapidly alternated the light polarization between right and left circular in order to reduce vector light shifts and enable lock-in detection. The detected signal was demodulated at the PEM frequency (42 kHz) and the free-precession-decay signal was analyzed to extract the precession frequencies.

Two important systematic errors required special consideration. The first arose due to a collisional interaction of the ^{201}Hg atoms with the walls of the cylindrical vapor cell, causing a ≈ 50 mHz quadrupolar shift. The quadrupolar wall shift led to resolved splitting of the Zeeman frequencies for ^{201}Hg. The quadrupolar wall shift, and an optical method to cancel it, was recently studied in detail by Peck *et al.* (2016) for Cs atoms, although it should be noted that in this case the quadrupolar wall shift turns out to be of electronic origin rather than nuclear as is the case for Hg. The second systematic error arose because the experimental apparatus was attached to the Earth, while the Hg spins were effectively decoupled from the Earth's rotation during the probe stage (since the spins were freely precessing). Consequently, the Hg isotopes exhibited apparent precession at the rotation rate of the Earth $\Omega_E \approx 2\pi \times 11.6$ μHz. This effect, known as the gyrocompass effect (Heckel *et al.*, 2008), can be understood as the result of viewing an inertial system, the Hg spins, from a

noninertial frame, the surface of the rotating Earth. The gyrocompass effect was studied with even greater precision in the work of Brown *et al.* (2010) and Gemmel *et al.* (2010). Both systematic effects were constrained at or below the statistical sensitivity of the experiment by orienting the apparatus so that uncertainty in the effects were quadratic in the misalignment angles.

The experiment establishing the strongest laboratory-scale limit on monopole-dipole couplings of neutrons was that of Tullney *et al.* (2013), shown by the dotted black curve in the upper plot of Fig. 13. In the experiment of Tullney *et al.* (2013), the spin precession frequencies of colocated gaseous samples of ^{3}He and ^{129}Xe were measured using a multichannel, low-T_c superconducting quantum interference device (SQUID) to monitor the magnetization. This avoided issues related to light shifts that can be problematic in optical atomic magnetometry experiments (Acosta *et al.*, 2006; Jackson Kimball *et al.*, 2013; Jackson Kimball, Dudley *et al.*, 2017). The source mass was a cylindrical unpolarized BGO crystal ($Bi_4Ge_3O_{12}$) whose position could be modulated using a compressed-air driven piston between ≈ 2 and ≈ 200 mm from a ^{3}He/^{129}Xe cell in order to modulate the strength of the exotic interaction. The BGO crystal was chosen as the source mass based on its high nucleon number density, low conductivity (and thus low Johnson-Nyquist noise), and its vanishingly small low-field magnetic susceptibility.

At sub-mm distance scales, limits on monopole-dipole interactions of the neutron have been obtained by the experiments of Petukhov *et al.* (2010), Bulatowicz *et al.* (2013), and Guigue *et al.* (2015) shown by short-dashed, solid, and dotted red (dark gray) curves, respectively, in the upper plot of Fig. 13. Bulatowicz *et al.* (2013) employed a dual species xenon NMR gyroscope with polarized ^{129}Xe and ^{131}Xe to search for a monopole-dipole interaction when a zirconia rod was moved near the NMR cell. Again the technique of comagnetometry was utilized: by simultaneously comparing the precession frequencies of the two Xe isotopes, magnetic field changes were distinguished from frequency shifts due to the monopole-dipole coupling between the polarized Xe nuclei and the zirconia rod source mass. The experiments of Petukhov *et al.* (2010) and Guigue *et al.* (2015) used measurements of hyperpolarized ^{3}He to constrain the contribution of short-range monopole-dipole interactions to relaxation rates. Although it is outside the range of the parameter space plotted in Fig. 13, the work of Jenke *et al.* (2014) established the strongest bounds on $|g_p g_s|/\hbar c$ for distances between 1 and 100 μm. In the experiment of Jenke *et al.* (2014), transitions between quantum states of ultracold neutrons confined vertically above a horizontal mirror by the Earth's gravity were driven by resonantly oscillating the mirror position. At even shorter distance ranges, $10^{-10} \lesssim \lambda \lesssim 10^{-7}$ m, the most stringent laboratory constraints on monopole-dipole interactions come from measurement of the diffraction of a cold neutron beam as it passed through a noncentrosymmetric quartz crystal (Fedorov, Kuznetsov, and Voronin, 2013), setting the bound $|g_p g_s|/\hbar c \lesssim 10^{-12}$. The experiment of Afach *et al.* (2015) used colocated samples of ultracold neutrons and ^{199}Hg atoms to obtain constraints at a level similar to that of Petukhov *et al.* (2010).

2. Electrons

The lower plot of Fig. 13 shows constraints on monopole-dipole interactions of electrons. Most of the best limits for electrons come from a series of experiments using spin-polarized torsion pendulums carried out at the University of Washington (Heckel *et al.*, 2008; Hoedl *et al.*, 2011; Terrano *et al.*, 2015), shown by the red (dark gray) curves indicated in the plot. A diagram of the spin-polarized torsion pendulum setup used by Terrano *et al.* (2015) is shown in Fig. 15. The key piece of the experimental apparatus was a ring of 20 equally magnetized segments of alternating high- and low-spin density materials. The 20-pole spin ring was the active element of the torsion-pendulum detector. The high-spin density material was alnico and the low-spin density material was $SmCo_5$; a substantial degree of the magnetization of $SmCo_5$ comes from the orbital motion of electrons while the magnetization of alnico is almost entirely due to the electrons' spin. The magnetization of each alnico wedge is tuned by a localized external field so that the spin-polarized torsion pendulum has negligible variation in magnetization. Then either an unpolarized copper attractor or spin-polarized attractor (identical to the pendulum detector) was rotated below the torsion pendulum at a frequency ω, producing a modulated torque at 10ω as the source's high mass (or spin) density wedges passed below the high- or low-spin density segments of the pendulum. The pendulum's and both
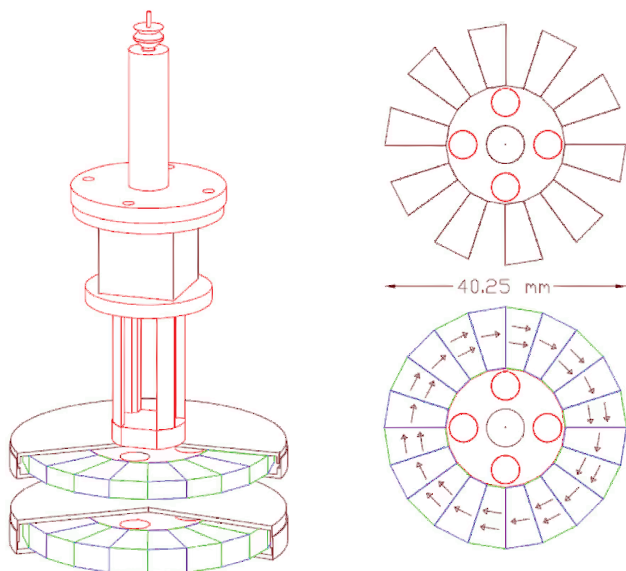

FIG. 15. The left panel shows the 20-pole spin-polarized torsion pendulum and the right panel shows the unpolarized and polarized sources (upper and lower figures, respectively) used to search for monopole-dipole and dipole-dipole interactions in the experiment of Terrano *et al.* (2015). The μ-metal shielding surrounding the spin-polarized pendulum and the sources is cut away to show the alternating alnico (green) and $SmCo_5$ (blue) segments and one of the four pairs of calibration cylinders (red). The mirror cube (in the middle of the pendulum's support structure) is used to monitor the pendulum twist angle. The entire apparatus is contained within a system of magnetic shields. The arrows on the spin attractor indicate net spin density and direction of the alternating segments. From Terrano *et al.*, 2015.

attractors' four cylinders (either tungsten or vacuum) provided gravitational calibration signals at 4ω. The twisting of the pendulum was measured optically using a reflector cube, and the torque was inferred from a harmonic analysis of the pendulum twist angle. The experimental setup allowed the attractors to be moved close to the pendulum, with a minimum separation of ≈ 4 mm. The experiment of Heckel *et al.* (2008) used a similar spin-polarized torsion pendulum but with the Earth and Sun as source masses. Hoedl *et al.* (2011) used a semiconductor-grade silicon single crystal attached to an ultrapure titanium bar as the torsion pendulum in order to have a highly nonmagnetic detector, and then used a ferromagnet as a dipole source; this setup enabled the spin source to be brought into close proximity of the detector, allowing sensitivity to monopole-dipole forces with ranges of fractions of a mm (i.e., boson masses $\gtrsim 1$ meV).

Strong laboratory constraints on monopole-dipole couplings of electrons were also obtained by Ni *et al.* (1999) by using a paramagnetic salt (TbF_3) and a dc SQUID to search for induced spin polarization in the TbF_3 sample caused by the proximity of a copper mass. This approach was recently improved upon by Crescini *et al.* (2017), who used a dc SQUID to measure variation of the magnetization of a GSO crystal (Gd_2SiO_5) housed within a superconducting shield as a function of the distance to a lead mass under cryogenic conditions. Important constraints on both electron and neutron monopole-dipole interactions were also obtained in the experiment of Wineland *et al.* (1991). They carried out measurements on trapped $^9Be^+$ ions as an applied magnetic field was reversed relative to the local gravitation field g: the resulting frequency shift between the $^9Be^+$ $^2S_{1/2}|F=1, M=0\rangle$ and $^2S_{1/2}|F=1, M=-1\rangle$ states was constrained to be $< 13.4\,\mu$Hz, leading to the limits shown in the lower plot of Fig. 13 with the short-dashed black line.

3. Protons

The middle plot of Fig. 13 shows constraints on monopole-dipole interactions of protons. Here experimental limits are somewhat sparser. Most measurements using atomic vapor comagnetometers to search for exotic spin-dependent interactions use noble gases with valence neutrons, and therefore, as discussed previously, they are insensitive to proton couplings. Experiments using spin-polarized torsion pendulums or solid-state systems are sensitive to electron couplings. The laboratory-range experiment of Youdin *et al.* (1996), whose established constraints are shown by the long-dashed black curve, is an exception. Youdin *et al.* (1996) searched for monopole-dipole couplings between a 475-kg lead mass and the spins of ^{133}Cs and ^{199}Hg atoms using colocated atomic magnetometers (consisting of a Cs vapor cell sandwiched between a pair of ^{199}Hg cells contained within a system of magnetic shields, with laser optical pumping and probing of the atomic spins). Youdin *et al.* (1996) originally interpreted the results of their experiment to constrain only electron and neutron spin couplings. However, because the ^{133}Cs nucleus has a valence proton, Jackson Kimball (2015) noted that in this case the single-particle Schmidt model, semiempirical models, and large-scale nuclear shell-model calculations are all in reasonable agreement concerning the contribution of the

valence proton spin to the nuclear spin of ^{133}Cs. Therefore the experiment of Youdin *et al.* (1996) reliably establishes laboratory constraints on exotic monopole-dipole couplings of the proton. Similarly, at short ranges, the experiments of Petukhov *et al.* (2010) and Chu *et al.* (2013) established constraints for protons because of the well-understood contribution of the proton spin to the nuclear spin of ^{3}He (Anthony *et al.*, 1996; Jackson Kimball, 2015). Chu *et al.* (2013) searched for a spin-precession frequency shift of polarized ^{3}He when an unpolarized mass (either a ceramic block or a liquid mixture of $\approx 1\%$ MnCl$_2$ in pure water) was moved between 5 cm and 10 μm of the ^{3}He vapor cell. The particular source masses were chosen based on their nucleon densities, low magnetic impurities and magnetic susceptibilities, and minimal influence on the NMR measurement procedure. Although the work of Tullney *et al.* (2013) also used polarized ^{3}He, because the technique of comagnetometry with ^{129}Xe is employed and there is considerable uncertainty regarding the contribution of the proton spin to the ^{129}Xe nuclear spin (Jackson Kimball, 2015), we do not infer a limit on monopole-dipole interactions of the proton from this work. Recently Jackson Kimball, Dudley *et al.* (2017) completed a search for a long-range monopole-dipole coupling of the proton spin to the mass of the Earth using a ^{85}Rb/^{87}Rb comagnetometer, improving on the long-range limits of Youdin *et al.* (1996) by over 3 orders of magnitude. The experiment of Jackson Kimball, Dudley *et al.* (2017) employed overlapping ensembles of ^{85}Rb and ^{87}Rb atoms contained within an evacuated, antirelaxation-coated vapor cell and simultaneously measured the spin-precession frequencies using optical magnetometry techniques (Budker and Jackson Kimball, 2013) as the magnetic field was reversed relative to the direction of the gravitational field, similar to the experiment of Venema *et al.* (1992) discussed earlier. The measurement of Jackson Kimball, Dudley *et al.* (2017) established the best constraint on the proton GDM. The experiment was ultimately limited by systematic effects related to scattered light and magnetic field gradients.

4. Astrophysical constraints

The solid double green (gray) curves and light green (gray) striped shading in Fig. 13 shows the parameter space excluded by astrophysical considerations. Raffelt (2012) argued that the coupling constants g$_s$ and g$_p$ are individually constrained, and thus constraints on their product g$_s$g$_p$ can be derived. The scalar coupling constant g$_s$ is constrained by laboratory searches for monopole-monopole interactions [the potential $\mathcal{V}_1(r)$, Eq. (49)—see the review by Adelberger *et al.* (2009) and also Sec. VIII]. The pseudoscalar coupling constant g$_p$ for nucleons is constrained by the measured neutrino signal from supernova 1987A: the ≈ 10 s duration of the signal excludes excessive new energy losses (Raffelt and Seckel, 1988; Turner, 1988), although this constraint is based on the bremsstrahlung process in the collapsed supernova core and thus suffers from significant uncertainties related to dense nuclear matter effects (Janka *et al.*, 1996), and recent calculations (Blum and Kushnir, 2016; Chang, Essig, and McDermott, 2017; Hardy and Lasenby, 2017; Mahoney,

Leibovich, and Zentner, 2017) have suggested these limits may be weaker than first estimated and as displayed in Fig. 13. The pseudoscalar coupling constant g$_p$ for electrons is constrained by star cooling rates (Raffelt and Weiss, 1995). Although the astrophysical constraints on $|g_p g_s|/\hbar c$ are more stringent than the laboratory limits in all cases, there is both a degree of model specificity (Massó and Redondo, 2005) and some degree of uncertainty regarding the accuracy of stellar models (Hardy and Lasenby, 2017). Furthermore, it is possible that a so-called "chameleon mechanism" that screens interactions in regions of space with high mass density could invalidate astrophysical bounds on new interactions (Jain and Mandal, 2006). Thus direct laboratory measurements play a crucial, comparatively less ambiguous role in determining the existence of exotic spin-dependent interactions even when they are somewhat less sensitive than astrophysical bounds.

F. Experimental constraints on dipole-dipole interactions

Experimental searches for monopole-dipole interactions have certain appeal because such couplings violate invariance under both time reversal and spatial inversion, and hence one expects negligible background from standard model physics. Dipole-dipole couplings, on the other hand, are even under both T and P and can arise from standard model physics. In this sense, dipole-dipole couplings may be problematic for exotic physics searches because one must carefully account for standard model physics effects. Nonetheless, there has been impressive recent progress in laboratory searches for exotic dipole-dipole interactions.

1. Constraints on $\mathcal{V}_3(r)$

The best limit on long-range pseudoscalar dipole-dipole interactions [of the form given by the $\mathcal{V}_3$ potential described in Eq. (62)] between neutrons was achieved in the experiment of Vasilakis *et al.* (2009) (solid black curve in the upper plot of Fig. 16) using the setup shown in Fig. 17. The measurement technique is based on the principles of spin-exchange-relaxation-free (SERF) magnetometry (Allred *et al.*, 2002; Kornack and Romalis, 2002; Kominis *et al.*, 2003; Kornack, Ghosh, and Romalis, 2005). The atomic sample consists of overlapping ensembles of potassium (K) and ^{3}He at relatively high vapor densities (^{3}He density $\approx 10^{20}$ atoms/cm^3 and K density $\approx 10^{14}$ atoms/cm^3). The K sample is polarized through optical pumping and the ^{3}He sample is polarized through spin-exchange collisions with K. The vapor cell is located within a five-layer μ-metal shield fitted with internal coils used to cancel residual magnetic fields and create a small field $\mathcal{B}$ parallel to the propagation direction of the pump beam. Under these experimental conditions, for which the Larmor frequencies are comparable to or smaller than the frequency of spin-exchange collisions, the spin-exchange interaction between K atoms and the polarized ^{3}He vapor strongly couples the two spin ensembles (Kornack and Romalis, 2002; Kornack, Ghosh, and Romalis, 2005). In a spherical cell this coupling can be represented as an effective magnetic field $\mathcal{B}_{\text{eff}}$ experienced by one spin species due to the average magnetization **M** of the other. The applied field $\mathcal{B}$ is tuned so that it approximately cancels the $\mathcal{B}_{\text{eff}}$ experienced by
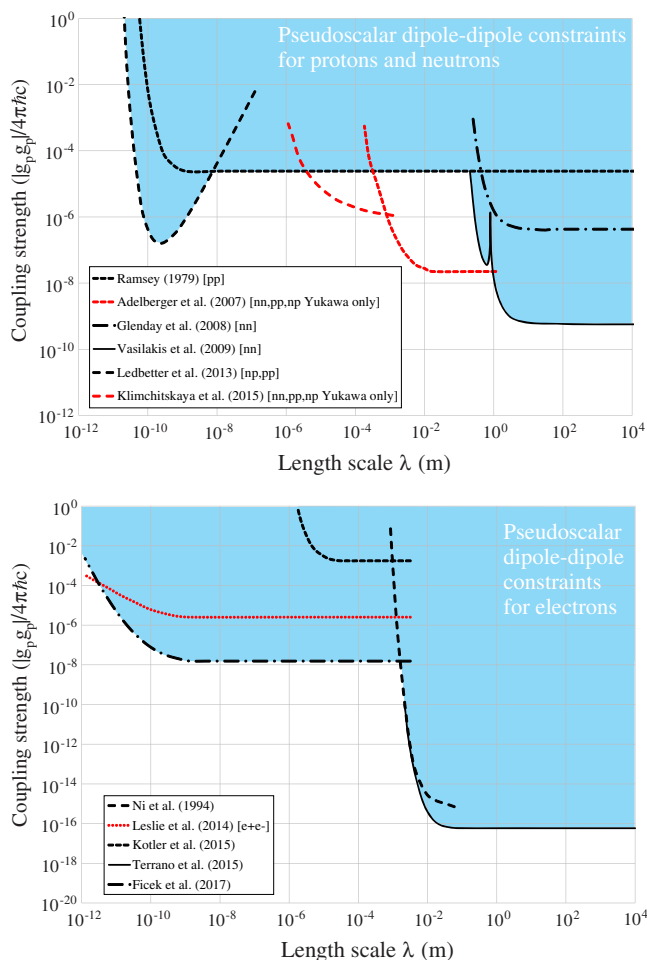
FIG. 16. Laboratory constraints [shaded light blue (gray), see text for discussion of individual experiments] on pseudoscalar dipole-dipole couplings $|g_p g_p|/(4\pi\hbar c)$ [the $\mathcal{V}_3$ potential as described in Eq. (62)], between nucleons and electrons as a function of the range λ of the interaction. The short- and long-dashed red (dark gray) lines in the upper plot show constraints derived from spin-independent measurements that apply only to the Yukawa form of the pseudoscalar interaction [Eq. (67)]. The dotted red (dark gray) line in the lower plot shows constraints based on positronium spectroscopy which in order to be compared with electron-electron constraints must assume *CPT* invariance.

the K atoms. The K atoms are then effectively in a zero-field environment. Because the ^{3}He magnetization **M** adiabatically follows $\mathcal{B}$, components of $\mathcal{B}$ transverse to $\hat{z}$ are automatically compensated by $\mathcal{B}_{\text{eff}}$ to first order. Such cancellation occurs only for interactions that couple to spins in proportion to their magnetic moments, leaving the K-^{3}He comagnetometer sensitive to inertial rotation (Kornack, Ghosh, and Romalis, 2005) and anomalous spin couplings (Vasilakis *et al.*, 2009). Thus the self-compensating K-^{3}He comagnetometer enables one to use high-sensitivity SERF magnetometry techniques for detection of anomalous spin-dependent interactions causing precession about axes transverse to $\hat{z}$.

The K spin polarization along $\hat{x}$ is determined by measuring optical rotation of an off-resonant, linearly polarized probe light beam [see, for example, the review by Budker *et al.* (2002) for a discussion of optical rotation]. After residual
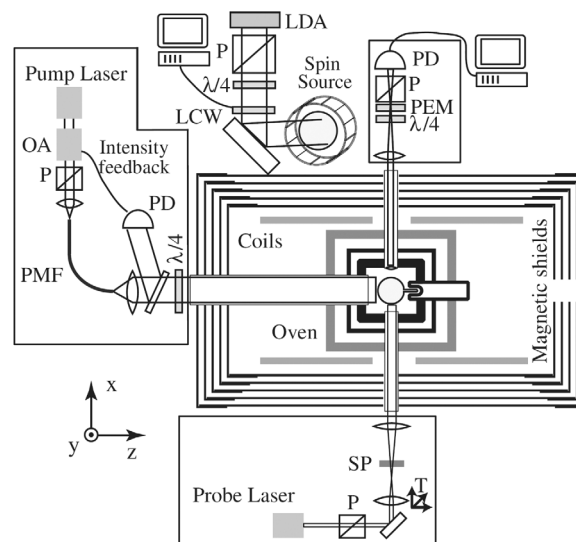

FIG. 17. Experimental setup. PD = photodiode, SP = stress plate to control polarization of the probe beam, T = translation stage to shift the probe beam, P = polarizer, PMF = polarization maintaining fiber, OA = optical amplifier, LCW = liquid crystal wave plate, PEM = photoelastic modulator, $\lambda/4$ = quarter-wave plate, and LDA = laser diode array. From Vasilakis *et al.* (2009).

magnetic fields and light shifts are eliminated using zeroing routines [described in detail by Kornack, Ghosh, and Romalis (2005)], the K spin polarization along $\hat{x}$ can arise only due to nonmagnetic, spin-dependent interactions, offering a highly sensitive probe of such anomalous interactions. The spin source in the experiment of Vasilakis *et al.* (2009) consisted of a dense ($\approx 3 \times 10^{20}$ cm^{-1}), highly polarized ($\approx 15\%$ polarization) ^{3}He gas located approximately 50 cm from the cell. The nuclear-spin direction of the ^{3}He sample was reversed at a 0.18 Hz rate by adiabatic fast passage. After approximately one month of data acquisition, no anomalous effect was detected at a level corresponding to a magnetic field value less than an aT (10^{-14} G).

Constraints on pseudoscalar dipole-dipole couplings between protons at the molecular scale were deduced by Ramsey (1979) based on molecular beam experiments with hydrogen (H$_2$). Comparing the measurements of Harrick *et al.* (1953) to calculations of the magnetic dipole-dipole interaction between the protons in H$_2$ limited the possible contribution of an exotic dipole-dipole interaction to spin-dependent energy splittings, establishing the constraint shown by the short-dashed black curve in the upper plot of Fig. 16. Ledbetter, Romalis, and Jackson Kimball (2013) obtained the constraints on proton-proton and neutron-proton pseudoscalar dipole-dipole couplings shown by the long-dashed black curve in the upper plot of Fig. 16 by comparing NMR measurements to theoretical calculations of indirect nuclear dipole-dipole coupling (J coupling) in deuterated molecular hydrogen (HD). The Hamiltonian describing J coupling has the form $\mathcal{J}\mathbf{I}_1 \cdot \mathbf{I}_2$ ($\mathbf{I}_{1,2}$ are the nuclear spins and $\mathcal{J}$ parametrizes the interaction strength) and arises due to a second-order hyperfine interaction where the interaction between the nuclear spins is mediated through the electron cloud. The

measurements from which Ledbetter, Romalis, and Jackson Kimball (2013) extracted constraints were performed with HD in the gas phase: thus the internuclear vector $\hat{\mathbf{r}}$ was randomly reoriented due to collisions. This effect leads to an averaging of Eq. (62), so that its distance scaling becomes proportional to $e^{-r/\lambda}/\lambda^2 r$. The collisional averaging reduces sensitivity to exotic dipole-dipole forces for which λ differs significantly from the mean internuclear separation, as seen in Fig. 16. Of interest in regard to the constraints derived from J coupling in HD are more recent measurements and calculations (Garbacz, 2014; Neronov and Seregin, 2015).

Other notable experiments searching for exotic dipole-dipole couplings of nucleons include the work of Glenday *et al.* (2008), an experiment similar to that of Vasilakis *et al.* (2009) that employed a dual-species ^{3}He-^{129}Xe maser as the detector, and constraints from Adelberger *et al.* (2007) and Klimchitskaya and Mostepanenko (2015) based on short-range tests of the gravitational inverse-square law and the Casimir effect. The work of Adelberger *et al.* (2007) and Klimchitskaya and Mostepanenko (2015), which actually searched for spin-independent interactions, constrained only the Yukawa form of the pseudoscalar coupling [Eq. (67)] and are thus more model specific than the other laboratory searches considered. The constraints from Adelberger *et al.* (2007) and Klimchitskaya and Mostepanenko (2015) do not apply to the derivative form [Eq. (68)] that would be expected for Goldstone bosons such as the axion. Constraints on spin-dependent interactions derived from experimental searches for spin-independent interactions are also considered by Aldaihan *et al.* (2017).

For electrons, the experiments of Ni *et al.* (1994) and Terrano *et al.* (2015) established the most stringent constraints on pseudoscalar dipole-dipole forces at interaction ranges $\gtrsim 1$ mm (solid and long-dashed black curves, respectively, in the lower plot of Fig. 16). The experiment of Terrano *et al.* (2015) was addressed in the preceding section on monopole-dipole interactions (see Fig. 15 and surrounding discussion). Ni *et al.* (1994) used a SQUID to measure the magnetization of a paramagnetic salt (TbF$_3$) induced by dipole-dipole interactions with rotating spin-polarized samples (Dy$_6$Fe$_{23}$ and HoFe$_3$). From atomic scales up to a mm, the agreement between energy structure calculations and spectroscopic measurements in He (Ficek *et al.*, 2017) provide the most stringent constraints, shown by the black dot-dashed line in the lower plot of Fig. 16. Also of interest are electron spin resonance measurements in iron using a scanning tunneling microscope (STM) by Luo *et al.* (2017).

2. Constraints on $\mathcal{V}_2(r)$

Figure 18 shows the laboratory constraints on axial-vector dipole-dipole couplings $|g_A g_A|/(4\pi\hbar c)$ described by the $\mathcal{V}_2$ potential in the MWDM formalism [Eq. (64)]. In terms of experiments, the critical difference between the $\mathcal{V}_2$ and $\mathcal{V}_3$ potentials is the scaling with particle separation: the $\mathcal{V}_2$ potential scales as $1/r$ whereas the $\mathcal{V}_3$ potential scales as $1/r^3$. Thus experiments searching for dipole-dipole interactions can have vastly different sensitivities to the two different potentials.

An example illustrating the importance of the distance scaling is the work of Hunter *et al.* (2013) which established
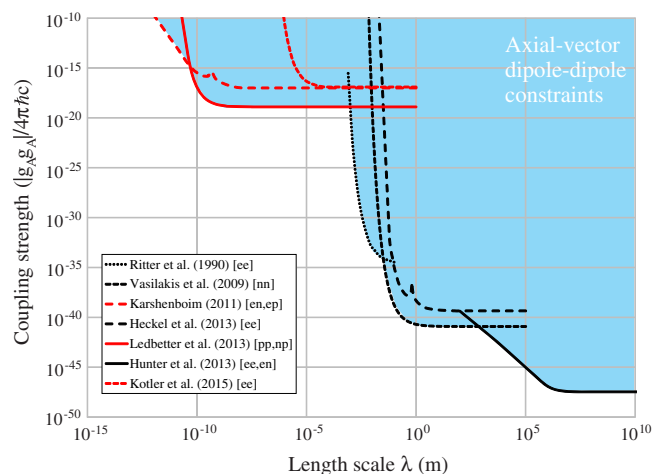

FIG. 18. Laboratory constraints [shaded light blue (gray), see text for discussion of individual experiments] on axial-vector dipole-dipole couplings $|g_A g_A|/(4\pi\hbar c)$ [the $\mathcal{V}_2$ potential as described in Eq. (64)], for various particles as a function of the range λ of the interaction.

the long-range axial-vector constraints shown by the solid black curve in Fig. 18. Hunter *et al.* (2013) took advantage of the large number of polarized electrons in the Earth: there are $\approx 10^{49}$ unpaired electron spins in the Earth, yielding $\approx 10^{42}$ polarized geoelectrons polarized by the Earth's magnetic field. Thus the number of polarized geoelectrons exceeds that of a typical laboratory source by a factor of $\gtrsim 10^{17}$. However, a typical laboratory source of polarized electrons can be placed closer than a meter away from a detector whereas the mean distance of a polarized geoelectron is $\gtrsim 10^5$ m from a detector on the surface of the Earth. For pseudoscalar dipole-dipole interactions, the $1/r^3$ distance scaling makes searches for exotic interactions with geoelectrons less competitive than searches employing polarized laboratory sources. On the other hand, the $1/r$ scaling of the axial-vector interaction makes the large number of polarized geoelectrons a much stronger source with which to search for long-range interactions. Hunter *et al.* (2013) used data from optical atomic magnetometers (Venema *et al.*, 1992; Peck *et al.*, 2012) and a spin-polarized torsion pendulum (Heckel *et al.*, 2008) to derive the limits shown in Fig. 18. The experiments of Heckel *et al.* (2008) and Peck *et al.* (2012) utilized rotatable mounts for their entire experimental apparatus in order to modulate the signal from the polarized geoelectrons, a technique also employed in the experiment of Brown *et al.* (2010).

Many of the experiments searching for exotic dipole-dipole interactions previously discussed also place strong constraints on axial-vector interactions between various particles (Heckel *et al.*, 2008; Vasilakis *et al.*, 2009; Ledbetter, Romalis, and Jackson Kimball, 2013). Between a μm and a mm, the best direct constraint on axial-vector dipole-dipole interactions between electrons comes from the measurement of the magnetic dipole-dipole interaction between two trapped ^{88}Sr$^+$ ions (Kotler *et al.*, 2014; Kotler, Ozeri, and Jackson Kimball, 2015). Kotler *et al.* (2014) trapped two ^{88}Sr$^+$ ions using a linear radio-frequency Paul trap, and the ions were initialized in an entangled state that was insensitive to spatially

homogeneous magnetic field noise. This technique enabled precise measurement of the magnetic dipole-dipole interaction between the ions, which when compared to a straightforward calculation gave good agreement at a level of ≈ 200 μHz. Kotler, Ozeri, and Jackson Kimball (2015) then used the agreement between experiment and theory to limit the strength of exotic dipole-dipole interactions as shown by the short-dashed red (dark gray) curve in Fig. 18. Ritter *et al.* (1990) (black dotted curve in Fig. 18) carried out an experiment with a spin-polarized torsion pendulum made from Dy_6Fe_{23}, which had the characteristic that at a particular temperature (between 265 and 280 K) the magnetization due to the orbital motion of the electrons approximately canceled the magnetization from the electron spins, allowing a torsion pendulum with large net intrinsic spin but small magnetic moment, a similar idea to that behind the later work of the University of Washington group discussed previously (Heckel *et al.*, 2008; Terrano *et al.*, 2015). Karshenboim (2010a, 2010b, 2010c) compared spectroscopic measurements of hyperfine structure to QED calculations for various atomic systems in order to derive constraints on axial-vector interactions, the strongest constraints coming from hydrogen, deuterium, and ^{3}He$^+$.

3. Astrophysical constraints

It should be noted that laboratory limits on pseudoscalar interactions are weaker than relevant astrophysical constraints on g$_p$ from the neutrino signal from SN 1987A (Engel, Seckel, and Hayes, 1990), the metallicity of stars (Haxton and Lee, 1991), the maximum brightness of red giants (Raffelt and Weiss, 1995), and null searches for axion emission from the Sun (Derbin *et al.*, 2009). However, these astrophysical constraints do not necessarily apply to axial-vector or vector interactions (Dobrescu and Mocioiu, 2006). Since both the $\mathcal{V}_2$ and $\mathcal{V}_3$ potentials can be generated by spin-1 bosons, astrophysical constraints, specific to the vertex-level interactions for spin-0 bosons (Dobrescu and Mocioiu, 2006; Raffelt, 1999), do not apply in general to the $\mathcal{V}_2$ and $\mathcal{V}_3$ potentials and are therefore not shown in Figs. 16 and 18.

G. Experimental constraints on other forms of spin-dependent interactions

A number of experiments have searched for some of the other forms of exotic spin-dependent potentials enumerated by Dobrescu and Mocioiu (2006) [Eqs. (49)–(59)]. For example, Vasilakis *et al.* (2009) and Hunter *et al.* (2013) specifically searched for the $\mathcal{V}_{11}$ potential [Eq. (56)]. Jackson Kimball, Boyd, and Budker (2010) used measurements and calculated cross sections for spin exchange between alkali-metal atoms and noble gases (specifically sodium and helium) to constrain anomalous spin-dependent forces between nuclei at the atomic scale, and established the first limits on the $\mathcal{V}_8$ potential [Eq. (54)]. Hunter and Ang (2014) used polarized geoelectrons to constrain many of the other velocity-dependent potentials: $\mathcal{V}_{6,7}$, $\mathcal{V}_8$, $\mathcal{V}_{15}$, and $\mathcal{V}_{16}$ [Eqs. (53), (54), (58), and (59), respectively]. Yan and Snow (2013) used measurements of a P-odd spin rotation when a cold neutron beam passed through a liquid ^{4}He target to set limits on $\mathcal{V}_{12+13}$ at short ranges ($10^{-6} \lesssim \lambda \lesssim 1$ m), and Yan *et al.*

(2015) used ^{3}He spin-relaxation rates with the Earth as an unpolarized source mass to constrain $\mathcal{V}_{12+13}$ at long ranges ($\lambda \gtrsim 1$ m). Piegsa and Pignol (2012) were able to establish bounds on $\mathcal{V}_{4+5}$ at the mm scale for neutrons using Ramsey's method of separated oscillatory fields with a cold neutron beam that traveled past a nearby copper plate. Heckel *et al.* (2008) constrained long-range velocity-dependent potentials between their torsion pendulum and the Moon and the Sun. Ficek *et al.* (2018) compared spectroscopic measurements and theoretical calculations for antiprotonic He to obtain the first constraints on exotic spin-dependent semileptonic interactions between matter and antimatter.

Measurements of atomic parity violation as described in Sec. IV can be used to search for interactions mediated by exotic bosons since several of the MWDM potentials violate P. Indeed, some of the best constraints on interactions mediated by new spin-1 (Z') bosons have been derived from atomic parity violation experiments (Bouchiat and Fayet, 2005; Davoudiasl, Lee, and Marciano, 2012; Dzuba, Flambaum, and Stadnik, 2017).

It also bears mentioning that there have been several tests of the universality of free fall (UFF) performed with spin-polarized objects, in particular, with cold atoms (Fray *et al.*, 2004; Tarallo *et al.*, 2014; Duan *et al.*, 2016). At present, such experiments are orders of magnitude less sensitive to the potentials described in Eqs. (49)–(59) than the experiments described in Secs. VII.E and VII.F. The basic reason for this is that free-fall experiments essentially measure the spatial derivative of $\mathcal{V}_i$ whereas the experiments using optical atomic magnetometers or torsion pendulums measure the energy shift due to $\mathcal{V}_i$ directly. Section X discusses UFF tests using both polarized and unpolarized test masses along with other experimental probes of the equivalence principle.

As noted in Sec. VII.B, there are a variety of other theories predicting spin-dependent interactions that are not well described by the potentials outlined in Eqs. (49)–(59), and several experiments have specifically sought to measure such effects. Glenday *et al.* (2008), Heckel *et al.* (2008), and Vasilakis *et al.* (2009) searched for the hypothetical ghost condensate resulting from spontaneous breaking of Lorentz symmetry (Arkani-Hamed *et al.*, 2004, 2005). Vasilakis *et al.* (2009) and Hunter *et al.* (2013) searched for the potentials arising from unparticles (Georgi, 2007; Liao and Liu, 2007). Many experiments have analyzed their results in terms of gravitational torsion (Heckel *et al.*, 2008; Jackson Kimball, Boyd, and Budker, 2010; Ledbetter, Romalis, and Jackson Kimball, 2013; Lehnert, Snow, and Yan, 2014; Kotler, Ozeri, and Jackson Kimball, 2015). Ivanov and Snow (2017) proposed that gravitational torsion generates a new type of P-even and T-odd potentials that can be probed using spin-polarized particles moving through unpolarized matter that is rotating in the laboratory frame. Lehnert *et al.* (2017) experimentally investigated a different deviation from the predictions of general relativity known as nonmetricity by measuring the rotation of neutron spins as the neutrons propagate though liquid helium. Undoubtedly, the rich theoretical landscape of exotic spin-dependent interactions will continue to inspire a vibrant array of experiments as many possible interactions still remain unexplored.

H. Emerging ideas

A major new direction in the search for exotic spin-dependent interactions is the push to study oscillating and transient signals from fields comprised of new bosons such as axions, ALPs, and hidden photons that may constitute dark matter or dark energy. These ideas are discussed in Sec. IX, and include global networks of optical atomic magnetometers (Pospelov *et al.*, 2013; Pustelny *et al.*, 2013) and atomic clocks (Derevianko and Pospelov, 2014) to search for correlated transient signals heralding new physics that might arise from topological defects (Pospelov *et al.*, 2013; Stadnik and Flambaum, 2014b) or clumps of virialized ultralight fields (Derevianko, 2016). There are also new experiments using NMR (Budker *et al.*, 2014), atomic spectroscopy (Stadnik and Flambaum, 2014a), and resonant electromagnetic detectors (Chaudhuri *et al.*, 2015) to search for coherently oscillating dark matter fields. A related proposal is that of Romalis and Caldwell (2013), who noted that cosmological scalar fields, which may explain dark energy, have local spatial gradients that could have detectable electromagnetic couplings.

There are also new ideas being developed for novel sources and detectors that can be used to search for exotic spin-dependent interactions. Chu *et al.* (2015) proposed the use of new paramagnetic insulators, in particular, gadolinium gallium garnet ($Gd_3Ga_5O_{12}$ or GGG), to search for spin-dependent interactions. Ledbetter *et al.* (2012) proposed a new class of liquid state nuclear-spin comagnetometers with potential sensitivities in the 10^{-11} Hz range for 1 d of measurement and Limes, Sheng, and Romalis (2018) demonstrated new techniques for He-Xe comagnetometry offering superior stability and accuracy. Another new concept being developed by Arvanitaki and Geraci (2014) combines the techniques used in short-distance tests of gravity employing torsion pendulums (Kapner *et al.*, 2007) and microcantilevers (Geraci *et al.*, 2008) with those used in NMR experiments in order to search for short-range monopole-dipole interactions.

Jackson Kimball, Sushkov, and Budker (2016) recently predicted that a ferromagnetic needle will precess about the axis of a magnetic field at a Larmor frequency Ω when $I\Omega \ll N\hbar$, where I is the moment of inertia of the needle about the precession axis and N is the number of polarized spins in the needle. In this regime the needle behaves as a gyroscope with spin $N\hbar$ maintained along the easy axis of the needle by the crystalline and shape anisotropy. Such a precessing ferromagnetic needle is a correlated system of N spins that can be used to measure magnetic fields for long times. In principle, by taking advantage of rapid averaging of quantum uncertainty, the sensitivity of a precessing needle magnetometer can far surpass that of magnetometers based on spin precession of atoms in the gas phase. Under conditions where noise from coupling to the environment is subdominant, the scaling with measurement time t of the quantum- and detection-limited magnetometric sensitivity is $t^{-3/2}$. If a magnetometer based on a precessing ferromagnetic needle can be experimentally realized, a measurement of needle precession averaged over $\approx 10^3$ s could reach a sensitivity to exotic electron-spin-dependent couplings at an energy scale of $\approx 10^{-26}$ eV. If such an experimental sensitivity could be achieved in practice, it would probe exotic spin-dependent interactions more than 5 orders of magnitude weaker than present laboratory limits.

VIII. SEARCHES FOR EXOTIC SPIN-INDEPENDENT INTERACTIONS

A. Introduction

One of the exotic potentials described by the MWDM formalism deserves special attention, namely, $\mathcal{V}_1$ [Eq. (49)]—the sole potential among those discussed in Sec. VII that has no dependence on the spins of the interacting fermions. Experimental searches for such exotic spin-independent interactions have a long history, mostly from the perspective of tests of the inverse-square law (ISL) of gravity. Originally the idea was to see if the gravitational force law followed the form (Adelberger, Heckel, and Nelson, 2003)

$$\mathbf{F}_G(r) = -G\frac{m_X m_Y}{r^{2+\epsilon}}\hat{\mathbf{r}}, \qquad (81)$$

where $\mathbf{F}_G$ is the gravitational force between test masses m_X and m_Y separated by a distance r, G is Newton's gravitational constant, and ϵ is a parameter characterizing deviation from the ISL. Since the r^{-2} scaling of the gravitational force law derives from the geometry of three-dimensional space, it turns out generally that a force law of the form given by Eq. (81) is difficult to motivate from a theoretical perspective. Instead, the modern perspective follows the MWDM formulation, positing a Yukawa-like deviation from the ISL; the common $\alpha - \lambda$ parametrization (Talmadge *et al.*, 1988) found in the literature proposes a modified form of the gravitational potential given by

$$V'(r) = -\frac{Gm_X m_Y}{r}(1 + \alpha e^{-r/\lambda}), \qquad (82)$$

where the parameter α characterizes the strength and λ characterizes the range of the modified gravitational interaction. From the point of view of quantum field theory, such a modification of the gravitational interaction is equivalent to effects generated by the exchange of a new boson as in the MWDM formalism. Typically in the literature such a Yukawa-like, spin-independent interaction is referred to as a *fifth force* (Fujii, 1971; Fischbach *et al.*, 1986). Correspondence between the two viewpoints can be made explicit: exchange of scalar or vector bosons between fermions X and Y can be described by

$$\alpha = \frac{\hbar c}{4\pi Gm_X m_Y}(g_s^X g_s^Y - g_v^X g_v^Y), \qquad (83)$$

where $g_{s,v}^{X,Y}$ characterizes the vertex-level scalar (subscript s) or vector (subscript v) coupling generating a long-range $\mathcal{V}_1$ potential [Eq. (49)]. The range λ is understood in this case to be the reduced Compton wavelength of the new scalar or vector boson. Although there have been numerous alternative theoretical proposals for specific forms of modified gravitational potentials, to a large degree these considerations are moot for experimental work since all searches for ISL violations have to date returned null results; Eq. (82) is entirely adequate for phenomenological comparison of

different experimental constraints. In the event a violation is detected, however, it will be necessary to pursue determination of the specific form of the new interaction.

There have been a number of recent comprehensive reviews on the topic of ISL tests and searches for exotic spin-independent interactions; we refer the interested reader to the works by Adelberger, Heckel, and Nelson (2003), Gundlach (2005), Onofrio (2006), Newman, Berg, and Boynton (2009), Antoniadis *et al.* (2011), Fischbach and Talmadge (2012), Lamoreaux (2012), Murata and Tanaka (2015), and Brax, Fichet, and Pignol (2017) for more details on this subject. In this section we offer a brief overview of the field and recent developments.

B. Motivation and theoretical landscape

Theories motivating searches for ISL violations and fifth forces are often inspired by the inherent conflict between general relativity and quantum field theory. One aspect of this conflict is the *hierarchy problem*, the enormous gulf between the Higgs mass and the Planck mass (discussed in Sec. VII.B). An influential theoretical suggestion that inspired a new generation of short-range ISL tests was the proposal by Arkani-Hamed, Dimopoulos, and Dvali (1998, 1999) that the hierarchy problem could be resolved if there existed relatively large (sub-mm scale) extra compact spatial dimensions in which gravitons could propagate but standard model particles could not. In this scenario, n extra dimensions beyond the ordinary four are compactified with characteristic radius R and the hierarchy problem is resolved by setting the "true" Planck mass $M_{\mathrm{Pl}} \approx M_{\mathrm{EW}}$, the electroweak scale. The observed long-range strength of gravity is a result of the dilution of the field through the extra dimensions, so from Gauss's law the apparent "four-dimensional" Planck mass $M_{\mathrm{Pl}}{}^{*} = \sqrt{\hbar c/G}$ is given by

$$(M_{\mathrm{Pl}}{}^{*})^2 \approx M_{\mathrm{Pl}}{}^2 \left(\frac{R}{\ell_{\mathrm{Pl}}}\right)^n \approx \frac{c^n R^n}{\hbar^n} M_{\mathrm{Pl}}{}^{2+n}, \qquad (84)$$

where $\ell_{\mathrm{Pl}} = \hbar/M_{\mathrm{Pl}}c$ is the true Planck length. Setting $M_{\mathrm{Pl}} \approx M_{\mathrm{EW}}$, for $n = 2$, $R \approx 100~\mu$m. Although recent experiments (Kapner *et al.*, 2007; Bezerra *et al.*, 2011; Sushkov *et al.*, 2011a; Yang *et al.*, 2012; Kamiya *et al.*, 2015; Chen *et al.*, 2016; Tan *et al.*, 2016) and astrophysical constraints (Arkani-Hamed, Dimopoulos, and Dvali, 1999; Barger *et al.*, 1999; Cullen and Perelstein, 1999; Hall and Smith, 1999) have excluded the $n = 2$ possibility, scenarios with $n \geq 3$ and variations on the ideas of Arkani-Hamed, Dimopoulos, and Dvali (1998) involving, for example, extra dimensions with nonuniform compactification scales (Lykken and Nandi, 2000) and alternative metrics for the extra dimensions (Randall and Sundrum, 1999b), including the possibility of infinite-sized extra dimensions (Randall and Sundrum, 1999a), are still viable and provide motivation for continued tests of the ISL.

A second aspect of the conflict between general relativity and quantum field theory is the *cosmological constant problem* or *vacuum energy catastrophe* (Weinberg, 1989). Observational evidence suggests that the accelerating expansion of the Universe may be explained by a nonzero

cosmological constant associated with a vacuum energy density $\rho_{\mathrm{vac}} \approx 4 \times 10^3$ eV/cm^3, the so-called dark energy. However, rough estimates of ρ_{vac} based on the standard model assuming no new physics up to the Planck scale suggest a vacuum energy density $\approx 10^{122}$ eV/cm^3, a staggering discrepancy. The vacuum energy scale derived from cosmological observations corresponds to a length scale

$$\ell_{\mathrm{vac}} \approx \sqrt{4}\frac{\hbar c}{\rho_{\mathrm{vac}}} \approx 100~\mu\mathrm{m}. \qquad (85)$$

A suggested theoretical path toward resolving the cosmological constant problem is the proposal that somehow the gravitational interaction with vacuum fluctuations "cuts off" at length scales $\lesssim \ell_{\mathrm{vac}}$ (Sundrum, 1999), indicating that one might generically expect a change in gravitational physics below $\approx 100~\mu$m. It is suggestive that two of the most significant theoretical problems confronting quantum theories of gravity both indicate a benchmark scale of $\approx 100~\mu$m where a deviation from the ISL might be expected.

As noted in Sec. VIII.A, the existence of new scalar or vector bosons could also give rise to apparent violations of the ISL due to the appearance of a new Yukawa potential between fermions. Such new bosons commonly appear in grand unification theories such as string theory (Bailin and Love, 1987) as well as in related theories involving extra dimensions such as those previously discussed (Antoniadis, Dimopoulos, and Dvali, 1998), supersymmetric theories (Taylor, 1990), and many others (Adelberger, Heckel, and Nelson, 2003; Antoniadis *et al.*, 2011; Dobrescu and Mocioiu, 2006). Two specific examples from string theory are often cited as possible targets of searches: radions (Brans and Dicke, 1961), which are scalar bosons related to the radius of extra dimensions, and dilatons (Arvanitaki, Huang, and Van Tilburg, 2015), which are scalar bosons that determine the interactions between particles in string theory. Particles such as radions and dilatons are known collectively as moduli, scalar bosons whose expectation values determine key parameters in string theory (Schellekens, 2013).

Another important theoretical motivation to search for new scalar bosons is the idea of *quintessence*, the proposal that the accelerating expansion of the Universe is a result of the potential energy of a scalar field; for reviews see Padmanabhan (2003), Peebles and Ratra (2003), Frieman, Turner, and Huterer (2008), Linder (2008), and Tsujikawa (2013). Furthermore, there have been a number of proposals that attempt to explain dark energy as a modification of gravity at cosmological distance scales; for a review, see Joyce *et al.* (2015). To produce the observed accelerating expansion, the modification of gravity would correspond to a long-range scalar interaction. However, modified gravity at such large distance scales immediately confronts stringent observational tests at the solar system scale and shorter distances (Will, 2014) and is ruled out. To avoid these observational constraints, there have been a number of proposals that the new scalar component of gravity is somehow screened within the solar system, for example, via self-interactions (Khoury and Weltman, 2004b; Olive and Pospelov, 2008), modified Newtonian dynamics [MOND; see, for example, the work of

Milgrom (1983)], or other nonlinearities (Vainshtein, 1972). These screening mechanisms are, in turn, associated with new particles such as chameleons (Khoury, 2013) and galileons (Nicolis, Rattazzi, and Trincherini, 2009) that can be searched for in laboratory experiments.

C. Laboratory tests

Many experimental searches for fifth forces and tests of the ISL employ torsion pendulums, an experimental technique discussed in Sec. VII.E in the context of searches for spin-dependent interactions (see Fig. 15 and surrounding discussion). Torsion-pendulum tests of the ISL are reviewed by Adelberger *et al.* (2009) and Newman, Berg, and Boynton (2009); recent torsion-pendulum experiments by Kapner *et al.* (2007), Yang *et al.* (2012), and Tan *et al.* (2016) have established the most stringent constraints on α for $10^{-5} \lesssim \lambda \lesssim 10^{-2}$ m [Eq. (82)], probing the theoretically interesting region of parameter space covering up to 3 orders of magnitude below the nominal strength of gravity around the dark energy scale of $\ell_{vac} \approx 100\ \mu$m. Between 5 and 15 μm, the best constraint on a fifth force comes from measurements employing a $\approx 1\ \mu$g test mass attached to a cryogenic microcantilever and a source mass with alternating 100-μm-wide gold and silicon strips that are moved beneath the cantilever (Geraci *et al.*, 2008).

A feature common to all recent torsion-pendulum tests of the ISL and microcantilever experiments is the use of a thin conducting membrane between the source and test masses that acts as an electrostatic shield. Because of the challenges related to manufacturing conducting membranes thinner than a few microns, experimental tests of the ISL below a few microns have generally had to contend with distant-dependent electromagnetic forces due to the Casimir effect (Lamoreaux, 1997) and electrostatic patch potentials (Kim *et al.*, 2010; Sushkov *et al.*, 2011b). The Casimir effect [reviewed by Lamoreaux (2005), for example] is the attraction or repulsion between objects due to modification of the electromagnetic vacuum modes in the space between the objects, which appears as an additional short-range force. Precise comparisons between Casimir effect measurements and calculations provide some of the best constraints on fifth forces for $10^{-7} \lesssim \lambda \lesssim 10^{-5}$ m (Masuda and Sasaki, 2009; Bezerra *et al.*, 2011; Sushkov *et al.*, 2011a). Experiments by Chen *et al.* (2016) employing a micromechanical torsional oscillator have recently probed the $4 \times 10^{-8} \lesssim \lambda \lesssim 10^{-5}$ m range by coating the surface of an alternating density source mass with gold in order to keep the Casimir effect uniform as the position of the source mass is varied (Matloob and Falinejad, 2001; Decca *et al.*, 2005), improving on the Casimir effect measurement constraints on α by several orders of magnitude. Of note at this distance scale are continuing efforts to use ultracold atoms as force sensors near dielectric surfaces to probe short-range gravity (Ferrari *et al.*, 2006; Wolf *et al.*, 2007; Sorrentino *et al.*, 2009; Pelle *et al.*, 2013).

At even smaller length scales, on the order of 0.01 to 10 nm, the best constraints on fifth forces come from experiments measuring the scattering of neutrons off of noble gas atoms (Pokotilovski, 2006; Nesvizhevsky, Pignol, and Protasov,

2008; Kamiya *et al.*, 2015). Atomic and molecular spectroscopy can also produce meaningful constraints at this length scale. In particular, spectroscopy of atomic hydrogen (Wan-Ping, Peng, and Hao-Xue, 2015; Dahia and Lemos, 2016a) and molecular hydrogen (H_2, HD, and D_2) (Gato-Rivera, 2015; Salumbides *et al.*, 2015) has been used in conjunction with theoretical calculations of atomic and molecular energy levels to constrain the models of gravity postulating extra dimensions discussed in Sec. VIII.B.

Another closely related class of experimental probes of gravity involve tests of the Einstein equivalence principle (EEP) that underpins general relativity. The EEP states that any local experiment (local in the sense that gravitational tidal effects may be neglected) cannot distinguish between a gravitational field and an acceleration of the laboratory. Tests of the EEP are discussed in Sec. X and include recent precise measurements of the gravitational redshift using atom interferometry by Müller, Peters, and Chu (2010), Poli *et al.* (2011), and Zhou *et al.* (2015) that verify the predictions of general relativity with an accuracy better than 10^{-8}. An alternative approach to testing the EEP employing atomic spectroscopy has achieved a sensitivity matching that of atom interferometry: Hohensee *et al.* (2013) used measurements of the transition frequency between two nearly degenerate opposite-parity states of atomic dysprosium over the course of two years to constrain electron-related anomalies in gravitational redshifts at the 10^{-8} level.

As mentioned in Sec. VIII.B, theoretical attempts to ascribe the accelerating expansion of the Universe to a long-range modification of gravity appear to require a screening mechanism in order to evade experimental limits on fifth forces. Experiments using atom interferometry have established the most stringent constraints on such theories (Burrage *et al.*, 2016; Elder *et al.*, 2016). Hamilton *et al.* (2015) used a Cs matter-wave interferometer near a spherical source mass in an ultrahigh vacuum chamber, thereby reducing any screening mechanisms by searching for a fifth force with individual atoms rather than bulk matter (in contrast to the torsion pendulum, microcantilever, and Casimir-effect experiments).

It is notable that the types of scalar particles that would mediate fifth forces, such as dilatons (Van Tilburg *et al.*, 2015), may also constitute the dark matter (in the same way that the axions and ALPs mediating spin-dependent interactions can be dark matter, as mentioned in Sec. VII.H). Consequently, atomic physics techniques can be employed to search for dark matter scalar bosons as discussed in detail in Sec. IX. There are also a number of new proposals on the horizon that promise improved sensitivity to spin-independent interactions at various length scales and new ways to test the EEP and ISL: examples include experiments employing optically trapped microspheres and nanospheres (Geraci, Papp, and Kitching, 2010; Geraci and Goldman, 2015), Bose-Einstein condensates (Dimopoulos and Geraci, 2003), novel atom interferometry experiments (Hohensee *et al.*, 2012), and measurements employing trapped neutrons (Abele *et al.*, 2010). An alternative way to look for exotic interactions is to see if, for example, a mass can source a scalar field that changes fundamental constants; such an experiment

can be competitive with those searching directly for new forces as surveyed in this section (Leefer *et al.*, 2016).

IX. SEARCHES FOR LIGHT DARK MATTER

A. Introduction

A variety of astrophysical and cosmological measurements (Bertone, Hooper, and Silk, 2005; Feng, 2010; Gorenstein and Tucker, 2014) strongly suggest that over 80% of all matter in the Universe is invisible, nonluminous dark matter. Understanding the microscopic DM nature is one of the paramount goals of cosmology, astrophysics, and particle physics, since it will not only reveal the origins of the dominant constituent of matter in the Universe but also offer insight into the cosmology of the early Universe, uncover new physical laws, and potentially lead to the discovery of other fundamental forces.

The evidence for DM is derived from observations of DM's gravitational effects at the galactic scale and larger: galactic rotation curves (Zwicky, 1933; Rubin and Ford, 1970; Rubin, Ford, and Thonnard, 1980), gravitational lensing (Tyson, Kochanski, and Dell'Antonio, 1998; Refregier, 2003), the bullet cluster (Clowe *et al.*, 2006) and other galactic cluster studies (Lewis, Buote, and Stocke, 2003), large-scale structure of the Universe (Allen *et al.*, 2003), supernovae surveys (Riess *et al.*, 1998; Perlmutter *et al.*, 1999), and the cosmic microwave background radiation (Komatsu *et al.*, 2011). All these observations point toward the existence of DM. In order to fully elucidate the nature of DM, terrestrial experiments seek to measure nongravitational interactions of DM with standard model particles and fields. However, the vast extrapolation from the $\gtrsim 10$ kpc distances associated with astrophysical observations to particle physics phenomena accessible to laboratory-scale experiments leaves open a vast number of plausible theoretical possibilities worth exploring.

In order to develop an experimental strategy for terrestrial DM detection, it is useful to consider what can be surmised about the local DM environment of our Solar System based on astrophysical observations. The local DM density is best estimated from the galactic rotation curve of the Milky Way, which it turns out is rather challenging to measure from the vantage point of our Solar System. Furthermore, in the end, the galactic rotation curve offers only incomplete information on the local DM density since it is sensitive to the integrated mass density between our location and the center of the Galaxy, and the mass density near the Galactic center is notoriously difficult to determine. Nonetheless, based on numerical models (Bergström, Ullio, and Buckley, 1998) and observations of other similar spiral galaxies (Salucci and Borriello, 2003), it is believed that the Milky Way is embedded within and rotates through a spherical DM halo.

The commonly used standard halo model predicts that the DM energy density local to the Solar System is $\rho_{\rm DM} \approx 0.3\text{--}0.4$ GeV/cm^3; this corresponds to a mass density equivalent to one hydrogen atom per a few cm^3. Further, in the galactic rest frame the velocity distribution of DM objects is isotropic and quasi-Maxwellian, with dispersion $v \approx 290$ km/s and a cutoff above the galactic escape velocity of $v_{\rm esc} \approx 550$ km/s (Freese, Lisanti, and Savage, 2013).

The Milky Way rotates through the DM halo with the Sun moving at ≈ 220 km/s roughly toward the Cygnus constellation. Therefore one may think of a DM "wind" impinging upon the Earth, with typical relative velocities $v_g \approx 300$ km/s $\approx 10^{-3} c$. The speed of the Earth with respect to the DM halo is also seasonally modulated at a level of $\approx 10\%$ due to the Earth's orbit around the Sun. Furthermore, the prevailing view based on astrophysical observations is that the DM is cold, i.e., moving with velocities much smaller than the speed of light.

To date, experimental efforts to detect DM have largely focused on weakly interacting massive particles (WIMPs), with masses between 10 and 1000 GeV (Bertone, Hooper, and Silk, 2005; Feng, 2010). Despite considerable effort, there are no conclusive signs of WIMP DM interactions, even as experimental sensitivities have improved rapidly in recent years. While the WIMP is theoretically well motivated, it is by no means the only DM candidate. Observational limits permit the mass of DM constituents to be as low as 10^{-33} GeV or as high as 10^{48} GeV. A number of candidates inhabit this vast parameter space, ranging from ultralight axions and axionlike particles, which are discussed in relation to new interactions in Secs. VII and VIII, to more complex dark sectors that lead to composite DM "clumps."

While particle detectors work by measuring energy deposition, precision measurement techniques are well suited for detecting candidates that act as coherent entities on the scale of individual detectors (or networks of detectors). Aided by recent advances in fields such as optical and atomic interferometry, magnetometry, and atomic clocks, several promising new experimental concepts have been recently proposed to employ these technologies to search for DM candidates with masses between 10^{-33} and 10^{-12} GeV. Methods to probe ultraheavy, composite DM candidates with astrophysical and terrestrial measurements have also emerged.

The key idea behind these concepts is that light DM particles have large mode occupation numbers and their phenomenology is described by a classical field. For this mass range the DM candidates are necessarily bosonic: noninteracting fermionic candidates would require larger masses to reproduce the standard halo model velocity distribution [if the mass of the DM particle is smaller than ≈ 10 eV then the corresponding Fermi velocity exceeds the galactic escape velocity, see Derevianko (2016)]. The lower-mass limit of 10^{-24} eV comes from requiring that the de Broglie wavelength is smaller than the size of galaxies where gravitational signatures of DM have been observed. While such classical fields may arise in a wide variety of DM models, their effects on standard model particles include a finite number of possibilities (see Table II): the classical field can cause precession of nuclear and electron spins, drive currents in electromagnetic systems, and induce equivalence-principle-violating accelerations of matter (Graham and Rajendran, 2013). They could also modulate the values of the fundamental "constants" of nature, which can induce changes in atomic transition frequencies (Derevianko and Pospelov, 2014; Arvanitaki, Huang, and Van Tilburg, 2015) and local gravitational field (Geraci and Derevianko, 2016). Some of these phenomena have been searched for in other

TABLE II.   Current experimental efforts in searches for bosonic ultralight dark matter candidates. The table lists illustrative couplings of bosonic ultralight dark matter candidates (scalar φ, axion a, and dark photon A'_μ) to SM fields, and their experimental effects. h, $G^{\mu\nu}$, $F^{\mu\nu}$, and ψ represent, respectively, SM Higgs, gluon, photon, and fermion fields, or operators of that form. $\mathcal{O}_{\mathrm{SM}}$ stands for terms from the SM Lagrangian density. $n = 1$, 2 for linear and quadratic couplings. Axion E&M refers to the coupling between axions and the electromagnetic field (photons) and EMF stands for electromotive force. Free fields cause signal oscillations at the field Compton frequency and self-interacting fields forming DM "clumps" can cause transient effects. Specific experiments are discussed in Sec. IX.B. The table is not exhaustive, as, for example, the GPS.DM and GNOME experiments could be sensitive to monopole topological defects which require vector fields. Adapted from Graham, Kaplan *et al.*, 2016.

Spin	Type	Operator	Interaction	DM effects	Searches
0	Scalar	$\varphi h^\dagger h$, $\phi^n \mathcal{O}_{\mathrm{SM}}$	Higgs portal or dilaton	Fundamental constant variation	Atomic clocks, GPS.DM
		$a G^{\mu\nu}\tilde{G}_{\mu\nu}$	Axion QCD	Nucleon EDM	CASPEr electric
	Pseudoscalar	$a F^{\mu\nu}\tilde{F}_{\mu\nu}$	Axion E&M	EMF along B field	ADMX, CULTASK, MADMAX
		$(\partial_\mu a)\bar{\psi}\gamma^\mu\gamma_5\psi$	Axion fermion	Spin torque	CASPEr wind, GNOME, QUAX
1	Vector	$F'_{\mu\nu}F^{\mu\nu}$	Vector-photon mixing	EMF in vacuum	DM Radio, ADMX
		$F'_{\mu\nu}\bar{\psi}\sigma^{\mu\nu}\psi$	Dipole operator	Spin torque	CASPEr wind
	Axial vector	$A'_\mu\bar{\psi}\gamma^\mu\gamma^5\psi$	Minimally coupled	Spin torque	CASPEr wind

contexts described throughout this review (see Secs. II, VII, VIII, X, and XI). Here we examine the particular characteristics of effects induced by light DM fields and how precision measurement techniques such as NMR, atomic and SQUID magnetometry, electromagnetic resonators, atomic and optical interferometers, and atomic clocks can be used to search for these effects. When the mass of the particle constituting the DM is sufficiently light, the classical DM field leads to persistent time-varying signals that are localized in frequency at the DM mass, enabling rejection of technical noise while permitting signal amplification through resonant schemes. The classical fields sourced by "clumpy" DM could cause transient signals that can be observed by correlating output from multiple synchronized detectors.

The entire field of laboratory cosmology, where table-top-scale precision measurement experiments search for terrestrial signatures of effects related to light DM, has emerged as a vibrant research area over the last few years with a number of promising new proposals joining several ongoing experiments. As noted, based purely on the known properties of DM, the range of parameter space to be explored is vast. However, experiments can be guided by clues from other fields of physics suggesting mysteries that can be solved by postulating, for example, new DM candidates with particular properties—this is what distinguishes the most theoretically well-motivated light DM candidates (by the Occam's razor principle).

Among the most well-motivated light DM candidates is the QCD axion, discussed in Sec. VII.A.3; experimental axion searches were recently reviewed by Graham *et al.* (2015). Axions can naturally constitute a significant fraction of DM: for example, they can be produced in sufficient abundance in the early Universe via the so-called vacuum realignment process (Abbott and Sikivie, 1983; Dine and Fischler, 1983; Preskill, Wise, and Wilczek, 1983). This process results from a misalignment between the axion field generated when axions are first produced via spontaneous symmetry breaking and the minimum of the potential generated by QCD interactions. Since the axion field is initially perturbed from the QCD potential minimum, it will oscillate; these oscillations are not significantly damped over the age of the Universe and in fact in most models it is the energy stored in these coherent oscillations of

the axion field that constitute the mass energy ascribed to DM (Dine and Fischler, 1983; Preskill, Wise, and Wilczek, 1983; Duffy and Bibber, 2009). Similar scenarios describe the production of most light bosons. Another axion production mechanism is through the decay of topological defects such as domain walls or strings (Davis, 1985; Nagasawa and Kawasaki, 1994; Chang, Hagmann, and Sikivie, 1998), where the topological defects interpolate between regions of space with different axion vacuum fields which can exist, for example, due to nontrivial vacuum structure (i.e., multiple equivalent local minima in the self-interaction potential).

QCD axions couple to photon, gluon, and fermion spins over a predictable range of axion mass-coupling strength parameter space (Abbott and Sikivie, 1983; Dine and Fischler, 1983; Preskill, Wise, and Wilczek, 1983). There are three possible interactions of axions with standard model particles and fields: axions can couple to electromagnetism, induce EDMs for nucleons (see Sec. V) via interaction with the gluon field, and can cause precession of electron and nucleon spins (see Table II).

There are robust astrophysical constraints on QCD axions with masses $\gtrsim 10$ meV based on the observation of the neutrino signal from supernova 1987A and star cooling (Raffelt, 1999). Heavier axions would have produced observable effects in astrophysical objects, and much heavier axions would already have been seen in terrestrial experiments. Constraints have also been considered for QCD axions with masses $\lesssim 1$ μeV based on cosmology. However, these constraints depend upon assumptions about unknown initial conditions of the Universe. Such lighter-mass QCD axions were never ruled out by either experimental or astrophysical observations, but theory prejudice held that they were less likely based on cosmology. It has now been realized that this was based on a particular scenario for the earliest epochs in the Universe, a time about which we know little. Since the inception of this cosmological argument against lower-mass QCD axions, inflation has become the dominant paradigm for the birth of the Universe. This along with other factors led to alternative possibilities for axion production in the early Universe which allow a much larger mass range for the QCD axion, and in fact bestow the lighter axions with a strong theoretical motivation (Freivogel, 2010; Linde, 1988).

Going beyond the QCD axions, SM extensions offer a plenitude of ultralight DM candidates. We collectively refer to such candidates as virialized ultralight fields (VULFs). Possibilities are compiled in Table II, where the fields are characterized by their spin and intrinsic parity. As noted, in the considered mass range (<10 eV) the DM candidates are necessarily bosonic. In particular, spin-1 particles, commonly referred to as dark or hidden photons (see Sec. VII.B.5), could conceivably constitute a substantial fraction of the DM (Arias *et al.*, 2012; Nelson and Scholtz, 2011; Foot and Vagnozzi, 2015). Table II also indicates various potential DM couplings to SM fields. More broadly, the possible *nongravitational* couplings can be classified according to "portals" that correspond to different gauge invariant operators of the SM fields coupling to operators that contain fields from the dark sector. This phenomenological approach is widely used in particle physics for searches of DM and dark forces (Rouven *et al.*, 2013). For example, for scalar DM fields φ, the following portals may arise (Derevianko and Pospelov, 2014):

$$\mathcal{L}_1 = \frac{\partial_\mu \varphi}{\Lambda} \sum_{\text{SM particles}} c_\psi \bar{\psi} \gamma_\mu \gamma_5 \psi \qquad \text{axionic portal,}$$

$$\mathcal{L}_2 = \frac{\varphi}{\Lambda} \sum_{\text{SM particles}} c_\psi^{(s)} m_\psi \bar{\psi} \psi \qquad \text{linear scalar,}$$

$$\mathcal{L}_3 = \frac{\varphi^2}{\Lambda^2} \sum_{\text{SM particles}} c_\psi^{(2s)} m_\psi \bar{\psi} \psi \qquad \text{quadratic scalar,}$$

$$\mathcal{L}_4 = \frac{i\varphi^* \partial_\mu \varphi}{\Lambda^2} \sum_{\text{SM particles}} g_\psi \bar{\psi} \gamma_\mu \psi \qquad \text{current-current.}$$

Here ψ are SM fermion fields with associated masses m_ψ, Λ are the energy scales, and c_i are individual coefficients that can take on different values depending on the type of ψ. This classification can be generalized to include the SM gauge bosons, for example, of the form $\varphi F_{\mu\nu} F^{\mu\nu}$ for electromagnetism and extended further to nonscalar DM fields.

While the phenomenological portal classification is broad, one should be aware of certain existing astrophysical and laboratory constraints on the coupling strengths or energy scales Λ. For example, the hypothesized DM fields can mediate forces and thus the limits from fifth-force experiments (Sec. VIII) immediately apply. Thereby an experiment searching for DM signatures through a specific portal must probe yet unexplored parameter space. In some cases, the broader search may soften such constraints. For example, the discussed bounds on the QCD axion are relaxed for ALPs (Massó and Redondo, 2005). ALPs are pseudoscalar particles similar in nature to the QCD axion that do not solve the strong *CP* problem, but rather emerge naturally from other frameworks such as string theory. ALPs may also have the properties necessary to solve the hierarchy problem, as discussed in Sec. VII.B.

As mentioned earlier, a distinct theoretical possibility is that DM is not distributed uniformly but rather occurs in the form of clumps. Even the ever-present gravitational interaction leads to instabilities and clumping. Examples of clumpy objects include "dark stars" (Kolb and Tkachev, 1993;

Barranco and Bernal, 2011; Iwazaki, 2015; Braaten, Mohapatra, and Zhang, 2016), Q balls (Coleman, 1985; Kusenko and Steinhardt, 2001), solitons, and clumps formed due to dissipative interactions in the DM sector. Alternatively, a significant fraction of the DM mass energy could be stored in "topological defects" manifesting as monopoles, strings, or domain walls (Vilenkin, 1985). If DM takes such a form, terrestrial detectors would not register a continuous oscillating signal associated with VULFs, but rather would observe transient events associated with the passage of the detector through such a DM object (Pospelov *et al.*, 2013; Derevianko and Pospelov, 2014; Budker and Derevianko, 2015). Self-interacting fields can include bosonic and fermionic DM candidates. The characteristic spatial extent of topological defects is determined by the Compton wavelength of the underlying DM field. For an Earth-sized object, the characteristic mass is $\approx 10^{-14}$ eV which places such DM fields in the category of ultralight candidates.

B. Experimental searches

Axion and ALP searches can be classified into different categories depending on where the detected particles are produced. For example, in "light shining through walls" (LSW) experiments (Robilliard *et al.*, 2007; Redondo and Ringwald, 2011), axions are created in the experiment from an intense laser light field and a static field of a strong magnet which facilitates mixing between photons and axions. These axions are then detected by converting them back to photons after they cross a wall that is transparent to them but completely blocks the light. In "helioscope" experiments (Raffelt, 1999; Graham *et al.*, 2015), the task of producing axions or ALPs is "subcontracted" to the Sun (hence the name), but detection is accomplished as in LSW experiments. Finally, "haloscopes" directly detect the DM from the galactic halo. In a somewhat complementary approach, indirect experiments search for modifications of the known interactions via exchange of virtual exotic particles. Such experiments include the "fifth-force" searches and experiments looking for exotic spin-dependent interactions or modification of fundamental constants in the presence of massive and/or spin-polarized objects that presumably act as sources of the virtual exotic particles. We discuss some examples of direct experimental searches of different kinds next, while indirect searches are discussed in Secs. VII and VIII. The direct detection of clumpy DM objects requires networks of precision measurement tools, and we discuss here two ongoing searches with magnetometers and atomic clocks.

1. Microwave cavity axion experiments

Microwave cavity searches for dark matter axions were reviewed by Bradley *et al.* (2003). The first experiment to search for light DM composed of QCD axions was the ADMX, which began its work in the 1990s (Asztalos *et al.*, 2001, 2010). This experiment exploits the coupling of the QCD axion to the electromagnetic field to convert axions into microwave photons in a strong magnetic field $\mathcal{B}$ (Fig. 19). In general, pseudoscalar particles such as axions and ALPs can
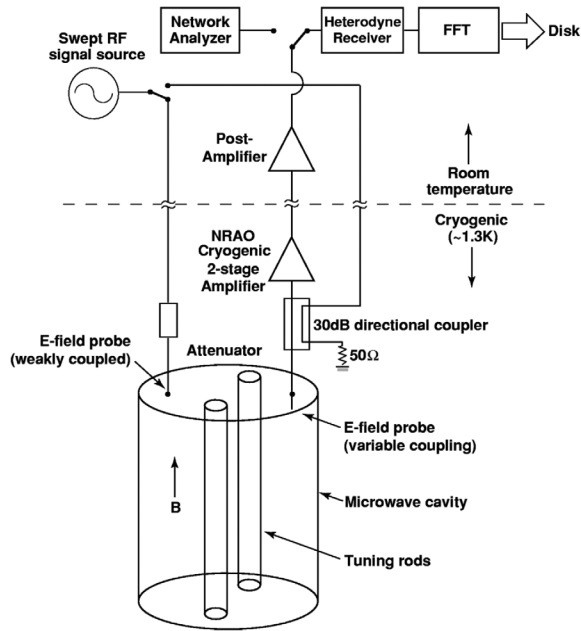
FIG. 19. Schematic diagram of the ADMX experiment. Photons produced in the microwave cavity by the interaction of an axion field $a(\mathbf{r}, t)$ with the magnetic field $\mathcal{B}$ [Eq. (86)] are detected by the electric field probes. Tuning rods enable the resonant frequency of the cavity to be scanned to search for axions of different masses. (Fields from the rf signal source can be sent through the setup for calibration purposes.) The signals are recorded after multiple amplification stages and heterodyning. The 2001 experiment employed cryogenic heterojunction field-effect transistors built by the National Radio Astronomy Observatory (NRAO), while new versions of ADMX employ SQUID amplifiers (Asztalos *et al.*, 2010). From Asztalos *et al.*, 2001.

be produced by the interaction of two photons via a process known as the Primakoff effect (Primakoff, 1951), and consequently an axion and ALP interacting with an electromagnetic field can produce a photon via the inverse Primakoff effect (Raffelt and Seckel, 1988). This process was proposed by Sikivie (1983, 1985) as a method to search for DM axions (haloscope experiment) as well as axions emitted by the Sun (helioscope experiment). The nonrelativistic Lagrangian describing this interaction is

$$\mathcal{L}_{a\gamma\gamma} = g_\gamma \frac{\alpha}{\pi} \frac{a(\mathbf{r}, t)}{f_a} \mathcal{E} \cdot \mathcal{B}, \tag{86}$$

where g_γ is the coupling constant describing the strength of the axion-photon interaction, α is the fine-structure constant, $a(\mathbf{r}, t)$ is the axion field, f_a is the symmetry breaking scale associated with the axion (see Sec. VII.C), and $\mathcal{E}$ and $\mathcal{B}$ are the electric and magnetic fields. This interaction corresponds to the axion-E&M entry in Table II. In the ADMX experiment, $\mathcal{B}$ is generated with a superconducting solenoid and $\mathcal{E}$ is the electric field of the resultant microwave photon produced by the inverse Primakoff effect. The resonant frequency of the cavity can be tuned so that it matches the frequency of the microwave photons produced by the interaction of $a(\mathbf{r}, t)$ with $\mathcal{B}$, which have energy corresponding to

$$E_\gamma \approx m_a c^2 + \tfrac{1}{2} m_a c^2 \beta^2, \tag{87}$$

where m_a is the axion mass and $\beta = v/c \approx 10^{-3}$ is the relative velocity of the laboratory with respect to the rest frame of the axion field. As noted in the Introduction to this section, the dispersion of the axion velocities is roughly on the same order as β, i.e., $\Delta\beta \approx 10^{-3}$, so the axionic DM would produce a relatively narrow microwave resonance:

$$\Delta\omega/\omega \sim (\Delta\beta)^2 \sim 10^{-6}. \tag{88}$$

ADMX is to date the first and only experiment to probe the particularly interesting region of parameter space corresponding to standard QCD axion models, namely, the KSVZ and Dine-Fischler-Srednicki-Zhitnitskii (DFSZ) family of models (Kim, 1979; Shifman, Vainshtein, and Zakharov, 1980; Zhitnitskii, 1980; Dine, Fischler, and Srednicki, 1981), in a band of axion masses near $\approx 2 \times 10^{-6}$ to $\approx 4 \times 10^{-6}$ eV. A new effort to extend the ADMX experiment to search for higher mass axions using correspondingly higher frequency microwave cavities, known as HAYSTAC—Haloscope At Yale Sensitive To Axion Cold dark matter (van Bibber and Carosi, 2013), has recently produced its first results (Brubaker *et al.*, 2017). HAYSTAC was able to probe higher axion masses with improved sensitivity by pushing to lower temperatures and leveraging recent progress in quantum electronics; HAYSTAC has probed the KSVZ parameter space in a band of axion masses near $\approx 24 \times 10^{-6}$ eV (Brubaker *et al.*, 2017). The ADMX and HAYSTAC Collaborations plan a systematic search for QCD axions with masses between $m_a c^2 \approx 10^{-6}$ and $\approx 10^{-4}$ eV by 2021.

Another significant microwave cavity experimental program is underway at the Center for Axion and Precision Physics Research (CAPP) at KAIST in South Korea (Youn, 2016; Semertzidis, 2017), where researchers are developing stronger magnets, new low-noise amplifiers (e.g., based on Josephson parametric amplifiers), and superconducting cavities with novel designs to increase their Q and expand their volume. The CAPP haloscope, known as CULTASK (CAPP's ultra low temperature axion search in Korea), aims to target an axion mass range near $\approx 10^{-5}$ eV.

A new broadband axion DM haloscope experiment aimed at detecting axions with $m_a \approx 10^{-4}$ eV proposed by Jaeckel and Redondo (2013) is under development at the Max Planck Institute for Physics (Caldwell *et al.*, 2017). This project, named MADMAX, is based on axion-photon conversion at the transition between different dielectric media. By using ≈ 80 dielectric disks immersed in a ≈ 10 T magnetic field, the emitted power is enhanced by a factor of $\approx 10^5$ over that from a single mirror (flat dish antenna).

2. Spin-precession axion experiments

A new experiment recently proposed by Budker *et al.* (2014) to search for lighter QCD axions and ALPs using different couplings from those exploited in ADMX and similar microwave cavity experiments is the cosmic axion spin precession experiment (CASPEr). CASPEr exploits both the axion-gluon coupling, which generates a time-varying

EDM of nuclei[6] (CASPEr electric), and the coupling of the axion to nuclear spins (CASPEr wind); see Graham and Rajendran (2013). CASPEr uses NMR techniques for detecting spin precession caused by background axion DM. This approach complements ADMX, HAYSTAC, and CULTASK which are sensitive to higher axion masses and a different coupling.

The key idea underlying the CASPEr concept is that axion DM can cause the precession of nuclear spins in a manner similar to that discussed for exotic spin-dependent interactions and EDMs (Secs. VII and V, respectively). Nuclear spins in a noncentrosymmetric crystal, such as a ferroelectric, experience a large effective electric field (Leggett, 1978; Mukhamedjanov and Sushkov, 2005), a phenomenon analogous to the large internal effective electric fields experienced by electrons in polar molecules (Graham and Rajendran, 2011). The coupling of the axion DM field to nuclear spins (via the generation of electric dipole moments through the axion-gluon coupling) in such a material has the form of a pseudomagnetic field $\mathcal{B}_1^*$ oscillating at the axion Compton frequency. If the external bias magnetic field $\mathcal{B}_0$ is set to a value such that the nuclear spin splitting matches this frequency, a resonance condition is achieved, and the nuclear spins and the corresponding magnetization **M** tilt and undergo Larmor precession (see Fig. 20). A sensitive magnetometer, such as a SQUID, placed next to the sample, detects the oscillating transverse magnetization. The experimental protocol of CASPEr electric is to sweep the externally applied bias magnetic field and search for a nonzero magnetometer response, which is a signature of spin coupling to the axion DM field. CASPEr electric has the potential to reach sensitivity to QCD axions over a mass range of $10^{-14} \lesssim m_a c^2 \lesssim 10^{-9}$ eV and search a significant fraction of unexplored parameter space for ALPs up to masses of $\approx 10^{-7}$ eV (Budker *et al.*, 2014; Jackson Kimball *et al.*, 2017).

CASPEr wind is an example of an experiment specifically sensitive to ALP DM (at least in its present form, it will not have sufficient sensitivity to reach parameter space corresponding to the QCD axion). CASPEr wind is analogous to CASPEr electric, except that the pseudomagnetic field $\mathcal{B}_1^*$ is generated by a different mechanism: the coupling of nuclear spins to the spatial gradient of the ALP DM field (the so-called "ALP wind"). This enables the use of materials such as liquid xenon without electric fields. Xenon can be efficiently spin polarized to enhance the signal. A variety of experimental approaches (Jackson Kimball *et al.*, 2017), including the use of atomic magnetometers (Graham *et al.*, 2017) and zero-to-ultralow-field NMR (Garcon *et al.*, 2018), have been proposed as methods to search for the ALP wind. Abel *et al.* (2017) used the CASPEr wind approach to analyze data

---

[6]As noted by Schiff (1963), the interaction of an EDM of a pointlike particle with an applied electrostatic field is screened in atomic systems, since the constituent charged particles redistribute themselves to cancel the field. However, the screening is incomplete because of finite nuclear size and relativistic effects, which can even enhance the atomic EDM relative to the electron or nuclear EDM in heavy atoms (see Sec. V).
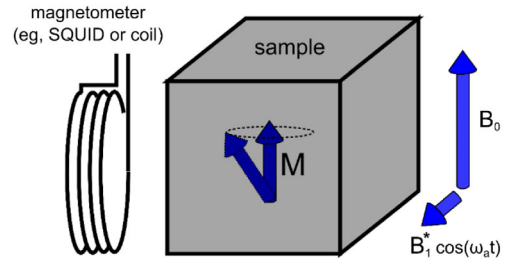

FIG. 20. Experimental concept of CASPEr. The oscillating axion field $a(\mathbf{r}, t)$ acts as a pseudomagnetic field $\mathcal{B}_1^*$, either by inducing an oscillating EDM via the axion-gluon interaction that couples to an electric field (CASPEr electric), or via the interaction of spins with the gradient of $a(\mathbf{r}, t)$ arising from the motion of the sample through the axion field (CASPEr wind). The oscillating $\mathcal{B}_1^*$ causes polarized nuclear spins to tip away from the leading field $\mathcal{B}_0$ and precess at the Larmor frequency. The approach is based on the principles of NMR experiments. From Budker *et al.*, 2014.

from a search for the neutron EDM to constrain ALP DM with $10^{-24} \lesssim m_a c^2 \lesssim 10^{-17}$ eV.

In the KSVZ family of QCD axion models (Kim, 1979; Shifman, Vainshtein, and Zakharov, 1980), the coupling of the axion to electron spins is nominally zero, whereas in the DFSZ family of models (Zhitnitskii, 1980; Dine, Fischler, and Srednicki, 1981), the axion is predicted to couple to the electron spin. Thus, in addition to searches for axion couplings to nuclear spins as searched for in CASPEr, it is of interest to search for axion-electron couplings: this is the target of the QUAX (quaerere axion) experiment (Ruoso *et al.*, 2016). The essence of the experiment, originally outlined by Krauss *et al.* (1985), Barbieri *et al.* (1989), Turner (1990), and Kakhidze and Kolokolov (1991), is quite similar to that of CASPEr, with the important difference that in the QUAX experiment a yttrium iron garnet (YIG) sphere is used as the sample of polarized electron spins as opposed to the polarized nuclear samples studied in CASPEr.

3. Radio axion searches

ADMX, CASPEr, and related experiments are also sensitive to another class of particles known as dark or hidden photons (Wagner *et al.*, 2010), discussed in Sec. VII.B.5. As with ordinary photons, hidden photons are vector particles with spin 1. However, hidden photons have mass and could constitute the DM in a manner similar to axions and ALPs (Arkani-Hamed *et al.*, 2009). Hidden-photon DM can be described as a weakly coupled "hidden electric field," oscillating at the hidden-photon Compton frequency and able to penetrate shielding (Jackson Kimball *et al.*, 2016). At low frequencies (where the wavelength is long compared to the size of the shielding), the interaction of electrons in the shielding material with the hidden-photon field generates a real, oscillating magnetic field. It was recently proposed that such hidden-photon DM can be searched for using a tunable, resonant LC circuit designed to couple to this magnetic field, a "dark matter radio" (Chaudhuri *et al.*, 2015). Hidden-photon DM has an enormous range of possible Compton frequencies, but current experiments (such as ADMX, which is also

sensitive to hidden photons) search only over a few narrow parts of that range (Wagner *et al.*, 2010). In contrast, DM radio has potential sensitivity many orders of magnitude beyond current limits over an extensive range of hidden-photon masses, with $10^{-12} \lesssim m_{\gamma'} c^2 \lesssim 10^{-3}$ eV, where $m_{\gamma'}$ is the hidden-photon mass.

Related proposals for broadband axion and ALP detection with *LC* circuits were developed by Sikivie, Sullivan, and Tanner (2014) and Kahn, Safdi, and Thaler (2016). The concept of these experiments can be understood by noting that the axion-photon coupling effectively modifies Maxwell's equations (Sikivie, 1983, 1985) such that dark matter axions and ALPs generate an oscillating current density in the presence of a magnetic field. These ideas also apply to the high-frequency (10 to 100 GHz) axion search proposed by the MADMAX Collaboration (Jaeckel and Redondo, 2013).

4. Atomic clocks, accelerometers, and spectroscopy

As noted in the Introduction to this section, one of the generic signals VULFs can produce are time-oscillating interactions. An example is DM consisting of dilatons, ultralight scalar particles arising in string theories (Arvanitaki, Huang, and Van Tilburg, 2015). As with axions and ALPs, dilatons form a gas described as a scalar field oscillating at the Compton frequency of the dilaton. This field feebly interacts with normal matter leading to a temporal variation of fundamental constants which in turn affects the "ticking" rates of atomic clocks. Since clocks based on distinct atomic transitions have different sensitivities to a change of constants such as the fine-structure constant α, comparison between such clocks is a sensitive way to detect the variation of the constants (see Sec. II), including those caused by a time-varying DM field. A "differential atomic clock" based on microwave transitions between nearly degenerate metastable states in dysprosium was used by Van Tilburg *et al.* (2015) to search for dilatons in the mass range of 10^{-24} to 10^{-16} eV, improving existing constraints on the electron coupling of a DM dilaton by up to 4 orders of magnitude. These limits were further improved by Hees *et al.* (2016). Modern atomic clocks based on single trapped ions (Huntemann *et al.*, 2016) and ensembles of neutral atoms in optical lattices (Nemitz *et al.*, 2016) are reaching into relative frequency instability levels of a part in 10^{18}, promising a boost in the sensitivity of dilaton searches by about 2 orders of magnitude in the near future.

Also of note is that recently Graham, Kaplan *et al.* (2016) proposed using accelerometers (e.g., torsion balances and atom interferometers) to search for DM-induced forces $-\nabla[M_a(\mathbf{r}, t)c^2]$, where M_a is the DM-renormalized atomic mass. For atomic interferometers, the effects of atomic mass variation during the interferometric sequence and also DM-induced renormalization of the local gravity g dominate over the direct DM-induced forces (Geraci and Derevianko, 2016). Accelerometers are particularly sensitive to vector and scalar VULFs.

Arvanitaki, Dimopoulos, and Van Tilburg (2017) proposed an entirely new spectroscopic scheme for detection of bosonic DM with boson masses between 0.2 and 20 eV: a search for resonant transitions between states in polyatomic molecules driven by the oscillating DM field.

5. Exotic spin-dependent forces due to axions and ALPs

Section VII explores the exotic spin-dependent interactions generated by axions, ALPs, and dark or hidden photons. A recent proposal by Arvanitaki and Geraci (2014) to search for short-range monopole-dipole interactions between nuclei using NMR techniques, the axion resonant interaction detection experiment (ARIADNE), has particular relevance to axion DM searches. The aim of ARIADNE is to detect monopole-dipole interactions between the spins of ^{3}He nuclei and a rotating unpolarized tungsten attractor. The geometry of the experiment is specially designed to be sensitive to QCD axions in the range $10^{-6} \lesssim m_a c^2 \lesssim 10^{-3}$ eV (Geraci *et al.*, 2017). The upper end of the axion mass range to be explored by ARIADNE, well within the astrophysically and cosmologically allowed regions, is particularly difficult for DM detection experiments such as ADMX and CASPEr to access, and so ARIADNE has the potential to fill in an important gap in the explored axion parameter space.

6. Magnetometer and clock networks for detection of transient dark matter signals

If a detection of the QCD axion or other VULF candidates is made, a network of such experiments can be used to verify it, since the signal in all of them should be centered at the axion or ALP Compton frequency, a fundamental constant. A network would also enable the study of spatial coherence of the DM field (Derevianko, 2016) and search for deviations from the standard halo model predictions due to nonuniform or nonisotropic DM flows (Duffy and Sikivie, 2008). Networks of sensors are crucial in order to search for clumpy DM. Here the searches rely on the characteristic time delay of DM-induced signals between the nodes (see Fig. 21), as on average the clumps would sweep the network at galactic velocities.

The global network of optical magnetometers to search for exotic physics (GNOME) Collaboration (Pospelov *et al.*,
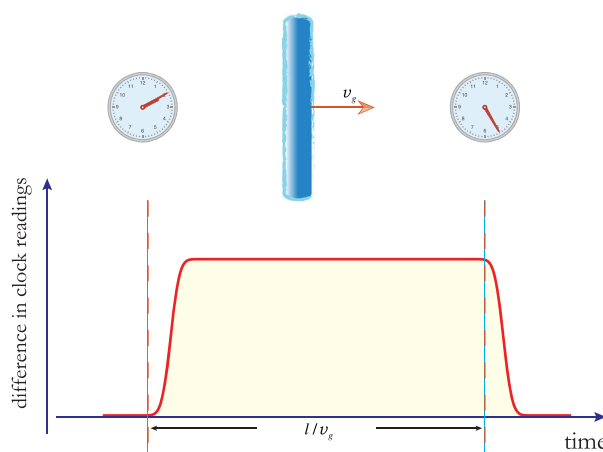

FIG. 21. Spatially separated and initially synchronized identical clocks are expected to exhibit a distinct desynchronization and resynchronization pattern due to an encounter with a DM object. Two clocks are separated by a distance ℓ, and because the wall propagates through the network with a speed $v_g \approx 300$ km/s, the characteristic "hump" persists over time ℓ / v_g. Adapted from Derevianko and Pospelov, 2014.

2013; Pustelny *et al.*, 2013) is searching for such transient signals due to the passage of the Earth through compact DM objects, such as DM domain walls (Pospelov *et al.*, 2013) or DM "stars" (Jackson Kimball, Budker *et al.*, 2018), that couple to atomic spins (similar to the ALP wind coupling searched for by CASPEr). While a single magnetometer system could detect such transient events, it would be exceedingly difficult to confidently distinguish a true signal generated by light DM from "false positives" induced by occasional abrupt changes of magnetometer operational conditions (e.g., magnetic-field spikes, laser-light-mode jumps, electronic noise, etc.). Effective vetoing of false positive events requires an array of magnetometers. Furthermore, there are key benefits in terms of noise suppression and event characterization to widely distributing the magnetometers geographically; see Fig. 22. The Laser Interferometer Gravitational Wave Observatory (LIGO) Collaboration has developed sophisticated data analysis techniques to search for similar correlated "burst" signals from a worldwide network of gravitational-wave detectors (Anderson *et al.*, 2001; Allen *et al.*, 2012), and the GNOME Collaboration has demonstrated that these data analysis techniques can be adapted to analyze data from the GNOME (Pustelny *et al.*, 2013). Presently the GNOME consists of over ten dedicated atomic magnetometers located at stations throughout the world.

If DM leads to the variation of fundamental constants, DM clumps can also manifest themselves as "glitches" of atomic clocks, for example, those onboard satellites of the Global Positioning System (Derevianko and Pospelov, 2014): if particular interactions exist, the clocks would become desynchronized as they are swept by a DM object (Fig. 21). The glitches would propagate through the GPS constellation at galactic velocities ≈ 300 km/s characteristic of the DM halo. The GPS.DM Collaboration is mining over a decade of archival GPS data to hunt for such DM objects, effectively using the GPS constellation as a 50 000-km-aperture DM detector. While the initial search has not found evidence for
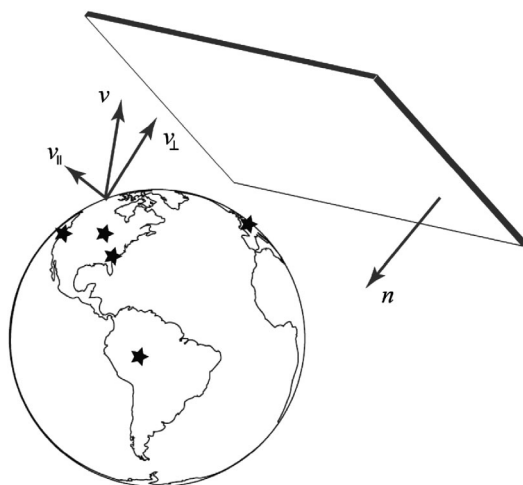

FIG. 22. Schematic of an axion and ALP domain-wall crossing event as searched for by the GNOME. The crossings recorded in four distinct locations (marked with stars) allow determination of the normal velocity $v_\perp$ to the wall and prediction of the timing of the fifth event. From Pospelov *et al.*, 2013.

such DM objects at the current search sensitivity, it improves the current constraints on certain DM couplings by several orders of magnitude (Roberts *et al.*, 2017). Recently, it was also shown that a single optical atomic clock (composed of two independent clock ensembles probed by the same laser) can be sensitive to transient DM interactions and constraints on scalar quadratic DM-clock couplings have been obtained by Wcisło *et al.* (2016). While this colocated clock technique can be used to place limits on DM-clock couplings, the positive DM detection still requires a geographically distributed network. Transient variations of fundamental constants can also be searched for with a global network of laser interferometers (Stadnik and Flambaum, 2015b, 2016).

X. GENERAL RELATIVITY AND GRAVITATION

A. Tests of the Einstein equivalence principle

The equivalence principle can be traced back to the 16th-century observation that all bodies fall to Earth at the same rate of acceleration (Will, 2014). This was a remarkable discovery for it leads to the conclusion that a body's mass is proportional to its weight. The constant of proportionality seems to be independent of material composition or any other detail of the body. That is the basic principle of the equivalence of gravitational mass and inertial mass.

Within the framework of Einstein's theory of general relativity (GR), there is the Einstein equivalence principle (EEP), which includes the following postulates (Will, 2014):

(1) The weak equivalence principle (WEP): the trajectory of a freely falling "test" body is independent of its internal structure and composition. All bodies in a common gravitational field fall with the same acceleration according to WEP. This is also called the universality of free fall (UFF).
(2) Local Lorentz invariance (LLI): the outcome of any local nongravitational experiment conducted in free fall is independent of the velocity and the orientation of the apparatus.
(3) Local position invariance (LPI): the outcome of any local nongravitational experiment is independent of where and when in the Universe it is performed.

Different versions of the EEP appear in the literature; precise formulations of its variants are discussed by Casola, Liberati, and Sonego (2015). AMO tests of LLI are discussed in Sec. XI. Tests of LPI include searches for the temporal and spatial variations of fundamental constants as discussed in detail in Sec. II.

Both GR and the SM are assumed to be low-energy limits of a more complete theory at the high-energy scale. The EEP implies a universal coupling between matter and gravity, i.e., all forms of matter or energy respond to gravity in the same way. However, this may not be the case for most theories aimed at unifying all four fundamental interactions, such as string theories. Any theories in which the coupling constants are spatially dependent violate the WEP, as discussed in Sec. II. On the other hand, the WEP can be tested with experiments complementary to those used to test fundamental constant variation. Thus WEP tests provide additional opportunities to open a low-energy window into the nature

of unification theories. Various theoretical arguments that the EEP is violated at small but measurable levels are discussed in detail by Damour (2012). "Runaway dilaton" models (Damour and Polyakov, 1994; Damour, Piazza, and Veneziano, 2002; Damour, 2012) estimated that the onset of WEP violation may start just beyond the sensitivity of current experiments.

Tests of the equivalence principle as well as more general tests of gravity are reviewed by Will (2014). A review of the past WEP tests and future proposals is given by Sondag and Dittus (2016). Modern tests of the WEP include torsion-balance experiments, free-fall experiments, and the measurement of relative motions of celestial bodies (for example, lunar laser ranging). To quantify violations of WEP, we suppose that the gravitational mass of a body m_g is not equal to its inertial mass m_I. Then the acceleration a of a body in a gravitational field g is given by $\mathbf{a} = (m_g/m_I)\mathbf{g}$. To test WEP, one compares the accelerations a_1 and a_2 of two falling bodies which differ in their composition, and measures the "Eötvös" ratio η

$$\eta = 2\left|\frac{a_1 - a_2}{a_1 + a_2}\right|. \tag{89}$$

The "Eöt-Wash" torsion-balance experiments tested WEP to 10^{-13} by comparing differential accelerations of beryllium-aluminum and beryllium-titanium test-body pairs (Schlamminger *et al.*, 2008; Wagner *et al.*, 2012). Lunar laser-ranging experiments, which measure the differential accelerations of the Earth and the Moon toward the Sun, provided similarly stringent limits to the violation of the equivalence principle (Williams, Turyshev, and Boggs, 2004, 2012). Both the torsion-balance and lunar-laser ranging WEP tests are close to their fundamental limits of accuracy. Macroscopic (i.e., classical) Earth-based free-fall WEP tests are less accurate, reaching the 10^{-10} level (Kuroda and Mio, 1989).

Significant improvement in probing WEP is expected to come from future space-based missions. MicroSCOPE is a Centre National d'Études Spatiales (CNES) and European Space Agency (ESA) gravity-research minisatellite mission (Bergé, Touboul, and Rodrigues, 2015) that aims to test the WEP in space to 10^{-15} by comparing the acceleration experienced by two free-falling test masses in the Earth's gravity field. First results of the MicroSCOPE mission (Touboul *et al.*, 2017), constraints on the violation of the weak equivalence principle by a light scalar dilaton (Bergé *et al.*, 2018), and limits for new long-range forces (Fayet, 2018) were reported. Other macroscopic proposals to test the WEP include the sounding rocket principle of equivalence measurement (Reasenberg *et al.*, 2012) (free-fall stratosphere experiment), Galileo Galilei (Nobili *et al.*, 2012) (space-based torsion-balance experiment), the satellite test of the equivalence principle (Overduin *et al.*, 2012) (free-fall space-based experiment), and others.

The WEP test using both quantum and classical objects was reported by Peters, Chung, and Chu (1999). This experiment compared the values for the local acceleration due to the Earth's gravity g obtained using an atom interferometer based on a fountain of ^{133}Cs laser-cooled atoms and a Michelson-interferometer classical gravimeter which used macroscopic glass object, demonstrating agreement to 7 parts in 10^9. In

subsequent related work, Merlet *et al.* (2010) compared the performance of optical and atom-interferometric gravimeters. Francis *et al.* (2015) reported an international comparison of 25 different gravimeters. Freier *et al.* (2016) reported absolute measurements with a mobile atom-interferometric gravimeter, demonstrating an accuracy of 39 nm/s^2 and long-term stability of 0.5 nm/s^2.

The theoretical framework for WEP tests in the quantum domain is discussed by Herrmann, Dittus, and Lämmerzahl (2012). Weak equivalence tests using quantum matter were made possible by techniques for production and control of ultracold atoms and by the attainment of dilute atomic Bose-Einstein condensates (BECs) (Cornell and Wieman, 2002; Ketterle, 2002). Atom interferometers measuring the difference in phase between matter waves traveling along different paths can be used as accelerometers, offering potential precision tests of GR with quantum rather than classical matter. A good general review of atom interferometry is given by Cronin, Schmiedmayer, and Pritchard (2009) and Tino and Kasevich (2014). Hogan, Johnson, and Kasevich (2009), Kleinert *et al.* (2015), and Tino and Kasevich (2014) reviewed the light-pulse atom interferometry which is employed in most high-precision measurements mentioned in this review and its applications to tests of fundamental physics.

Fully quantum WEP tests with atomic interferometry directly compare the phase shifts of two different types of matter waves without the use of classical gravimeters. The potential of matter-wave interferometers using quantum gases for probing fundamental concepts of quantum mechanics and GR has been discussed by Dimopoulos *et al.* (2007), Herrmann, Dittus, and Lämmerzahl (2012), Müntinga *et al.* (2013), and Biedermann *et al.* (2015). Testing the limits of quantum-mechanical superpositions with different systems was discussed by Arndt and Hornberger (2014).

The sensitivity of atom interferometers to WEP violations increases linearly with the momentum difference between the two matter waves emerging from a beam splitter and quadratically with the time of free fall. Sensitivity can be increased by increasing the momentum difference or the time in free fall (or both). Therefore, the space-based experiments promise a breakthrough in sensitivity because of long free-fall times. Current and proposed tests of gravity with atom interferometry include splitting free-falling BECs in atomic fountains (Schlippert *et al.*, 2014; Hartwig *et al.*, 2015), drop towers (Müntinga *et al.*, 2013), parabolic flights (Geiger *et al.*, 2011; Barrett *et al.*, 2016), sounding rocket missions (Seidel *et al.*, 2015), and outer space (Tino *et al.*, 2013; D. N. Aguilera *et al.*, 2014; Williams *et al.*, 2016).

A number of experiments, implementing the longest atom-interferometry times to date, have been performed in Stanford's 10-m atomic fountain (Dickerson *et al.*, 2013), where superpositions of atomic wave packets with spatial separations of up to 50 cm were created (Kovachy, Asenbaum *et al.*, 2015). An important step was the preparation through atomic lensing of narrow momentum distributions corresponding to effective temperatures in the pK regime (Kovachy, Hogan *et al.*, 2015).

Gravity gradients pose a major challenge for high-precision tests of the WEP with atom interferometry. They degrade contrast in the interference signal and impose severe

requirements on the level at which the relative positions and velocities of the initial wave packets for the two atomic species must be controlled. Otherwise, gravity gradients could mimic spurious violations of the WEP. These difficulties can be mitigated by employing wave packets with narrower position and momentum widths until reaching the Heisenberg uncertainty limit. A scheme to compensate the effects of gravity gradients and overcome these difficulties was recently proposed (Roura, 2017) and has been demonstrated experimentally (D'Amico *et al.*, 2017; Overstreet *et al.*, 2018). Overstreet *et al.* (2018) showed that one can reduce the systematic effects associated with gravity gradients in WEP tests to 1 part in 10^{14}. This makes atom interferometry competitive with tests employing macroscopic masses.

In 2010, a preparation and observation of a Bose-Einstein condensate during free fall in a 146-m-tall evacuated drop tower of the Center of Applied Space Technology and Microgravity (ZARM) in Bremen, Germany was reported (van Zoest *et al.*, 2010). The realization of an asymmetric Mach-Zehnder interferometer operated with a Bose-Einstein condensate in extended free fall at ZARM was reported by Müntinga *et al.* (2013). These proof-of-principle experiments demonstrated a feasibility of coherent matter-wave experiments in microgravity paving the way toward for matter-wave experiments in space. In 2017, the QUANTUS Collaboration (Seidel *et al.*, 2015) conducted a successful MAIUS 1 (matter-wave interferometry in microgravity) experiment aboard a sounding rocket at altitude up to 243 km above the Earth's surface, well above the Kármán line that marks the boundary of outer space (the International Space Station's orbit is about 400 km above the surface of the Earth). About 100 discrete matter-wave experiments were conducted during the six-minute experimental phase of this flight.

Atom-interferometry quantum tests of the universality of free fall with cold rubidium ^{85}Rb and ^{87}Rb atoms were performed by Fray *et al.* (2004) and Bonnin *et al.* (2013) at the 10^{-7} level. A scheme to suppress common-mode noise in lasers used for atom interferometry was demonstrated by Zhou *et al.* (2015), resulting in a measurement of $\eta(^{87}$Rb, ^{85}Rb$) = (2.8 \pm 3.0) \times 10^{-8}$.

One of the advantages for using cold atom clouds for gravity tests is the opportunity to perform qualitatively different WEP tests with well-characterized "test masses" with a definite spin for a search of the spin-gravity coupling effects. Tarallo *et al.* (2014) reported such an experimental comparison of the gravitational interaction for a ^{88}Sr (boson, $I = 0$) with that of a ^{87}Sr (fermion, $I = 9/2$). The Eötvös ratio and possible spin-gravity coupling were constrained at the 10^{-7} level. Note that such a test is completely insensitive to the types of spin-gravity interactions probed in spin-precession experiments such as those of Venema *et al.* (1992) and Jackson Kimball, Dudley *et al.* (2017); see the discussion in Sec. VII.G.

Duan *et al.* (2016) reported a test of the universality of free fall with ^{87}Rb atoms in different spin orientations. They used a Mach-Zehnder–type atom interferometer to alternately measure the free-fall acceleration of the atoms in $m_F = +1$ and -1 magnetic sublevels, with the resultant Eötvös ratio of $\eta = (0.2 \pm 1.2) \times 10^{-7}$. Improved results were reported by Zhang *et al.* (2018).

Rosi *et al.* (2017) reported a novel WEP test performed on rubidium atoms prepared in coherent superpositions of different energy eigenstates. A Bragg atom interferometer in a gravity gradiometer configuration was used to compare their free fall. This experiment tested quantum aspects of EEP that have no classical counterpart. Rosi *et al.* (2017) also measured the Eötvös ratio of atoms in two hyperfine levels with relative uncertainty in the range of 10^{-9}.

Geiger and Trupke (2018) proposed an experiment to study the possible influence of entanglement between two test masses on the universality of free fall. They devised a test of the weak equivalence principle with ^{85}Rb and ^{87}Rb atoms entangled by a vacuum stimulated rapid adiabatic passage protocol implemented in a high-finesse optical cavity.

The first quantum test of the UFF with matter waves of two different atomic species was reported by Schlippert *et al.* (2014). This experiment compared the free-fall accelerations of laser-cooled ensembles of ^{87}Rb and ^{39}K atoms by measuring the gravitationally induced shift in two Mach-Zehnder–type interferometers. Schlippert *et al.* (2014) measured the Eötvös ratio

$$\eta_{\text{Rb,K}} = 2 \frac{g_{\text{Rb}} - g_{\text{K}}}{g_{\text{Rb}} + g_{\text{K}}} = (0.3 \pm 5.4) \times 10^{-7}, \qquad (90)$$

where g_{Rb} and g_{K} are free-fall accelerations of the ^{87}Rb and ^{39}K atoms, respectively. A nonzero value of the Eötvös ratio would indicate a UFF violation resulting from either a difference of the inertial and gravitational masses or an additional (unknown) force which depends on the composition of the atomic species and differs for ^{87}Rb and ^{39}K atoms. The same apparatus may be used to improve the precision by 2 orders of magnitudes to the ppb level.

Hartwig *et al.* (2015) proposed a long base line atom interferometer test of EEP with Rb and Yb. With over 10 m of free fall, their experiment is estimated to reach 7×10^{-13} accuracy in the Eötvös ratio. Use of the heavy alkaline earth Yb will broaden the scope of atom-interferometric EEP tests in view of EEP violation parametrization based on the dilaton model described by Damour (2012).

A number of quantum WEP tests in microgravity are being pursued, with the promise of greatly increased precision over current quantum tests. This is a goal of the QUANTUS Collaboration previously mentioned. The I.C.E. (Interférometrie atomique á sources Cohérentes pour l'Espace—Coherent atom interferometry for space applications) experiment (Geiger *et al.*, 2011) is a compact and transportable atom interferometer, designed to test WEP by comparing the accelerations of free-falling clouds of ultracold Rb and K atoms inside an airplane in free fall. Searching for WEP violation at high precision is the primary science objectives of the SpaceTime Explorer and QUantum Equivalence Space Test (STE-QUEST) space mission (D. N. Aguilera *et al.*, 2014; Altschul *et al.*, 2015) designed to measure the Eötvös ratio between matter waves of two Rb isotopes in a differential atom interferometer at the 2×10^{-15} uncertainty level. Although QUEST was not selected for the European Space Agency M3 Cosmic Vision Programme, it demonstrated the potential of future space-based quantum

WEP tests. Other proposals for quantum atom-interferometry space-based WEP tests include the Quantum Test of the Equivalence principle and Space Time (QTEST) (Williams *et al.*, 2016) and a Quantum WEP test (Q-WEP) (Tino *et al.*, 2013) on the International Space Station.

B. Determination of the Newtonian gravitational constant

The Newtonian gravitational constant G was the second fundamental constant subject to an absolute measurement, which was first conducted by Cavendish (1798)). The 2014 CODATA recommended value (Mohr, Newell, and Taylor, 2016) is $G = 6.67408(31) \times 10^{-11}$ m^3 kg^{-1} s^{-2}. The relative standard uncertainty in G of 4.7×10^{-5} is by far the largest of any of the primary fundamental constants, exceeding that of the Boltzmann constant k by 2 orders of magnitude. The slow rate of progress in reducing the uncertainty in G and large unresolved disagreements between the most precise measurements is a matter of concern in the precision-measurement community (Schlamminger, 2014; Anderson *et al.*, 2015; Schlamminger, Gundlach, and Newman, 2015; Rothleitner and Schlamminger, 2017). Reflecting the isolation of gravity and GR from the standard model, G is also unique among the fundamental constants in having no dependence upon any of the other constants included in the CODATA least-squares fit (Mohr, Newell, and Taylor, 2016).

The first experimental observation of a gravitational shift of a de Broglie wave was made in 1974 using neutron interferometry in the Earth's gravitational field (Colella, Overhauser, and Werner, 1975). Until 2014, all experimental determinations that contributed to the CODATA recommended value of G involved measurement of classical forces. The first atom-interferometric measurements of G were performed by Bertoldi *et al.* (2006) and Fixler *et al.* (2007). These experiments demonstrated the gravitational action of a laboratory source mass upon an atomic de Broglie wavelength, an intrinsically quantum-mechanical effect. They yielded values of G consistent with the CODATA recommended value then, but with much larger uncertainties. Atom-interferometric measurements of G certainly offer the prospect of having systematic uncertainties qualitatively different from those of classical experiments, and they may eventually provide a link between G and other fundamental constants, as in the example of the dependence of the fine-structure constant α on the ratio $\hbar/M(^{87}\text{Rb})$. Rosi *et al.* (2014) reported an atom-interferometric determination of G with a relative standard uncertainty of 0.015%. Their measurement was included in the least-squares fit that determined the 2014 CODATA recommended value.

The coupling of the initial position and velocity of the atomic wave packets to gravity gradients has so far been the main source of systematics in the gradiometry measurements for the determination of G with atom interferometry. However, it was argued that the compensation technique of Roura (2017) can also be exploited in this context to achieve accuracies competitive with those of measurements employing macroscopic masses or even better (D'Amico *et al.*, 2017; Rosi, 2018). Past and ongoing G determinations based on atom interferometry were reviewed by Rosi (2016).

The use of multiple atomic samples in an interferometer also enables measurements of higher-order spatial derivatives of the gravity field. Rosi *et al.* (2015) reported the first direct measurement of the gravity-field curvature based on three conjugated atom interferometers. The gravity curvature was produced by nearby source masses along one axis. In the experimental set up designed by Rosi *et al.* (2015), three atomic clouds launched in the vertical direction are simultaneously interrogated by the same atom-interferometry sequence probing the gravity field at three equally spaced positions. Such an atomic sensor is capable of measuring gravity, gravity gradient, and curvature along the vertical direction at the same time, important for geodesy studies and Earth monitoring applications. The same scheme may be used for a novel approach to the G measurement.

Asenbaum *et al.* (2017) used a dual light-pulse atom interferometer to measure a phase shift associated with spacetime-curvature induced tidal forces on the wave function of a single quantum system. A macroscopic spatial superposition state in each interferometer, extending over 16 cm, acted as a nonlocal probe of the spacetime manifold.

C. Detection of gravitational waves

The detection of the gravitational waves (GW) by the Advanced LIGO in 2015 (Abbott *et al.*, 2016a, 2016b) initiated the field of gravitational-wave astronomy. This opens a new window on the Universe since many of the GW cosmic sources do not have detectable electromagnetic emissions. Theoretical physics implications of the observed binary black-hole mergers and probes of new physics and cosmology enabled by the detection of the gravitational waves are described by Yunes, Yagi, and Pretorius (2016). Once at full sensitivity, the Advanced LIGO detectors will be able to see inspiralling binaries made up of two 1.4 solar-mass neutron stars to a distance of 300 megaparsecs (Mpc, 1 parsec = 3.3 light years) and coalescing black-hole systems at the cosmological distance, to the redshifts $z = 0.4$, significantly increasing the number of potentially detectable events. Advanced LIGO at full capacity will be essentially operating at the quantum noise limit. With the Advanced Virgo GW detector in Italy along with future detectors, the GW signals may be triangulated. There are already proposals for 10 and 40 km laser interferometers, the Einstein telescope (Sathyaprakash *et al.*, 2012), and the cosmic explorer (Abbott *et al.*, 2017), significantly longer than the Advanced LIGO 4 km arms, and thus able to measure lower frequencies at smaller fractional sensitivity.

The detection capability of the laser interferometry terrestrial detectors is limited to GWs with frequencies above $\approx$10 Hz by the seismic noise and Newtonian noise (fluctuations of the terrestrial gravity field which creates a tidal effect on separated test masses) (Saulson, 1984). The ability to detect gravitational waves of lower frequencies will significantly increase the number of binary star mergers from which the gravitational waves may be detected and allow for longer observation of the inspiralling binary stars before the merger. Stochastic gravitational waves, i.e., relic GWs from the early evolution of the Universe, from cosmological (and possibly unforeseen) sources, such as inflation and reheating, a network of cosmic strings, or phase transitions in the early Universe, etc., can also be easier to detect at these low

frequencies; see Dimopoulos *et al.* (2008). Proposals for the detection of the gravitational waves at lower frequencies include the space-based laser interferometry detector [laser interferometer space antenna (LISA) (Danzmann *et al.*, 2011) and evolved-LISA (eLISA) (Amaro-Seoane *et al.*, 2012)] and both terrestrial and space-based matter-wave detectors, using either atom interferometers or atomic clocks (Tino and Vetrano, 2007; Dimopoulos *et al.*, 2008; Hogan *et al.*, 2011; Yu and Tinto, 2011; Graham *et al.*, 2013; Chiow, Williams, and Yu, 2015; Chaibi *et al.*, 2016; Graham, Hogan *et al.*, 2016; Hogan and Kasevich, 2016; Kolkowitz *et al.*, 2016).

Terrestrial atom interferometers have been proposed (Dimopoulos *et al.*, 2008; Chaibi *et al.*, 2016) for GW detection in the 0.3 to 3 Hz frequency band. Chaibi *et al.* (2016) proposed a new detection strategy based on a correlated array of atom interferometers which allows reduction of the Newtonian noise limiting all ground-based GW detectors below ≈10 Hz. The matter-wave laser interferometer gravitation antenna (MIGA) is a hybrid detector that couples laser and matter-wave interferometry aimed at both the geophysical studies and subhertz GWs detection in a low-noise underground laboratory to minimize effects of laboratory vibrations (Geiger *et al.*, 2015).

LISA and eLISA are space-based laser interferometric detectors analogous to LIGO, to be composed of three spacecraft forming either a two- or three-arm Michelson interferometer (Danzmann *et al.*, 2011; Amaro-Seoane *et al.*, 2012), with the GW frequency-detection range from 0.1 mHz to 1 Hz.

Both atomic clocks and atom-interferometry technologies improved tremendously over the past decade, also leading to fast development of the gravitational-wave detection schemes (Dimopoulos *et al.*, 2008; Hogan *et al.*, 2011; Graham *et al.*, 2013; Chiow, Williams, and Yu, 2015; Chaibi *et al.*, 2016; Graham, Hogan *et al.*, 2016; Hogan and Kasevich, 2016; Kolkowitz *et al.*, 2016) with improved sensitivities, realistic requirements for the underlying technologies, and addressing some problems (Bender, 2011, 2014) of earlier proposals. The intrinsic noise sources and sensitivity limits of atom-based versus light-based interferometers for GW detection are being clarified (Bender, 2011, 2014; Baker and Thorpe, 2012). Most importantly, the restriction of a space-based atom-interferometry GW detector to a relatively short base line ≈1000 km, in comparison with LISA, was lifted in the recent 2016 proposal (Hogan and Kasevich, 2016). Because of considerable evolution of the AMO GW detector proposals, we briefly describe only the most recent proposals based on atom interferometers and atomic clocks.

Hogan and Kasevich (2016) proposed a space-based GW detector based on two satellites with light-pulse atom interferometers separated by a long base line (over 100 000 km), capable of detecting GWs in the 0.1-mHz to 1-Hz frequency band. The light pulses are sent back and forth across the base line from alternating directions, driving atomic single-photon transitions. The use of single-photon transitions in alkaline-earth atoms (Sr) with long lifetimes of the excited state significantly reduces laser frequency noise (Graham *et al.*, 2013) in comparison to the GW detector proposals based on alkali-metal atoms requiring implementation of two-photon transitions (Dimopoulos *et al.*, 2008). The GWs are detected by monitoring the phase difference between the two interferometers caused by the variation of the light travel time across the base line due to a passing GW. As described by Graham, Hogan *et al.* (2016), the atom-interferometric GW detector essentially compares time kept by the laser and atom "clocks." A gravitational wave affects the flat-space relation between these clocks by a factor proportional to the distance between them, and such change oscillates in time with the frequency of the gravitational wave resulting in a detectable signal.

In previous proposals (Dimopoulos *et al.*, 2008; Graham *et al.*, 2013), the same laser would drive atom transitions at both ends, requiring the laser to remain collimated over the optical path between two satellites, significantly restricting the maximum base line length. In the Hogan and Kasevich (2016) scheme, both satellites house a master laser and a local-oscillator laser that have sufficient intensity to drive transitions in the local atom interferometer. The master laser beam interacts with its satellite's atomic cloud and then propagates to the second satellite acting now as a reference beam which does not have to be collimated as it reaches the opposite satellite. A local oscillator in the other satellite is phase referenced or phase locked to the incoming reference laser beam and drives the transitions in this satellite's atomic cloud. An identical scheme is implemented in the reverse direction. Since much less intensity of the reference beam is required for phase reference than for atomic excitations, this scheme allows for a much larger base line leading to enhanced sensitivity, simplified atom optics, and reduced atomic-source flux requirements. Such a GW detector scheme with 12 photon recoil atom optics and 6×10^8 m base line is projected to exceed the sensitivity of proposed the LISA detector by a factor of 10 (Hogan and Kasevich, 2016).

Graham, Hogan *et al.* (2016) proposed an atom-interferometric GW detector that can operate in a resonant detection mode and can switch between the broadband and narrow-band detection modes to increase sensitivity.

Geiger (2017) reviewed the perspective of using atom interferometry for GW detection in the mHz to about 10 Hz frequency band.

Kolkowitz *et al.* (2016) proposed using a two-satellite scheme sharing ultrastable optical laser light over a single base line, with atomic optical lattice clocks (rather than atom interferometers) as sensitive, narrow-band detectors of the local frequency of the shared laser light. A passing GW induces effective Doppler shifts and the GW signal is detected as a differential frequency shift of the shared laser light due to the relative velocity of the satellites. Such a scheme can detect GWs with frequencies ranging from 3 mHz to 10 Hz without loss of sensitivity. The clock scheme may be integrated with an optical interferometric detector. The next stage of matter-wave gravitational detector development is a demonstration of ground-based prototype systems and characterization of the noise sources.

D. Gravity experiments with antimatter

One of the recent foci of the experimental efforts on matter-antimatter comparisons is testing whether antimatter is affected by gravity in the same way as matter. For example, the CERN based GBAR Collaboration is developing a

technique (Pérez *et al.*, 2015) where they will first create a positive ion consisting of an antiproton and two positrons that will be sympathetically cooled with Be^+ ions and then "gently" photoionized to produce a cold neutral antihydrogen atom that will fall under gravity over a known distance before being detected. The AEgIS experiment at CERN is also aimed at the direct measurement of the Earth's gravitational acceleration on antihydrogen but has a completely different design (Testera *et al.*, 2015). In the AEgIS expariment, a cold, pulsed beam of antihydrogen will pass through a moiré deflectometer (Aghion *et al.*, 2014), coupled to a position-sensitive detector to measure the strength of the gravitational interaction between matter and antimatter to a precision of 1%. A second goal of the AEgIS experiment is to carry out spectroscopic measurements on antihydrogen atoms. There is a possibility of laser cooling of the negative ion of lanthanum (La, $Z = 57$) (Jordan *et al.*, 2015). Laser-cooled La^- might be used for sympathetic cooling of antiprotons for subsequent antihydrogen formation (Kellerbauer *et al.*, 2009).

A method to directly measure the ratio of the gravitational to inertial mass of antimatter accomplished by searching for the free fall (or rise) of ground-state antihydrogen atoms was proposed by the ALPHA Collaboration (Amole *et al.*, 2013). The antihydrogen atoms are released from the trap; the escaping anti-atoms are then detected when they annihilate on the trap wall.

One should emphasize that the possibility of the difference in gravity between matter and antimatter is already constrained, under some assumptions, at the 1 ppm level by experiments of Gabrielse *et al.* (1999) which found no differences in gravitational redshift of matter and antimatter clocks. Ulmer *et al.* (2015) interpreted their result for the sidereal variation of the q/m ratios given by Eq. (46) as a test of the weak equivalence principle for baryonic antimatter. Following Hughes and Holzscheiter (1991), they expressed a possible gravitational anomaly acting on antimatter with a parameter a_g, which modifies the effective Newtonian gravitational potential U to give $a_g U$, setting an upper limit of $|a_g - 1| < 8.7 \times 10^{-7}$. The role of the internal kinetic energy of bound systems of matter in tests of the Einstein equivalence principle was considered by Hohensee, Müller, and Wiringa (2013), letting the limits on equivalence principle violations in antimatter from tests using bound systems of normal matter. We emphasized that any difference between matter and antimatter gravity would run into theoretical conceptual troubles (Karshenboim, 2016).

Furthermore, as discussed in previous sections, there have been numerous and stringent matter-based tests of the equivalence principle and *CPT* invariance, and these must have a direct bearing on the proposed tests with antimatter, especially considering that most of the mass of the antiproton comes from the quark binding energy (i.e., the gluon field). The true antimatter mass and energy content of the antiproton in the form of antiquarks can reasonably be assumed to be less than or about 1%, while the antimatter content of ordinary matter due to virtual particles is non-negligible. This implies that there is a connection between matter-based equivalence principle tests and proposed antihydrogen experiments. Another compelling, albeit model-dependent, argument

(Adelberger *et al.*, 1991) limits the difference between gravitational acceleration for matter and antimatter to less than a part in 10^5 or perhaps much better (considering the considerably more sensitive updated versions of the torsion-pendulum experiment). It is based on reasonable assumptions of equivalence principle violations arising from a scalar or vector gravitational coupling and combining data from the exquisitely precise measurements using torsion pendulums with stringent limits on *CPT* invariance.

E. Other AMO tests of gravity

A test of the local Lorentz invariance of post-Newtonian gravity was performed by Müller *et al.* (2008) by monitoring the Earth's gravity with a Mach-Zehnder atom interferometer (see Sec. XI). Hohensee *et al.* (2012) proposed an experimental realization of the gravitational Aharonov-Bohm effect: measurement of phase shifts with an atom interferometer due to a gravitational potential U in the absence of a gravitational force. A pair of laboratory masses will be used as a source of the gravitational potential. A matter-wave interferometry experiment to measure such phase shifts in the absence of a classical force is currently under construction at the University of California, Berkeley (Hohensee *et al.*, 2012).

Testing subgravitational forces on atoms from a miniature, in-vacuum source mass was reported by Jaffe *et al.* (2016).

Tests of gravity are interconnected with the searches for exotic forces. Leefer *et al.* (2016) suggested and implemented the use of atomic spectroscopy to search for Yukawa-type fifth forces. By studying the behavior of atomic transition frequencies at varying distances away from massive bodies (e.g., the Sun, the Moon, heavy masses in the laboratory), Leefer *et al.* (2016) placed constraints on possible nongravitational interactions of a scalar field with the photon, electron, and nucleons. This work also placed constraints on combinations of interaction parameters that cannot otherwise be probed with traditional anomalous-force measurements. Leefer *et al.* (2016) suggested further measurements to improve on the current level of sensitivity. Such measurements include the use of more precise atomic clocks and other systems (molecular, highly charged ionic and nuclear transitions), and implementing different experimental geometries (e.g., the size of the effect can be increased by up to 4 orders of magnitude by measuring atomic transition frequencies first on the Earth, then on a space probe headed toward the Sun).

XI. LORENTZ SYMMETRY TESTS

Local Lorentz invariance is one of the foundations of the current laws of physics: the outcome of any local nongravitational experiment is independent of the velocity and the orientation of the (freely falling) apparatus. The first test of Lorentz invariance was Michelson's 1881 experiment (Michelson, 1881) aimed at detecting the ether (erroneously assumed to be the medium for electromagnetic wave propagation). This experiment was further improved by Michelson and Morley (1887). Michelson and Morley's apparatus measured the interference between two beams of light traveling back and forth along two perpendicular paths. This light

interferometer was rotated relative to the Earth to test the isotropy of the speed of light.

In the 1960s, the first spectroscopic tests of Lorentz symmetry were performed by Hughes, Robinson, and Beltran-Lopez (1960) and Drever (1961) where they searched for sidereal variation of NMR lines in ^{7}Li. The Hughes-Drever tests were inspired by Cocconi and Salpeter (1958) who suggested that it might be possible, based on Mach's principle, for inertial mass to acquire a tensor character due to aniso-tropic distribution of matter in the Universe. This would cause a particle's inertial mass to depend on the orientation of its orbit with respect to the matter anisotropy, which in turn would generate energy shifts in atoms and nuclei. Experiments similar to the Hughes-Drever test have come to be known as "clock-comparison tests" in which the frequencies of different atomic "clock" transitions are com-pared as the clocks rotate with the Earth. Since these early tests, the field of Lorentz symmetry tests has flourished, encompassing almost all fields of physics (Mattingly, 2005; Liberati and Maccione, 2009; Kostelecký and Russell, 2011). The *Data Tables for Lorentz and CPT Violation* by Kostelecký and Russell (2017) provides yearly updates of experimental progress of the last decade and gives tables of the measured and derived values of coefficients for Lorentz and *CPT* violation in the standard model extension discussed later. The listed experiments include searches for Lorentz violation (LV) in the matter, photon, neutrino, and gravity sectors. The *Data Tables for Lorentz and CPT Violation* has grown in length by 50% in the past 3 years demonstrating a large number of new experiments in many sectors.

This recent interest in tests of Lorentz symmetries is motivated by theoretical developments in quantum gravity suggesting that Lorentz symmetry may be violated at some energies, tremendous progress in experimental precision, and development of a theoretical framework to analyze different classes of experiments. A particular attraction of the LLI tests is the possibility of a positive result: a confirmed measurement of Lorentz violation would be an unambiguous signal of new physics. The natural energy scale for strong LV induced by quantum gravity is the Planck scale ($M_{\text{Pl}} \approx 10^{19}$ GeV/c^2), which is far beyond the reach of existing observations: even ultrahigh energy cosmic rays still fall 8 orders of magnitude short of the Planck scale. The good news is that strong LV at the Planck scale may also lead to small but potentially observable low-energy LV. Therefore, high-precision tests of LLI with matter, gravity, or light may provide insight into possible new physics and set limits on various theories such as quantum gravity. The bad news is that there are no predictions of the magnitude of LV violation at low energies. Lorentz-violating effects may be suppressed by some power of the ratio R between the electroweak scale and the natural (Planck) energy scale for strings: $R = m_{\text{ew}}/M_{\text{Pl}} = 2 \times 10^{-17}$ (Kostelecký and Potting, 1995) or electron mass to Plank scale 4×10^{-23} (Liberati and Maccione, 2009).

Lorentz violation tests are analyzed in the context of an effective field theory known as the SME. Two approaches are used when constructing such an effective field theory to describe Lorentz violations (Kostelecký and Potting, 1995; Colladay and Kostelecký, 1998; Myers and Pospelov, 2003):

(1) add renormalizable Lorentz-violating terms to the standard model Lagrangian and (2) explicitly break Lorentz invariance by introducing nonrenormalizable operators.

In minimal SME, corresponding to the first approach, the standard model Lagrangian is augmented with every possible combination of the SM fields that are not term-by-term Lorentz invariant, while maintaining gauge invariance, energy-momentum conservation, and Lorentz invariance of the total action (Colladay and Kostelecký, 1998). Separate violations of LLI are possible for each type of particle, making it essential to verify LLI in different systems at a high level of precision. Liberati and Maccione (2009) reviewed nonmini-mal SME experimental tests, and all current limits are given in the 2017 edition of the *Data Tables for Lorentz and CPT Violation* (Kostelecký and Russell, 2017). We limit this review to recent AMO tests and proposals. The diverse set of AMO Lorentz-symmetry tests involves experiments with atomic clocks (Wolf *et al.*, 2006), other precision spectros-copy measurements (Hohensee *et al.*, 2013), magnetometers (Smiciklas *et al.*, 2011; Allmendinger, Heil *et al.*, 2014), electromagnetic cavities (Eisele, Nevsky, and Schiller, 2009), and quantum-information-trapped-ion technologies (Pruttivarasin *et al.*, 2015).

In minimal SME, a general expression for the quadratic Hermitian Lagrangian density describing a single spin-1/2 Dirac fermion of mass m (electron, proton, or neutron) in the presence of Lorentz violation is given by (Kostelecký and Lane, 1999)

$$\mathcal{L} = \tfrac{1}{2} i c \bar{\psi} \Gamma_\nu \overleftrightarrow{\partial^\nu} \psi - Mc^2 \bar{\psi}\psi, \qquad (91)$$

where ψ is a four-component Dirac spinor,

$$f \overleftrightarrow{\partial^\nu} g = f \partial^\nu g - g \partial^\nu f,$$
$$M = m + a_\mu \gamma^\mu + b_\mu \gamma_5 \gamma^\mu + \tfrac{1}{2} H_{\mu\nu} \sigma^{\mu\nu}, \qquad (92)$$

and

$$\Gamma_\nu = \gamma_\nu + c_{\mu\nu}\gamma_\nu + d_{\mu\nu}\gamma_5\gamma_\nu + e_\nu + i\gamma_5 f_\nu + \tfrac{1}{2}g_{\lambda\mu\nu}\sigma_{\lambda\mu}. \qquad (93)$$

The first terms in the expressions for M and Γ_ν give the usual SM Lagrangian. Lorentz violation is quantified by the parameters a_μ, b_μ, $c_{\mu\nu}$, $d_{\mu\nu}$, e_μ, f_μ, $g_{\lambda\mu\nu}$, and $H_{\mu\nu}$. The coefficients in Eq. (92) have dimensions of mass; the coefficients in Eq. (93) are dimensionless. The field operators in Eqs. (92) and (93) containing the coefficients $c_{\mu\nu}$, $d_{\mu\nu}$, and $H_{\mu\nu}$ are even under *CPT* and the remaining ones are odd under *CPT*. The framework of interpreting the laboratory experi-ments involving monitoring atomic or nuclear frequencies in terms of the SME coefficients is described in detail by Kostelecký and Lane (1999) and Kostelecký and Mewes (2002). Such atomic experiments may be interpreted as Lorentz-invariance tests for the photon, electron, and nuclear constituents, such as proton and neutron, with varying sensitivities to different combinations of LLI effects. A number of experiments are sensitive to either electron or nucleon sectors, with photon contributions appearing in all atomic experiments. AMO tests of LLI also include testing

isotropy of gravity; a test of the LLI of post-Newtonian gravity was performed by Müller *et al.* (2008) by monitoring the Earth's gravity with a Mach-Zehnder atom interferometer. Expressed within the standard model extension, the analysis limits four coefficients describing anisotropic gravity at the ppb level and three others at the 10 ppm level. Using the SME, Müller *et al.* (2008) explicitly demonstrated how their experiment actually compares the isotropy of gravity and electromagnetism.

A. Electron sector of the SME

Testing LLI of the electron motion in an atom has the advantage of testing for new physics in a well-understood system. In atomic experiments aimed at the LLI tests in the electron-photon sector (Hohensee *et al.*, 2013; Pruttivarasin *et al.*, 2015), one searches for variations of the atomic energy levels when the orientation of the electronic wave function is rotated with respect to a standard reference frame. Generally, one uses the Sun centered celestial-equatorial frame (SCCEF) for the analysis of the experiments (Kostelecký and Mewes, 2002), indicated by the coordinate indices T, X, Y, and Z. For example, the $c_{\mu\nu}$ tensor has nine components that need to be experimentally determined: parity even c_{TT} and c_{JK}, and parity odd c_{TJ}, where $J, K = X, Y, Z$. The elements c_{JK} which describe the dependence of the kinetic energy on the direction of the momentum have a leading order time-modulation period related to the sidereal day (12- and 24-hr modulations) in the laboratory experiments described later. The c_{TJ} and c_{TT} describe the dependence of the kinetic energy on the boost of the laboratory frame and have a leading order time-modulation period related to the sidereal year. The terms c_{TJ} are proportional to the ratio of the Earth's orbital velocity to the speed of light $\beta_\oplus \approx 10^{-4}$; and the c_{TT} term is suppressed by $\beta_\oplus^2 \approx 10^{-8}$, resulting in a weaker bound on these components of the $c_{\mu\nu}$ tensor. The indices (0,1, 2, 3) are used for the laboratory frame. The most sensitive LLI tests for electrons have been conducted with neutral Dy atoms (Hohensee *et al.*, 2013) and Ca$^+$ ions (Pruttivarasin *et al.*, 2015) as described next.

Violations of Lorentz invariance in bound electronic states result in a perturbation of the Hamiltonian that can be described by Kostelecký and Lane (1999) and Hohensee *et al.* (2013)

$$\delta H = -\left(C_0^{(0)} - \frac{2U}{3c^2}c_{00}\right)\frac{\mathbf{p}^2}{2m_e} - \frac{1}{6m_e}C_0^{(2)}T_0^{(2)}, \quad (94)$$

where **p** is the momentum of a bound electron. The second term in the parentheses gives the leading order gravitational redshift anomaly in terms of the Newtonian potential U. We refer the interested reader to Kostelecký and Tasson (2011) for the study of the gravitational couplings of matter in the presence of Lorentz and *CPT* violation and the derivation of the relativistic quantum Hamiltonian from the gravitationally coupled minimal SME. The parameters $C_0^{(0)}$ and $C_0^{(2)}$ are elements of the $c_{\mu\nu}$ tensor in the laboratory frame introduced by Eq. (93):

$$C_0^{(0)} = c_{00} + (2/3)c_{jj}, \quad (95)$$

$$C_0^{(2)} = c_{jj} + (2/3)c_{33}, \quad (96)$$

where $j = 1, 2, 3$. The $C_{\pm1}^{(2)}$ and $C_{\pm2}^{(2)}$ do not contribute to the energy shift of bound states. The values of the $C_0^{(0)}$ and $C_0^{(2)}$ in the laboratory frame are the functions of the $c_{\mu\nu}$ tensor in the SCCEF frame and the velocity and orientation of the lab.

The nonrelativistic form of the $T_0^{(2)}$ operator is $T_0^{(2)} = \mathbf{p}^2 - 3p_z^2$. Predicting the energy shift due to LV involves calculating of the expectation value of the Hamiltonian (94) for the atomic states of interest. The larger the matrix elements, the more sensitive is this atomic state. One has to take into account that only a transition-energy shift can be measured, so the difference of the sensitivities of the upper and lower states is important for the final experimental analysis in terms of the $c_{\mu\nu}$ tensor. The most accurate tests in the electron-photon sector can be conducted in atoms or ions with the highest possible sensitivities which are amenable to high-precision measurement techniques. Since the operators in Eq. (94) contain the second power of the momentum operator p, the corresponding matrix elements are expected to be large for orbitals with large kinetic energy. This happens for atomic $4f$ electrons localized deep inside the atom in the area of large (negative) potential and kinetic energy in some atomic systems.

We note that the formalism is the same for the LV violation in the nuclei, and the expectation values of the same operators (but for the nuclear states) determine the sensitivity.

1. LLI tests with dysprosium

A joint test of local Lorentz invariance and the Einstein equivalence principle for electrons was reported by Hohensee *et al.* (2013) using long-term measurements of the transition frequency between two nearly degenerate states of atomic dysprosium.

Dy, a lanthanide element with partially filled electronic $4f$ shells, has two near-degenerate, low-lying excited states with significant momentum quadrupole moments, opposite parity, and leading configurations $[Xe]4f^{10}5d6s$, $J = 10$ (state A) and $[Xe]4f^95d^26s$, $J = 10$ (state B). The energy difference between states A and B can be measured directly by driving an electric dipole transition with a radio-frequency (rf) field. The average shift in the $B \to A$ transition frequency ω_{rf}, properly weighted for transition frequencies for different magnetic sublevels, is given by

$$\frac{\delta\omega_{rf}}{2\pi} = (10^{14} \text{ Hz})\left[500\left(C_0^{(0)} - \frac{2U_\odot}{3c^2}c_{00}\right) + 9.1C_0^{(2)}\right], \quad (97)$$

where $U_\odot$ is the Sun's gravitational potential. The sign of the frequency shift is opposite for ^{162}Dy and ^{164}Dy. The uncertainty in the numerical coefficient in front of the first term in the square brackets may be large due to the compilations in the evaluation of the matrix elements of the p^2 operator. There is no LV contribution from the nucleus since both Dy isotopes

used in the experiment, ^{162}Dy and ^{164}Dy, have nuclear spin $I = 0$.

The Dy experiment used repeated measurements acquired over nearly 2 years to obtain constraints on eight of the nine elements of the $c_{\mu\nu}$ tensor. Hohensee *et al.* (2013) tightened the previous limits (Altschul, 2006, 2010; Müller *et al.*, 2007) on four of the six parity-even components by factors ranging from 2 to 10, limiting Lorentz violation for electrons at the level of 10^{-17} for the c_{JK} components. Previous studies used rotating optical Fabry-Pérot resonators and microwave whispering-gallery sapphire resonators (Müller *et al.*, 2007) and high-energy astrophysical sources (Altschul, 2006, 2010) to constrain $c_{\mu\nu}$ coefficients for electrons.

Hohensee *et al.* (2013) also improved bounds on gravitational redshift anomalies for electrons (Vessot *et al.*, 1980; Hohensee *et al.*, 2011) by 2 orders of magnitude to 10^{-8}.

2. LLI test with calcium ion

Pruttivarasin *et al.* (2015) performed a test of Lorentz symmetry using an electronic analog of a Michelson-Morley experiment using the $^2D_{5/2}$ atomic states of a ^{40}Ca$^+$ ion with anisotropic electron momentum distributions. A pair of ^{40}Ca$^+$ ions was trapped in a linear Paul trap, with a static magnetic field applied defining the eigenstates of the system. The direction of this magnetic field changes with respect to the Sun as the Earth rotates, resulting in a rotation of the interferometer as illustrated in Fig. 23.

In the magnetic field, the $3d^2D_{5/2}$ atomic state splits into six states with the magnetic quantum numbers $m_J = \pm 1/2, \pm 3/2$, and $\pm 5/2$. Using the Hamiltonian given by Eq. (94), and calculating the corresponding matrix elements of the $T_0^{(2)}$
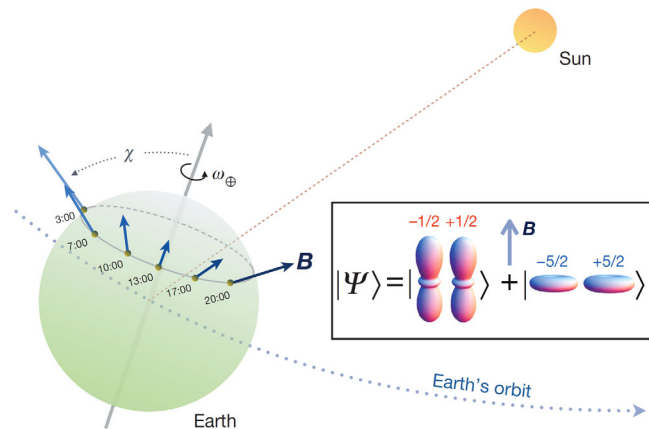

FIG. 23. Rotation of the quantization axis of the experiment with respect to the Sun as the Earth rotates. A magnetic field (B) is applied vertically in the laboratory frame to define the eigenstates of the system. As the Earth rotates with an angular frequency given by $\omega_\oplus = 2\pi/(23.93\ \text{h})$, the orientation of the magnetic field and, consequently, that of the electron wave packet (as shown in the inset in terms of probability envelopes) changes with respect to the Sun's rest frame. The angle χ is the colatitude of the experiment. From Pruttivarasin *et al.*, 2015.

operator, the energy shift of these $^2D_{5/2}$ atomic states induced by the Lorenz violation in the electron-photon sector is given by

$$\frac{\delta E}{h} = [(2.16 \times 10^{15}) - (7.42 \times 10^{14})m_J^2]C_0^{(2)}. \quad (98)$$

Since the LV energy shift depends on the magnetic quantum number, monitoring the energy difference between the $m_J = \pm 1/2$ and the $\pm 5/2$ Zeeman substates during the Earth's rotation probes the c_{JK} components of the LV tensor. The frequency difference (in Hz) between the LV shifts of the $m_J = 5/2$ and $1/2$ substates of the $3d\,^2D_{5/2}$ manifold is given by

$$\frac{1}{h}(E_{m_J=5/2} - E_{m_J=1/2}) = [-4.45(9) \times 10^{15}\ \text{Hz}]C_0^{(2)}. \quad (99)$$

This experiment is not sensitive to the scalar $C_0^{(0)}$ coefficient of Eq. (94).

The main source of decoherence in this experiment is magnetic field noise, since it also shifts the energies of the Zeeman substates. This problem is resolved by applying quantum-information inspired techniques and creating a two-ion product state that is insensitive to magnetic field fluctuation to first order. The energy difference between the two-ion states $|\pm 5/2, \mp 5/2\rangle$ and $|\pm 1/2, \mp 1/2\rangle$ was measured for 23 h, resulting in the limit of $h \times 11$ mHz. Pruttivarasin *et al.* (2015) pointed out that the experimental results may be interpreted in terms of either photon or electron LV violation described via $c'_{\mu\nu} = c_{\mu\nu} + k_{\mu\nu}/2$, where the first term refers to the electron LV and the second term to the photon LV. The Ca$^+$ experiment improved the limits to the c'_{JK} coefficients of the LV violation in the electron-photon sector to the 10^{-18} level. Because the ^{40}Ca$^+$ nucleus has nuclear spin $I = 0$, there is no nuclear LV contribution, just as in the case of the Dy experiment. The same experiment can be interpreted as testing anisotropy in the speed of light with the sensitivity similar to that of more recent work reported by Nagel *et al.* (2015).

3. Future prospects and other experiments

With optimization, both Dy and Ca$^+$ experiments could yield significantly improved constraints. An optimized Dy experiment may reach sensitivities on the order of 9×10^{-20} in 1 yr for the c_{JK} components (Hohensee *et al.*, 2013).

Further significant improvement of LV constraints calls for another system with a long-lived or ground state that has a large $\langle j|T_0^{(2)}|j\rangle$ matrix element. Dzuba *et al.* (2016) carried out a systematic study of this quantity for various systems and identified general rules for the enhancement of the reduced matrix elements of the $T^{(2)}$ operator. They identified the ytterbium ion Yb$^+$ to be an ideal system for future LV tests with high sensitivity, as well as excellent experimental controllability. The sensitivity of the $4f^{13}6s^2\ ^2F_{7/2}$ state of Yb$^+$ to LV is over an order of magnitude higher than that of the Ca$^+$ $^2D_{5/2}$ state. This state also has an exceptionally long lifetime on the order of several years (Huntemann *et al.*,

2012), so the proposed experiment is not limited by spontaneous decay during a measurement in contrast to the Ca$^+$ case.

Experimental techniques for precision control and manipulation of Yb$^+$ atomic states are particulary well developed owing to atomic clock (Huntemann *et al.*, 2016) and quantum-information (Islam *et al.*, 2013) applications making it an excellent candidate for searches of the Lorentz-violation signature.

Dzuba *et al.* (2016) estimated that experiments with the metastable $4f^{13}6s^2\ {}^2F_{7/2}$ state of Yb$^+$ can reach sensitivities of 1.5×10^{-23} for the c_{JK} coefficients, over 10^5 times more stringent than the current best limits. Moreover, the projected sensitivity to the c_{TJ} coefficients will be at the level of 1.5×10^{-19}, below the ratio between the electroweak and Planck energy scales. Similar sensitivities may potentially be reached for LV tests with highly charged ions (Dzuba *et al.*, 2016; Shaniv *et al.*, 2018), given future development of experimental techniques for these systems (Schmöger *et al.*, 2015).

Shaniv *et al.* (2018) proposed a broadly applicable experimental scheme to search for the LLI violation with atomic systems using dynamic decoupling which can be implemented in current atomic clocks experiments, with both single ions and arrays of neutral atoms. Moreover, this scheme can be performed on systems with no optical transitions, and therefore it is also applicable to highly charged ions which exhibit particularly high sensitivity to Lorentz-invariance violation.

Another interesting future possibility is measuring transition energies of rare-earth ions doped in crystalline lattices, which can be highly sensitive to the electron SME parameters (Harabati *et al.*, 2015).

Also of note is the work of Botermann *et al.* (2014), testing the time dilation predictions of special relativity, using a clock-comparison test performed at relativistic speeds using Li$^+$ ions in a storage ring. Another test of time dilation was reported by Delva *et al.* (2017) who searched for variations of the frequency differences between four strontium optical lattice clocks in different locations in Europe, connected by fiber optic links.

B. Proton and neutron sectors of the SME

1. Cs clock experiment

Another example of a clock-comparison test is the work of Wolf *et al.* (2006) who used a cold Cs atomic clock to test LLI in the matter sector, setting limits on the tensor Lorentz-violating coefficients for the proton. The Cs clock, which is also the primary frequency standard defining the second, operates on the $|F = 3\rangle \leftrightarrow |F = 4\rangle$ hyperfine transition of the ^{133}Cs $6S_{1/2}$ ground state, where $\mathbf{F} = \mathbf{J} + \mathbf{I}$ is the total angular momentum and Cs nuclear spin is $I = 7/2$. In the magnetic field, $F = 3$ and 4 clock states split into seven and nine Zeeman substates with $m_F = [-3, 3]$ and $[-4, 4]$, respectively. The atomic clock operates on the

$$|F = 3, m_F = 0\rangle \leftrightarrow |F = 4, m_F = 0\rangle \qquad (100)$$

hyperfine transition at 9.2 GHz, which is insensitive to both Lorentz violation and first-order magnetic field effects. The

other transitions with $\delta m_F \neq 0$ are used for magnetic field characterization. To test Lorentz symmetry, Wolf *et al.* (2006) monitored a combination of clock and

$$|F = 3, m_F = 3\rangle \leftrightarrow |F = 4, m_F = 3\rangle, \qquad (101)$$

$$|F = 3, m_F = -3\rangle \leftrightarrow |F = 4, m_F = -3\rangle \qquad (102)$$

transitions to form a combined observable

$$\nu_c = \nu_{+3} + \nu_{-3} - 2\nu_0. \qquad (103)$$

The ν_0, ν_{+3}, and ν_{-3} are frequencies of Eqs. (100), (101), and (102) transitions. The combined observable is used to avoid the dominant noise source—the first-order Zeeman shift due to the magnetic field fluctuations which strongly affect the states with $m_F \neq 0$, but cancels for the $\pm m_F$ combination. Since the m_F is the same for upper and lower states of all transitions, there is no Lorentz-violating tensor component from the electron sector. Since the ^{133}Cs nucleus has one unpaired proton, the experiment is interpreted in terms of the proton LV parameters of the $c_{\mu\nu}$ tensor, using the Schmidt nuclear model. The Cs clock experiment sets the limits for parameters for the proton at the 10^{-21}–10^{-25} level. A reanalysis of this experiment using an improved model linking the frequency shift of the ^{133}Cs hyperfine Zeeman transitions and SME coefficients of proton and neutron carried out by Pihan-Le Bars *et al.* (2017) placed improved bounds on the LV for the proton and the neutron.

2. Comagnetometer experiments

Some of the most stringent clock-comparison tests of LLI (Brown *et al.*, 2010; Smiciklas *et al.*, 2011) have been carried out using the self-compensating SERF comagnetometry scheme (Kornack and Romalis, 2002; Kornack, Ghosh, and Romalis, 2005), which was also used for constraining anomalous dipole-dipole interactions (Vasilakis *et al.*, 2009) as discussed in detail in Sec. VII.

The experiment of Brown *et al.* (2010) employs over-lapping ensembles of K and ^{3}He coupled via spin-exchange collisions. The atoms are in the low-magnetic-field SERF regime where broadening of the Zeeman resonances due to spin-exchange collisions is eliminated. The magnetic field along the z direction is tuned to the compensation point where the K-^{3}He SERF comagnetometer is insensitive to magnetic fields but highly sensitive to anomalous interactions that do not scale with the magnetic moments. The spin polarization of the K atoms along the x direction, probed via optical rotation with a linearly polarized laser beam propagating along x, is given to leading order by

$$P_x^e = P_z^e \frac{\gamma_e}{\Gamma_{\text{rel}}} \left(\beta_y^N - \beta_y^e + \frac{\Omega_y}{\gamma_N} \right), \qquad (104)$$

where β_y^N and β_y^e describe the phenomenological SME background fields along the y direction coupling to the ^{3}He nucleus (N) and valence electron (e) of K, respectively, P_z^e is

the K electron spin polarization along z, Γ_{rel} is the relaxation rate for K polarization, γ_e and γ_N are the gyromagnetic ratios for electrons and ^{3}He nuclei, respectively, and Ω_y is the rotation rate of the apparatus. A number of steps are taken to eliminate various sources of noise and systematic error. For example, the signal described by Eq. (104) depends explicitly on the rotation rate of the apparatus, so a nonzero P_x^e is generated by the gyrocompass effect due to the Earth's rotation (Venema *et al.*, 1992; Heckel *et al.*, 2008). To compensate for this effect, the experiment is mounted on a rotary platform. Figure 24 shows the change in the comagnetometer signal for a 180° rotation as a function of the initial platform angle, demonstrating a significant effect of Earth's rotation on P_x^e. In order to test LLI, the orientation of the apparatus is alternated between north-south or east-west (marked by crosses on the plot of Fig. 24) every 22 s over the course of many days. Nonzero values of β_y^N or β_y^e lead to sidereal oscillation of the amplitude of the difference between the north-south or east-west signals. The results of the measurements, carried out over 143 days, are consistent with no LLI violation. Combined with the constraints on electron couplings to SME background fields from Heckel *et al.* (2008), the results of this experiment probe neutron couplings to SME background fields at energy scales $\approx 10^{-25}$ eV (Brown *et al.*, 2010).

The closely related experiment of Smiciklas *et al.* (2011) uses a ^{21}Ne-Rb-K SERF comagnetometer with a shot-noise-limited sensitivity to LLI violations that is an order of magnitude better than the K-^{3}He comagetometer. Additionally, because the nuclear spin of ^{21}Ne is $I = 3/2$, the ^{21}Ne-Rb-K comagnetometer is sensitive to tensor anisotropies as well as the vector anisotropies probed by the K-^{3}He comagetometer ($I = 1/2$ for ^{3}He). A new version of this experiment, performed at the South Pole to better control for the gyrocompass effect (Hedges, Smiciklas, and Romalis, 2015), is expected to improve on these constraints by yet another order of magnitude.

A different scheme was used by Allmendinger, Heil *et al.* (2014) to test LV in the neutron sector at a similar level of accuracy by measuring precession of overlapping ensembles of ^{3}He and ^{129}Xe atoms [although note the discussion between Allmendinger, Schmidt *et al.* (2014) and Romalis *et al.* (2014) regarding these results].
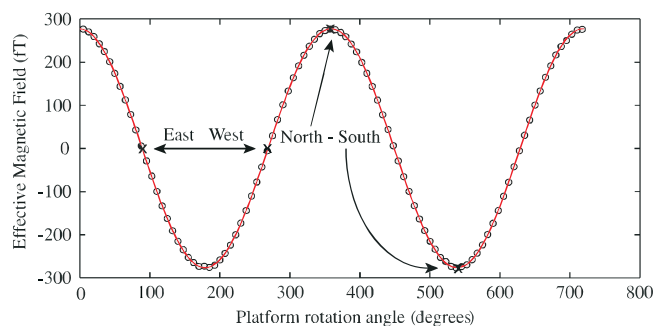

FIG. 24. Change of K-^{3}He self-compensating SERF comagnetometer signal for 180° platform rotation as a function of the initial platform angle. From Brown *et al.*, 2010.

C. Quartz oscillators

Lo *et al.* (2016) proposed and demonstrated a novel approach to LLI tests in the matter sector taking advantage of new, compact, and reliable quartz oscillator technology. Violations of LLI in the matter and photon sector of the SME generate anisotropies in particles' inertial masses and the elastic constants of solids, giving rise to anisotropies in the resonance frequencies of acoustic modes in solids. Thus the spatial-orientation dependence of acoustic resonances can be used to constrain LV: the initial experiment of Lo *et al.* (2016) set constraints on certain SME parameters some 3 orders of magnitude more stringent than other laboratory tests and 10 times more stringent than astrophysical limits.

D. Photon sector of the SME

At the close of this section, we return to the experimental setup that was the basis of the first tests of Lorentz invariance, the rotating interferometer. Recent experiments with rotating optical and microwave resonators establish some of the most stringent constraints on LV in the photon sector (Müller *et al.*, 2007; Eisele, Nevsky, and Schiller, 2009; Herrmann *et al.*, 2009; Hohensee *et al.*, 2010; Nagel *et al.*, 2015; Chen, Magoulakis, and Schiller, 2016). For example, Eisele, Nevsky, and Schiller (2009) searched for a spatial anisotropy of the speed of light using two orthogonal standing-wave optical cavities contained in a single block of glass with ultralow thermal expansion coefficient. The orthogonal cavities were probed with a laser and rotated nearly 200 000 times over the course of 13 months using an air cushion rotation table with low axis wobble, low vibration level, and active stabilization of optical elements. The quantity of interest in the experiment was the spatial-orientation dependence of the beat frequency between the light from the two cavities, which was found to be invariant at a level below a part in 10^{17}. The experiment of Nagel *et al.* (2015) improved upon this result by a factor of 10 through the use of two cryogenic cylindrical copper cavities loaded with identical sapphire dielectric crystals whose axes were oriented orthogonally to one another. Whispering gallery mode resonances near 13 GHz were excited and the apparatus was rotated with a period of ≈ 100 s. Again the observable was the spatial-orientation dependence of the beat frequency between the signals from the two microwave cavities. Compared to the original experiments of Michelson and Morley (1887), this is an improvement of 17 orders of magnitude. Kostelecký, Melissinos, and Mewes (2016) also point out that gravitational-wave detectors, km-scale laser interferometers with exquisite sensitivity, establish constraints on certain LV parameters of the SME that are several orders of magnitude more stringent than previous limits. Even more stringent constraints come from reinterpretation of existing data: Flambaum and Romalis (2017) noted that by analyzing the Coulomb interactions between the constituent particles of atoms and nuclei, comagnetometer experiments testing LLI (Smiciklas *et al.*, 2011) established that the speed of light is isotropic to a part in 10^{28}.

XII. SEARCH FOR VIOLATIONS OF QUANTUM STATISTICS, SPIN-STATISTICS THEOREM

The concept of *identical particles* is unique to quantum physics. In contrast to, for example, identical twins or so-called "standard-candle" supernovae, all electrons, helium atoms, ^{85}Rb nuclei, etc., are truly identical to each other. This means that if we have a wave function representing a system containing identical particles, particle densities should not change upon interchange of two identical particles. As a consequence, the wave function should either remain invariant or change sign under permutation of identical particles. This is the essence of the permutation-symmetry postulate (PSP). The spin-statistics theorem (SST) dictates which of the two options is realized given the particular intrinsic spin of the particles. (This connection is nontrivial and, one might argue, *a priori* unexpected.) The resulting division of particles into fermions and bosons is one of the cornerstones of modern physics.

The SST is proved in the framework of relativistic field theory using the assumptions of causality and Lorentz invariance in $3 + 1$ spacetime dimensions, along with a number of more subtle implicit assumptions enumerated by Wichmann (2001).

While it is difficult to build a consistent relativistic theory incorporating SST and PSP violations (a feat that has not as yet been accomplished, to our knowledge), it is necessary to put these properties to rigorous tests given their fundamental importance to our understanding of nature. One may think of such tests as probing all the assumptions in the SST proof as well as providing a possible experimental window into theories that go beyond conventional field theory, for instance, string theory. For example, plausible theoretical scenarios for small spin-statistics violations include excitations of higher dimensions allowing particles to possess wrong-symmetry states in the usual three-dimensional space while maintaining the correct symmetry in an N-dimensional space (Greenberg and Mohapatra, 1989).

Since all our observations so far are consistent with PSP and SST, the experiments should search for small violations of PSP and SST, the effects sometimes referred to as "violations of quantum statistics."

Comprehensive reviews of the literature on the spin-statistics connection and related issues such as the Pauli exclusion principle and particle indistinguishably, including theoretical background and experimental searches, can be found in a book edited by Hilborn and Tino (2000) and a paper by Curceanu, Gillaspy, and Hilborn (2012). Here we limit our discussion to examples of recent experiments of atomic, molecular, and optical techniques that are used in this field.

The strongest limit on a possible violation of the Pauli exclusion principle for electrons currently comes from the VIP experiment at Gran Sasso (Marton *et al.*, 2013). Here strong electric current is flown through a copper sample and Pauli-forbidden atomic transitions involving occupied atomic orbitals are searched for by measuring x rays at the anticipated transition energy. The limit on the probability for two electrons to be in a symmetry-forbidden state is currently $< 4.7 \times 10^{-29}$ with expected improvement in the upgraded VIP2 experiment by a further 2 orders of magnitude (Shi *et al.*, 2016; Marton *et al.*, 2017).

Molecular spectroscopy has played an important historical role in establishing the experimental basis for the PSP and the SST (Curceanu, Gillaspy, and Hilborn, 2012). The general idea is that in a molecule containing two identical nuclei rotational states corresponding to the overall molecular wave function being symmetric (in the case of half-integer-spin nuclei) or antisymmetric (in the case of integer-spin nuclei) are forbidden by quantum statistics, and so the spectral lines involving these molecular states are absent from the molecular spectrum. A powerful experimental methodology for testing for statistics violations is to look for such forbidden lines (Tino, 2001).

Recent experiments (Cancio Pastor *et al.*, 2015) using saturated-absorption cavity ring-down spectroscopy searched for forbidden rovibrational lines at a $4.25\ \mu$m wavelength in the spectra of the ^{12}C^{16}O$_2$ molecule containing two bosonic oxygen nuclei. They limited the relative probability for the molecule to be in a wrong-symmetry state at the $< 3.8 \times 10^{-12}$ level, significantly improving on earlier results. An interesting extension is to molecules containing more than two identical nuclei that would allow one to probe for more complex permutation symmetries than are allowed for just two identical particles (Tino, 2000, 2001).

An experimental test of Bose-Einstein (BE) statistics and, consequently, the SST as it applies to photons interacting with atoms was carried out by English, Yashchuk, and Budker (2010). The experiment, extending earlier work (DeMille *et al.*, 1999), used a selection rule for atomic transitions that is closely related to the Landau-Yang theorem (Landau, 1948; Yang, 1950) in high-energy physics. The selection rule states that two collinear, equal-frequency, photons cannot be in a state of total angular momentum 1. An example in high-energy physics is that the neutral spin-1 Z_0 boson cannot decay to two photons. (According to the Particle Data Group, the branching ratio for this process is limited to $< 5.2 \times 10^{-5}$, although there are additional reasons that suppress such decay.) For atoms, the selection rule means that two collinear equal-frequency photons cannot stimulate a transition between atomic states of total angular momentum 0 and 1. The experiment employed an atomic beam of barium optically excited in a power-buildup cavity and resulted in a limit for two photons to be in the wrong (i.e., fermionic) symmetry state of $< 4.0 \times 10^{-11}$. Further improvements by several orders of magnitude are expected in ongoing experiments using ultracold Sr atoms (Guzman, Inaki, and Penaflor, 2015).

As mentioned, quantum-statistics violation would be an effect outside of the framework of conventional field theory, in contrast to most other "exotic" effects discussed in this review. Combined with the absence of a consistent alternative framework, discussion of such effects often leads to conceptual difficulties, including questions such as what is the experiment really testing, and how can we compare results from different experiments, etc.

The results of some early experiments were dismissed as they did not take into account a so-called *superselection rule* stating that the permutation symmetry of a system of identical particles cannot change in the course of the system's evolution. Being truly identical implies that the particles cannot be distinguished by any measurement. In particular, this means that all operators corresponding to physical observables

must commute with all exchange operators ξ, for example, $[H, \xi] = 0$ for any Hamiltonian H. This fact is used by Amado and Primakoff (1980) to derive the aforementioned superselection rule, which implies

$$\langle A|H|S \rangle = 0, \qquad (105)$$

where $|S\rangle$ and $|A\rangle$ are exchange symmetric and antisymmetric states, respectively. The superselection rule prevents, for example, the transition between a symmetric and antisymmetric state (as was searched for in some early experiments purporting to test the SST) based purely on the fact that the particles are identical and not on the PSP or SST. However, it is important here to note that the superselection rule does not prevent creation of particles with mixed statistics. The quon algebra (Greenberg, 1991; Greenberg and Hilborn, 1999), for example, takes advantage of this exception by postulating creation and annihilation operators which do not obey the usual commutation relations, leading to the creation of particle states which are neither symmetric nor antisymmetric. Another immediate consequence of the superselection rule is that a description in terms of a wave function with a mixed permutation symmetry is not acceptable and a density matrix should be used instead. A further discussion of these points and related references can be found in the paper by Elliott *et al.* (2012).

XIII. CONCLUSION

AMO physics has been crucially important in laying the foundation of our understanding of the fundamental laws of nature ever since the advent of precision spectroscopy in the 19th century. The most remarkable success is the discovery of the inevitability of quantum theory and its subsequent spectacular development, including firming up such fundamental concepts as indistinguishability of identical particles, the spin-statistics connection, the role of discrete symmetries such as parity and time-reversal invariance, entanglement, relativistic quantum mechanics, and quantum field theory, and many others. From the early days, AMO physics has been closely connected to astronomy and astrophysics, from the discovery of new elements in the solar spectrum to determining the velocities of stars and measuring the expansion of the Universe via redshifts of spectral lines. The list of seminal fundamental physics discoveries using AMO techniques can, of course, be made almost arbitrarily long.

Remarkably, two centuries after its birth, the field of precision AMO tests of fundamental physics continues to be at the forefront of discovery, showing no signs of slowing down. Conversely, with collider physics becoming more and more expensive and potentially reaching saturation in terms of accessible particle energies and intensities, AMO physics complements high-energy physics and, in some cases, provides powerful ways to indirectly explore potential new phenomena at energy scales reaching orders of magnitude beyond what can be expected to be directly accessible with accelerators in the foreseeable future.

Having powerful AMO tools for fundamental physics inquiry is especially important because there are many basic properties of the Universe that we do not understand.

• What are dark matter and dark energy?
• Why is there so much more matter in the Universe than antimatter?
• Why are the masses of all known particles so much smaller than the fundamental energy scales such as the grand unification and the Planck scales?
• Why do strong interactions appear to respect the *CP* symmetry?
• What lies beyond the standard model of particles and interactions?
• How can general relativity be unified with quantum theory?

These questions are, in a sense, "urgent." For instance, dark matter constitutes most of the mass in galaxies including our own, and so it is likely that a discovery of the dark matter composition is "around the corner."

We hope that with this review we have succeeded in conveying our own excitement and anticipation of forthcoming paradigm-shifting discoveries in fundamental physics with atoms, molecules, and light.

APPENDIX A: NOTATIONS, UNITS, AND ABBREVIATIONS

1. Atomic and molecular properties as encoded in spectroscopic notation

Atoms and molecules make wonderful clocks and precision measurement instruments because their electronic states offer

read, write, and storage capabilities extending across many decades of bandwidth. Key properties of a given state can be understood by symmetry considerations for which an understanding of conventional spectroscopic notation is a useful aid. We present a brief summary of notation that is germane to most of the specific examples discussed in this review. The concepts can be found on display in the periodic table of the elements constructed for use in atomic spectroscopy (Dragoset *et al.*, 2017). More comprehensive accounts can be found in Bunker *et al.* (1997), Schutte *et al.* (1997a, 1997b), and Martin and Wiese (2002).

2. Atomic symmetries

The conventional periodic table of the elements (Dragoset *et al.*, 2017) is laid out in a way that displays the *Aufbau* principle. As the atomic number Z increases, electrons are added one by one to atomic electron shells. These are labeled by the integer principal quantum number $n \geq 1$ and orbital angular momentum quantum number l $(0 \leq l < n)$. These two quantum numbers are encountered in the nonrelativistic quantum theory of the hydrogen atom. The beginning of the nth row of the periodic table marks the start of filling the electron shell $n, 0$, and the end marks the filling of an electron shell.

This representation of atomic structure is only an approximate model, but it also defines a zeroth-order basis of many-electron wave functions that can be consistently improved upon and enlarged by techniques of quantum many-body theory. Good guidance for rough estimates of energies and transition probabilities is communicated in a standard notation. This notation expresses in order of descending magnitude of energy: the atomic mean field (configuration), the electron-electron interaction (term), the spin-orbit interaction (electronic level), the possible electron-nucleus interactions (hyperfine level), and the projection of the total angular momentum (Zeeman sublevel).

We illustrate this using the example of the ground state of cerium (Ce, Z = 58). Its electron configuration is conventionally described as

$$1s^2 2s^2 2p^6 3s^2 3p^6 3d^{10} 4s^2 4p^6 4d^{10} 5s^2 5p^6 4f^1 5d^1 6s^2. \quad (A1)$$

Here s, p, d, and f designate $l = 0$, 1, 2, and 3, and the superscripts designate occupation numbers. Thus, starting from the left, Eq. (A1) indicates that there are two electrons in the $n = 1$, $l = 0$ shell, two more in the 2, 0 subshell of the $n = 2$ shell, six more in the 2, 1 subshell, and so on up to the last closed subshell $5p$. That consolidated list of subshells is the same as that for the ground state of Xe, so it is convenient to rewrite Eq. (A1) as

$$[\text{Xe}]4f5d6s^2, \quad (A2)$$

where no superscript indicates single occupancy of the electron shell.

This shows that Ce has four electrons outside an isotropic closed-shell Xe-like core. These electrons determine the symmetries of the electronic wave function and have predominant influence on the atom's chemical and physical properties.

There are 140 independent electronic states that are members of the Eq. (A2) configuration. These are differentiated by the term and level hierarchies. The ground state of Ce has the term and level designation

$$[\text{Xe}]4f5d6s^2 \, {}^1G_4^\circ. \quad (A3)$$

Four properties are encoded in the rightmost expression ${}^1G_4^\circ$ of Eq. (A3):

- The state's total electronic spin angular momentum S (in units of $\hbar$), which is encoded as $2S + 1$ in the ${}^1G$ superscript. Here the state is a "spin singlet" with $S = 0$.
- The state's total electronic orbital angular momentum L (in units of $\hbar$), which is encoded as a capital letter. The string $SPDFGHIK$ expresses the character values for $0 \leq L \leq 7$. Here the state has $L = 4$.
- The state's total electronic angular momentum J (in units of $\hbar$), which is shown in the ${}^1G_4^\circ$ subscript. Here $J = 4$, consistent with $L = 4$ and $S = 0$.
- The state's parity under inversion of spatial coordinates. This is sometimes shown by $\circ$ if the parity is odd, and the superscript is omitted for even-parity states. Indeed it is redundant, because the parity is given by (-1) to the power of $\sum_k l_k$, where the sum runs over all atomic electrons. Here it is odd, which is readily verified since $4f$ is the only electron shell that makes an odd contribution to the sum.

Of these four indices, only two are exact: parity (to the extent that electroweak interactions are negligible) and total angular momentum J (in cases where there is no nuclear angular momentum or neglecting hyperfine structure). Concerning J, when there is no hyperfine structure, the application of a weak magnetic field reveals that the ground level has $2J + 1$ distinct Zeeman sublevels. As for S and L, there are cases in which it is meaningful to consider them as good quantum numbers. For example, helium was once considered to consist of two elements, orthohelium and parahelium, because it evinced distinctive singlet and triplet spectra, between which there seemed to be no connection (Keesom, 1942). Now we understand those to be spectra associated with states that are (predominantly) $S = 0$ and 1, respectively. In many cases of atoms with several valence electrons, different configurations and terms are strongly mixed, and the dominant configuration and LS term are listed. Indeed, our example expression, Eq. (A3), is a case in point. The Ce ground state approximately described by Eq. (A3) is, in fact, a mixture of different configuration and terms, where the weight of Eq. (A3) is about 60% (Kramida, Ralchenko, and Reader, 2018).

When the atomic nucleus has no angular momentum, as is the case for all even-even isotopes in their nuclear ground state, then a level designation such as Eq. (A3) identifies $2J + 1$ degenerate states, corresponding to the distinct values of M_J, the projection of $\mathbf{J}$ upon some arbitrary quantization axis. When the nucleus has spin $\mathbf{I} \neq 0$, then the total atomic angular momentum is designated $\mathbf{F} = \mathbf{I} + \mathbf{J}$. As before, the corresponding quantum numbers are I, J, and F. The

magnetic quantum number of an atomic state M_F takes one of $2F + 1$ discrete values. The separate values of F correspond to different relative arrangements of electronic and nuclear magnetic and electric moments, whereby they have slightly different energies. These energy differences were called "hyperfine structures" when they were first interpreted by Pauli (1924), because they were a minute detail of atomic spectra.

3. Molecular symmetries

The molecular term symbols that designate the electronic states of a diatomic molecule take the form

$$^{2S+1}\Lambda^{(+/-)}_{\Omega,(g/u)}. \tag{A4}$$

The symbols Λ, S, and Ω are analogous to their atomic counterparts L, S, and J. Indeed, S designates the same net electronic spin in both cases. In the body frame of the molecule, i.e., a frame in which the internuclear axis is fixed in space, rotations of all electrons about the internuclear axis commute with the Hamiltonian, so projections of electronic angular momentum upon that axis can be taken to be good quantum numbers. The absolute value of the projection upon this axis of electronic orbital angular momentum L is designated Λ (in units of $\hbar$). Thus, $\Lambda = 0, 1, 2, 3, \ldots$, designated, respectively, by uppercase Greek letters Σ, Π, Δ, Φ, etc. in analogy with the atomic S, P, D, F, etc.. As atomic L is to Λ, so is atomic J to Ω, which is the magnitude of the projection of electronic total angular momentum upon the internuclear axis, again in units of $\hbar$. As for J in atoms, Ω is an integer or half integer. As an example, we consider a state of the thorium oxide molecule ThO that is mentioned in Sec. V.F.2. Its electronic state is labeled there as $^3\Delta_1$, thus $S = 1$, $\Lambda = 2$, and $\Omega = 1$.

For isolated molecules, only total angular momentum is rigorously conserved. Total angular momentum and parity also depend on the rotational motion of the molecule. The rotational quantum number is designated $J = 0, 1, 2, \ldots$; the corresponding inversion symmetry is $(-1)^J$. For homonuclear diatomic molecules, there is an additional quantum number associated with inversion with respect to the symmetry plane bisecting the line connecting the two nuclei. It can be even (German "gerade") or odd ("ungerade") under this transformation, which is represented in the term symbol as g or u.

Finally, there is a symmetry of the molecular Hamiltonian under reflection in any plane that contains the internuclear axis. The electronic wave function may be even or odd under this transformation, which accounts for the $+$ or $-$ superscript that is an option in Eq. (A4). It is used only for Σ states, the best-known example being the $^3\Sigma_g^-$ ground state of molecular oxygen O_2.

4. Units

The International System of Units (SI) is used throughout this paper, unless noted otherwise. Atomic units are often used in the source literature. In atomic units, the values of elementary charge e, the electron mass m_e, and the reduced Planck constant $\hbar$ have a numerical value of 1, and the electric constant ϵ_0 has a numerical value of $1/(4\pi)$. The conversion between SI and atomic units for commonly used quantities, including formulas and numerical values, is given, for example, in Table XXXVII of Mohr, Newell, and Taylor (2016), p. 62. For example, the atomic unit of the electric field is $\mathcal{E}_{at} = e/(4\pi\epsilon_0 a_0^2)$.

5. Symbols and abbreviations

The common mathematical symbols and abbreviations which appear throughout the review are listed in Tables III and IV for convenience. Section-specific notations are given under the section headings. The designations specific to a single subtopic and used only briefly are not tabulated here, but are defined the first time they are introduced. CODATA

TABLE III.   Mathematical symbols used and their meanings.

Symbol	Meaning
c	speed of light
ϵ_0	electric constant
G	Newtonian constant of gravitation
h	Planck constant, $\hbar = h/2\pi$
e	elementary charge
α	fine-structure constant
R_∞	Rydberg constant
a_0	Bohr radius
μ_N	nuclear magneton
G_F	Fermi constant
g	local acceleration due to the Earth's gravity
m_e	electron mass
m_p	proton mass
M_Z	Z-boson mass
θ_W	weak mixing angle
σ_i	Pauli matrices $i = 1, 2, 3$
γ_μ	Dirac matrices $\mu = 0, 1, 2, 3$
γ_5	Dirac matrix associated with pseudoscalars
$\sigma^{\mu\nu}$	$\sigma^{\mu\nu} = \frac{i}{2}(\gamma^\mu\gamma^\nu - \gamma^\nu\gamma^\mu)$
$\mathbf{s}$	single electron spin
$\mathbf{S}$	multielectron atom total spin
$\mathbf{p}$	linear momentum
$\mathcal{E}$	electric field (vector)
$\mathcal{B}$	magnetic field (vector)
C, P, T	charge conjugation, parity, and time-reversal transformations
$\mu = m_p/m_e$	proton to electron mass ratio, $\bar{\mu} = 1/\mu$ (Sec. II)
K	dimensionless sensitivity factor of an energy level to α variation (Sec. II)
K_μ	dimensionless sensitivity factor of an energy level to μ variation (Sec. II)
m_q	average mass of light quarks (Sec. II)
Λ_{QCD}	QCD energy scale (Sec. II)
κ	dimensionless sensitivity factor of an energy level to a variation of $X_q = m_q/\Lambda_{QCD}$ (Sec. II)
k_X	dimensionless factor quantifying the spatial variation of the fundamental constant X (Sec. II)
Q_W	nuclear weak charge (Sec. IV)
$\mathbf{d}$	electric dipole moment (Sec. V)
$\mathcal{P}$	dimensionless electrical polarization (Sec. V)
$\mathcal{S}$	Schiff moment (Sec. V)
$\tilde{d}$	chromo-EDM (Sec. V)
$\hat{\sigma}$	unit vector along spin (Sec. VII)

TABLE IV.   Acronyms and abbreviations.

Abbreviation	Meaning
ALPs	axionlike particles
AMO	atomic, molecular, and optical physics
APV	atomic parity violation
CPT	combined operation *CPT*
CPV	*CP* violation
cEDM	chromo-EDM
DFSZ	Dine-Fischler-Srednicki-Zhitnitskii
DM	dark matter
EDM	electric dipole moment
eEDM	electron EDM
EEP	Einstein equivalence principle
GDM	gravitational dipole moment
GR	general relativity
GPS	Global Positioning System
GW	gravitational wave
HCI	highly charged ion
ISL	inverse-square law
KSVZ	Kim-Shifman-Vainshtein-Zakharov
LHC	Large Hadron Collider
LLI	local Lorentz invariance
LPI	local position invariance
LV	Lorentz symmetry violation
MQM	magnetic quadrupole moment
MWDM	Moody-Wilczek-Dobrescu-Mocioiu
NAM	nuclear anapole moment
NIST	National Institute of Standards and Technology
NMR	nuclear magnetic resonance
nr	nonrelativistic
PSP	permutation-symmetry postulate
QCD	quantum chromodynamics
SCCEF	Sun centered celestial-equatorial frame
SLI	semileptonic interaction
SM	standard model
SME	standard model extension
SMt	Schiff moment
SQUID	superconducting quantum interference device
SST	spin-statistics theorem
SUSY	supersymmetry
T,PV	simultaneous *T* and *P* violation
TV	*T* violating but *P* conserving
UFF	universality of free fall
VULF	virialized ultralight field
WEP	weak equivalence principle
WIMP	weakly interacting massive particle

and Particle Data Group designations are adopted in the review for common quantities. Every effort is made to use notations and abbreviations which most commonly appear in the literature.

REFERENCES

Aad, G., *et al.* (ATLAS Collaboration), 2012, "Observation of a new particle in the search for the Standard Model Higgs boson with the ATLAS detector at the LHC," Phys. Lett. B **716**, 1.

Abbott, B. P., *et al.*, 2017, "Exploring the sensitivity of next generation gravitational wave detectors," Classical Quantum Gravity **34**, 044001.

Abbott, B. P., *et al.* (LIGO Scientific Collaboration and Virgo Collaboration), 2016a, "GW151226: Observation of gravitational waves from a 22-solar-mass binary black hole coalescence," Phys. Rev. Lett. **116**, 241103.

Abbott, B. P., *et al.* (LIGO Scientific Collaboration and Virgo Collaboration), 2016b, "Observation of gravitational waves from a binary black hole merger," Phys. Rev. Lett. **116**, 061102.

Abbott, L. F., and P. Sikivie, 1983, "A cosmological bound on the invisible axion," Phys. Lett. B **120**, 133.

Abe, M., G. Gopakumar, M. Hada, B. P. Das, H. Tatewaki, and D. Mukherjee, 2014, "Application of relativistic coupled-cluster theory to the effective electric field in YbF," Phys. Rev. A **90**, 022501.

Abel, C., *et al.*, 2017, "Search for axionlike dark matter through nuclear spin precession in electric and magnetic fields," Phys. Rev. X **7**, 041034.

Abele, H., T. Jenke, H. Leeb, and J. Schmiedmayer, 2010, "Ramsey's method of separated oscillating fields and its application to gravitationally induced quantum phase shifts," Phys. Rev. D **81**, 065019.

Abrahamyan, S., *et al.*, 2012, "Measurement of the neutron radius of ^{208}Pb through parity violation in electron scattering," Phys. Rev. Lett. **108**, 112502.

Ackerman, Lotty, Matthew R. Buckley, Sean M. Carroll, and Marc Kamionkowski, 2009, "Dark matter and dark radiation," Phys. Rev. D **79**, 023519.

Acosta, V., M. P. Ledbetter, S. M. Rochester, D. Budker, D. F. Jackson Kimball, D. C. Hovde, W. Gawlik, S. Pustelny, J. Zachorowski, and V. V. Yashchuk, 2006, "Nonlinear magneto-optical rotation with frequency-modulated light in the geophysical field range," Phys. Rev. A **73**, 053404.

Adam, R., *et al.* (Planck Collaboration), 2016, "Planck 2015 results," Astron. Astrophys. **594**, A1.

Adelberger, E. G., J. H. Gundlach, B. R. Heckel, S. Hoedl, and S. Schlammiger, 2009, "Torsion balance experiments: A low-energy frontier of particle physics," Prog. Part. Nucl. Phys. **62**, 102.

Adelberger, E. G., B. R. Heckel, S. Hoedl, C. D. Hoyle, D. J. Kapner, and A. Upadhye, 2007, "Particle-physics implications of a recent test of the gravitational inverse-square law," Phys. Rev. Lett. **98**, 131104.

Adelberger, E. G., B. R. Heckel, and A. E. Nelson, 2003, "Tests of the gravitational inverse-square law," Annu. Rev. Nucl. Part. Sci. **53**, 77.

Adelberger, E. G., B. R. Heckel, C. W. Stubbs, and Y. Su, 1991, "Does antimatter fall with the same acceleration as ordinary matter?," Phys. Rev. Lett. **66**, 850.

Adkins, Gregory S., Minji Kim, Christian Parsons, and Richard N. Fell, 2015, "Three-photon-annihilation contributions to positronium energies at order ma^7," Phys. Rev. Lett. **115**, 233401.

Afach, S., *et al.*, 2015, "Constraining interactions mediated by axion-like particles with ultracold neutrons," Phys. Lett. B **745**, 58.

Aghion, S., *et al.*, 2014, "A moiré deflectometer for antimatter," Nat. Commun. **5**, 4538.

Aguilera, D. N., *et al.*, 2014, "STE-QUEST—test of the universality of free fall using cold atom interferometry," Classical Quantum Gravity **31**, 115010; "Corrigendum: STE-QUEST—test of the universality of free fall using cold atom interferometry," **31**, 159502 (2014).

Ahmadi, M., *et al.*, 2016, "An improved limit on the charge of antihydrogen from stochastic acceleration," Nature (London) **529**, 373.

Ahmadi, M., *et al.*, 2017a, "Observation of the $1s-2s$ transition in trapped antihydrogen," Nature (London) **541**, 506.

Ahmadi, M., *et al.*, 2017b, "Observation of the hyperfine spectrum of antihydrogen," Nature (London) **548**, 66.

Aidala, C., S. Bass, D. Hasch, and G. Mallot, 2013, "The spin structure of the nucleon," Rev. Mod. Phys. **85**, 655.

Aldaihan, S., D. E. Krause, J. C. Long, and W. M. Snow, 2017, "Calculations of the dominant long-range, spin-independent contributions to the interaction energy between two nonrelativistic Dirac fermions from double-boson exchange of spin-0 and spin-1 bosons with spin-dependent couplings," Phys. Rev. D **95**, 096005.

Allen, B., W. G. Anderson, P. R. Brady, D. A. Brown, and J. D. E. Creighton, 2012, "FINDCHIRP: an algorithm for detection of gravitational waves from inspiraling compact binaries," Phys. Rev. D **85**, 122006.

Allen, S. W., R. W. Schmidt, A. C. Fabian, and H. Ebeling, 2003, "Cosmological constraints from the local X-ray luminosity function of the most X-ray-luminous galaxy clusters," Mon. Not. R. Astron. Soc. **342**, 287.

Allmendinger, F., W. Heil, S. Karpuk, W. Kilian, A. Scharth, U. Schmidt, A. Schnabel, Y. Sobolev, and K. Tullney, 2014, "New limit on Lorentz-invariance- and *CPT*-violating neutron spin interactions using a free-spin-precession ^{3}He-^{129}Xe comagnetometer," Phys. Rev. Lett. **112**, 110801.

Allmendinger, F., U. Schmidt, W. Heil, S. Karpuk, A. Scharth, Yu. Sobolev, and K. Tullney, 2014, "Allmendinger *et al.* reply," Phys. Rev. Lett. **113**, 188902.

Allred, J. C., R. N. Lyman, T. W. Kornack, and M. V. Romalis, 2002, "High-sensitivity atomic magnetometer unaffected by spin-exchange relaxation," Phys. Rev. Lett. **89**, 130801.

Alonso, A. M., B. S. Cooper, A. Deller, S. D. Hogan, and D. B. Cassidy, 2015, "Controlling positronium annihilation with electric fields," Phys. Rev. Lett. **115**, 183401.

Altmann, R. K., S. Galtier, L. S. Dreissen, and K. S. E. Eikema, 2016, "High-precision Ramsey-comb spectroscopy at deep ultraviolet wavelengths," Phys. Rev. Lett. **117**, 173201.

Altschul, B., 2006, "Limits on Lorentz violation from synchrotron and inverse compton sources," Phys. Rev. Lett. **96**, 201101.

Altschul, B., 2010, "Laboratory bounds on electron Lorentz violation," Phys. Rev. D **82**, 016002.

Altschul, B., *et al.*, 2015, "Quantum tests of the Einstein equivalence principle with the STE-QUEST space mission," Adv. Space Res. **55**, 501.

Altuntas, Emine, Jeffrey Ammon, Sidney B. Cahn, and David DeMille, 2017, "Measuring nuclear spin dependent parity violation with molecules: Experimental methods and analysis of systematic errors," arXiv:1711.01988.

Altuntas, Emine, Jeffrey Ammon, Sidney B. Cahn, and David DeMille, 2018, "Demonstration of a sensitive method to measure nuclear spin-dependent parity violation," arXiv:1801.05316.

Amado, R. D., and H. Primakoff, 1980, "Comments on testing the Pauli principle," Phys. Rev. C **22**, 1338.

Amaro, P., S. Schlesser, M. Guerra, E.-O. Le Bigot, J.-M. Isac, P. Travers, J. P. Santos, C. I. Szabo, A. Gumberidze, and P. Indelicato, 2012, "Absolute measurement of the relativistic magnetic dipole transition energy in heliumlike argon," Phys. Rev. Lett. **109**, 043005.

Amaro-Seoane, P., *et al.*, 2012, "Low-frequency gravitational-wave science with eLISA/NGO," Classical Quantum Gravity **29**, 124016.

Amole, C., *et al.*, 2012, "Resonant quantum transitions in trapped antihydrogen atoms," Nature (London) **483**, 439.

Amole, C., *et al.*, 2014, "An experimental limit on the charge of antihydrogen," Nat. Commun. **5**, 3955.

Amole, C., *et al.* (ALPHA Collaboration), 2013, "Description and first application of a new technique to measure the gravitational mass of antihydrogen," Nat. Commun. **4**, 1785.

Anderson, J. D., G. Schubert, V. Trimble, and M. R. Feldman, 2015, "Measurements of Newton's gravitational constant and the length of day," Europhys. Lett. **110**, 10002.

Anderson, W. G., P. R. Brady, J. D. E. Creighton, and E. E. Flanagan, 2001, "Excess power statistic for detection of burst sources of gravitational radiation," Phys. Rev. D **63**, 042003.

Andreas, S., 2012, "Update on hidden sectors with dark forces and dark matter," *Proceedings of the 8th Patras Workshop on Axions, WIMPs and WISPs*, Report No. DESY-PROC-2012-04, arXiv:1211.5160.

Andresen, G. B., *et al.*, 2011, "Confinement of antihydrogen for 1,000 seconds," Nat. Phys. **7**, 558.

Androic, D., *et al.*, 2013, "First determination of the weak charge of the proton," Phys. Rev. Lett. **111**, 141803.

Ansel'm, A. A., 1982, "Possible new long-range interaction and methods for detecting it," Pis'ma Zh. Eksp. Teor. Fiz. **36**, 46 [JETP Lett. **36**, 46 (1982) [http://www.jetpletters.ac.ru/ps/1330/article_20100.pdf]].

Anthony, P. L., *et al.*, 1996, "Deep inelastic scattering of polarized electrons by polarized ^{3}He and the study of the neutron spin structure," Phys. Rev. D **54**, 6620.

Antognini, Aldo, *et al.*, 2013, "Proton structure from the measurement of $2s - 2p$ transition frequencies of muonic hydrogen," Science **339**, 417.

Antoniadis, I., S. Dimopoulos, and G. Dvali, 1998, "Millimetre-range forces in superstring theories with weak-scale compactification," Nucl. Phys. B **516**, 70.

Antoniadis, I., *et al.*, 2011, "Short-range fundamental forces," C.R. Phys. **12**, 755.

Antypas, D., and D. S. Elliott, 2011, "Measurements of the static polarizability of the $8s^2S_{1/2}$ state of atomic cesium," Phys. Rev. A **83**, 062511.

Antypas, D., and D. S. Elliott, 2013a, "Measurement of a weak transition moment using two-pathway coherent control," Phys. Rev. A **87**, 042505.

Antypas, D., and D. S. Elliott, 2013b, "Measurement of the radial matrix elements of the $6s^2S_{1/2} \rightarrow 7p^2P_J$ transitions in atomic cesium," Phys. Rev. A **88**, 052516.

Antypas, D., and D. S. Elliott, 2014, "Measurement of weak optical transition moments through two-pathway coherent control," Can. J. Chem. **92**, 144.

Aoyama, T., M. Hayakawa, T. Kinoshita, and M. Nio, 2008, "Revised value of the eighth-order QED contribution to the anomalous magnetic moment of the electron," Phys. Rev. D **77**, 053012.

Appelquist, Thomas, Bogdan A. Dobrescu, and Adam R. Hopper, 2003, "Nonexotic neutral gauge bosons," Phys. Rev. D **68**, 035012.

Arias, P., D. Cadamuro, M. Goodsell, J. Jaeckel, J. Redondo, and A. Ringwald, **2012**, "WISPy cold dark matter," J. Cosmol. Astropart. Phys. 06, 013.

Arkani-Hamed, N., S. Dimopoulos, and G. R. Dvali, 1998, "The hierarchy problem and new dimensions at a millimeter," Phys. Lett. B **429**, 263.

Arkani-Hamed, N., D. P. Finkbeiner, T. R. Slatyer, and N. Weiner, 2009, "A theory of dark matter," Phys. Rev. D **79**, 015014.

Arkani-Hamed, Nima, Hsin-Chia Cheng, Markus A. Luty, and Shinji Mukohyama, 2004, "Ghost condensation and a consistent infrared modification of gravity," J. High Energy Phys. 05, 074.

Arkani-Hamed, Nima, Hsin-Chia Cheng, Markus A. Luty, and Jesse Thaler, 2005, "Universal dynamics of spontaneous Lorentz violation and a new spin-dependent inverse-square law force," J. High Energy Phys. 07, 029.

Arkani-Hamed, Nima, Savas Dimopoulos, and Gia Dvali, 1999, "Phenomenology, astrophysics, and cosmology of theories with

submillimeter dimensions and TeV scale quantum gravity," Phys. Rev. D **59**, 086004.

Arkani-Hamed, Nima, and Savas Dimopoulos, 2005, "Supersymmetric unification without low energy supersymmetry and signatures for fine-tuning at the LHC," J. High Energy Phys. 06, 73.

Arndt, M., and K. Hornberger, 2014, "Testing the limits of quantum mechanical superpositions," Nat. Phys. **10**, 271.

Arnison, G., *et al.*, 1983a, "Experimental observation of isolated large transverse energy electrons with associated missing energy at $\sqrt{s} = 540$ Gev," Phys. Lett. B **122**, 103.

Arnison, G., *et al.*, 1983b, "Experimental observation of lepton pairs of invariant mass around 95 Gev/c^2 at the CERN SPS collider," Phys. Lett. B **126**, 398.

Arrington, John, and Ingo Sick, 2015, "Evaluation of the proton charge radius from electronproton scattering," J. Phys. Chem. Ref. Data **44**, 031204.

Artemyev, A. N., V. M. Shabaev, I. I. Tupitsyn, G. Plunien, and V. A. Yerokhin, 2007, "QED calculation of the $2p_{3/2} - 2p_{1/2}$ transition energy in boronlike argon," Phys. Rev. Lett. **98**, 173004.

Artemyev, A. N., V. M. Shabaev, V. A. Yerokhin, G. Plunien, and G. Soff, 2005, "QED calculation of the $n = 1$ and $n = 2$ energy levels in He-like ions," Phys. Rev. A **71**, 062104.

Arvanitaki, A., S. Dimopoulos, S. Dubovsky, N. Kaloper, and J. March-Russell, 2010, "String axiverse," Phys. Rev. D **81**, 123530.

Arvanitaki, A., S. Dimopoulos, and K. Van Tilburg, 2017, "Resonant absorption of bosonic dark matter in molecules," arXiv:1709.05354.

Arvanitaki, A., and A. A. Geraci, 2014, "Resonantly detecting axionmediated forces with nuclear magnetic resonance," Phys. Rev. Lett. **113**, 161801.

Arvanitaki, A., J. Huang, and K. Van Tilburg, 2015, "Searching for dilaton dark matter with atomic clocks," Phys. Rev. D **91**, 015015.

Asenbaum, P., C. Overstreet, T. Kovachy, D. D. Brown, J. M. Hogan, and M. A. Kasevich, 2017, "Phase shift in an atom interferometer due to spacetime curvature across its wave function," Phys. Rev. Lett. **118**, 183602.

Ashby, N., T. P. Heavner, S. R. Jefferts, T. E. Parker, A. G. Radnaev, and Y. O. Dudin, 2007, "Testing local position invariance with four cesium-fountain primary frequency standards and four NIST hydrogen masers," Phys. Rev. Lett. **98**, 070802.

Aspelmeyer, M., T. J. Kippenberg, and F. Marquardt, 2014, "Cavity optomechanics," Rev. Mod. Phys. **86**, 1391.

Asztalos, S., *et al.*, 2001, "Large-scale microwave cavity search for dark-matter axions," Phys. Rev. D **64**, 092003.

Asztalos, S. J., *et al.*, 2010, "Squid-based microwave cavity search for dark-matter axions," Phys. Rev. Lett. **104**, 041301.

Aubin, S., *et al.*, 2013, "Atomic parity non-conservation: the francium anapole project of the FrPNC collaboration at TRIUMF," Hyperfine Interact. **214**, 163.

Auerbach, N., V. V. Flambaum, and V. Spevak, 1996, "Collective T- and P-odd electromagnetic moments in nuclei with octupole deformations," Phys. Rev. Lett. **76**, 4316.

Avelino, P. P., C. J. A. P. Martins, N. J. Nunes, and K. A. Olive, 2006, "Reconstructing the dark energy equation of state with varying couplings," Phys. Rev. D **74**, 083508.

Bagdonaite, J., M. Daprà, P. Jansen, H. L. Bethlem, W. Ubachs, S. Muller, C. Henkel, and K. M. Menten, 2013, "Robust constraint on a drifting proton-to-electron mass ratio at $z = 0.89$ from methanol observation at three radio telescopes," Phys. Rev. Lett. **111**, 231101.

Bagdonaite, J., P. Jansen, C. Henkel, H. L. Bethlem, K. M. Menten, and W. Ubachs, 2013, "A stringent limit on a drifting proton-to-electron mass ratio from alcohol in the early universe," Science **339**, 46.

Bagdonaite, J., E. J. Salumbides, S. P. Preval, M. A. Barstow, J. D. Barrow, M. T. Murphy, and W. Ubachs, 2014, "Limits on a gravitational field dependence of the proton-electron mass ratio from H$_2$ in white dwarf stars," Phys. Rev. Lett. **113**, 123002.

Bailin, David, and Alex Love, 1987, "Kaluza-Klein theories," Rep. Prog. Phys. **50**, 1087.

Baker, C. A., *et al.*, 2006, "Improved experimental limit on the electric dipole moment of the neutron," Phys. Rev. Lett. **97**, 131801.

Baker, J. G., and J. I. Thorpe, 2012, "Comparison of atom interferometers and light interferometers as space-based gravitational wave detectors," Phys. Rev. Lett. **108**, 211101.

Balazs, C., G. White, and J. Yue, 2017, "Effective field theory, electric dipole moments and electroweak baryogenesis," J. High Energy Phys. 03, 30.

Ban, Shufang, Jacek Dobaczewski, Jonathan Engel, and A. Shukla, 2010, "Fully self-consistent calculations of nuclear Schiff moments," Phys. Rev. C **82**, 015501.

Banks, T., and A. Zaks, 1982, "On the phase structure of vector-like gauge theories with massless fermions," Nucl. Phys. B **196**, 189.

Barbieri, R., M. Cerdonio, G. Fiorentini, and S. Vitale, 1989, "Axion to magnon conversion. A scheme for the detection of galactic axions," Phys. Lett. B **226**, 357.

Barger, V., T. Han, C. Kao, and R.-J. Zhang, 1999, "Astrophysical constraints on large extra dimensions," Phys. Lett. B **461**, 34.

Barkov, L. M., and M. S. Zolotorev, 1978, "Measuring optical activity of bismuth vapour," Pis'ma Zh. Eksp. Teor. Fiz. **28**, 544 [JETP Lett. **28**, 503 (1978), http://www.jetpletters.ac.ru/ps/1578/article_24213.pdf].

Baron, J., *et al.*, 2014, "Order of magnitude smaller limit on the electric dipole moment of the electron," Science **343**, 269.

Baron, J., *et al.* (ACME Collaboration), 2017, "Methods, analysis, and the treatment of systematic errors for the electron electric dipole moment search in thorium monoxide," New J. Phys. **19**, 073029.

Barr, S. M., 1992a, "Measurable T- and P-odd electron-nucleon interactions from Higgs-boson exchange," Phys. Rev. Lett. **68**, 1822.

Barr, S. M., 1992b, "T-and P-odd electron-nucleon interactions and the electric dipole moments of large atoms," Phys. Rev. D **45**, 4148.

Barr, S. M., 1993, "A review of *CP* violation in atoms," Int. J. Mod. Phys. A **08**, 209.

Barr, S. M., and A. Zee, 1990, "Electric dipole moment of the electron and of the neutron," Phys. Rev. Lett. **65**, 21.

Barranco, J., and A. Bernal, 2011, "Self-gravitating system made of axions," Phys. Rev. D **83**, 043525.

Barrett, B., L. Antoni-Micollier, L. Chichet, B. Battelier, T. Lévèque, A. Landragin, and P. Bouyer, 2016, "Dual matter-wave inertial sensors in weightlessness," Nat. Commun. **7**, 13786.

Bassi, A., K. Lochan, S. Satin, T. P. Singh, and H. Ulbricht, 2013, "Models of wave-function collapse, underlying theories, and experimental tests," Rev. Mod. Phys. **85**, 471.

Beck, B. R., J. A. Becker, P. Beiersdorfer, G. V. Brown, K. J. Moody, J. B. Wilhelmy, F. S. Porter, C. A. Kilbourne, and R. L. Kelley, 2007, "Energy splitting of the ground-state doublet in the nucleus ^{229}Th," Phys. Rev. Lett. **98**, 142501.

Beck, B. R., C. Y. Wu, P. Beiersdorfer, G. V. Brown, J. A. Becker, K. J. Moody, J. B. Wilhelmy, F. S. Porter, C. A. Kilbourne, and R. L. Kelley, 2009, "Improved value for the energy splitting of the ground-state doublet in the nucleus ^{229m}Th," Report No. LLNL-PROC-415170.

Beiersdorfer, P., 2010, "Testing QED and atomic-nuclear interactions with high-Z ions," J. Phys. B **43**, 074032.

Beiersdorfer, P., E. Träbert, G. V. Brown, J. Clementson, D. B. Thorn, M. H. Chen, K. T. Cheng, and J. Sapirstein, 2014, "Hyperfine splitting of the $2s_{1/2}$ and $2p_{1/2}$ levels in Li- and Be-like ions of $^{141}_{59}$Pr," Phys. Rev. Lett. **112**, 233003.

Beiersdorfer, P., *et al.*, 2001, "Hyperfine structure of hydrogenlike thallium isotopes," Phys. Rev. A **64**, 032506.

Beloy, K., A. Borschevsky, P. Schwerdtfeger, and V. V. Flambaum, 2010, "Enhanced sensitivity to the time variation of the fine-structure constant and m_p/m_e in diatomic molecules: A closer examination of silicon monobromide," Phys. Rev. A **82**, 022106.

Bender, P. L., 2011, "Comment on "Atomic gravitational wave interferometric sensor," Phys. Rev. D **84**, 028101.

Bender, P. L., 2014, "Comparison of atom interferometry with laser interferometry for gravitational wave observations in space," Phys. Rev. D **89**, 062004.

Bennett, G. W., *et al.*, 2006, "Final report of the E821 muon anomalous magnetic moment measurement at BNL," Phys. Rev. D **73**, 072003.

Bennett, S. C., and C. E. Wieman, 1999, "Measurement of the $6S \rightarrow 7S$ transition polarizability in atomic cesium and an improved test of the standard model," Phys. Rev. Lett. **82**, 2484.

Berengut, J. C., V. A. Dzuba, and V. V. Flambaum, 2010, "Enhanced laboratory sensitivity to variation of the fine-structure constant using highly-charged ions," Phys. Rev. Lett. **105**, 120801.

Berengut, J. C., V. A. Dzuba, and V. V. Flambaum, 2011, "Transitions in Zr, Hf, Ta, W, Re, Hg, Ac and U ions with high sensitivity to variation of the fine structure constant," Phys. Rev. A **84**, 054501.

Berengut, J. C., V. A. Dzuba, V. V. Flambaum, J. A. King, M. G. Kozlov, M. T. Murphy, and J. K. Webb, 2011, "Atomic Transition Frequencies, Isotope Shifts, and Sensitivity to Variation of the Fine Structure Constant for Studies of Quasar Absorption Spectra," in *From Varying Couplings to Fundamental Physics. Astrophysics and Space Science Proceedings*, edited by C. Martins and P. Molaro (Springer, Berlin).

Berengut, J. C., V. A. Dzuba, V. V. Flambaum, and A. Ong, 2011, "Hole transitions in multiply-charged ions for precision laser spectroscopy and searching for α-variation," Phys. Rev. Lett. **106**, 210802.

Berengut, J. C., V. A. Dzuba, V. V. Flambaum, and A. Ong, 2012a, "Highly charged ions with E1, M1, and E2 transitions within laser range," Phys. Rev. A **86**, 022517.

Berengut, J. C., V. A. Dzuba, V. V. Flambaum, and A. Ong, 2012b, "Optical transitions in highly-charged californium ions with high sensitivity to variation of the fine-structure constant," Phys. Rev. Lett. **109**, 070802.

Berengut, J. C., V. A. Dzuba, V. V. Flambaum, and S. G. Porsev, 2009, "Proposed experimental method to determine α sensitivity of splitting between ground and 7.6 eV isomeric states in ^{229}Th," Phys. Rev. Lett. **102**, 210801.

Berengut, J. C., and V. V. Flambaum, 2012, "Manifestations of a spatial variation of fundamental constants on atomic clocks, Oklo, meteorites, and cosmological phenomena," Europhys. Lett. **97**, 20006.

Berengut, J. C., V. V. Flambaum, J. A. King, S. J. Curran, and J. K. Webb, 2011, "Is there further evidence for spatial variation of fundamental constants?," Phys. Rev. D **83**, 123506.

Berengut, J. C., V. V. Flambaum, and A. Ong, 2013, "Testing spatial α-variation with optical atomic clocks based on highly charged ions," Eur. Phys. J. Web Conf. **57**, 02001.

Berengut, J. C., V. V. Flambaum, A. Ong, J. K. Webb, J. D. Barrow, M. A. Barstow, S. P. Preval, and J. B. Holberg, 2013, "Limits on the dependence of the fine-structure constant on gravitational potential from white-dwarf spectra," Phys. Rev. Lett. **111**, 010801.

Berengut, J. C., E. M. Kava, and V. V. Flambaum, 2012, "Is there a spatial gradient in values of the fine-structure constant? A reanalysis of the results," Astron. Astrophys. **542**, A118.

Berengut, J. C., *et al.*, 2018, "Probing new light force-mediators by isotope shift spectroscopy," Phys. Rev. Lett. **120**, 091801.

Bergé, J., P. Touboul, and M. Rodrigues for the MICROSCOPE team, 2015, "Status of MICROSCOPE, a mission to test the equivalence principle in space," J. Phys. Conf. Ser. **610**, 012009.

Bergé, Joel, Philippe Brax, Gilles Métris, Martin Pernot-Borràs, Pierre Touboul, and Jean-Philippe Uzan, 2018, "MICROSCOPE mission: First constraints on the violation of the weak equivalence principle by a light scalar dilaton," Phys. Rev. Lett. **120**, 141101.

Bergström, L., P. Ullio, and J. H. Buckley, 1998, "Observability of γ rays from dark matter neutralino annihilations in the Milky Way halo," Astropart. Phys. **9**, 137.

Bernauer, J. C., *et al.* (A1 Collaboration), 2010, "High-precision determination of the electric and magnetic form factors of the proton," Phys. Rev. Lett. **105**, 242001.

Bernreuther, Werner, and Mahiko Suzuki, 1991, "The electric dipole moment of the electron," Rev. Mod. Phys. **63**, 313.

Bertoldi, A., G. Lamporesi, L. Cacciapuoti, M. de Angelis, M. Fattori, T. Petelski, A. Peters, M. Prevedelli, J. Stuhler, and G. M. Tino, 2006, "Atom interferometry gravity-gradiometer for the determination of the Newtonian gravitational constant G," Eur. Phys. J. D **40**, 271.

Bertone, G., 2013, Ed., *Particle Dark Matter: Observations, Models and Searches* (Cambridge University, Cambridge, UK).

Bertone, G., D. Hooper, and J. Silk, 2005, "Particle dark matter: Evidence, candidates and constraints," Phys. Rep. **405**, 279.

Beyer, A., *et al.*, 2017, "The Rydberg constant and proton size from atomic hydrogen," Science **358**, 79.

Bezerra, V. B., G. L. Klimchitskaya, V. M. Mostepanenko, and C. Romero, 2011, "Constraints on non-Newtonian gravity from measuring the Casimir force in a configuration with nanoscale rectangular corrugations," Phys. Rev. D **83**, 075004.

Biedermann, G. W., X. Wu, L. Deslauriers, S. Roy, C. Mahadeswaraswamy, and M. A. Kasevich, 2015, "Testing gravity with cold-atom interferometers," Phys. Rev. A **91**, 033629.

Biesheuvel, J., J.-P. Karr, L. Hilico, K. S. E. Eikema, W. Ubachs, and J. C. J. Koelemeij, 2016, "Probing QED and fundamental constants through laser spectroscopy of vibrational transitions in HD$^+$," Nat. Commun. **7**, 10385.

BIPM, 2014, "SI Brochure: The International System of Units (SI) [8th edition, 2006; updated in 2014]," available online: http://www.bipm.org/en/publications/si-brochure.

Bishof, Michael, *et al.*, 2016, "Improved limit on the ^{225}Ra electric dipole moment," Phys. Rev. C **94**, 025501.

Bjorken, James D., and S. D. Drell, 1964, *Relativistic Quantum Mechanics* (McGraw-Hill, New York).

Blatt, J. M., and V. F. Weisskopf, 1979, *Theoretical Nuclear Physics* (Springer, New York).

Blatt, S., *et al.*, 2008, "New limits on coupling of fundamental constants to gravity using ^{87}Sr optical lattice clocks," Phys. Rev. Lett. **100**, 140801.

Bloch, I., J. Dalibard, and S. Nascimbène, 2012, "Quantum simulations with ultracold quantum gases," Nat. Phys. **8**, 267.

Bloch, I., J. Dalibard, and W. Zwerger, 2008, "Many-body physics with ultracold gases," Rev. Mod. Phys. **80**, 885.

Bluhm, R., V. A. Kostelecký, and N. Russell, 1997, "Testing *CPT* with anomalous magnetic moments," Phys. Rev. Lett. **79**, 1432.

Blum, K., and D. Kushnir, 2016, "Neutrino signal of collapse-induced thermonuclear supernovae: The case for prompt black hole formation in SN 1987A," Astrophys. J. **828**, 31.

Blundell, S. A., W. R. Johnson, and J. Sapirstein, 1990, "High-accuracy calculation of the $6S_{1/2}$ to $7S_{1/2}$ parity-nonconserving transition in atomic cesium and implications for the standard model," Phys. Rev. Lett. **65**, 1411.

Bonnin, A., N. Zahzam, Y. Bidel, and A. Bresson, 2013, "Simultaneous dual-species matter-wave accelerometer," Phys. Rev. A **88**, 043615.

Botermann, Benjamin, *et al.*, 2014, "Test of time dilation using stored Li$^+$ ions as clocks at relativistic speed," Phys. Rev. Lett. **113**, 120405.

Bouchendira, R., P. Cladé, S. Guellati-Khélifa, F. Nez, and F. Biraben, 2011, "New determination of the fine structure constant and test of the quantum electrodynamics," Phys. Rev. Lett. **106**, 080801.

Bouchiat, C., and P. Fayet, 2005, "Constraints on the parity-violating couplings of a new gauge boson," Phys. Lett. B **608**, 87.

Bouchiat, C., and C. A. Piketty, 1983, "Parity violation in atomic cesium and alternatives to the standard model of electroweak interaction," Phys. Lett. B **128**, 73.

Bouchiat, C., and C. A. Piketty, 1991, "Nuclear spin dependent atomic parity violation, nuclear anapole moments and the hadronic axial neutral current," Z. Phys. C **49**, 91.

Bouchiat, M. A., and C. Bouchiat, 1974, "Parity violation induced by weak neutral currents in atomic physics. I," J. Phys. Conf. Ser. **35**, 899.

Bouchiat, M. A., and C. Bouchiat, 1975, "Parity violation induced by weak neutral currents in atomic physics. II," J. Phys. (France) **36**, 493.

Bouchiat, M.-A., and C. Bouchiat, 1997, "Parity violation in atoms," Rep. Prog. Phys. **60**, 1351.

Bouchiat, M. A., J. Guena, L. Pottier, and L. Hunter, 1984, "New observation of a parity violation in cesium," Phys. Lett. B **134**, 463.

Bouchiat, Marie-Anne, 2007, "Linear Stark shift in dressed atoms as a signal to measure a nuclear anapole moment with a cold-atom fountain or interferometer," Phys. Rev. Lett. **98**, 043003.

Braaten, E., A. Mohapatra, and H. Zhang, 2016, "Dense axion stars," Phys. Rev. Lett. **117**, 121801.

Bradley, R., J. Clarke, D. Kinion, L. J. Rosenberg, K. van Bibber, S. Matsuki, M. Mück, and P. Sikivie, 2003, "Microwave cavity searches for dark-matter axions," Rev. Mod. Phys. **75**, 777.

Brans, C., and R. H. Dicke, 1961, "Mach's principle and a relativistic theory of gravitation," Phys. Rev. **124**, 925.

Brax, P., S. Fichet, and G. Pignol, 2017, "Bounding quantum dark forces," arXiv:1710.00850.

Brown, B. A., G. F. Bertsch, L. M. Robledo, M. V. Romalis, and V. Zelevinsky, 2017, "Nuclear matrix elements for tests of local lorentz invariance violation," Phys. Rev. Lett. **119**, 192504.

Brown, B. A., A. Derevianko, and V. V. Flambaum, 2009, "Calculations of the neutron skin and its effect in atomic parity violation," Phys. Rev. C **79**, 035501.

Brown, J. M., S. J. Smullin, T. W. Kornack, and M. V. Romalis, 2010, "New limit on Lorentz- and *CPT*-violating neutron spin interactions," Phys. Rev. Lett. **105**, 151604.

Brown, R. C., S. Wu, J. V. Porto, C. J. Sansonetti, C. E. Simien, S. M. Brewer, J. N. Tan, and J. D. Gillaspy, 2013, "Quantum interference and light polarization effects in unresolvable atomic lines: Application to a precise measurement of the ^{6,7}Li D$_2$ lines," Phys. Rev. A **87**, 032504; **88**, 069902(E) (2013).

Brubaker, B. M., *et al.*, 2017, "First results from a microwave cavity axion search at 24 μeV," Phys. Rev. Lett. **118**, 061302.

Bruhns, H., J. Braun, K. Kubiček, J. R. Crespo López-Urrutia, and J. Ullrich, 2007, "Testing QED screening and two-loop contributions with He-like ions," Phys. Rev. Lett. **99**, 113001.

Bubin, Sergiy, Oleg V. Prezhdo, and Kálmán Varga, 2013, "Instability of tripositronium," Phys. Rev. A **87**, 054501.

Buckley, Matthew R., and Michael J. Ramsey-Musolf, 2012, "Precision probes of a leptophobic boson," Phys. Lett. B **712**, 261.

Bucksbaum, P. H., E. D. Commins, and L. R. Hunter, 1981, "Observations of parity nonconservation in atomic thallium," Phys. Rev. D **24**, 1134.

Budker, D., and A. Derevianko, 2015, "A data archive for storing precision measurements," Phys. Today **68**, 10.

Budker, D., W. Gawlik, D. F. Kimball, S. M. Rochester, V. V. Yashchuk, and A. Weis, 2002, "Resonant nonlinear magneto-optical effects in atoms," Rev. Mod. Phys. **74**, 1153.

Budker, D., P. W. Graham, M. Ledbetter, S. Rajendran, and A. O. Sushkov, 2014, "Proposal for a cosmic axion spin precession experiment (CASPEr)," Phys. Rev. X **4**, 021030.

Budker, D., and D. F. Jackson Kimball, 2013, Eds., *Optical Magnetometry* (Cambridge University, Cambridge, UK).

Budker, D., and M. Romalis, 2007, "Optical magnetometry," Nat. Phys. **3**, 227.

Budker, Dmitry, 1999, "Parity Nonconservation in Atoms," in *Physics Beyond the Standard Model, Proceedings of the Fifth Intrnational WEIN Symposium*, edited by P. Herczeg, C. M. Hoffman, and H. V. Klapdor-Kleingrothaus (World Scientific, Singapore), p. 418.

Budker, Dmitry, Derek F. Kimball, and David P. DeMille, 2008, *Atomic physics: an exploration through problems and solutions* (Oxford University, New York).

Bulatowicz, M., R. Griffith, M. Larsen, J. Mirijanian, C. B. Fu, E. Smith, W. M. Snow, H. Yan, and T. G. Walker, 2013, "Laboratory search for a long-range T-odd, P-odd interaction from axionlike particles using dual-species nuclear magnetic resonance with polarized ^{129}Xe and ^{131}Xe gas," Phys. Rev. Lett. **111**, 102001.

Bunker, P. R., C. J. H. Schutte, J. T. Hougen, I. M. Mills, J. K. G. Watson, and B. P. Winnewisser, 1997, "Notations and conventions in molecular spectroscopy: Part 3. Permutation and permutation-inversion symmetry notation (IUPAC Recommendations 1997)," Pure Appl. Chem. **69**, 1651.

Burrage, C., A. Kuribayashi-Coleman, J. Stevenson, and B. Thrussell, **2016**, "Constraining symmetron fields with atom interferometry," J. Cosmol. Astropart. Phys. **12**, 041.

Cacciapuoti, L., *et al.*, 2007, "Atomic clock ensemble in space: Scientific objectives and mission status," Nucl. Phys. B, Proc. Suppl. **166**, 303.

Cadoret, M., E. de Mirandes, P. Cladé, S. Guellati-Khélifa, C. Schwob, F. Nez, L. Julien, and F. Biraben, 2008, "Combination of Bloch oscillations with a Ramsey-Bordé interferometer: New determination of the fine structure constant," Phys. Rev. Lett. **101**, 230801.

Cahn, S. B., J. Ammon, E. Kirilov, Y. V. Gurevich, D. Murphree, R. Paolino, D. A. Rahmlow, M. G. Kozlov, and D. DeMille, 2014, "Zeeman-tuned rotational level-crossing spectroscopy in a diatomic free radical," Phys. Rev. Lett. **112**, 163002.

Cairncross, William B., Daniel N. Gresh, Matt Grau, Kevin C. Cossel, Tanya S. Roussy, Yiqi Ni, Yan Zhou, Jun Ye, and Eric A. Cornell, 2017, "Precision measurement of the electron's electric dipole moment using trapped molecular ions," Phys. Rev. Lett. **119**, 153001.

Caldwell, A., G. Dvali, B. Majorovits, A. Millar, G. Raffelt, J. Redondo, O. Reimann, F. Simon, F. Steffen, and Madmax Working Group, 2017, "Dielectric Haloscopes: A New Way to Detect Axion Dark Matter," Phys. Rev. Lett. **118**, 091801.

Campbell, C. J., A. G. Radnaev, A. Kuzmich, V. A. Dzuba, V. V. Flambaum, and A. Derevianko, 2012, "A single-ion nuclear clock for metrology at the 19th decimal place," Phys. Rev. Lett. **108**, 120802.

Cancio Pastor, P., I. Galli, G. Giusfredi, D. Mazzotti, and P. De Natale, 2015, "Testing the validity of Bose-Einstein statistics in molecules," Phys. Rev. A **92**, 063820.

Carlson, C. E., 2015, "The proton radius puzzle," Prog. Part. Nucl. Phys. **82**, 59.

Carroll, S. M., and G. B. Field, 1994, "Consequences of propagating torsion in connection-dynamic theories of gravity," Phys. Rev. D **50**, 3867.

Cartan, É., 1922, "On a generalization of the Riemann curvature concept and space with torsion," C.R. Acad. Sci. (Paris) **174**, 593.

Cartan, É., 1923, "On varieties of affine connections and the theory of general relativity (part I)," Ann. Sci. Ec. Norm. Super. **40**, 325.

Cartan, É., 1924, "On varieties of affine connections and the theory of general relativity (part I)," Ann. Sci. Ec. Norm. Super. **41**, 1.

Cartan, É., 1925, "On varieties of affine connections and the theory of general relativity (part II)," Ann. Sci. Ec. Norm. Super. **42**, 17.

Casalbuoni, R., S. de Curtis, D. Dominici, and R. Gatto, 1999, "Bounds on new physics from the new data on parity violation in atomic cesium," Phys. Lett. B **460**, 135.

Casola, Eolo Di, Stefano Liberati, and Sebastiano Sonego, 2015, "Nonequivalence of equivalence principles," arXiv:1310.7426v2.

Cassidy, D. B., 2018, "Experimental progress in positronium laser physics," Eur. Phys. J. D **72**, 53.

Cassidy, D. B., T. H. Hisakado, H. W. K. Tom, and A. P. Mills, 2012a, "Efficient production of Rydberg positronium," Phys. Rev. Lett. **108**, 043401.

Cassidy, D. B., T. H. Hisakado, H. W. K. Tom, and A. P. Mills, 2012b, "Optical spectroscopy of molecular positronium," Phys. Rev. Lett. **108**, 133402.

Cassidy, D. B., T. H. Hisakado, H. W. K. Tom, and A. P. Mills, 2012c, "Positronium hyperfine interval measured via saturated absorption spectroscopy," Phys. Rev. Lett. **109**, 073401.

Cassidy, D. B., and A. P. Mills, 2007, "The production of molecular positronium," Nature (London) **449**, 195.

Cavendish, H., 1798, "Experiments to determine the density of the Earth. By Henry Cavendish, Esq. F. R. S. and A. S.," Philos. Trans. R. Soc. London **88**, 469.

Chaibi, W., R. Geiger, B. Canuel, A. Bertoldi, A. Landragin, and P. Bouyer, 2016, "Low frequency gravitational wave detection with ground-based atom interferometer arrays," Phys. Rev. D **93**, 021101.

Chand, H., R. Srianand, P. Petitjean, and B. Aracil, 2004, "Probing the cosmological variation of the fine-structure constant: Results based on VLT-UVES sample," Astron. Astrophys. **417**, 853.

Chang, J. H., R. Essig, and S. D. McDermott, 2017, "Revisiting Supernova 1987A constraints on dark photons," J. High Energy Phys. 01, 107.

Chang, S., C. Hagmann, and P. Sikivie, 1998, "Studies of the motion and decay of axion walls bounded by strings," Phys. Rev. D **59**, 023505.

Chantler, C. T., *et al.*, 2012, "Testing three-body quantum electrodynamics with trapped Ti^{20+} ions: Evidence for a Z-dependent divergence between experiment and calculation," Phys. Rev. Lett. **109**, 153001.

Chantler, C. T., *et al.*, 2013, "Chantler *et al.* reply," Phys. Rev. Lett. **110**, 159302.

Charlton, M., and J. W. Humberston, 2000, *Positron Physics*, edited by M. Charlton and J. W. Humberston (Cambridge University Press, Cambridge, UK), p. 464.

Chatrchyan, S., *et al.*, 2012, "Observation of a new boson at a mass of 125 GeV with the CMS experiment at the LHC," Phys. Lett. B **716**, 30.

Chaudhuri, S., P. W. Graham, K. Irwin, J. Mardon, S. Rajendran, and Y. Zhao, 2015, "Radio for hidden-photon dark matter detection," Phys. Rev. D **92**, 075012.

Chen, Q., E. Magoulakis, and S. Schiller, 2016, "High-sensitivity crossed-resonator laser apparatus for improved tests of Lorentz invariance and of space-time fluctuations," Phys. Rev. D **93**, 022003.

Chen, Y.-J., W. K. Tham, D. E. Krause, D. López, E. Fischbach, and R. S. Decca, 2016, "Stronger limits on hypothetical Yukawa interactions in the 30–8000 nm range," Phys. Rev. Lett. **116**, 221102.

Cheng, Cunfeng, Aernout P. P. van der Poel, Paul Jansen, Marina Quintero-Pérez, Thomas E. Wall, Wim Ubachs, and Hendrick L. Bethlem, 2016, "Molecular fountain," Phys. Rev. Lett. **117**, 253201.

Chengalur, J. N., and N. Kanekar, 2003, "Constraining the variation of fundamental constants using 18 cm OH lines," Phys. Rev. Lett. **91**, 241302.

Chikashige, Y., R. Mohapatra, and R. Peccei, 1981, "Are there real Goldstone bosons associated with broken lepton number?," Phys. Lett. B **98**, 265.

Chin, C., and V. V. Flambaum, 2006, "Enhanced sensitivity to fundamental constants in ultracold atomic and molecular systems near Feshbach resonances," Phys. Rev. Lett. **96**, 230801.

Chin, C., V. V. Flambaum, and M. G. Kozlov, 2009, "Ultracold molecules: new probes on the variation of fundamental constants," New J. Phys. **11**, 055048.

Chiow, S.-W., J. Williams, and N. Yu, 2015, "Laser-ranging long-baseline differential atom interferometers for space," Phys. Rev. A **92**, 063613.

Cho, D., K. Sangster, and E. A. Hinds, 1989, "Tenfold improvement of limits on T violation in thallium fluoride," Phys. Rev. Lett. **63**, 2559.

Cho, D., K. Sangster, and E. A. Hinds, 1991, "Search for time-reversal-symmetry violation in thallium fluoride using a jet source," Phys. Rev. A **44**, 2783.

Choi, J., and D. S. Elliott, 2016, "Measurement scheme and analysis for weak ground-state-hyperfine-transition moments through two-pathway coherent control," Phys. Rev. A **93**, 023432.

Chu, P.-H., E. Weisman, C.-Y. Liu, and J. C. Long, 2015, "Search for exotic short-range interactions using paramagnetic insulators," Phys. Rev. D **91**, 102006.

Chu, P.-H., *et al.*, 2013, "Laboratory search for spin-dependent short-range force from axionlike particles using optically polarized ^{3}He gas," Phys. Rev. D **87**, 011105(R).

Chu, S., 1998, "Nobel Lecture: The manipulation of neutral particles," Rev. Mod. Phys. **70**, 685.

Chupp, Tim, 2010, "Permanent electric dipole moments of atoms and molecules," Adv. At. Mol. Opt. Phys. **59**, 129.

Chupp, Timothy, Peter Fierlinger, Michael Ramsey-Musolf, and Jaideep Singh, 2017, "Electric Dipole Moments of the Atoms, Molecules, Nuclei and Particles," arXiv:1710.02504.

Chupp, Timothy, and Michael Ramsey-Musolf, 2015, "Electric dipole moments: A global analysis," Phys. Rev. C **91**, 035502.

Cirigliano, V., Yingchuan Li, S. Profumo, and M. J. Ramsey-Musolf, **2010**, "MSSM baryogenesis and electric dipole moments: an update on the phenomenology," J. High Energy Phys. 01, 002.

Clowe, D., M. Bradač, A. H. Gonzalez, M. Markevitch, S. W. Randall, C. Jones, and D. Zaritsky, 2006, "A direct empirical proof of the existence of dark matter," Astrophys. J. Lett. **648**, L109.

Cocconi, Giuseppe, and E Salpeter, 1958, "A search for anisotropy of inertia," Il Nuovo Cimento **10**, 646.

Cohen-Tannoudji, C. N., 1998, "Nobel Lecture: Manipulating atoms with photons," Rev. Mod. Phys. **70**, 707.

Colella, R., A. W. Overhauser, and S. A. Werner, 1975, "Observation of gravitationally induced quantum interference," Phys. Rev. Lett. **34**, 1472.

Coleman, S., 1985, "Q-balls," Nucl. Phys. B **262**, 263.

Colladay, D., and V. A. Kostelecký, 1998, "Lorentz-violating extension of the standard model," Phys. Rev. D **58**, 116002.

Commins, E. D., and P. H. Bucksbaum, 1983, *Weak Interactions of Leptons and Quarks* (Cambridge University, Cambridge, England).

Commins, E. D., and D. P. DeMille, 2009, "The electric dipole moment of the electron," in *Lepton Dipole Moments*, edited by B. L. Roberts and W. J. Marciano (World Scientific, Singapore).

Commins, Eugene D., 2012, "Electron spin and its history," Annu. Rev. Nucl. Part. Sci. **62**, 133.

Commins, Eugene D., J. D. Jackson, and David P. DeMille, 2007, "The electric dipole moment of the electron: An intuitive explanation for the evasion of Schiff's theorem," Am. J. Phys. **75**, 532.

Conti, R., P. Bucksbaum, S. Chu, E. Commins, and L. Hunter, 1979, "Preliminary observation of parity nonconservation in atomic thallium," Phys. Rev. Lett. **42**, 343.

Conti, R. S., and I. B. Khriplovich, 1992, "New limits on T-odd, P-even interactions," Phys. Rev. Lett. **68**, 3262.

Cornell, E. A., and C. E. Wieman, 2002, "Nobel Lecture: Bose-Einstein condensation in a dilute gas, the first 70 years and some recent experiments," Rev. Mod. Phys. **74**, 875.

Costa de Beauregard, O., 1942, "Sur la dynamique des milieux doués dune densité de moment cinétique propre," C.R. Hebd. Seances Acad. Sci. **214**, 904.

Costa de Beauregard, O., 1964, "Translational inertial spin effect with moving particles," Phys. Rev. **134**, B471.

Crescini, N., C. Braggio, G. Carugno, P. Falferi, A. Ortolan, and G. Ruoso, 2017, "Improved constraints on monopoledipole interaction mediated by pseudo-scalar bosons," Phys. Lett. B **773**, 677.

Crewther, R. J., P. Di Vecchia, G. Veneziano, and E. Witten, 1979, "Chiral estimate of the electric dipole moment of the neutron in quantum chromodynamics," Phys. Lett. B **88**, 123.

Cronin, A. D., J. Schmiedmayer, and D. E. Pritchard, 2009, "Optics and interferometry with atoms and molecules," Rev. Mod. Phys. **81**, 1051.

Cullen, S., and M. Perelstein, 1999, "SN1987A constraints on large compact dimensions," Phys. Rev. Lett. **83**, 268.

Curceanu, C., J. D. Gillaspy, and R. C. Hilborn, 2012, "Resource letter SS-1: The spin-statistics connection," Am. J. Phys. **80**, 561.

Cvetic, M., and P. Langacker, 1996, "Implications of Abelian extended gauge structures from string models," Phys. Rev. D **54**, 3570.

Czarnecki, A., and R. Szafron, 2016, "Light-by-light scattering in the Lamb shift and the bound electron *g* factor," Phys. Rev. A **94**, 060501.

Dahia, F., and A. S. Lemos, 2016a, "Constraints on extra dimensions from atomic spectroscopy," Phys. Rev. D **94**, 084033.

Dahia, F., and A. S. Lemos, 2016b, "Is the proton radius puzzle evidence of extra dimensions?," Eur. Phys. J. C **76**, 435.

Daido, R., and F. Takahashi, 2017, "The sign of the dipole–dipole potential by axion exchange," Phys. Lett. B **772**, 127.

D'Amico, G., G. Rosi, S. Zhan, L. Cacciapuoti, M. Fattori, and G. M. Tino, 2017, "Canceling the gravity gradient phase shift in atom interferometry," Phys. Rev. Lett. **119**, 253201.

Damour, T., 2012, "Theoretical aspects of the equivalence principle," Classical Quantum Gravity **29**, 184001.

Damour, T., F. Piazza, and G. Veneziano, 2002, "Runaway dilaton and equivalence principle violations," Phys. Rev. Lett. **89**, 081601.

Damour, T., and A. M. Polyakov, 1994, "The string dilation and a least coupling principle," Nucl. Phys. B **423**, 532.

Danzmann, K., *et al.*, 2011, "LISA: Unveiling a hidden universe," Assessment Study Report ESA/SRE 3, 2.

Davis, R. L., 1985, "Goldstone bosons in string models of galaxy formation," Phys. Rev. D **32**, 3172.

Davoudiasl, H., H.-S. Lee, and W. J. Marciano, 2012, "'Dark' Z implications for parity violation, rare meson decays, and Higgs physics," Phys. Rev. D **85**, 115019.

Davoudiasl, Hooman, Hye Sung Lee, and William J. Marciano, 2014, "Muon $g - 2$, rare kaon decays, and parity violation from dark bosons," Phys. Rev. D **89**, 095006.

Decca, R. S., D. López, H. B. Chan, E. Fischbach, D. E. Krause, and C. R. Jamell, 2005, "Constraining new forces in the Casimir regime using the isoelectronic technique," Phys. Rev. Lett. **94**, 240401.

Delaunay, C., C. Frugiuele, E. Fuchs, and Y. Soreq, 2017, "Probing new spin-independent interactions through precision spectroscopy in atoms with few electrons," Phys. Rev. D **96**, 115002.

Delaunay, C., R. Ozeri, G. Perez, and Y. Soreq, 2016, "Probing the atomic Higgs force," arXiv:1601.05087.

Delva, P., *et al.*, 2017, "Test of special relativity using a fiber network of optical clocks," Phys. Rev. Lett. **118**, 221102.

DeMille, D., F. Bay, S. Bickman, D. Kawall, L. Hunter, D. Krause, S. Maxwell, and K. Ulmer, 2001, "Search for the electric dipole moment of the electron using metastable PbO," in *Art and Symmetry in Experimental Physics* (American Institute of Physics, Melville, NY), Vol. 596, p. 72.

DeMille, D., D. Budker, N. Derr, and E. Deveney, 1999, "Search for exchange-antisymmetric two-photon states," Phys. Rev. Lett. **83**, 3978.

DeMille, D., S. B. Cahn, D. Murphree, D. A. Rahmlow, and M. G. Kozlov, 2008, "Using molecules to measure nuclear spin-dependent parity violation," Phys. Rev. Lett. **100**, 023003.

DeMille, D., S. Sainis, J. Sage, T. Bergeman, S. Kotochigova, and E. Tiesinga, 2008, "Enhanced sensitivity to variation of m_e/m_p in molecular spectra," Phys. Rev. Lett. **100**, 043202.

DeMille, David, 1995, "Parity nonconservation in the $6s^2 \, {}^1S_0 \rightarrow 6s5d \, {}^3D_1$ transition in atomic ytterbium," Phys. Rev. Lett. **74**, 4165.

de Nijs, A. J., W. Ubachs, and H. L. Bethlem, 2014, "Ramsey-type microwave spectroscopy on CO (a$^3\Pi$)," J. Mol. Spectrosc. **300**, 79.

Denis, Malika, and Timo Fleig, 2016, "In search of discrete symmetry violations beyond the standard model: Thorium monoxide reloaded," J. Chem. Phys. **145**, 214307.

Derbin, A. V., A. I. Egorov, I. A. Mitropol'sky, V. N. Muratova, D. A. Semenov, and E. V. Unzhakov, 2009, "Search for resonant absorption of solar axions emitted in M1 transition in ^{57}Fe nuclei," Eur. Phys. J. C **62**, 755.

Derevianko, A., 2000, "Reconciliation of the measurement of parity-nonconservation in Cs with the standard model," Phys. Rev. Lett. **85**, 1618.

Derevianko, A., V. A. Dzuba, and V. V. Flambaum, 2012, "Highly charged ions as a basis of optical atomic clockwork of exceptional accuracy," Phys. Rev. Lett. **109**, 180801.

Derevianko, A., and M. Pospelov, 2014, "Hunting for topological dark matter with atomic clocks," Nat. Phys. **10**, 933.

Derevianko, Andrei, 2016, "Detecting dark matter waves with a network of precision measurement tools," arXiv:1605.09717.

Derevianko, Andrei, and S. G. Porsev, 2007, "Theoretical overview of atomic parity violation: Recent developments and challenges," Eur. Phys. J. A **32**, 517.

Derevianko, Andrei, and Sergey G. Porsev, 2002, "Reevaluation of the role of nuclear uncertainties in experiments on atomic parity violation with isotopic chains," Phys. Rev. A **65**, 052115.

Desplanques, Bertrand, John F. Donoghue, and Barry R. Holstein, 1980, "Unified treatment of the parity violating nuclear force," Ann. Phys. (N.Y.) **124**, 449.

Deutsch, Martin, 1951, "Evidence for the formation of positronium in gases," Phys. Rev. **82**, 455.

Dickenson, G. D., M. L. Niu, E. J. Salumbides, J. Komasa, K. S. E. Eikema, K. Pachucki, and W. Ubachs, 2013, "Fundamental vibration of molecular hydrogen," Phys. Rev. Lett. **110**, 193601.

Dickerson, S. M., J. M. Hogan, A. Sugarbaker, D. M. S. Johnson, and M. A. Kasevich, 2013, "Multiaxis inertial sensing with long-time point source atom interferometry," Phys. Rev. Lett. **111**, 083001.

Dimopoulos, S., and H. Georgi, 1981, "Softly broken supersymmetry and SU(5)," Nucl. Phys. B **193**, 150.

Dimopoulos, S., and A. A. Geraci, 2003, "Probing submicron forces by interferometry of Bose-Einstein condensed atoms," Phys. Rev. D **68**, 124021.

Dimopoulos, S., P. W. Graham, J. M. Hogan, and M. A. Kasevich, 2007, "Testing general relativity with atom interferometry," Phys. Rev. Lett. **98**, 111102.

Dimopoulos, S., P. W. Graham, J. M. Hogan, M. A. Kasevich, and S. Rajendran, 2008, "Atomic gravitational wave interferometric sensor," Phys. Rev. D **78**, 122002.

Dine, M., and W. Fischler, 1983, "The not-so-harmless axion," Phys. Lett. B **120**, 137.

Dine, M., W. Fischler, and M. Srednicki, 1981, "A simple solution to the strong *CP* problem with a harmless axion," Phys. Lett. B **104**, 199.

Dine, Michael, and Alexander Kusenko, 2003, "Origin of the matter-antimatter asymmetry," Rev. Mod. Phys. **76**, 1.

Dinh, T. H., A. Dunning, V. A. Dzuba, and V. V. Flambaum, 2009, "Sensitivity of hyperfine structure to nuclear radius and quark mass variation," Phys. Rev. A **79**, 054102.

Di Piazza, A., C. Müller, K. Z. Hatsagortsyan, and C. H. Keitel, 2012, "Extremely high-intensity laser interactions with fundamental quantum systems," Rev. Mod. Phys. **84**, 1177.

DiSciacca, J., *et al.*, 2013, "One-particle measurement of the antiproton magnetic moment," Phys. Rev. Lett. **110**, 130801.

Dobrescu, Bogdan A., 2005, "Massless gauge bosons other than the photon," Phys. Rev. Lett. **94**, 151802.

Dobrescu, Bogdan A., and Irina Mocioiu, **2006**, "Spin-dependent macroscopic forces from new particle exchange," J. High Energy Phys. 11, 005.

Dolgov, A. D., and V. A. Novikov, 2012, "*CPT*, Lorentz invariance, mass differences, and charge non-conservation," JETP Lett. **95**, 594.

Dragoset, R. A., A. Musgrove, C. W. Clark, W. C. Martin, and K. Olsen, 2017, "Periodic table of the elements," NIST SP 966 [http://physics.nist.gov/pt].

Drake, G. W. F., Mark M. Cassar, and Razvan A. Nistor, 2002, "Ground-state energies for helium, H⁻, and Ps⁻," Phys. Rev. A **65**, 054501.

Drake, G. W. F., and Z.-C. Yan, 2008, "High-precision spectroscopy as a test of quantum electrodynamics in light atomic systems," Can. J. Phys. **86**, 45.

Drever, R. W. P., 1961, "A search for anisotropy of inertial mass using a free precession technique," Philos. Mag. **6**, 683.

Duan, Xiao-Chun, Xiao-Bing Deng, Min-Kang Zhou, Ke Zhang, Wen-Jie Xu, Feng Xiong, Yao-Yao Xu, Cheng-Gang Shao, Jun Luo, and Zhong-Kun Hu, 2016, "Test of the universality of free fall with atoms in different spin orientations," Phys. Rev. Lett. **117**, 023001.

Dubielzig, T., M. Niemann, A.-G. Paschke, M. Carsjens, M. Kohnen, and C. Ospelkaus, 2013, "Quantum logic enabled test of discrete

symmetries," in APS Division of Atomic, Molecular and Optical Physics Meeting Abstracts.

Dubovsky, S., and G. Hernández-Chifflet, **2015**, "Heating up the Galaxy with hidden photons," J. Cosmol. Astropart. Phys. 12, 054.

Duffy, L. D., and P. Sikivie, 2008, "Caustic ring model of the Milky Way halo," Phys. Rev. D **78**, 063508.

Duffy, Leanne D., and Karl van Bibber, 2009, "Axions as dark matter particles," New J. Phys. **11**, 105008.

Dufour, G., D. B. Cassidy, P. Crivelli, P. Debu, A. Lambrecht, V. V. Nesvizhevsky, S. Reynaud, A. Y. Voronin, and T. E. Wall, 2015, "Prospects for studies of the free fall and gravitational quantum states of antimatter," Adv. High Energy Phys. **2015**, 379642.

Dzuba, V. A., J. C. Berengut, V. V. Flambaum, and B. Roberts, 2012, "Revisiting parity nonconservation in cesium," Phys. Rev. Lett. **109**, 203003.

Dzuba, V. A., A. Derevianko, and V. V. Flambaum, 2012a, "Ion clock and search for the variation of the fine structure constant using optical transitions in Nd^{13+} and Sm^{15+}," Phys. Rev. A **86**, 054502.

Dzuba, V. A., A. Derevianko, and V. V. Flambaum, 2012b, "High-precision atomic clocks with highly charged ions: Nuclear-spin-zero f^{12}-shell ions," Phys. Rev. A **86**, 054501; **87**, 029906 (2013).

Dzuba, V. A., and V. V. Flambaum, 2009a, "Calculation of the (T, P)-odd electric dipole moment of thallium and cesium," Phys. Rev. A **80**, 062509.

Dzuba, V. A., and V. V. Flambaum, 2009b, "Search for variation of the fundamental constants in atomic, molecular, and nuclear spectra," Can. J. Phys. **87**, 25.

Dzuba, V. A., V. V. Flambaum, and J. S. M. Ginges, 2001, "Calculations of parity-nonconserving $s - d$ amplitudes in Cs, Fr, Ba⁺, and Ra⁺," Phys. Rev. A **63**, 062101.

Dzuba, V. A., V. V. Flambaum, and Hidetoshi Katori, 2015, "Optical clock sensitive to variation of the fine structure constant based on the Ho^{14+} ion," Phys. Rev. A **91**, 022119.

Dzuba, V. A., V. V. Flambaum, and I. B. Khriplovich, 1986, "Enhancement of P- and T-nonconserving effects in rare-earth atoms," Z. Phys. D **1**, 243.

Dzuba, V. A., V. V. Flambaum, and S. G. Porsev, 2009, "Calculation of (p, t)-odd electric dipole moments for the diamagnetic atoms ^{129}Xe, ^{171}Yb, ^{199}Hg, ^{211}Rn, and ^{225}Ra," Phys. Rev. A **80**, 032120.

Dzuba, V. A., V. V. Flambaum, M. S. Safronova, S. G. Porsev, T. Pruttivarasin, M. A. Hohensee, and H. Häffner, 2016, "Strongly enhanced effects of Lorentz symmetry violation in entangled Yb⁺ ions," Nat. Phys. **12**, 465.

Dzuba, V. A., V. V. Flambaum, and Y. V. Stadnik, 2017, "Probing low-mass vector bosons with parity nonconservation and nuclear anapole moment measurements in atoms and molecules," Phys. Rev. Lett. **119**, 223201.

Dzuba, V. A., V. V. Flambaum, and O. P. Sushkov, 1989, "Summation of the high orders of perturbation theory for the parity nonconserving E1-amplitude of the 6S-7S transition in the caesium atom," Phys. Lett. A **141**, 147.

Dzuba, V. A., V. V. Flambaum, and O. P. Sushkov, 1995, "Calculation of energy levels, E1 transition amplitudes, and parity violation in francium," Phys. Rev. A **51**, 3454.

Dzuba, V. A., V. V. Flambaum, and J. K. Webb, 1999a, "Calculations of the relativistic effects in many-electron atoms and space-time variation of fundamental constants," Phys. Rev. A **59**, 230.

Dzuba, V. A., V. V. Flambaum, and J. K. Webb, 1999b, "Space-time variation of physical constants and relativistic corrections in atoms," Phys. Rev. Lett. **82**, 888.

Dzuba, V. A., V. V. Flambaum, J. S. M. Ginges, and M. G. Kozlov, 2002, "Electric dipole moments of Hg, Xe, Rn, Ra, Pu, and TlF

induced by the nuclear Schiff moment and limits on time-reversal violating interactions," Phys. Rev. A **66**, 012111.

Dzuba, V. A., C. Harabati, W. R. Johnson, and M. S. Safronova, 2001, "Breit correction to the parity-nonconservation amplitude in cesium," Phys. Rev. A **63**, 044103.

Dzuba, V. A., M. S. Safronova, U. I. Safronova, and V. V. Flambaum, 2015, "Actinide ions for testing the spatial α-variation hypothesis," Phys. Rev. A **92**, 060502.

Eckel, S., P. Hamilton, E. Kirilov, H. W. Smith, and D. DeMille, 2013, "Search for the electron electric dipole moment using Ω-doublet levels in PbO," Phys. Rev. A **87**, 052130.

Edwards, N. H., S. J. Phipp, P. E. G. Baird, and S. Nakayama, 1995, "Precise measurement of parity nonconserving optical rotation in atomic thallium," Phys. Rev. Lett. **74**, 2654.

Eides, M. I., and V. A. Shelyuto, 2017, "One more hard three-loop correction to parapositronium energy levels," arXiv:1705.09166.

Eides, Michael I., Howard Grotch, and Valery A Shelyuto, 2001, "Theory of light hydrogenlike atoms," Phys. Rep. **342**, 63.

Eills, J., J. W. Blanchard, L. Bougas, M. G. Kozlov, A. Pines, and D. Budker, 2017, "Measuring molecular parity nonconservation using nuclear magnetic resonance spectroscopy," arXiv:1707.01759.

Einstein, A., 1916, "The basis of the general theory of relativity," Ann. Phys. (Berlin) **354**, 769.

Eisele, C., A. Y. Nevsky, and S. Schiller, 2009, "Laboratory test of the isotropy of light propagation at the 10^{-17} level," Phys. Rev. Lett. **103**, 090401.

Elder, B., J. Khoury, P. Haslinger, M. Jaffe, H. Müller, and P. Hamilton, 2016, "Chameleon dark energy and atom interferometry," Phys. Rev. D **94**, 044051.

Elliott, S. R., B. H. LaRoque, V. M. Gehman, M. F. Kidd, and M. Chen, 2012, "An improved limit on Pauli-exclusion-principle forbidden atomic transitions," Found. Phys. **42**, 1015.

Engel, J., D. Seckel, and A. C. Hayes, 1990, "Emission and detectability of hadronic axions from SN1987A," Phys. Rev. Lett. **65**, 960.

Engel, J., and P. Vogel, 1989, "Spin-dependent cross sections of weakly interacting massive particles on nuclei," Phys. Rev. D **40**, 3132.

Engel, Jonathan, Michael J. Ramsey-Musolf, and U. van Kolck, 2013, "Electric dipole moments of nucleons, nuclei, and atoms: The Standard Model and beyond," Prog. Part. Nucl. Phys. **71**, 21.

English, D., V. V. Yashchuk, and D. Budker, 2010, "Spectroscopic test of Bose-Einstein statistics for photons," Phys. Rev. Lett. **104**, 253604.

Epp, S. W., 2013, "Comment on "Testing three-body quantum electrodynamics with trapped Ti^{20+} ions: Evidence for a Z-dependent divergence between experiment and calculation"," Phys. Rev. Lett. **110**, 159301.

Fadeev, P., F. Ficek, Y. V. Stadnik, M. G. Kozlov, V. V. Flambaum, and D. Budker, 2018, "Revisiting spin-dependent forces mediated by new bosons: Potentials in the coordinate-space representation for macroscopic and sub-atomic-scale experiments," to be published.

Fayet, P., 2004, "Light spin-1/2 or spin-0 dark matter particles," Phys. Rev. D **70**, 023514.

Fayet, P., 2018, "MICROSCOPE limits for new long-range forces and implications for unified theories," Phys. Rev. D **97**, 055039.

Fayet, Pierre, 2007, "U-boson production in e^+e^- annihilations, ψ and γ decays, and light dark matter," Phys. Rev. D **75**, 115017.

Fedorov, V. V., I. A. Kuznetsov, and V. V. Voronin, 2013, "A search for nEDM and new constraints on short-range "pseudo-magnetic" interaction using neutron optics of noncentrosymmetric crystal," Nucl. Instrum. Methods Phys. Res., Sect. B **309**, 237.

Feng, J. L., 2010, "Dark matter candidates from particle physics and methods of detection," Annu. Rev. Astron. Astrophys. **48**, 495.

Feng, Jonathan L., 2013, "Naturalness and the status of supersymmetry," Annu. Rev. Nucl. Part. Sci. **63**, 351.

Ferrari, G., N. Poli, F. Sorrentino, and G. M. Tino, 2006, "Long-lived Bloch oscillations with bosonic Sr atoms and application to gravity measurement at the micrometer scale," Phys. Rev. Lett. **97**, 060402.

Ferrell, S. J., A. Cingöz, A. Lapierre, A.-T. Nguyen, N. Leefer, D. Budker, V. V. Flambaum, S. K. Lamoreaux, and J. R. Torgerson, 2007, "Investigation of the gravitational-potential dependence of the fine-structure constant using atomic dysprosium," Phys. Rev. A **76**, 062104.

Ficek, F., P. Fadeev, V. V. Flambaum, D. F. Jackson Kimball, M. G. Kozlov, Y. V. Stadnik, and D. Budker, 2018, "Constraints on exotic spin-dependent interactions between matter and antimatter from antiprotonic helium spectroscopy," Phys. Rev. Lett. **120**, 183002.

Ficek, Filip, Derek F. Jackson Kimball, Mikhail G. Kozlov, Nathan Leefer, Szymon Pustelny, and Dmitry Budker, 2017, "Constraints on exotic spin-dependent interactions between electrons from helium fine-structure spectroscopy," Phys. Rev. A **95**, 032505.

Firestone, R. B., and V. S. Shirley, 1998, Eds., *Table of Isotopes* (Wiley, New York).

Fischbach, E., and D. E. Krause, 1999, "Constraints on light pseudoscalars implied by tests of the gravitational inverse-square law," Phys. Rev. Lett. **83**, 3593.

Fischbach, E., D. Sudarsky, A. Szafer, C. Talmadge, and S. H. Aronson, 1986, "Reanalysis of the Eötvös experiment," Phys. Rev. Lett. **56**, 3.

Fischbach, E., and C. L. Talmadge, 2012, *The Search for non-Newtonian Gravity* (Springer, New York).

Fischler, Willy, Sonia Paban, and Scott Thomas, 1992, "Bounds on microscopic physics from P and T violation in atoms and molecules," Phys. Lett. B **289**, 373.

Fitzakerley, D. W., *et al.* (ATRAP Collaboration), 2016, "Electron-cooled accumulation of 4×10^9 positrons for production and storage of antihydrogen atoms," J. Phys. B **49**, 064001.

Fixler, J. B., G. T. Foster, J. M. McGuirk, and M. A. Kasevich, 2007, "Atom interferometer measurement of the Newtonian constant of gravity," Science **315**, 74.

Flambaum, V., S. Lambert, and M. Pospelov, 2009, "Scalar-tensor theories with pseudoscalar couplings," Phys. Rev. D **80**, 105021.

Flambaum, V. V., 2006a, "Enhanced effect of temporal variation of the fine structure constant and the strong interaction in ^{229}Th," Phys. Rev. Lett. **97**, 092502.

Flambaum, V. V., 2006b, "Enhanced effect of temporal variation of the fine-structure constant in diatomic molecules," Phys. Rev. A **73**, 034101.

Flambaum, V. V., 2016, "Enhancing the effect of Lorentz invariance and Einstein's equivalence principle violation in nuclei and atoms," Phys. Rev. Lett. **117**, 072501.

Flambaum, V. V., D. DeMille, and M. G. Kozlov, 2014, "Time-reversal symmetry violation in molecules induced by nuclear magnetic quadrupole moments," Phys. Rev. Lett. **113**, 103003.

Flambaum, V. V., V. A. Dzuba, and C. Harabati, 2017, "Effect of nuclear quadrupole moments on parity nonconservation in atoms," Phys. Rev. A **96**, 012516.

Flambaum, V. V., and J. S. M. Ginges, 2002, "Nuclear Schiff moment and time-invariance violation in atoms," Phys. Rev. A **65**, 032113.

Flambaum, V. V., A. A. Gribakina, G. F. Gribakin, and M. G. Kozlov, 1994, "Structure of compound states in the chaotic spectrum of the Ce atom: Localization properties, matrix elements, and enhancement of weak perturbations," Phys. Rev. A **50**, 267.

Flambaum, V. V., and I. B. Khriplovich, 1980, "P-odd nuclear forces—a source of parity violation in atoms," Zh. Eksp. Teor. Fiz. **79**, 1656 [Sov. Phys. JETP **52**, 835 (1980), http://www.jetp.ac.ru/cgi-bin/e/index/e/52/5/p835?a=list].

Flambaum, V. V., and I. B. Khriplovich, 1985a, "New bounds on the electric dipole moment of the electron and on T-odd electron-nucleon coupling," Zh. Eksp. Teor. Fiz. **89**, 1505 [JETP **62**, 872 (1985), http://www.jetp.ac.ru/cgi-bin/dn/e_062_05_0872.pdf].

Flambaum, V. V., and I. B. Khriplovich, 1985b, "On the enhancement of parity nonconserving effects in diatomic molecules," Phys. Lett. A **110**, 121.

Flambaum, V. V., I. B. Khriplovich, and O. P. Sushkov, 1984, "Nuclear anapole moments," Phys. Lett. B **146**, 367.

Flambaum, V. V., and M. G. Kozlov, 2007, "Enhanced sensitivity to the time variation of the fine-structure constant and m_p/m_e in diatomic molecules," Phys. Rev. Lett. **99**, 150801.

Flambaum, V. V., D. B. Leinweber, A. W. Thomas, and R. D. Young, 2004, "Limits on variations of the quark masses, qcd scale, and fine structure constant," Phys. Rev. D **69**, 115006.

Flambaum, V. V., and M. V. Romalis, 2017, "Limits on Lorentz invariance violation from Coulomb interactions in nuclei and atoms," Phys. Rev. Lett. **118**, 142501.

Flambaum, V. V., Y. V. Stadnik, M. G. Kozlov, and A. N. Petrov, 2013, "Enhanced effects of temporal variation of the fundamental constants in $^2\Pi_{1/2}$-term diatomic molecules: ^{207}Pb^{19}F," Phys. Rev. A **88**, 052124.

Flambaum, V. V., and A. F. Tedesco, 2006, "Dependence of nuclear magnetic moments on quark masses and limits on temporal variation of fundamental constants from atomic clock experiments," Phys. Rev. C **73**, 055501.

Fleig, Timo, 2017, "$\mathcal{P}$, $\mathcal{T}$-odd and magnetic hyperfine-interaction constants and excited-state lifetime for HfF$^+$," Phys. Rev. A **96**, 040502.

Fleig, Timo, and Malaya K. Nayak, 2013, "Electron electric-dipole-moment interaction constant for HfF$^+$ from relativistic correlated all-electron theory," Phys. Rev. A **88**, 032514.

Fleurbaey, H., S. Galtier, S. Thomas, M. Bonnaud, L. Julien, F. Biraben, F. Nez, M. Abgrall, and J. Guéna, 2018, "New measurement of the $1s - 3s$ transition frequency of hydrogen: contribution to the proton charge radius puzzle," arXiv:1801.08816.

Foot, R., and S. Vagnozzi, 2015, "Dissipative hidden sector dark matter," Phys. Rev. D **91**, 023512.

Fortier, T. M., *et al.*, 2007, "Precision atomic spectroscopy for improved limits on variation of the fine structure constant and local position invariance," Phys. Rev. Lett. **98**, 070801.

Fortson, E. N., Y. Pang, and L. Wilets, 1990, "Nuclear-structure effects in atomic parity nonconservation," Phys. Rev. Lett. **65**, 2857.

Fortson, N., P. Sandars, and S. Barr, 2003, "The search for a permanent electric dipole moment," Phys. Today **56**, 33.

Fortson, Norval, 1993, "Possibility of measuring parity nonconservation with a single trapped atomic ion," Phys. Rev. Lett. **70**, 2383.

Francis, O., *et al.*, 2015, "CCM.G-K2 key comparison," Metrologia **52**, 07009.

Fray, S., C. A. Diez, T. W. Hänsch, and M. Weitz, 2004, "Atomic interferometer with amplitude gratings of light and its applications to atom based tests of the equivalence principle," Phys. Rev. Lett. **93**, 240404.

Freese, Katherine, Mariangela Lisanti, and Christopher Savage, 2013, "Colloquium: Annual modulation of dark matter," Rev. Mod. Phys. **85**, 1561.

Freier, C., M. Hauth, V. Schkolnik, B. Leykauf, M. Schilling, H. Wziontek, H.-G. Scherneck, J. Müller, and A. Peters, 2016, "Mobile quantum gravity sensor with unprecedented stability," J. Phys. Conf. Ser. **723**, 012050.

Freivogel, B., **2010**, "Anthropic explanation of the dark matter abundance," J. Cosmol. Astropart. Phys. 03, 021.

Frieman, J. A., M. S. Turner, and D. Huterer, 2008, "Dark energy and the accelerating universe," Annu. Rev. Astron. Astrophys. **46**, 385.

Frolov, A., 2005, "Positron annihilation in the positronium negative ion Ps," Phys. Lett. A **342**, 430.

Frolov, A. M., and D. M. Wardlaw, 2008, "Stability of the five-body bi-positronium ion Ps$_2$e$^-$," Phys. Lett. A **372**, 6721.

Fujii, Y., 1971, "Dilaton and possible non-Newtonian gravity," Nature Phys. Sci. **234**, 5.

Fukuyama, Takeshi, 2012, "Searching for new physics beyond the standard model in electric dipole moment," Int. J. Mod. Phys. A **27**, 1230015.

Gabrielse, G., S. F. Hoogerheide, J. Dorr, and E. Novitski, 2014, "Precise Matter and Antimatter Tests of the Standard Model with e^-, e^+, p, $\bar{p}$ and $\bar{H}$," in *Fundamental Physics in Particle Traps*, Springer Tracts in Modern Physics, Vol. 256, edited by W. Quint and M. Vogel (Springer, Berlin/Heidelberg), p. 1.

Gabrielse, G., A. Khabbaz, D. S. Hall, C. Heimann, H. Kalinowsky, and W. Jhe, 1999, "Precision mass spectroscopy of the antiproton and proton using simultaneously trapped particles," Phys. Rev. Lett. **82**, 3198.

Gacesa, M., and R. Côté, 2014, "Photoassociation of ultracold molecules near a Feshbach resonance as a probe of the electron-proton mass ratio variation," J. Mol. Spectrosc. **300**, 124.

Gambini, R., and J. Pullin, 2003, "Discrete quantum gravity," Int. J. Mod. Phys. D **12**, 1775.

Garbacz, P., 2014, "Spin-spin coupling in the HD molecule determined from ^{1}H and ^{2}H NMR experiments in the gas-phase," Chem. Phys. **443**, 1.

Garcon, A., *et al.*, 2018, "The Cosmic Axion Spin Precession Experiment (CASPEr): a dark-matter search with nuclear magnetic resonance," Quantum Science and Technology **3**, 014008.

Gato-Rivera, B., 2015, "Constraining extra space dimensions using precision molecular spectroscopy," J. Phys. Conf. Ser. **626**, 012052.

Gavela, M. B., P. Hernández, J. Orloff, and O. Pène, 1994, "Standard model CP-violation and baryon asymmetry," Mod. Phys. Lett. A **09**, 795.

Geiger, R., 2017, "Future gravitational wave detectors based on atom interferometry," in *An Overview of Gravitational Waves: Theory, Sources and Detection*, edited by G. Augar and E. Plagnol (World Scientific, Singapore), pp. 285–313, arXiv:1611.09911.

Geiger, R., and M Trupke, 2018, "Proposal for a quantum test of the weak equivalence principle with entangled atomic species," Phys. Rev. Lett. **120**, 043602.

Geiger, R., *et al.*, 2011, "Detecting inertial effects with airborne matter-wave interferometry," Nat. Commun. **2**, 474.

Geiger, R., *et al.*, 2015, "Matter-wave laser interferometric gravitation antenna (MIGA): New perspectives for fundamental physics and geosciences," *Proceedings of the 50th Rencontres de Moriond "100 years after GR", La Thuile (Italy)*, arXiv:1505.07137.

Gelmini, G., S. Nussinov, and T. Yanagida, 1983, "Does nature like Nambu-Goldstone bosons?," Nucl. Phys. B **219**, 31.

Gelmini, G., and M. Roncadelli, 1981, "Left-handed neutrino mass scale and spontaneously broken lepton number," Phys. Lett. B **99**, 411.

Gemmel, C., *et al.*, 2010, "Limit on Lorentz and CPT violation of the bound neutron using a free precession ^{3}He/^{129}Xe comagnetometer," Phys. Rev. D **82**, 111901(R).

Georgescu, I. M., S. Ashhab, and F. Nori, 2014, "Quantum simulation," Rev. Mod. Phys. **86**, 153.

Georgi, Howard, 2007, "Unparticle physics," Phys. Rev. Lett. **98**, 221601.

Geraci, A., and H. Goldman, 2015, "Sensing short range forces with a nanosphere matter-wave interferometer," Phys. Rev. D **92**, 062002.

Geraci, A. A., S. B. Papp, and J. Kitching, 2010, "Short-range force detection using optically cooled levitated microspheres," Phys. Rev. Lett. **105**, 101101.

Geraci, A. A., S. J. Smullin, D. M. Weld, J. Chiaverini, and A. Kapitulnik, 2008, "Improved constraints on non-Newtonian forces at 10 microns," Phys. Rev. D **78**, 022002.

Geraci, A. A., *et al.*, 2017, "Progress on the ARIADNE axion experiment," arXiv:1710.05413.

Geraci, Andrew A., and Andrei Derevianko, 2016, "Sensitivity of atom interferometry to ultralight scalar field dark matter," Phys. Rev. Lett. **117**, 261301.

Germann, Matthias, Xin Tong, and Stefan Willitsch, 2014, "Observation of electric-dipole-forbidden infrared transitions in cold molecular ions," Nat. Phys. **10**, 820.

Gharibnejad, H., and A. Derevianko, 2015, "Dark forces and atomic electric dipole moments," Phys. Rev. D **91**, 035007.

Gillaspy, J. D., 2014, "Precision spectroscopy of trapped highly charged heavy elements: pushing the limits of theory and experiment," Phys. Scr. **89**, 114004.

Ginges, J. S. M., and V. V. Flambaum, 2004, "Violations of fundamental symmetries in atoms and tests of unification theories of elementary particles," Phys. Rep. **397**, 63.

Giudice, Gian Francesco, and Andrea Romanino, 2006, "Electric dipole moments in split supersymmetry," Phys. Lett. B **634**, 307.

Glauber, R. J., 2006, "Nobel lecture: One hundred years of light quanta," Rev. Mod. Phys. **78**, 1267.

Glenday, A. G., C. E. Cramer, D. F. Phillips, and R. L. Walsworth, 2008, "Limits on anomalous spin-spin couplings between neutrons," Phys. Rev. Lett. **101**, 261801.

Godun, R. M., P. B. R. Nisbet-Jones, J. M. Jones, S. A. King, L. A. M. Johnson, H. S. Margolis, K. Szymaniec, S. N. Lea, K. Bongs, and P. Gill, 2014, "Frequency ratio of two optical clock transitions in ^{171}Yb$^+$ and constraints on the time variation of fundamental constants," Phys. Rev. Lett. **113**, 210801.

Goldman, N., G. Juzeliūnas, P. Öhberg, and I. B. Spielman, 2014, "Light-induced gauge fields for ultracold atoms," Rep. Prog. Phys. **77**, 126401.

Gomes Ferreiraa, F. A., P. C. Maltab, L. P. R. Ospedalc, and J. A. Helayël-Netod, 2015, "Topologically massive spin-1 particles and spin-dependent potentials," Eur. Phys. J. C **75**, 238.

Gomez, E., S. Aubin, G. D. Sprouse, L. A. Orozco, and D. P. DeMille, 2007, "Measurement method for the nuclear anapole moment of laser-trapped alkali-metal atoms," Phys. Rev. A **75**, 033418.

Gomez, E., L. A. Orozco, and G. D. Sprouse, 2006, "Spectroscopy with trapped francium: advances and perspectives for weak interaction studies," Rep. Prog. Phys. **69**, 79.

Gorenstein, P., and W. Tucker, 2014, "Astronomical signatures of dark matter," Adv. High Energy Phys. **2014**, 878203.

Graham, P. W., J. M. Hogan, M. A. Kasevich, and S. Rajendran, 2013, "New method for gravitational wave detection with atomic sensors," Phys. Rev. Lett. **110**, 171102.

Graham, P. W., J. M. Hogan, M. A. Kasevich, and S. Rajendran, 2016, "Resonant mode for gravitational wave detectors based on atom interferometry," Phys. Rev. D **94**, 104022.

Graham, P. W., I. G. Irastorza, S. K. Lamoreaux, A. Lindner, and K. A. van Bibber, 2015, "Experimental searches for the axion and axion-like particles," Annu. Rev. Nucl. Part. Sci. **65**, 485.

Graham, P. W., D. E. Kaplan, J. Mardon, S. Rajendran, and W. A. Terrano, 2016, "Dark matter direct detection with accelerometers," Phys. Rev. D **93**, 075029.

Graham, P. W., D. E. Kaplan, J. Mardon, S. Rajendran, W. A. Terrano, L. Trahms, and T. Wilkason, 2017, "Spin precession experiments for light axionic dark matter," arXiv:1709.07852.

Graham, P. W., David E. Kaplan, and Surjeet Rajendran, 2015, "Cosmological relaxation of the electroweak scale," Phys. Rev. Lett. **115**, 221801.

Graham, P. W., and S. Rajendran, 2011, "Axion dark matter detection with cold molecules," Phys. Rev. D **84**, 055013.

Graham, P. W., and S. Rajendran, 2013, "New observables for direct detection of axion dark matter," Phys. Rev. D **88**, 035023.

Graner, B., Y. Chen, E. G. Lindahl, and B. R. Heckel, 2016, "Reduced limit on the permanent electric dipole moment of ^{199}Hg," Phys. Rev. Lett. **116**, 161601.

Gray, C. G., G. Karl, and V. A. Novikov, 2010, "Magnetic multipolar contact fields: The anapole and related moments," Am. J. Phys. **78**, 936.

Greenberg, O. W., 1991, "Particles with small violations of Fermi or Bose statistics," Phys. Rev. D **43**, 4111.

Greenberg, O. W., 2002, "*CPT* violation implies violation of Lorentz invariance," Phys. Rev. Lett. **89**, 231602.

Greenberg, O. W., and Robert C. Hilborn, 1999, "Quon statistics for composite systems and a limit on the violation of the Pauli principle for nucleons and quarks," Phys. Rev. Lett. **83**, 4460.

Greenberg, O. W., and R. N. Mohapatra, 1989, "Phenomenology of small violations of Fermi and Bose statistics," Phys. Rev. D **39**, 2032.

Greiner, Walter, 2000, *Relativistic Quantum Mechanics Wave Equations* (Springer, Berlin), 3rd ed.

Gresh, D., W. Cairncross, K. Cossel, M. Grau, K. B. Ng, Y. Zhou, Y. Ni, J. Ye, and E. Cornell, 2016, "Progress of the JILA electron EDM experiment," *Bulletin of the Americal Physical Society*, Vol. 61, No. 8, Abstract H5.00007.

Griffith, W. C., M. D. Swallows, T. H. Loftus, M. V. Romalis, B. R. Heckel, and E. N. Fortson, 2009, "Improved limit on the permanent electric dipole moment of ^{199}Hg," Phys. Rev. Lett. **102**, 101601.

Guéna, J., M. Abgrall, D. Rovera, P. Rosenbusch, M. E. Tobar, P. Laurent, A. Clairon, and S. Bize, 2012, "Improved tests of local position invariance using ^{87}Rb and ^{133}Cs fountains," Phys. Rev. Lett. **109**, 080801.

Guéna, J., P. Rosenbusch, P. Laurent, M. Abgrall, D. a. Rovera, G. Santarelli, M. E. Tobar, S. Bize, and A. Clairon, 2010, "Demonstration of a dual alkali Rb/Cs atomic fountain clock," IEEE Trans. Ultrason. Ferroelectr. Freq. Control **57**, 647.

Guéna, J., *et al.*, 2012, "Progress in atomic fountains at LNE-SYRTE," IEEE Trans. Ultrason. Ferroelectr. Freq. Control **59**, 391.

Guigue, M., D. Jullien, A. K. Petukhov, and G. Pignol, 2015, "Constraining short-range spin-dependent forces with polarized ^{3}He," Phys. Rev. D **92**, 114001.

Gumberidze, A., *et al.*, 2005, "Quantum electrodynamics in strong electric fields: The ground-state Lamb shift in hydrogenlike uranium," Phys. Rev. Lett. **94**, 223001.

Gundlach, J. H., 2005, "Laboratory tests of gravity," New J. Phys. **7**, 205.

Guzman, J., T. Inaki, and A. Penaflor, 2015, "Search for violations of Bose-Einstein statistics using ultra-cold Sr atoms," in *APS Division of Atomic, Molecular and Optical Physics Meeting Abstracts*.

Haber, H. E., G. L. Kane, and T. Sterling, 1979, "The fermion mass scale and possible effects of Higgs bosons on experimental observables," Nucl. Phys. B **161**, 493.

Hall, J. L., 2006, "Nobel lecture: Defining and measuring optical frequencies," Rev. Mod. Phys. **78**, 1279.

Hall, L. J., and D. Smith, 1999, "Cosmological constraints on theories with large extra dimensions," Phys. Rev. D **60**, 085008.

Hamilton, P., M. Jaffe, P. Haslinger, Q. Simmons, H. Müller, and J. Khoury, 2015, "Atom-interferometry constraints on dark energy," Science **349**, 849.

Hammond, R. T., 1995, "Upper limit on the torsion coupling constant," Phys. Rev. D **52**, 6918.

Hanneke, D., R. A. Carollo, and D. A. Lane, 2016, "High sensitivity to variation in the proton-to-electron mass ratio in O_2^+," Phys. Rev. A **94**, 050101.

Hanneke, D., S. Fogwell, and G. Gabrielse, 2008, "New measurement of the electron magnetic moment and the fine structure constant," Phys. Rev. Lett. **100**, 120801.

Hänsch, T. W., 2006, "Nobel Lecture: Passion for precision," Rev. Mod. Phys. **78**, 1297.

Happer, W., Y.-Y. Jau, and T. Walker, 2010, *Optically Pumped Atoms* (Wiley-VCH, Berlin).

Happer, William, 1972, "Optical Pumping," Rev. Mod. Phys. **44**, 169.

Harabati, C., V. A. Dzuba, V. V. Flambaum, and M. A. Hohensee, 2015, "Effects of Lorentz-symmetry violation on the spectra of rare-earth ions in a crystal field," Phys. Rev. A **92**, 040101.

Hardy, E., and R. Lasenby, **2017**, "Stellar cooling bounds on new light particles: plasma mixing effects," J. High Energy Phys. 02, 33.

Hari Dass, N. D., 1976, "Experimental tests for some quantum effects in gravitation," Phys. Rev. Lett. **36**, 393.

Haroche, S., 2013, "Nobel lecture: Controlling photons in a box and exploring the quantum to classical boundary," Rev. Mod. Phys. **85**, 1083.

Harrick, N. J., R. G. Barnes, P. J. Bray, and N. F. Ramsey, 1953, "Nuclear radiofrequency spectra of D_2 and H_2 in intermediate and strong magnetic fields," Phys. Rev. **90**, 260.

Hartwig, J., S. Abend, C. Schubert, D. Schlippert, H. Ahlers, K. Posso-Trujillo, N. Gaaloul, W. Ertmer, and E. M. Rasel, 2015, "Testing the universality of free fall with rubidium and ytterbium in a very large baseline atom interferometer," New J. Phys. **17**, 035011.

Haxton, W. C., and K. Y. Lee, 1991, "Red-giant evolution, metallicity, and new bounds on hadronic axions," Phys. Rev. Lett. **66**, 2557.

Haxton, W. C., and C. E. Wieman, 2001, "Atomic parity nonconservation and nuclear anapole moments," Annu. Rev. Nucl. Part. Sci. **51**, 261.

Haxton, Wick C., and Barry R. Holstein, 2013, "Hadronic parity violation," Prog. Part. Nucl. Phys. **71**, 185.

Hayes, A. C., J. L. Friar, and P. Möller, 2008, "Splitting sensitivity of the ground and 7.6 eV isomeric states of ^{229}Th," Phys. Rev. C **78**, 024311.

Heavner, T. P., E. A. Donley, F. Levi, G. Costanzo, T. E. Parker, J. H. Shirley, N. Ashby, S. Barlow, and S. R. Jefferts, 2014, "First accuracy evaluation of NIST-F2," Metrologia **51**, 174.

Heckel, B., 2016, http://online.kitp.ucsb.edu/online/nuclear-c16/heckel/options.html.

Heckel, B. R., E. G. Adelberger, C. E. Cramer, T. S. Cook, S. Schlamminger, and U. Schmidt, 2008, "Preferred-frame and *CP*-violation tests with polarized electrons," Phys. Rev. D **78**, 092006.

Hedges, Morgan, Marc Smiciklas, and Michael Romalis, 2015, "South Pole Lorentz invariance test," in *APS April Meeting Abstracts*, Vol. 1, p. 6003.

Hees, A., J. Guéna, M. Abgrall, S. Bize, and P. Wolf, 2016, "Searching for an oscillating massive scalar field as a dark matter candidate using atomic hyperfine frequency comparisons," Phys. Rev. Lett. **117**, 061301.

Hehl, Friedrich W., Paul von der Heyde, G. David Kerlick, and James M. Nester, 1976, "General relativity with spin and torsion: Foundations and prospects," Rev. Mod. Phys. **48**, 393.

Heinzen, D. J., and D. J. Wineland, 1990, "Quantum-limited cooling and detection of radio-frequency oscillations by laser-cooled ions," Phys. Rev. A **42**, 2977.

Heiße, F., *et al.*, 2017, "High-precision measurement of the proton's atomic mass," Phys. Rev. Lett. **119**, 033001.

Henkel, C., K. M. Menten, M. T. Murphy, N. Jethava, V. V. Flambaum, J. A. Braatz, S. Muller, J. Ott, and R. Q. Mao, 2009, "The density, the cosmic microwave background, and the proton-to-electron mass ratio in a cloud at redshift 0.9," Astron. Astrophys. **500**, 725.

Herrmann, S., H. Dittus, and C. Lämmerzahl (for the QUANTUS and PRIMUS teams), 2012, "Testing the equivalence principle with atomic interferometry," Classical Quantum Gravity **29**, 184003.

Herrmann, S., A. Senger, K. Möhle, M. Nagel, E. V. Kovalchuk, and A. Peters, 2009, "Rotating optical cavity experiment testing lorentz invariance at the 10^{-17} level," Phys. Rev. D **80**, 105011.

Hilborn, R. C., and G. M. Tino, 2000, Eds., *Spin-Statistics Connection and Commutation Relations: Experimental Tests and Theoretical Implications* (American Institute of Physics, New York).

Hill, R. J., 2017, "Review of experimental and theoretical status of the proton radius puzzle," Eur. Phys. J. Web Conf. **137**, 01023.

Hoedl, S. A., F. Fleischer, E. G. Adelberger, and B. R. Heckel, 2011, "Improved constraints on an axion-mediated force," Phys. Rev. Lett. **106**, 041801.

Hoekstra, S., 2016 (private communication).

Hogan, C. J., 2000, "Why the universe is just so," Rev. Mod. Phys. **72**, 1149.

Hogan, J. M., D. M. S. Johnson, and M. A. Kasevich, 2009, "Light-pulse atom interferometry," in *Atom Optics and Space Physics*, edited by E. Arimondo, W. Ertmer, W. P. Schleich, and E. M. Rasel (IOS, Amsterdam), p. 411, arXiv:0806.3261.

Hogan, J. M., and M. A. Kasevich, 2016, "Atom-interferometric gravitational-wave detection using heterodyne laser links," Phys. Rev. A **94**, 033632.

Hogan, J. M., *et al.*, 2011, "An atomic gravitational wave interferometric sensor in low earth orbit (AGIS-LEO)," Gen. Relativ. Gravit. **43**, 1953.

Hohensee, M. A., S. Chu, A. Peters, and H. Müller, 2011, "Equivalence principle and gravitational redshift," Phys. Rev. Lett. **106**, 151102.

Hohensee, M. A., B. Estey, P. Hamilton, A. Zeilinger, and H. Müller, 2012, "Force-free gravitational redshift: proposed gravitational Aharonov-Bohm experiment," Phys. Rev. Lett. **108**, 230404.

Hohensee, M. A., N. Leefer, D. Budker, C. Harabati, V. A. Dzuba, and V. V. Flambaum, 2013, "Limits on violations of Lorentz symmetry and the Einstein equivalence principle using radio-frequency spectroscopy of atomic dysprosium," Phys. Rev. Lett. **111**, 050401.

Hohensee, M. A., H. Müller, and R. B. Wiringa, 2013, "Equivalence principle and bound kinetic energy," Phys. Rev. Lett. **111**, 151102.

Hohensee, Michael A., Paul L. Stanwix, Michael E. Tobar, Stephen R. Parker, David F. Phillips, and Ronald L. Walsworth, 2010,

"Improved constraints on isotropic shift and anisotropies of the speed of light using rotating cryogenic sapphire oscillators," Phys. Rev. D **82**, 076001.

Holdom, Bob, 1986, "Two U(1)'s and ϵ charge shifts," Phys. Lett. B **166**, 196.

Hoogeveen, F., 1990, "The standard model prediction for the electric dipole moment of the electron," Nucl. Phys. B **341**, 322.

Hopkinson, D. A., and P. E. G. Baird, 2002, "An interferometric test of time reversal invariance in atoms," J. Phys. B **35**, 1307.

Hori, M., A. Sótér, and V. I. Korobov, 2014, "Proposed method for laser spectroscopy of pionic helium atoms to determine the charged-pion mass," Phys. Rev. A **89**, 042515.

Hori, M., *et al.*, 2011, "Two-photon laser spectroscopy of antiprotonic helium and the antiproton-to-electron mass ratio," Nature (London) **475**, 484.

Hori, M., *et al.*, 2016, "Buffer-gas cooling of antiprotonic helium to 1.5 to 1.7 K, and antiproton-to-electron mass ratio," Science **354**, 610.

Hornberger, K., S. Gerlich, P. Haslinger, S. Nimmrichter, and M. Arndt, 2012, "Colloquium: Quantum interference of clusters and molecules," Rev. Mod. Phys. **84**, 157.

Huber, Stephan J., Maxim Pospelov, and Adam Ritz, 2007, "Electric dipole moment constraints on minimal electroweak baryogenesis," Phys. Rev. D **75**, 036006.

Hudson, E. R., H. J. Lewandowski, B. C. Sawyer, and J. Ye, 2006, "Cold molecule spectroscopy for constraining the evolution of the fine structure constant," Phys. Rev. Lett. **96**, 143004.

Hudson, J. J., D. M. Kara, I. J. Smallman, B. E. Sauer, M. R. Tarbutt, and E. A. Hinds, 2011, "Improved measurement of the shape of the electron," Nature (London) **473**, 493.

Hughes, R. J., and M. H. Holzscheiter, 1991, "Constraints on the gravitational properties of antiprotons and positrons from cyclotron-frequency measurements," Phys. Rev. Lett. **66**, 854.

Hughes, V. W., H. G. Robinson, and V. Beltran-Lopez, 1960, "Upper limit for the anisotropy of inertial mass from nuclear resonance experiments," Phys. Rev. Lett. **4**, 342.

Huntemann, N., B. Lipphardt, C. Tamm, V. Gerginov, S. Weyers, and E. Peik, 2014, "Improved limit on a temporal variation of m_p/m_e from comparisons of Yb$^+$ and Cs atomic clocks," Phys. Rev. Lett. **113**, 210802.

Huntemann, N., M. Okhapkin, B. Lipphardt, S. Weyers, C. Tamm, and E. Peik, 2012, "High-accuracy optical clock based on the octupole transition in ^{171}Yb$^+$," Phys. Rev. Lett. **108**, 090801.

Huntemann, N., C. Sanner, B. Lipphardt, C. Tamm, and E. Peik, 2016, "Single-ion atomic clock with 3×10^{-18} systematic uncertainty," Phys. Rev. Lett. **116**, 063001.

Hunter, L., J. Gordon, S. Peck, D. Ang, and Lin J.-F., 2013, "Using the Earth as a polarized electron source to search for long-range spin-spin interactions," Science **339**, 928.

Hunter, L. R., and D. G. Ang, 2014, "Using geoelectrons to search for velocity-dependent spin-spin interactions," Phys. Rev. Lett. **112**, 091803.

Hutzler, Nicholas R., Hsin-I Lu, and John M. Doyle, 2012, "The buffer gas beam: An intense, cold, and slow source for atoms and molecules," Chem. Rev. **112**, 4803.

Hylleraas, Egil A., and Aadne Ore, 1947, "Binding energy of the positronium molecule," Phys. Rev. **71**, 493.

Inoue, T., *et al.*, 2015, "Experimental search for the electron electric dipole moment with laser cooled francium atoms," Hyperfine Interact. **231**, 157.

Ishida, A., 2015, "New precise measurement of the hyperfine splitting of positronium," J. Phys. Chem. Ref. Data **44**, 031212.

Ishida, A., T. Namba, S. Asai, T. Kobayashi, H. Saito, M. Yoshida, K. Tanaka, and A. Yamamoto, 2014, "New precision measurement of hyperfine splitting of positronium," Phys. Lett. B **734**, 338.

Islam, R., C. Senko, W. C. Campbell, S. Korenblit, J. Smith, A. Lee, E. E. Edwards, C.-C. J. Wang, J. K. Freericks, and C. Monroe, 2013, "Emergence and frustration of magnetism with variable-range interactions in a quantum simulator," Science **340**, 583.

Ivanov, A. N., and W. M. Snow, 2017, "Parity-even and time-reversal-odd neutron optical potential in spinning matter induced by gravitational torsion," Phys. Lett. B **764**, 186.

Iwazaki, A., 2015, "Axion stars and fast radio bursts," Phys. Rev. D **91**, 023008.

Jackson, J. D., 1999, *Classical Electrodynamics* (John Wiley & Sons, New York), 3rd ed.

Jackson Kimball, D. F., 2015, "Nuclear spin content and constraints on exotic spin-dependent couplings," New J. Phys. **17**, 073008.

Jackson Kimball, D. F., A. Boyd, and D. Budker, 2010, "Constraints on anomalous spin-spin interactions from spin-exchange collisions," Phys. Rev. A **82**, 062714.

Jackson Kimball, D. F., D. Budker, J. Eby, M. Pospelov, S. Pustelny, T. Scholtes, Y. V. Stadnik, A. Weis, and A. Wickenbrock, 2018, "Searching for axion stars and Q-balls with a terrestrial magnetometer network," Phys. Rev. D **97**, 043002.

Jackson Kimball, D. F., J. Dudley, Y. Li, D. Patel, and J. Valdez, 2017, "Constraints on long-range spin-gravity and monopole-dipole couplings of the proton," Phys. Rev. D **96**, 075004.

Jackson Kimball, D. F., J. Dudley, Y. Li, S. Thulasi, S. Pustelny, D. Budker, and M. Zolotorev, 2016, "Magnetic shielding and exotic spin-dependent interactions," Phys. Rev. D **94**, 082005.

Jackson Kimball, D. F., I. Lacey, J. Valdez, J. Swiatlowski, C. Rios, R. Peregrina-Ramirez, C. Montcrieffe, J. Kremer, J. Dudley, and C. Sanchez, 2013, "A dual-isotope rubidium comagnetometer to search for anomalous long-range spin-mass (spin-gravity) couplings of the proton," Ann. Phys. (Berlin) **525**, 514.

Jackson Kimball, D. F., S. K. Lamoreaux, and T. E. Chupp, 2013, "Tests of fundamental physics with optical magnetometers," in *Optical Magnetometry*, edited by D. Budker and D. F. Jackson Kimball (Cambridge University, Cambridge, UK).

Jackson Kimball, D. F., A. O. Sushkov, and D. Budker, 2016, "Precessing ferromagnetic needle magnetometer," Phys. Rev. Lett. **116**, 190801.

Jackson Kimball, D. F., *et al.*, 2017, "Overview of the Cosmic Axion Spin Precession Experiment (CASPEr)," arXiv:1711.08999.

Jaeckel, J., and J. Redondo, 2013, "Resonant to broadband searches for cold dark matter consisting of weakly interacting slim particles," Phys. Rev. D **88**, 115002.

Jaffe, M., P. Haslinger, V. Xu, P. Hamilton, A. Upadhye, B. Elder, J. Khoury, and H. Müller, 2016, "Testing sub-gravitational forces on atoms from a miniature, in-vacuum source mass," arXiv:1612.05171.

Jain, P., and S. Mandal, 2006, "Evading the astrophysical limits on light pseudoscalars," Int. J. Mod. Phys. D **15**, 2095.

Janka, H. T., W. Keil, G. Raffelt, and D. Seckel, 1996, "Nucleon spin fluctuations and the supernova emission of neutrinos and axions," Phys. Rev. Lett. **76**, 2621.

Jansen, P., H. L. Bethlem, and W. Ubachs, 2014, "Perspective: Tipping the scales: Search for drifting constants from molecular spectra," J. Chem. Phys. **140**, 010901.

Jansen, P., I. Kleiner, C. Meng, R. M. Lees, M. H. M. Janssen, W. Ubachs, and H. L. Bethlem, 2013, "Prospects for high-resolution microwave spectroscopy of methanol in a Stark-deflected molecular beam," Mol. Phys. **111**, 1923.

Jeet, J., C. Schneider, S. T. Sullivan, W. G. Rellergert, S. Mirzadeh, A. Cassanho, H. P. Jenssen, E. V. Tkalya, and E. R. Hudson, 2015, "Results of a direct search using synchrotron radiation for the low-energy ^{229}Th nuclear isomeric transition," Phys. Rev. Lett. **114**, 253001.

Jenke, T., *et al.*, 2014, "Gravity resonance spectroscopy constrains dark energy and dark matter scenarios," Phys. Rev. Lett. **112**, 151105.

Jentschura, U. D., 2011, "Lamb shift in muonic hydrogen II. Analysis of the discrepancy of theory and experiment," Ann. Phys. (Amsterdam) **326**, 516.

Johnson, W., M. Safronova, and U. Safronova, 2003, "Combined effect of coherent Z exchange and the hyperfine interaction in the atomic parity-nonconserving interaction," Phys. Rev. A **67**, 062106.

Johnson, W. R., I. Bednyakov, and G. Soff, 2001, "Vacuum-polarization corrections to the parity-nonconserving $6s - 7s$ transition amplitude in ^{133}Cs," Phys. Rev. Lett. **87**, 233001.

Johnson, Walter R., 2007, *Atomic Structure Theory—Lectures on Atomic Physics* (Springer-Verlag, Berlin).

Jones, A. C. L., T. H. Hisakado, H. J. Goldman, H. W. K. Tom, A. P. Mills, and D. B. Cassidy, 2014, "Doppler-corrected Balmer spectroscopy of Rydberg positronium," Phys. Rev. A **90**, 012503.

Jordan, E., G. Cerchiari, S. Fritzsche, and A. Kellerbauer, 2015, "High-resolution spectroscopy on the laser-cooling candidate La$^-$," Phys. Rev. Lett. **115**, 113001.

Joyce, A., B. Jain, J. Khoury, and M. Trodden, 2015, "Beyond the cosmological standard model," Phys. Rep. **568**, 1.

Jung, Martin, **2013**, "A robust limit for the electric dipole moment of the electron," J. High Energy Phys. 05, 168.

Jungmann, Klaus, 2013, "Searching for electric dipole moments," Ann. Phys. (Berlin) **525**, 550.

Kahn, Y., B. R. Safdi, and J. Thaler, 2016, "Broadband and resonant approaches to axion dark matter detection," Phys. Rev. Lett. **117**, 141801.

Kajita, M., 2017a, "Accuracy estimation of the ^{16}O$_2^+$ transition frequencies targeting the search for the variation in the proton-electron mass ratio," Phys. Rev. A **95**, 023418.

Kajita, M., 2017b, "Search for the variation in (m_p/m_e) using two vibrational transition frequencies of molecular ions," J. Phys. Soc. Jpn. **86**, 123301.

Kajita, M., G. Gopakumar, M. Abe, and M. Hada, 2014, "Characterizing of variation in the proton-to-electron mass ratio via precise measurements of molecular vibrational transition frequencies," J. Mol. Spectrosc. **300**, 99.

Kajita, M., G. Gopakumar, M. Abe, M. Hada, and M. Keller, 2014, "Test of m_p/m_e changes using vibrational transitions in N$_2^+$," Phys. Rev. A **89**, 032509.

Kakhidze, A. I., and I. V. Kolokolov, 1991, "Antiferromagnetic axion detector," Zh. Eksp. Teor. Fiz. **99**, 1077 [Sov. Phys. JETP **72**, 598 (1991)].

Kamiya, Y., K. Itagaki, M. Tani, G. N. Kim, and S. Komamiya, 2015, "Constraints on new gravitylike forces in the nanometer range," Phys. Rev. Lett. **114**, 161101.

Kane, Gordon L., 2002, "TASI lectures: weak scale supersymmetry—a top-motivated-bottom-up approach," arXiv:hep-ph/0202185.

Kanekar, N., 2011, "Constraining changes in the proton-electron mass ratio with inversion and rotational lines," Astrophys. J. Lett. **728**, L12.

Kanekar, N., W. Ubachs, K. M. Menten, J. Bagdonaite, A. Brunthaler, C. Henkel, S. Muller, H. L. Bethlem, and M. Daprà, 2015, "Constraints on changes in the proton-electron mass ratio using methanol lines," Mon. Not. R. Astron. Soc. **448**, L104.

Kapner, D. J., T. S. Cook, E. G. Adelberger, J. H. Gundlach, B. R. Heckel, C. D. Hoyle, and H. E. Swanson, 2007, "Tests of the gravitational inverse-square law below the dark-energy length scale," Phys. Rev. Lett. **98**, 021101.

Kara, D. M., I. J. Smallman, J. J. Hudson, B. E. Sauer, M. R. Tarbutt, and E. A. Hinds, 2012, "Measurement of the electron's electric dipole moment using YbF molecules: methods and data analysis," New J. Phys. **14**, 103051.

Karr, J.-P., 2014, "H$_2^+$ and HD: Candidates for a molecular clock," J. Mol. Spectrosc. **300**, 37.

Karshenboim, S. G., 2005, "Precision physics of simple atoms: QED tests, nuclear structure and fundamental constants," Phys. Rep. **422**, 1.

Karshenboim, S. G., 2010a, "Constraints on a long-range spin-dependent interaction from precision atomic physics," Phys. Rev. D **82**, 113013.

Karshenboim, S. G., 2010b, "Constraints on a long-range spin-independent interaction from precision atomic physics," Phys. Rev. D **82**, 073003.

Karshenboim, S. G., 2010c, "Precision physics of simple atoms and constraints on a light boson with ultraweak coupling," Phys. Rev. Lett. **104**, 220406.

Karshenboim, S. G., 2013, "Recent progress in determination of fundamental constants and fundamental physics at low energies," Ann. Phys. (Berlin) **525**, 472.

Karshenboim, Savely G., 2016, "Positronium, antihydrogen, light, and the equivalence principle," J. Phys. B **49**, 144001.

Kawall, D., 2011, "Searching for the electron EDM in a storage ring," J. Phys. Conf. Ser. **295**, 012031.

Keesom, W. H., 1942, *Helium* (Elsevier, New York).

Kellerbauer, A., C. Canali, A. Fischer, and U. Warring, 2009, "Ultracold antiprotons by indirect laser cooling," Hyperfine Interact. **194**, 77.

Kellerbauer, Alban, 2015, "Why antimatter matters," Eur. Rev. **23**, 45.

Ketterle, W., 2002, "Nobel lecture: When atoms behave as waves: Bose-Einstein condensation and the atom laser," Rev. Mod. Phys. **74**, 1131.

Khoury, J., 2013, "Chameleon field theories," Classical Quantum Gravity **30**, 214004.

Khoury, J., and A. Weltman, 2004a, "Chameleon cosmology," Phys. Rev. D **69**, 044026.

Khoury, J., and A. Weltman, 2004b, "Chameleon fields: Awaiting surprises for tests of gravity in space," Phys. Rev. Lett. **93**, 171104.

Khriplovich, I. B., 1991, *Parity Nonconservation in Atomic Phenomena* (Gordon and Breach, Philadelphia).

Khriplovich, I. B., and S. K. Lamoureaux, 1997, *CP Violation Without Strangeness* (Springer, Berlin).

Khriplovich, I. B., and A. R. Zhitnitsky, 1982, "What is the value of the neutron electric dipole moment in the Kobayashi-Maskawa model?," Phys. Lett. B **109**, 490.

Kim, J., 1979, "Weak-interaction singlet and strong *CP* invariance," Phys. Rev. Lett. **43**, 103.

Kim, J. E., and G. Carosi, 2010, "Axions and the strong *CP* problem," Rev. Mod. Phys. **82**, 557.

Kim, W.-J., A. O. Sushkov, D. A. R. Dalvit, and S. K. Lamoreaux, 2010, "Surface contact potential patches and Casimir force measurements," Phys. Rev. A **81**, 022505.

King, J. A., J. K. Webb, M. T. Murphy, V. V. Flambaum, R. F. Carswell, M. B. Bainbridge, M. R. Wilczynska, and F. E. Koch, 2012, "Spatial variation in the fine-structure constant—new results from VLT/UVES," Mon. Not. R. Astron. Soc. **422**, 3370.

Klaft, I., *et al.*, 1994, "Precision laser spectroscopy of the ground state hyperfine splitting of hydrogenlike ^{209}Bi^{82+}," Phys. Rev. Lett. **73**, 2425.

Kleinert, S., E. Kajari, A. Roura, and W. P. Schleich, 2015, "Representation-free description of light-pulse atom interferometry including non-inertial effects," Phys. Rep. **605**, 1.

Klimchitskaya, G. L., and V. M. Mostepanenko, 2015, "Improved constraints on the coupling constants of axion-like particles to nucleons from recent Casimir-less experiment," Eur. Phys. J. C **75**, 164.

Klinkenberg, P. F. A., 1952, "Tables of nuclear shell structure," Rev. Mod. Phys. **24**, 63.

Kluge, H.-J., *et al.*, 2008, "HITRAP: A facility at GSI for highly charged ions," Adv. Quantum Chem. **53**, 83.

Kobayashi, Jun, Atsushi Ogino, and Shin Inouye, 2015, "Ultracold molecular spectroscopy: toward the narrow-line cooling of molecules," New J. Phys. **17**, 035013.

Kobzarev, I. Yu., and L. B. Okun, 1962, "Gravitational interaction of fermions," Zh. Eksp. Teor. Fiz. **43**, 1904 [Sov. Phys. JETP **16**, 1343 (1963)].

Köhler, F., S. Sturm, A. Kracke, G. Werth, W. Quint, and K. Blaum, 2015, "The electron mass from g-factor measurements on hydrogen-like carbon ^{12}C^{5+}," J. Phys. B **48**, 144032.

Köhler, F., *et al.*, 2016, "Isotope dependence of the Zeeman effect in lithium-like calcium," Nat. Commun. **7**, 10246.

Kolb, E. W., and I. I. Tkachev, 1993, "Axion miniclusters and Bose stars," Phys. Rev. Lett. **71**, 3051.

Kolkowitz, S., I. Pikovski, N. Langellier, M. D. Lukin, R. L. Walsworth, and J. Ye, 2016, "Gravitational wave detection with optical lattice atomic clocks," Phys. Rev. D **94**, 124043.

Komatsu, E., *et al.*, 2011, "Seven-year Wilkinson microwave anisotropy probe," Astrophys. J. Suppl. Ser. **192**, 18.

Kominis, I. K., T. W. Kornack, J. C. Allred, and M. V. Romalis, 2003, "A subfemtotesla multichannel atomic magnetometer," Nature (London) **422**, 596.

Kornack, T. W., R. K. Ghosh, and M. V. Romalis, 2005, "Nuclear spin gyroscope based on an atomic comagnetometer," Phys. Rev. Lett. **95**, 230801.

Kornack, T. W., and M. V. Romalis, 2002, "Dynamics of two overlapping spin ensembles interacting by spin exchange," Phys. Rev. Lett. **89**, 253002.

Korobov, V. I., 2014, "Bethe logarithm for resonant states: Antiprotonic helium," Phys. Rev. A **89**, 014501.

Korobov, V. I., L. Hilico, and J.-P. Karr, 2014a, "$m\alpha^7$-order corrections in the hydrogen molecular ions and antiprotonic helium," Phys. Rev. Lett. **112**, 103003.

Korobov, V. I., L. Hilico, and J.-P. Karr, 2014b, "Theoretical transition frequencies beyond 0.1 ppb accuracy in H$_2^+$, HD$^+$, and antiprotonic helium," Phys. Rev. A **89**, 032511.

Korobov, V. I., L. Hilico, and J.-P. Karr, 2015, "Bound-state QED calculations for antiprotonic helium," Hyperfine Interact. **233**, 75–82.

Kostelecký, V. A., and C. D. Lane, 1999, "Constraints on Lorentz violation from clock-comparison experiments," Phys. Rev. D **60**, 116010.

Kostelecký, V. A., and M. Mewes, 2002, "Signals for Lorentz violation in electrodynamics," Phys. Rev. D **66**, 056005.

Kostelecký, V. A., and R. Potting, 1995, "*CPT*, strings, and meson factories," Phys. Rev. D **51**, 3923.

Kostelecký, V. A., and N. Russell, 2011, "Data tables for Lorentz and *CPT* violation," Rev. Mod. Phys. **83**, 11.

Kostelecký, V. A., and N. Russell, 2017, "Data tables for Lorentz and *CPT* violation," arXiv:0801.0287v10.

Kostelecký, V. A., and J. D. Tasson, 2011, "Matter-gravity couplings and Lorentz violation," Phys. Rev. D **83**, 016013.

Kostelecký, V. Alan, Adrian C Melissinos, and Matthew Mewes, 2016, "Searching for photon-sector Lorentz violation using gravitational-wave detectors," Phys. Lett. B **761**, 1.

Kostelecký, V. Alan, and Arnaldo J. Vargas, 2015, "Lorentz and *CPT* tests with hydrogen, antihydrogen, and related systems," Phys. Rev. D **92**, 056002.

Kotler, S., N. Akerman, N. Navon, Y. Glickman, and R. Ozeri, 2014, "Measurement of the magnetic interaction between two electrons," Nature (London) **510**, 376.

Kotler, S., R. Ozeri, and D. F. Jackson Kimball, 2015, "Constraints on exotic dipole-dipole couplings between electrons at the micrometer scale," Phys. Rev. Lett. **115**, 081801.

Kovachy, T., P. Asenbaum, C. Overstreet, C. A. Donnelly, S. M. Dickerson, A. Sugarbaker, J. M. Hogan, and M. A. Kasevich, 2015, "Quantum superposition at the half-metre scale," Nature (London) **528**, 530.

Kovachy, T., J. M. Hogan, A. Sugarbaker, S. M. Dickerson, C. A. Donnelly, C. Overstreet, and M. A. Kasevich, 2015, "Matter wave lensing to picokelvin temperatures," Phys. Rev. Lett. **114**, 143004.

Kozhedub, Y. S., O. V. Andreev, V. M. Shabaev, I. I. Tupitsyn, C. Brandau, C. Kozhuharov, G. Plunien, and T. Stöhlker, 2008, "Nuclear deformation effect on the binding energies in heavy ions," Phys. Rev. A **77**, 032501.

Kozlov, A., V. A. Dzuba, and V. V. Flambaum, 2013, "Prospects of biulding optical atomic clocks using Er I or Er III," Phys. Rev. A **88**, 032509.

Kozlov, M. G., 2009, "Λ-doublet spectra of diatomic radicals and their dependence on fundamental constants," Phys. Rev. A **80**, 022118.

Kozlov, M. G., V. A. Korol, J. C. Berengut, V. A. Dzuba, and V. V. Flambaum, 2004, "Space-time variation of the fine-structure constant and evolution of isotope abundances," Phys. Rev. A **70**, 062108.

Kozlov, M. G., L. N. Labzovskii, and A. O. Mitruschenkov, 1991, "Parity nonconservation in diatomic molecules is a strong constant magnetic field," Zh. Eksp. Teor. Fiz. **100**, 749 [Sov. Phys. JETP **73**, 415 (1991)].

Kozlov, M. G., and L. N. Labzowsky, 1995, "Parity violation effects in diatomics," J. Phys. B **28**, 1933.

Kozlov, M. G., and S. A. Levshakov, 2013, "Microwave and submillimeter molecular transitions and their dependence on fundamental constants," Ann. Phys. (Berlin) **525**, 452.

Kozlov, M. G., and S. G. Porsev, 1989, "The possibility to study the break of time-reversal invariance in atoms," Phys. Lett. A **142**, 233.

Kozlov, M. G., S. G. Porsev, and I. I. Tupitsyn, 2001, "High accuracy calculation of $6S \rightarrow 7S$ parity nonconserving amplitude in Cs," Phys. Rev. Lett. **86**, 3260.

Kozlov, M. G., M. S. Safronova, , J. R. Crespo López-Urrutia, and P. O. Schmidt, 2018, "Highly charged ions: optical clocks and applications in fundamental physics," arXiv:1803.06532.

Kozyrev, Ivan, Louis Baum, Kyle Matsuda, Benjamin L. Augenbraun, Loic Anderegg, Alexander P. Sedlack, and John M. Doyle, 2017, "Sisyphus laser cooling of a polyatomic molecule," Phys. Rev. Lett. **118**, 173201.

Kozyrev, Ivan, and Nicholas R. Hutzler, 2017, "Precision measurement of time-reversal symmetry violation with laser-cooled polyatomic molecules," Phys. Rev. Lett. **119**, 133002.

Kramida, A., Yu. Ralchenko, and J. Reader, and NIST ASD Team, 2018, NIST Atomic Spectra Database (version 5.5.2) (online), http://physics.nist.gov/asd, National Institute of Standards and Technology, Gaithersburg, MD.

Krauss, L., J. Moody, F. Wilczek, and D. E. Morris, 1985, "Calculations for cosmic axion detection," Phys. Rev. Lett. **55**, 1797.

Kubiček, K., J. Braun, H. Bruhns, J. R. Crespo López-Urrutia, P. H. Mokler, and J. Ullrich, 2012, "High-precision laser-assisted absolute determination of X-ray diffraction angles," Rev. Sci. Instrum. **83**, 013102.

Kubiček, K., P. H. Mokler, V. Mäckel, J. Ullrich, and J. R. C. López-Urrutia, 2014, "Transition energy measurements in hydrogenlike and heliumlike ions strongly supporting bound-state QED calculations," Phys. Rev. A **90**, 032508.

Kuchiev, M. Yu., and V. Flambaum, 2002, "QED radiative corrections to parity nonconservation in heavy atoms," Phys. Rev. Lett. **89**, 283002.

Kuchler, F., *et al.*, 2016, "A new search for the atomic EDM of ^{129}Xe at FRM-II," Hyperfine Interact. **237**, 95.

Kuroda, K., and N. Mio, 1989, "Test of a composition-dependent force by a free-fall interferometer," Phys. Rev. Lett. **62**, 1941.

Kuroda, N., *et al.*, 2014, "A source of antihydrogen for in-flight hyperfine spectroscopy," Nat. Commun. **5**, 3089.

Kusenko, A., and P. J. Steinhardt, 2001, "Q-ball candidates for self-interacting dark matter," Phys. Rev. Lett. **87**, 141301.

Lamm, H., 2017, "P—state positronium for precision physics: An ultrafine splitting at α^6," Phys. Rev. A **96**, 022515.

Lamoreaux, S. K., 1989, "Optical pumping technique for measuring small nuclear quadrupole shifts in $^1S_0$ atoms and testing spatial anisotropy," Nucl. Instrum. Methods Phys. Res., Sect. A **284**, 43.

Lamoreaux, S. K., 1997, "Demonstration of the Casimir force in the 0.6 to 6 μm range," Phys. Rev. Lett. **78**, 5.

Lamoreaux, S. K., 2005, "The Casimir force: background, experiments, and applications," Rep. Prog. Phys. **68**, 201.

Lamoreaux, S. K., 2012, "The Casimir force and related effects: The status of the finite temperature correction and limits on new long-range forces," Annu. Rev. Nucl. Part. Sci. **62**, 37.

Landau, L. D., 1948, Dokl. Akad. Nauk SSSR **60**, 207.

Langacker, Paul, 2009, "The physics of heavy Z' gauge bosons," Rev. Mod. Phys. **81**, 1199.

Laporte, O., 1924, "Die struktur des eisenspektrums (I)," Z. Phys. **23**, 135.

Latha, K. V. P., D. Angom, B. P. Das, and D. Mukherjee, 2009, "Probing *CP* violation with the electric dipole moment of atomic mercury," Phys. Rev. Lett. **103**, 083001; **115**, 059902(E) (2015).

Leanhardt, A. E., J. L. Bohn, H. Loh, P. Maletinsky, E. R. Meyer, L. C. Sinclair, R. P. Stutz, and E. A. Cornell, 2011, "High-resolution spectroscopy on trapped molecular ions in rotating electric fields: A new approach for measuring the electron electric dipole moment," J. Mol. Spectrosc. **270**, 1.

Le Dall, Matthias, Maxim Pospelov, and Adam Ritz, 2015, "Sensitivity to light weakly-coupled new physics at the precision frontier," Phys. Rev. D **92**, 016010.

Ledbetter, M. P., S. Pustelny, D. Budker, M. V. Romalis, J. W. Blanchard, and A. Pines, 2012, "Liquid-state nuclear spin comagnetometers," Phys. Rev. Lett. **108**, 243001.

Ledbetter, M. P., M. V. Romalis, and D. F. Jackson Kimball, 2013, "Constraints on short-range spin-dependent interactions from scalar spin-spin coupling in deuterated molecular hydrogen," Phys. Rev. Lett. **110**, 040402.

Lee, T. D., and C. N. Yang, 1956, "Question of parity conservation in weak interactions," Phys. Rev. **104**, 254.

Leefer, N., L. Bougas, D. Antypas, and D. Budker, 2014, "Towards a new measurement of parity violation in dysprosium," arXiv:1412.1245.

Leefer, N., A. Gerhardus, D. Budker, V. V. Flambaum, and Y. V. Stadnik, 2016, "Search for the effect of massive bodies on atomic spectra and constraints on Yukawa-type interactions of scalar particles," Phys. Rev. Lett. **117**, 271601.

Leefer, N., C. T. M. Weber, A. Cingöz, J. R. Torgerson, and D. Budker, 2013, "New limits on variation of the fine-structure constant using atomic dysprosium," Phys. Rev. Lett. **111**, 060801.

Leggett, A. J., 1978, "Macroscopic effect of P- and T-nonconserving interactions in ferroelectrics: A possible experiment?," Phys. Rev. Lett. **41**, 586.

Lehnert, R., W. M. Snow, Z. Xiao, and R. Xu, 2017, "Constraining spacetime nonmetricity with neutron spin rotation in liquid ^{4}He," Phys. Lett. B **772**, 865.

Lehnert, R., W. M. Snow, and H. Yan, 2014, "A first experimental limit on in-matter torsion from neutron spin rotation in liquid ^{4}He," Phys. Lett. B **730**, 353; Lehnert, R., W. M. Snow, and H. Yan, 2015, "Corrigendum to: A first experimental limit on in-matter torsion from neutron spin rotation in liquid ^{4}He," Phys. Lett. B **744**, 415.

Leitner, J., and S. Okubo, 1964, "Parity, charge conjugation, and time reversal in the gravitational interaction," Phys. Rev. **136**, B1542.

Lense, J., and H. Thirring, 1918, "On the influence of the proper rotation of a central body on the motion of the planets and the moon, according to Einstein's theory of gravitation," Phys. Z. **19**, 156.

Le Targat, R., *et al.*, 2013, "Experimental realization of an optical second with strontium lattice clocks," Nat. Commun. **4**, 2109; "Corrigendum: Experimental realization of an optical second with strontium lattice clocks," **4**, 2782 (2013).

Letokhov, V. S., 1975, "On difference of energy levels of left and right molecules due to weak interactions," Phys. Lett. A **53**, 275.

Levi, F., D. Calonico, C. E. Calosso, A. Godone, S. Micalizio, and G. A. Costanzo, 2014, "Accuracy evaluation of ITCsF2: a nitrogen cooled caesium fountain," Metrologia **51**, 270.

Levshakov, S. A., M. Centurión, P. Molaro, S. D'Odorico, D. Reimers, R. Quast, and M. Pollmann, 2006, "Most precise single redshift bound to $\Delta\alpha/\alpha$," Astron. Astrophys. **449**, 879.

Levshakov, S. A., F. Combes, F. Boone, I. I. Agafonova, D. Reimers, and M. G. Kozlov, 2012, "An upper limit to the variation in the fundamental constants at redshift $z = 5.2$," Astron. Astrophys. **540**, L9.

Levshakov, S. A., M. G. Kozlov, and D. Reimers, 2011, "Methanol as a tracer of fundamental constants," Astrophys. J. **738**, 26.

Levshakov, S. A., A. V. Lapinov, C. Henkel, P. Molaro, D. Reimers, M. G. Kozlov, and I. I. Agafonova, 2010, "Searching for chameleon-like scalar fields with the ammonia method. II. Mapping of cold molecular cores in NH_3 and HC_3N lines," Astron. Astrophys. **524**, A32.

Levshakov, S. A., P. Molaro, M. G. Kozlov, A. V. Lapinov, C. Henkel, D. Reimersi, T. Sakai, and I. I. Agafonova, 2011, "Searching for chameleon-like scalar fields," *From Varying Couplings to Fundamental Physics*, Astrophysics and Space Science Proceedings (Springer, Berlin), p. 103.

Levshakov, S. A., P. Molaro, A. V. Lapinov, D. Reimers, C. Henkel, and T. Sakai, 2010, "Searching for chameleon-like scalar fields with the ammonia method," Astron. Astrophys. **512**, A44.

Levshakov, S. A., P. Molaro, and D. Reimers, 2010, "Searching for spatial variations of α^2/μ in the Milky Way," Astron. Astrophys. **516**, A113.

Levshakov, S. A., D. Reimers, C. Henkel, B. Winkel, A. Mignano, M. Centurión, and P. Molaro, 2013, "Limits on the spatial variations of the electron-to-proton mass ratio in the galactic plane," Astron. Astrophys. **559**, A91.

Levshakov, S. A., D. Reimers, M. G. Kozlov, S. G. Porsev, and P. Molaro, 2008, "A new approach for testing variations of fundamental constants over cosmic epochs using FIR fine-structure lines," Astron. Astrophys. **479**, 719.

Lewenstein, M., A. Sanpera, V. Ahufinger, B. Damski, A. Sen, and U. Sen, 2007, "Ultracold atomic gases in optical lattices: mimicking condensed matter physics and beyond," Adv. Phys. **56**, 243.

Lewis, A. D., D. A. Buote, and J. T. Stocke, 2003, "Chandra observations of a2029: The dark matter profile down to below 0.01 rvir in an unusually relaxed cluster," Astrophys. J. **586**, 135.

Liao, Yi, and Ji-Yuan Liu, 2007, "Long-range electron spin-spin interactions from unparticle exchange," Phys. Rev. Lett. **99**, 191804.

Liberati, S., and L. Maccione, 2009, "Lorentz violation: Motivation and new constraints," Annu. Rev. Nucl. Part. Sci. **59**, 245.

Limes, M. E., D. Sheng, and M. V. Romalis, 2018, "^{3}He-^{129}Xe comagnetometery using ^{87}Rb detection and decoupling," Phys. Rev. Lett. **120**, 033401.

Linde, A. D., 1988, "Inflation and axion cosmology," Phys. Lett. B **201**, 437.

Linder, E. V., 2008, "The dynamics of quintessence, the quintessence of dynamics," Gen. Relativ. Gravit. **40**, 329.

Lintz, M., J. Guena, and M. A. Bouchiat, 2007, "Pump-probe measurement of atomic parity violation in cesium with a precision of 2.6%," Eur. Phys. J. A **32**, 525.

Liu, Yu-Sheng, David McKeen, and Gerald A. Miller, 2016, "Electrophobic scalar boson and muonic puzzles," Phys. Rev. Lett. **117**, 101801.

Lo, Anthony, Philipp Haslinger, Eli Mizrachi, Loïc Anderegg, Holger Müller, Michael Hohensee, Maxim Goryachev, and Michael E Tobar, 2016, "Acoustic tests of Lorentz symmetry using quartz oscillators," Phys. Rev. X **6**, 011018.

Loh, Huanqian, Kevin C. Cossel, M. C. Grau, K.-K. Ni, Edmund R. Meyer, John L. Bohn, Jun Ye, and Eric A. Cornell, 2013, "Precision spectroscopy of polarized molecules in an ion trap," Science **342**, 1220.

Lüders, Gerhart, and Bruno Zumino, 1957, "Some consequences of TCP-invariance," Phys. Rev. **106**, 385.

Ludlow, A. D., M. M. Boyd, J. Ye, E. Peik, and P. O. Schmidt, 2015, "Optical atomic clocks," Rev. Mod. Phys. **87**, 637.

Luo, P., J. Ding, J. Wang, and X. Ren, 2017, "Constraints on spin-dependent exotic interactions between electrons at the nanometer scale," Phys. Rev. D **96**, 055028.

Lykken, J., and S. Nandi, 2000, "Asymmetrical large extra dimensions," Phys. Lett. B **485**, 224.

Mäckel, V., R. Klawitter, G. Brenner, J. R. Crespo López-Urrutia, and J. Ullrich, 2011, "Laser spectroscopy on forbidden transitions in trapped highly charged Ar^{13+} ions," Phys. Rev. Lett. **107**, 143002.

Macpherson, M., K. Zetie, R. B. Warrington, D. N. Stacey, and J. Hoare, 1991, "Precise measurement of parity nonconserving optical rotation at 876 nm in atomic bismuth," Phys. Rev. Lett. **67**, 2784.

Mahoney, C., A. K. Leibovich, and A. R. Zentner, 2017, "Updated constraints on self-interacting dark matter from Supernova 1987A," Phys. Rev. D **96**, 043018.

Mantry, S., M. Pitschmann, and M. J. Ramsey-Musolf, 2014, "Distinguishing axions from generic light scalars using electric dipole moment and fifth-force experiments," Phys. Rev. D **90**, 054016.

Marciano, W. J., 1995, in *Precision Tests of the Standard Electroweak Model*, edited by P. Langacker (World Scientific, Singapore), p. 170.

Marciano, W. J., and A. I. Sanda, 1978, "Parity violation in atoms induced by radiative corrections," Phys. Rev. D **17**, 3055.

Martin, W. C., and W. L. Wiese, 2002, Atomic, Molecular, and Optical Physics Handbook (version 2.2) (online), https://www.nist.gov/pml/atomic-spectroscopy-compendium-basic-ideas-notation-data-and-formulas, National Institute of Standards and Technology, Gaithersburg, MD.

Martins, C. J. A. P., 2015, "Fundamental cosmology in the E-ELT era: the status and future role of tests of fundamental coupling stability," Gen. Relativ. Gravit. **47**, 1843.

Marton, J., *et al.*, 2013, "Testing the Pauli exclusion principle for electrons," J. Phys. Conf. Ser. **447**, 012070.

Marton, J., *et al.*, 2017, "VIP-2 at LNGS: An experiment on the validity of the Pauli exclusion principle for electrons," arXiv:1703.01615.

Massó, E., and J. Redondo, **2005**, "Evading astrophysical constraints on axion-like particles," J. Cosmol. Astropart. Phys. 09, 15.

Masuda, M., and M. Sasaki, 2009, "Limits on nonstandard forces in the submicrometer range," Phys. Rev. Lett. **102**, 171101.

Mathavan, Sreekanth C., Artem Zapara, Quinten Esajas, and Steven Hoekstra, 2016, "Deceleration of a supersonic beam of SrF molecules to 120 ms^{-1}," ChemPhysChem **17**, 3709.

Matloob, R., and H. Falinejad, 2001, "Casimir force between two dielectric slabs," Phys. Rev. A **64**, 042102.

Mattingly, D., 2005, "Modern tests of Lorentz invariance," Living Rev. Relativity **8**, 5.

McGuyer, B. H., M. McDonald, G. Z. Iwata, M. G. Tarallo, A. T. Grier, F. Apfelbeck, and T. Zelevinsky, 2015, "High-precision spectroscopy of ultracold molecules in an optical lattice," New J. Phys. **17**, 055004.

McKellar, Bruce H. J., S. R. Choudhury, Xiao-Gang He, and Sandip Pakvasa, 1987, "The neutron electric dipole moment in the standard KM model," Phys. Lett. B **197**, 556.

Meekhof, D. M., P. A. Vetter, P. K. Majumder, S. K. Lamoreaux, and E. N. Fortson, 1993, "High-precision measurement of parity non-conserving optical rotation in atomic lead," Phys. Rev. Lett. **71**, 3442.

Merlet, S., Q. Bodart, N. Malossi, A. Landragin, F. Pereira Dos Santos, O. Gitlein, and L. Timmen, 2010, "Comparison between two mobile absolute gravimeters: optical versus atomic interferometers," Metrologia **47**, L9.

Meyer, Edmund, and John Bohn, 2008, "Prospects for an electron electric-dipole moment search in metastable ThO and ThF$^+$," Phys. Rev. A **78**, 010502.

Meyer, Edmund, John Bohn, and Michael Deskevich, 2006, "Candidate molecular ions for an electron electric dipole moment experiment," Phys. Rev. A **73**, 062108.

Michelson, Albert A., 1881, "The relative motion of the Earth and the luminiferous ether," Am. J. Sci. **s3-22**, 120.

Michelson, Albert A., and Abraham Morley, 1887, "On the relative motion of the Earth and the luminiferous ether," Am. J. Sci. **s3-34**, 333.

Michishio, K., T. Kanai, S. Kuma, T. Azuma, K. Wada, I. Mochizuki, T. Hyodo, A. Yagishita, and Y. Nagashima, 2016, "Observation of a shape resonance of the positronium negative ion," Nat. Commun. **7**, 11060.

Milgrom, M., 1983, "A modification of the Newtonian dynamics as a possible alternative to the hidden mass hypothesis," Astrophys. J. **270**, 365.

Mills, Allen P., 1981, "Observation of the positronium negative ion," Phys. Rev. Lett. **46**, 717.

Mills, Jr., A. P., 2014, "Optical spectroscopy of atomic and molecular positronium," J. Phys. Conf. Ser. **488**, 012001.

Milstein, A. I., O. P. Sushkov, and I. S. Terekhov, 2002, "Radiative corrections and parity nonconservation in heavy atoms," Phys. Rev. Lett. **89**, 283003.

Milstein, A. I., O. P. Sushkov, and I. S. Terekhov, 2003, "Calculation of radiative corrections to the effect of parity nonconservation in heavy atoms," Phys. Rev. A **67**, 062103.

Miyazaki, A., T. Yamazaki, T. Suehara, T. Namba, S. Asai, T. Kobayashi, H. Saito, Y. Tatematsu, I. Ogawa, and T. Idehara, 2015, "First millimeter-wave spectroscopy of ground-state positronium," Prog. Theor. Exp. Phys. **2015**, 11C01.

Mohr, P. J., D. B. Newell, and B. N. Taylor, 2016, "CODATA recommended values of the fundamental physical constants: 2014," Rev. Mod. Phys. **88**, 035009.

Mohr, P. J., B. N. Taylor, and D. B. Newell, 2012, "CODATA recommended values of the fundamental physical constants: 2010," Rev. Mod. Phys. **84**, 1527.

Moody, J. E., and F. Wilczek, 1984, "New macroscopic forces?," Phys. Rev. D **30**, 130.

Mooser, A., S. Ulmer, K. Blaum, K. Franke, H. Kracke, C. Leiteritz, W. Quint, C. C. Rodegheri, C. Smorra, and J. Walz, 2014, "Direct high-precision measurement of the magnetic moment of the proton," Nature (London) **509**, 596.

Morgan, T. A., and A. Peres, 1962, "Direct test for the strong equivalence principle," Phys. Rev. Lett. **9**, 79.

Mukhamedjanov, T. N., and O. P. Sushkov, 2005, "Suggested search for ^{207}Pb nuclear Schiff moment in PbTiO$_3$ ferroelectric," Phys. Rev. A **72**, 034501.

Müller, H., S.-W. Chiow, S. Herrmann, S. Chu, and K.-Y. Chung, 2008, "Atom-interferometry tests of the isotropy of post-newtonian gravity," Phys. Rev. Lett. **100**, 031101.

Müller, H., A. Peters, and S. Chu, 2010, "A precision measurement of the gravitational redshift by the interference of matter waves," Nature (London) **463**, 926.

Müller, H., P. L. Stanwix, M. E. Tobar, E. Ivanov, P. Wolf, S. Herrmann, A. Senger, E. Kovalchuk, and A. Peters, 2007, "Tests of relativity by complementary rotating Michelson-Morley experiments," Phys. Rev. Lett. **99**, 050401.

Müntinga, H., *et al.*, 2013, "Interferometry with Bose-Einstein Condensates in Microgravity," Phys. Rev. Lett. **110**, 093602.

Murata, J., and S. Tanaka, 2015, "A review of short-range gravity experiments in the LHC era," Classical Quantum Gravity **32**, 033001.

Murphy, M. T., V. V. Flambaum, S. Muller, and C. Henkel, 2008, "Strong limit on a variable proton-to-electron mass ratio from molecules in the distant universe," Science **320**, 1611.

Murphy, M. T., V. V. Flambaum, J. K. Webb, V. A. Dzuba, J. X. Prochaska, and A. M. Wolfe, 2004, "Constraining variations in the fine-structure constant, quark masses and the strong interaction," in *Astrophysics, Clocks and Fundamental Constants*, Lecture Notes in Physics, Vol. 648, edited by S. G. Karshenboim and E. Peik (Springer, Berlin), p. 131.

Murphy, M. T., C. R. Locke, P. S. Light, A. N. Luiten, and J. S. Lawrence, 2012, "Laser frequency comb techniques for precise astronomical spectroscopy," Mon. Not. R. Astron. Soc. **422**, 761.

Murphy, M. T., J. K. Webb, and V. V. Flambaum, 2007, "Comment on "Limits on the time variation of the electromagnetic fine-structure constant in the low energy limit from absorption lines in the spectra of distant quasars"," Phys. Rev. Lett. **99**, 239001.

Murphy, M. T., J. K. Webb, and V. V. Flambaum, 2008a, "Revision of VLT/UVES constraints on a varying fine-structure constant," Mon. Not. R. Astron. Soc. **384**, 1053.

Murphy, M. T., J. K. Webb, and V. V. Flambaum, 2008b, "Revisiting VLT/UVES constraints on a varying fine-structure constant," in *Precision Spectroscopy in Astrophysics*, edited by N. C. Santos, L. Pasquini, A. C. M. Correia, and M. Romaniello (Springer-Verlag, Berlin/Heidelberg), p. 95.

Murphy, M. T., J. K. Webb, V. V. Flambaum, M. J. Drinkwater, F. Combes, and T. Wiklind, 2001a, "Improved constraints on possible variation of physical constants from H I 21-cm and molecular QSO absorption lines," Mon. Not. R. Astron. Soc. **327**, 1244.

Murphy, M. T., J. K. Webb, V. V. Flambaum, J. X. Prochaska, and A. M. Wolfe, 2001b, "Further constraints on variation of the fine-structure constant from alkali-doublet QSO absorption lines," Mon. Not. R. Astron. Soc. **327**, 1237.

Myers, R. C., and M. Pospelov, 2003, "Ultraviolet modifications of dispersion relations in effective field theory," Phys. Rev. Lett. **90**, 211601.

Nagahama, H., *et al.*, 2017, "Sixfold improved single particle measurement of the magnetic moment of the antiproton," Nat. Commun. **8**, 14084.

Nagasawa, M., and M. Kawasaki, 1994, "Collapse of axionic domain wall and axion emission," Phys. Rev. D **50**, 4821.

Nagashima, Y., 2014, "Experiments on positronium negative ions," Phys. Rep. **545**, 95.

Nagel, M., S. R. Parker, E. V. Kovalchuk, P. L. Stanwix, J. G. Hartnett, E. N. Ivanov, A. Peters, and M. E. Tobar, 2015, "Direct terrestrial test of Lorentz symmetry in electrodynamics to 10^{-18}," Nat. Commun. **6**, 8174.

Nakai, Yuichiro, and Matthew Reece, 2016, "Electric dipole moments in natural supersymmetry," arXiv:1612.08090.

Namba, Toshio, 2012, "Precise measurement of positronium," Prog. Theor. Exp. Phys. **2012**, 04D003.

Nanopoulos, D. V., Asim Yildiz, and Paul H. Cox, 1979, "On the electric dipole moment of the neutron," Phys. Lett. B **87**, 53.

Nelson, A. E., and J. Scholtz, 2011, "Dark light, dark matter, and the misalignment mechanism," Phys. Rev. D **84**, 103501.

Nemitz, N., T. Ohkubo, M. Takamoto, I. Ushijima, M. Das, N. Ohmae, and H. Katori, 2016, "Frequency ratio of Yb and Sr clocks with 5×10^{-17} uncertainty at 150 seconds averaging time," Nat. Photonics **10**, 258.

Neronov, Yu. I., and N. N. Seregin, 2015, "Determination of the spin-spin coupling constant of the HD isotopologue of hydrogen for the estimate of existence of nonelectromagnetic spin-dependent interaction," JETP Lett. **100**, 609.

Nesvizhevsky, V. V., G. Pignol, and K. V. Protasov, 2008, "Neutron scattering and extra-short-range interactions," Phys. Rev. D **77**, 034020.

Neville, D. E., 1980, "Experimental bounds on the coupling strength of torsion potentials," Phys. Rev. D **21**, 2075.

Neville, D. E., 1982, "Experimental bounds on the coupling of massless spin-1 torsion," Phys. Rev. D **25**, 573.

Newman, R. D., E. C. Berg, and P. E. Boynton, 2009, "Tests of the gravitational inverse square law at short ranges," Space Sci. Rev. **148**, 175.

Nguyen, A. T., D. Budker, D. DeMille, and M. Zolotorev, 1997, "Search for parity nonconservation in atomic dysprosium," Phys. Rev. A **56**, 3453.

Ni, W. T., T. C. P. Chui, S.-S. Pan, and B.-Y. Cheng, 1994, "Search for anomalous spin-spin interactions between electrons using a dc SQUID," Physica B (Amsterdam) **194**–**196**, 153.

Ni, W.-T., S.-S. Pan, H.-C. Yeh, L.-S. Hou, and J. Wan, 1999, "Search for an axionlike spin coupling using a paramagnetic salt with a dc SQUID," Phys. Rev. Lett. **82**, 2439.

Nicholson, T. L., *et al.*, 2015, "Systematic evaluation of an atomic clock at 2×10^{-18} total uncertainty," Nat. Commun. **6**, 6896.

Nicolis, A., R. Rattazzi, and E. Trincherini, 2009, "Galileon as a local modification of gravity," Phys. Rev. D **79**, 064036.

Nobili, A. M., *et al.*, 2012, "Galileo Galilei (GG): space test of the weak equivalence principle to 10^{-17} and laboratory demonstrations," Classical Quantum Gravity **29**, 184011.

Norrgard, E. B., E. R. Edwards, D. J. McCarron, M. H. Steinecker, D. DeMille, Shah Saad Alam, S. K. Peck, N. S. Wadia, and L. R. Hunter, 2017, "Hyperfine structure of the B$^3\Pi_1$ state and predictions of optical cycling behavior in the X → B transition of TlF," Phys. Rev. A **95**, 062506.

Norrgard, E. B., D. J. McCarron, M. H. Steinecker, M. R. Tarbutt, and D. DeMille, 2016, "Submillikelvin dipolar molecules in a radio-frequency magneto-optical trap," Phys. Rev. Lett. **116**, 063004.

Nörtershäuser, W., *et al.*, 2015, "Precision test of many-body QED in the Be$^+$ 2p fine structure doublet using short-lived isotopes," Phys. Rev. Lett. **115**, 033002.

Nuñez Portela, M., *et al.*, 2013, "Towards a precise measurement of atomic parity violation in a single Ra$^+$ ion," Hyperfine Interact. **214**, 157.

Olive, K. A., M. Peloso, and A. J. Peterson, 2012, "Where are the walls? Spatial variation in the fine-structure constant," Phys. Rev. D **86**, 043501.

Olive, K. A., M. Peloso, and J.-P. Uzan, 2011, "Wall of fundamental constants," Phys. Rev. D **83**, 043509.

Olive, K. A., and M. Pospelov, 2008, "Environmental dependence of masses and coupling constants," Phys. Rev. D **77**, 043524.

Ong, A., J. C. Berengut, and V. V. Flambaum, 2014, "Optical transitions in highly charged ions for detection of variations in the fine-structure constant," in *Fundamental Physics in Particle Traps*, Springer Tracts in Modern Physics, Vol. 256, edited by W. Quint and M. Vogel (Springer, Berlin), p. 293.

Onofrio, R., 2006, "Casimir forces and non-Newtonian gravitation," New J. Phys. **8**, 237.

Onofrio, Roberto, 2013, "Proton radius puzzle and quantum gravity at the Fermi scale," Europhys. Lett. **104**, 20002.

Overduin, J., F. Everitt, P. Worden, and J. Mester, 2012, "Step and fundamental physics," Classical Quantum Gravity **29**, 184012.

Overstreet, C., P. Asenbaum, T. Kovachy, R. Notermans, J. M. Hogan, and M. A. Kasevich, 2018, "Effective inertial frame in an atom interferometric test of the equivalence principle," Phys. Rev. Lett. **120**, 183604.

Pachucki, K., A. Czarnecki, U. D. Jentschura, and V. A. Yerokhin, 2005, "Complete two-loop correction to the bound-electron g factor," Phys. Rev. A **72**, 022108.

Padmanabhan, T., 2003, "Cosmological constant the weight of the vacuum," Phys. Rep. **380**, 235.

Pal, Rupsi, Dansha Jiang, M. S. Safronova, and U. I. Safronova, 2009, "Calculation of parity-nonconserving amplitude and other properties of Ra$^+$," Phys. Rev. A **79**, 062505.

Panda, C. D., *et al.*, 2016, "Stimulated Raman adiabatic passage preparation of a coherent superposition of ThO H$^3\Delta_1$ states for an improved electron electric-dipole-moment measurement," Phys. Rev. A **93**, 052110.

Papapetrou, A., 1949, "Non-symmetric stress-energy-momentum tensor and spin-density," Philos. Mag. Ser. 7 **40**, 937.

Park, Jee Woo, Zoe Z. Yan, Huanqian Loh, Sebastian A. Will, and Martin W. Zwierlein, 2017, "Second-scale nuclear spin coherence time of ultracold ^{23}Na^{40}K molecules," Science **357**, 372.

Parthey, C. G., *et al.*, 2011, "Precision spectroscopy on atomic hydrogen," in *Society of Photo-Optical Instrumentation Engineers (SPIE) Conference Series*, SPIE Proceedings Vol. 8132 (SPIE–International Society for Optical Engineering, Belling, WA), p. 813202.

Pašteka, L. F., A. Borschevsky, V. V. Flambaum, and P. Schwerdtfeger, 2015, "Search for the variation of fundamental constants: Strong enhancements in X$^2\Pi$ cations of dihalogens and hydrogen halides," Phys. Rev. A **92**, 012103.

Patrignani, C., *et al.* (Particle Data Group), 2016, "The review of particle physics," Chin. Phys. C **40**, 100001 [http://pdg.lbl.gov].

Pauli, W., 1924, "Zur Frage der theoretischen Deutung der Satelliten einiger Spektrallinien und ihrer Beeinflussung durch magnetische Felder," Naturwissenschaften **12**, 741.

Peccei, R., 2008, "The strong *CP* problem and axions," Lect. Notes Phys. **741**, 3.

Peccei, R., and H. Quinn, 1977a, "Constraints imposed by *CP* conservation in the presence of pseudoparticles," Phys. Rev. D **16**, 1791.

Peccei, R. D., and Helen R Quinn, 1977b, "*CP* conservation in the presence of pseudoparticles," Phys. Rev. Lett. **38**, 1440.

Peck, S. K., D. K. Kim, D. Stein, D. Orbaker, A. Foss, M. T. Hummon, and L. R. Hunter, 2012, "Limits on local Lorentz invariance in mercury and cesium," Phys. Rev. A **86**, 012109.

Peck, S. K., N. Lane, D. G. Ang, and L. R. Hunter, 2016, "Using tensor light shifts to measure and cancel a cell's quadrupolar frequency shift," Phys. Rev. A **93**, 023426.

Peebles, P. J. E., and B. Ratra, 2003, "The cosmological constant and dark energy," Rev. Mod. Phys. **75**, 559.

Peik, E., and M. Okhapkin, 2015, "Nuclear clocks based on resonant excitation of γ-transitions," C.R. Phys. **16**, 516.

Peik, E., and C. Tamm, 2003, "Nuclear laser spectroscopy of the 3.5 eV transition in ^{229}Th," Europhys. Lett. **61**, 181.

Peil, S., S. Crane, J. L. Hanssen, T. B. Swanson, and C. R. Ekstrom, 2013, "Tests of local position invariance using continuously running atomic clocks," Phys. Rev. A **87**, 010102.

Pelle, B., A. Hilico, G. Tackmann, Q. Beaufils, and F. Pereira dos Santos, 2013, "State-labeling Wannier-Stark atomic interferometers," Phys. Rev. A **87**, 023601.

Pendlebury, J. M., *et al.*, 2015, "Revised experimental upper limit on the electric dipole moment of the neutron," Phys. Rev. D **92**, 092003.

Peres, A., 1978, "Test of equivalence principle for particles with spin," Phys. Rev. D **18**, 2739.

Pérez, P., *et al.*, 2015, "The GBAR antimatter gravity experiment," Hyperfine Interact. **233**, 21.

Perlmutter, S., 2012, "Nobel Lecture: Measuring the acceleration of the cosmic expansion using supernovae," Rev. Mod. Phys. **84**, 1127.

Perlmutter, S., *et al.*, 1999, "Measurements of ω and λ from 42 high-redshift supernovae," Astrophys. J. **517**, 565.

Peskin, Michael E., and Daniel V. Schroeder, 1995, *An introduction to Quantum Field Theory* (Perseus Books, Reading, MA).

Peters, Achim, Keng Yeow Chung, and Steven Chu, 1999, "Measurement of gravitational acceleration by dropping atoms," Nature (London) **400**, 849.

Petrov, A. N., N. S. Mosyagin, T. A. Isaev, and A. V. Titov, 2007, "Theoretical study of hff$^+$ in search of the electron electric dipole moment," Phys. Rev. A **76**, 030501.

Petukhov, A. K., G. Pignol, D. Jullien, and K. H. Andersen, 2010, "Polarized ^{3}He as a probe for short-range spin-dependent interactions," Phys. Rev. Lett. **105**, 170401.

Phillips, W. D., 1998, "Nobel lecture: Laser cooling and trapping of neutral atoms," Rev. Mod. Phys. **70**, 721.

Phipp, S. J., N. H. Edwards, P. E. G. Baird, and S. Nakayama, 1996, "A measurement of parity non-conserving optical rotation in atomic lead," J. Phys. B **29**, 1861.

Piegsa, F. M., and G. Pignol, 2012, "Limits on the axial coupling constant of new light bosons," Phys. Rev. Lett. **108**, 181801.

Pihan-Le Bars, H., C. Guerlin, R.-D. Lasseri, J.-P. Ebran, Q. G. Bailey, S. Bize, E. Khan, and P. Wolf, 2017, "Lorentz-symmetry

test at Planck-scale suppression with nucleons in a spin-polarized ^{133}Cs cold atom clock," Phys. Rev. D **95**, 075026.

Pilipenko, S. V., 2013, "Paper-and-pencil cosmological calculator," arXiv:1303.5961.

Pohl, Randolf, 2016, "Laser spectroscopy of muonic hydrogen and the puzzling proton," J. Phys. Soc. Jpn. **85**, 091003.

Pohl, Randolf, Ronald Gilman, Gerald A. Miller, and Krzysztof Pachucki, 2013, "Muonic hydrogen and the proton radius puzzle," Annu. Rev. Nucl. Part. Sci. **63**, 175.

Pohl, Randolf, *et al.*, 2010, "The size of the proton," Nature (London) **466**, 213.

Pohl, Randolf, *et al.*, 2016, "Laser spectroscopy of muonic deuterium," Science **353**, 669.

Pokotilovski, Yu. N., 2006, "Constraints on new interactions from neutron scattering experiments," Phys. At. Nucl. **69**, 924.

Poli, N., C. W. Oates, P. Gill, and G. M. Tino, 2013, "Optical atomic clocks," Nuovo Cimento Rivista Serie **36**, 555.

Poli, N., F.-Y. Wang, M. G. Tarallo, A. Alberti, M. Prevedelli, and G. M. Tino, 2011, "Precision measurement of gravity with cold atoms in an optical lattice and comparison with a classical gravimeter," Phys. Rev. Lett. **106**, 038501.

Pollock, S. J., and M. C. Welliver, 1999, "Effects of neutron spatial distributions on atomic parity nonconservation in cesium," Phys. Lett. B **464**, 177.

Porsev, S. G., K. Beloy, and A. Derevianko, 2009, "Precision determination of electroweak coupling from atomic parity violation and implications for particle physics," Phys. Rev. Lett. **102**, 181601.

Porsev, S. G., K. Beloy, and A. Derevianko, 2010, "Precision determination of weak charge of ^{133}Cs from atomic parity violation," Phys. Rev. D **82**, 036008.

Porsev, S. G., K. V. Koshelev, I. I. Tupitsyn, M. G. Kozlov, D. Reimers, and S. A. Levshakov, 2007, "Transition frequency shifts with fine-structure-constant variation for Fe II: Breit and core-valence correlation corrections," Phys. Rev. A **76**, 052507.

Pospelov, M., S. Pustelny, M. P. Ledbetter, D. F. Jackson Kimball, W. Gawlik, and D. Budker, 2013, "Detecting domain walls of axionlike models using terrestrial experiments," Phys. Rev. Lett. **110**, 021803.

Pospelov, M., A. Ritz, and M. Voloshin, 2008, "Bosonic super-WIMPs as keV-scale dark matter," Phys. Rev. D **78**, 115012.

Pospelov, Maxim, 2009, "Secluded U(1) below the weak scale," Phys. Rev. D **80**, 095002.

Pospelov, Maxim, and Adam Ritz, 2005, "Electric dipole moments as probes of new physics," Ann. Phys. (Amsterdam) **318**, 119.

Pospelov, Maxim, and Adam Ritz, 2014, "CKM benchmarks for electron electric dipole moment experiments," Phys. Rev. D **89**, 056006.

Pospelov, Maxim, and Michael Romalis, 2004, "Lorentz invariance on trial," Phys. Today **57**, 40.

Prehn, Alexander, Martin Ibrügger, Rosa Glöckner, Gerhard Rempe, and Martin Zeppenfeld, 2016, "Optoelectrical cooling of polar molecules to submillikelvin temperatures," Phys. Rev. Lett. **116**, 063005.

Prescott, C. Y., *et al.*, 1978, "Parity non-conservation in inelastic electron scattering," Phys. Lett. B **77**, 347.

Preskill, J., M. B. Wise, and F. Wilczek, 1983, "Cosmology of the invisible axion," Phys. Lett. B **120**, 127.

Primakoff, H., 1951, "Photo-production of neutral mesons in nuclear electric fields and the mean life of the neutral meson," Phys. Rev. **81**, 899.

Pruttivarasin, T., M. Ramm, S. G. Porsev, I. I. Tupitsyn, M. S. Safronova, M. A. Hohensee, and H. Häffner, 2015, "Michelson-Morley analogue for electrons using trapped ions to test Lorentz symmetry," Nature (London) **517**, 592.

Puchalski, M., and K. Pachucki, 2014, "Quantum electrodynamics corrections to the 2P fine splitting in Li," Phys. Rev. Lett. **113**, 073004.

Purcell, E. M., and N. F. Ramsey, 1950, "On the possibility of electric dipole moments for elementary particles and nuclei," Phys. Rev. **78**, 807.

Pustelny, S., *et al.*, 2013, "The global network of optical magnetometers for exotic physics (GNOME): A novel scheme to search for physics beyond the standard model," Ann. Phys. (Berlin) **525**, 659.

Quintero-Pérez, M., T. E. Wall, S. Hoekstra, and H. L. Bethlem, 2014, "Preparation of an ultra-cold sample of ammonia molecules for precision measurements," J. Mol. Spectrosc. **300**, 112.

Rabey, I., J. Devlin, B. Sauer, J. Hudson, M. Tarbutt, and E. Hinds, 2016, "Sensitivity improvements to the YbF electron electric dipole moment experiment," in *APS Meeting Abstracts*.

Radžiūtė, Laima, Gediminas Gaigalas, Per Jönsson, and Jacek Bieroń, 2014, "Multiconfiguration Dirac-Hartree-Fock calculations of atomic electric dipole moments of ^{225}Ra, ^{199}Hg, and ^{171}Yb," Phys. Rev. A **90**, 012528.

Raffelt, G., 2012, "Limits on a *CP*-violating scalar axion-nucleon interaction," Phys. Rev. D **86**, 015001.

Raffelt, G., and D. Seckel, 1988, "Bounds on exotic-particle interactions from SN1987A," Phys. Rev. Lett. **60**, 1793.

Raffelt, G., and A. Weiss, 1995, "Red giant bound on the axion-electron coupling reexamined," Phys. Rev. D **51**, 1495.

Raffelt, G. G., 1999, "Particle physics from stars," Annu. Rev. Nucl. Part. Sci. **49**, 163.

Rahmani, H., R. Srianand, N. Gupta, P. Petitjean, P. Noterdaeme, and D. A. Vásquez, 2012, "Constraining the variation of fundamental constants at $z \approx 1.3$ using 21-cm absorbers," Mon. Not. R. Astron. Soc. **425**, 556.

Ramsey, N. F., 1979, "The tensor force between two protons at long range," Physica A (Amsterdam) **96**, 285.

Ramsey-Musolf, M. J., 1999, "Low-energy parity-violation and new physics," Phys. Rev. C **60**, 015501.

Ramsey-Musolf, Michael J., and Shelley A. Page, 2006, "Hadronic parity violation: A new view through the looking glass," Annu. Rev. Nucl. Part. Sci. **56**, 1.

Randall, L., and R. Sundrum, 1999a, "An alternative to compactification," Phys. Rev. Lett. **83**, 4690.

Randall, L., and R. Sundrum, 1999b, "Large mass hierarchy from a small extra dimension," Phys. Rev. Lett. **83**, 3370.

Reasenberg, R. D., B. R. Patla, J. D. Phillips, and R. Thapa, 2012, "Design and characteristics of a WEP test in a sounding-rocket payload," Classical Quantum Gravity **29**, 184013.

Redondo, J., and A. Ringwald, 2011, "Light shining through walls," Contemp. Phys. **52**, 211.

Refregier, A., 2003, "Weak gravitational lensing by large-scale structure," Annu. Rev. Astron. Astrophys. **41**, 645.

Regan, B., Eugene Commins, Christian Schmidt, and David DeMille, 2002, "New limit on the electron electric dipole moment," Phys. Rev. Lett. **88**, 071805.

Riess, A. G., 2012, "Nobel lecture: My path to the accelerating universe," Rev. Mod. Phys. **84**, 1165.

Riess, A. G., *et al.*, 1998, "Observational evidence from supernovae for an accelerating universe and a cosmological constant," Astron. J. **116**, 1009.

Ritter, R. C., C. E. Goldblum, W.-T. Ni, G. T. Gillies, and C. C. Speake, 1990, "Experimental test of equivalence principle with polarized masses," Phys. Rev. D **42**, 977.

Roberts, B. M., G. Blewitt, C. Dailey, M. Murphy, M. Pospelov, A. Rollings, J. Sherman, W. Williams, and A. Derevianko, 2017, "Search for domain wall dark matter with atomic clocks on board global positioning system satellites," Nat. Commun. **8**, 1195.

Roberts, B. M., V. A. Dzuba, and V. V. Flambaum, 2015, "Parity and time-reversal violation in atomic systems," Annu. Rev. Nucl. Part. Sci. **65**, 63.

Roberts, B. M., Y. V. Stadnik, V. A. Dzuba, V. V. Flambaum, N. Leefer, and D. Budker, 2014a, "Limiting P-odd interactions of cosmic fields with electrons, protons, and neutrons," Phys. Rev. Lett. **113**, 081601.

Roberts, B. M., Y. V. Stadnik, V. A. Dzuba, V. V. Flambaum, N. Leefer, and D. Budker, 2014b, "Parity-violating interactions of cosmic fields with atoms, molecules, and nuclei: Concepts and calculations for laboratory searches and extracting limits," Phys. Rev. D **90**, 096005.

Robilliard, C., R. Battesti, M. Fouche, J. Mauchain, A.-M. Sautivet, F. Amiranoff, and C. Rizzo, 2007, "No light shining through a wall: Results from a photoregeneration experiment," Phys. Rev. Lett. **99**, 190403.

Romalis, M. V., and R. R. Caldwell, 2013, "Laboratory search for a quintessence field," arXiv:1302.1579.

Romalis, Michael V., Dong Sheng, Brian Saam, and Thad G. Walker, 2014, "Comment on "new limit on lorentz-invariance- and *CPT*-violating neutron spin interactions using a free-spin-precession $^3\mathrm{He} - ^{129}\mathrm{Xe}$ comagnetometer"," Phys. Rev. Lett. **113**, 188901.

Rosenband, T., *et al.*, 2008, "Frequency ratio of Al$^+$ and Hg$^+$ single-ion optical clocks; metrology at the 17th decimal place," Science **319**, 1808.

Rosenberry, M., and T. Chupp, 2001, "Atomic electric dipole moment measurement using spin exchange pumped masers of $^{129}\mathrm{Xe}$ and $^3\mathrm{He}$," Phys. Rev. Lett. **86**, 22.

Rosi, G., 2016, "Challenging the "Big G" measurement with atoms and light," J. Phys. B **49**, 202002.

Rosi, G., 2018, "A proposed atom interferometry determination of G at 10^{-5} using a cold atomic fountain," Metrologia **55**, 50.

Rosi, G., L. Cacciapuoti, F. Sorrentino, M. Menchetti, M. Prevedelli, and G. M. Tino, 2015, "Measurement of the gravity-field curvature by atom interferometry," Phys. Rev. Lett. **114**, 013001.

Rosi, G., G. D'Amico, L. Cacciapuoti, F. Sorrentino, M. Prevedelli, M. Zych, Č. Brukner, and G. M. Tino, 2017, "Quantum test of the equivalence principle for atoms in coherent superposition of internal energy states," Nat. Commun. **8**, 15529.

Rosi, G., F. Sorrentino, L. Cacciapuoti, M. Prevedelli, and G. M. Tino, 2014, "Precision measurement of the Newtonian gravitational constant using cold atoms," Nature (London) **510**, 518.

Rosner, J. L., 1999, "Atomic parity violation and precision electroweak physics—An updated analysis," Phys. Rev. D **61**, 016006.

Rosner, Jonathan L., 2002, "Role of present and future atomic parity violation experiments in precision electroweak tests," Phys. Rev. D **65**, 073026.

Rothleitner, G. C., and S. Schlamminger, 2017, "Measurements of the Newtonian constant of gravitation," Rev. Sci. Instrum. **88**, 111101.

Roura, A., 2017, "Circumventing Heisenberg's uncertainty principle in atom interferometry tests of the equivalence principle," Phys. Rev. Lett. **118**, 160401.

Rouven, Essig, *et al.*, 2013, "Working Group Report: New Light Weakly Coupled Particles," Tech. Rep., arXiv:1311.0029.

Rubin, V. C., and W. K. Ford, Jr., 1970, "Rotation of the andromeda nebula from a spectroscopic survey of emission regions," Astrophys. J. **159**, 379.

Rubin, V. C., W. K. Ford, Jr., and N. Thonnard, 1980, "Rotational properties of 21 SC galaxies with a large range of luminosities and radii, from $\mathrm{NGC\,4605/R} = 4\,\mathrm{kpc}/\mathrm{to\,UGC\,2885/R} = 122\,\mathrm{kpc}$," Astrophys. J. **238**, 471.

Rudolph, J. K., *et al.*, 2013, "X-ray resonant photoexcitation: Linewidths and energies of Kα transitions in highly charged Fe ions," Phys. Rev. Lett. **111**, 103002.

Ruoso, G., A. Lombardi, A. Ortolan, R. Pengo, C. Braggio, G. Carugno, C. S. Gallo, and C. C. Speake, 2016, "The QUAX proposal: a search of galactic axion with magnetic materials," J. Phys. Conf. Ser. **718**, 042051.

Safronova, M. S., 2014, "Time Trials for Fundamental Constants," Physics Online Journal **7**, 117.

Safronova, M. S., V. A. Dzuba, V. V. Flambaum, U. I. Safronova, S. G. Porsev, and M. G. Kozlov, 2014a, "Atomic properties of Cd-like and Sn-like ions for the development of frequency standards and search for the variation of the fine-structure constant," Phys. Rev. A **90**, 052509.

Safronova, M. S., V. A. Dzuba, V. V. Flambaum, U. I. Safronova, S. G. Porsev, and M. G. Kozlov, 2014b, "Highly charged ions for atomic clocks, quantum information, and search for α variation," Phys. Rev. Lett. **113**, 030801.

Safronova, M. S., V. A. Dzuba, V. V. Flambaum, U. I. Safronova, S. G. Porsev, and M. G. Kozlov, 2014c, "Study of highly-charged Ag-like and In-like ions for the development of atomic clocks and search for α-variation," Phys. Rev. A **90**, 042513.

Safronova, M. S., and W. R. Johnson, 2000, "High-precision calculation of the parity-nonconserving amplitude in francium," Phys. Rev. A **62**, 022112.

Sahoo, B. K., 2010, "*Ab initio* studies of electron correlation effects in the atomic parity violating amplitudes in Cs and Fr," J. Phys. B **43**, 085005.

Sainis, S., J. Sage, E. Tiesinga, S. Kotochigova, T. Bergeman, and D. DeMille, 2012, "Detailed spectroscopy of the $\mathrm{Cs}_2 a^3\Sigma_u^+$ state and implications for measurements sensitive to variation of the electron-proton mass ratio," Phys. Rev. A **86**, 022513.

Sakharov, A. D., 1967, "Violation of *CP* invariance, C asymmetry, and baryon asymmetry of the universe," ZhETF Pis'ma **5**, 32 [JETP Lett. **5**, 24 (1967)].

Sakurai, J. J., and J. J. Napolitano, 2011, *Modern Quantum Mechanics* (Addison Wesley, Boston), 2nd ed.

Salucci, P., and A. Borriello, 2003, "The intriguing distribution of dark matter in galaxies," in *Particle Physics in the New Millennium* (Springer, New York), p. 66.

Salumbides, E. J., G. D. Dickenson, T. I. Ivanov, and W. Ubachs, 2011, "QED effects in molecules: Test on rotational quantum states of H$_2$," Phys. Rev. Lett. **107**, 043005.

Salumbides, E. J., A. N. Schellekens, B. Gato-Rivera, and W. Ubachs, 2015, "Constraints on extra dimensions from precision molecular spectroscopy," New J. Phys. **17**, 033015.

Sandars, P. G. H., 1965, "The electric dipole moment of an atom," Phys. Lett. **14**, 194.

Sandars, P. G. H., 1966, "Enhancement factor for the electric dipole moment of the valence electron in an alkali atom," Phys. Lett. **22**, 290.

Sandars, P. G. H., 1967, "Measurability of the proton electric dipole moment," Phys. Rev. Lett. **19**, 1396.

Santamaria, L., V. Di Sarno, I. Ricciardi, S. Mosca, M. De Rosa, G. Santambrogio, P. Maddaloni, and P. De Natale, 2014, "Assessing the time constancy of the proton-to-electron mass ratio by precision

ro-vibrational spectroscopy of a cold molecular beam," J. Mol. Spectrosc. **300**, 116.

Sapirstein, J., K. Pachucki, A. Veitia, and K. T. Cheng, 2003, "Radiative corrections to parity-nonconserving transitions in atoms," Phys. Rev. A **67**, 052110.

Sathyaprakash, B., *et al.*, 2012, "Scientific objectives of Einstein telescope," Classical Quantum Gravity **29**, 124013.

Sato, T., *et al.*, 2015, "EDM measurement in ^{129}Xe atom using dual active feedback nuclear spin maser," Hyperfine Interact. **230**, 147.

Saulson, P. R., 1984, "Terrestrial gravitational noise on a gravitational wave antenna," Phys. Rev. D **30**, 732.

Schabinger, B., S. Sturm, A. Wagner, J. Alonso, W. Quint, G. Werth, and K. Blaum, 2012, "Experimental g factor of hydrogenlike silicon-28," Eur. Phys. J. D **66**, 71.

Schellekens, A. N., 2013, "Life at the interface of particle physics and string theory," Rev. Mod. Phys. **85**, 1491.

Scherk, J., 1979, "Antigravity: a crazy idea?," Phys. Lett. B **88**, 265.

Schiff, L. I., 1963, "Measurability of nuclear electric dipole moments," Phys. Rev. **132**, 2194.

Schiller, S., 2007, "Hydrogenlike highly charged ions for tests of the time independence of fundamental constants," Phys. Rev. Lett. **98**, 180801.

Schiller, S., D. Bakalov, and V. I. Korobov, 2014, "Simplest molecules as candidates for precise optical clocks," Phys. Rev. Lett. **113**, 023004.

Schiller, S., *et al.*, 2009, "Einstein Gravity Explorer—a medium-class fundamental physics mission," Exp. Astron. **23**, 573.

Schlamminger, S., 2014, "Fundamental constants: A cool way to measure big G," Nature (London) **510**, 478.

Schlamminger, S., K.-Y. Choi, T. A. Wagner, J. H. Gundlach, and E. G. Adelberger, 2008, "Test of the equivalence principle using a rotating torsion balance," Phys. Rev. Lett. **100**, 041101.

Schlamminger, S., J. H. Gundlach, and R. D. Newman, 2015, "Recent measurements of the gravitational constant as a function of time," Phys. Rev. D **91**, 121101.

Schlippert, D., J. Hartwig, H. Albers, L. L. Richardson, C. Schubert, A. Roura, W. P. Schleich, W. Ertmer, and E. M. Rasel, 2014, "Quantum test of the universality of free fall," Phys. Rev. Lett. **112**, 203002.

Schmidt, B. P., 2012, "Nobel lecture: Accelerating expansion of the universe through observations of distant supernovae," Rev. Mod. Phys. **84**, 1151.

Schmidt, T., 1937, "Über die magnetischen momente der atomkerne," Z. Phys. **106**, 358.

Schmöger, L., *et al.*, 2015, "Coulomb crystallization of highly charged ions," Science **347**, 1233.

Schneider, G., *et al.*, 2017, "Double-trap measurement of the proton magnetic moment at 0.3 parts per billion precision," Science **358**, 1081.

Schutte, C. J. H., J. E. Bertie, P. R. Bunker, J. T. Hougen, I. M. Mills, J. K. G. Watson, and B. P. Winnewisser, 1997a, "Notations and conventions in molecular spectroscopy: Part 1. General spectroscopic notation (IUPAC Recommendations 1997)," Pure Appl. Chem. **69**, 1633.

Schutte, C. J. H., J. E. Bertie, P. R. Bunker, J. T. Hougen, I. M. Mills, J. K. G. Watson, and B. P. Winnewisser, 1997b, "Notations and conventions in molecular spectroscopy: Part 2. Symmetry notation (IUPAC Recommendations 1997)," Pure Appl. Chem. **69**, 1641.

Scott, D., 2006, "The standard cosmological model," Can. J. Phys. **84**, 419.

Seidel, S. T., M. D. Lachmann, D. Becker, J. Grosse, M. A. Popp, J. B. Wang, T. Wendrich, and E. M. Rasel, 2015, "Atom interferometry on sounding rockets," European Rocket and Balloon: Programmes and Related research, ESA Special Publications **730**, 309.

Seiferle, B., L. von der Wense, and P. G. Thirolf, 2017, "Lifetime measurement of the ^{229}Th nuclear isomer," Phys. Rev. Lett. **118**, 042501.

Semertzidis, Y., 2017, "The axion dark matter search at CAPP: a comprehensive approach," in *APS April Meeting Abstracts*.

Shabaev, V. M., A. N. Artemyev, V. A. Yerokhin, O. M. Zherebtsov, and G. Soff, 2001, "Towards a test of QED in investigations of the hyperfine splitting in heavy ions," Phys. Rev. Lett. **86**, 3959.

Shabaev, V. M., D. A. Glazov, N. S. Oreshkina, A. V. Volotka, G. Plunien, H.-J. Kluge, and W. Quint, 2006, "g-factor of heavy ions: A new access to the fine structure constant," Phys. Rev. Lett. **96**, 253002.

Shabaev, V. M., D. A. Glazov, G. Plunien, and A. V. Volotka, 2015, "Theory of bound-electron g factor in highly charged ions," J. Phys. Chem. Ref. Data **44**, 031205.

Shabaev, V. M., D. A. Glazov, M. B. Shabaeva, V. A. Yerokhin, G. Plunien, and G. Soff, 2002, "g factor of high-Z lithiumlike ions," Phys. Rev. A **65**, 062104.

Shabaev, V. M., K. Pachucki, I. I. Tupitsyn, and V. A. Yerokhin, 2005, "QED corrections to the parity-nonconserving $6S - 7S$ amplitude in ^{133}Cs," Phys. Rev. Lett. **94**, 213002.

Shabalin, E. P., 1978, "Electric dipole moment of the quark in a gauge theory with left handed-fermions," Yad. Fiz. **28**, 151 [Sov. J. Nucl. Phys. **28**, 75 (1978)].

Shaniv, R., R. Ozeri, M. S. Safronova, S. G. Porsev, V. A. Dzuba, V. V. Flambaum, and H. Häffner, 2018, "New ideas for tests of Lorentz invariance with atomic systems," Phys. Rev. Lett. **120**, 103202.

Shelkovnikov, A., R. J. Butcher, C. Chardonnet, and A. Amy-Klein, 2008, "Stability of the proton-to-electron mass ratio," Phys. Rev. Lett. **100**, 150801.

Shi, H., *et al.*, 2016, "Searches for the violation of Pauli exclusion principle at LNGS in VIP(-2) experiment," J. Phys. Conf. Ser. **718**, 042055.

Shifman, M., A. Vainshtein, and V. Zakharov, 1980, "Can confinement ensure natural *CP* invariance of strong interactions?," Nucl. Phys. B **166**, 493.

Sigurdson, K., A. Kurylov, and M. Kamionkowski, 2003, "Spatial variation of the fine-structure parameter and the cosmic microwave background," Phys. Rev. D **68**, 103509.

Sikivie, P., 1983, "Experimental tests of the "invisible" axion," Phys. Rev. Lett. **51**, 1415.

Sikivie, P., 1985, "Detection rates for "invisible"-axion searches," Phys. Rev. D **32**, 2988.

Sikivie, P., 2014, "Axion dark matter detection using atomic transitions," Phys. Rev. Lett. **113**, 201301.

Sikivie, P., N. Sullivan, and D. B. Tanner, 2014, "Proposal for axion dark matter detection using an LC circuit," Phys. Rev. Lett. **112**, 131301.

Sikivie, Pierre, 2012, "The strong *CP* problem," C.R. Phys. **13**, 176.

Singh, Yashpal, and B. K. Sahoo, 2015, "Rigorous limits on the hadronic and semileptonic *CP*-violating coupling constants from the electric dipole moment of ^{199}Hg," Phys. Rev. A **91**, 030501.

Skripnikov, L. V., 2016, "Combined 4-component and relativistic pseudopotential study of ThO for the electron electric dipole moment search," J. Chem. Phys. **145**, 214301.

Skripnikov, L. V., 2017, "Communication: Theoretical study of HfF$^+$ cation to search for the T,P-odd interactions," J. Chem. Phys. **147**, 021101.

Skripnikov, L. V., A. N. Petrov, and A. V. Titov, 2013, "Communication: Theoretical study of ThO for the electron electric dipole moment search," J. Chem. Phys. **139**, 221103.

Smiciklas, M., J. M. Brown, L. W. Cheuk, S. J. Smullin, and M. V. Romalis, 2011, "New test of local Lorentz invariance using a ^{21}Ne-Rb-K comagnetometer," Phys. Rev. Lett. **107**, 171604.

Smorra, C., *et al.*, 2015, "BASE—the baryon antibaryon symmetry experiment," Eur. Phys. J. Spec. Top. **224**, 3055.

Smorra, C., *et al.*, 2017, "A parts-per-billion measurement of the antiproton magnetic moment," Nature (London) **550**, 371.

Solà, J., 2013, "Cosmological constant and vacuum energy: old and new ideas," J. Phys. Conf. Ser. **453**, 012015.

Sondag, A., and H. Dittus, 2016, "Electrostatic positioning system for a free fall test at drop tower Bremen and an overview of tests for the weak equivalence principle in past, present and future," Adv. Space Res. **58**, 644.

Sorrentino, F., A. Alberti, G. Ferrari, V. V. Ivanov, N. Poli, M. Schioppo, and G. M. Tino, 2009, "Quantum sensor for atom-surface interactions below 10 μm," Phys. Rev. A **79**, 013409.

Srianand, R., H. Chand, P. Petitjean, and B. Aracil, 2004, "Limits on the time variation of the electromagnetic fine-structure constant in the low energy limit from absorption lines in the spectra of distant quasars," Phys. Rev. Lett. **92**, 121302.

Srianand, R., H. Chand, P. Petitjean, and B. Aracil, 2007, "Reply to the comment by M. T. Murphy, J. K. Webb, and V. V. Flambaum," Phys. Rev. Lett. **99**, 239002.

Stadnik, Y. V., V. A. Dzuba, and V. V. Flambaum, 2018, "Improved limits on axion-like-particle-mediated P, T-violating interactions between electrons and nucleons from electric dipole moments of atoms and molecules," Phys. Rev. Lett. **120**, 013202.

Stadnik, Y. V., and V. V. Flambaum, 2014a, "Axion-induced effects in atoms, molecules, and nuclei: Parity nonconservation, anapole moments, electric dipole moments, and spin-gravity and spin-axion momentum couplings," Phys. Rev. D **89**, 043522.

Stadnik, Y. V., and V. V. Flambaum, 2014b, "Searching for topological defect dark matter via nongravitational signatures," Phys. Rev. Lett. **113**, 151301.

Stadnik, Y. V., and V. V. Flambaum, 2015a, "Nuclear spin-dependent interactions: searches for WIMP, axion and topological defect dark matter, and tests of fundamental symmetries," Eur. Phys. J. C **75**, 110.

Stadnik, Y. V., and V. V. Flambaum, 2015b, "Searching for dark matter and variation of fundamental constants with laser and maser interferometry," Phys. Rev. Lett. **114**, 161301.

Stadnik, Y. V., and V. V. Flambaum, 2016, "Enhanced effects of variation of the fundamental constants in laser interferometers and application to dark-matter detection," Phys. Rev. A **93**, 063630.

Stadnik, Yevgeny V., and Victor V. Flambaum, 2014c, "New atomic probes for dark matter detection: Axions, axion-like particles and topological defects," Mod. Phys. Lett. A **29**, 1440007.

Stamper-Kurn, D. M., and M. Ueda, 2013, "Spinor Bose gases: Symmetries, magnetism, and quantum dynamics," Rev. Mod. Phys. **85**, 1191.

Streater, R. F., and A. S. Wightman, 2000, *PCT, Spin and Statistics, and All That* (Princeton University, Princeton, NJ).

Stueckelberg, E. C. G., 1948, "A possible new type of spin-spin interaction," Phys. Rev. **73**, 808.

Sturm, S., F. Köhler, J. Zatorski, A. Wagner, Z. Harman, G. Werth, W. Quint, C. H. Keitel, and K. Blaum, 2014, "High-precision measurement of the atomic mass of the electron," Nature (London) **506**, 467.

Sturm, S., M. Vogel, F. Köhler-Langes, W. Quint, K. Blaum, and G. Werth, 2017, "High-precision measurements of the bound electron's magnetic moment," Atoms **5**, 4.

Sturm, S., A. Wagner, M. Kretzschmar, W. Quint, G. Werth, and K. Blaum, 2013, "g-factor measurement of hydrogenlike ^{28}Si^{13+} as a challenge to QED calculations," Phys. Rev. A **87**, 030501.

Sturm, S., A. Wagner, B. Schabinger, J. Zatorski, Z. Harman, W. Quint, G. Werth, C. H. Keitel, and K. Blaum, 2011, "g factor of hydrogenlike ^{28}Si^{13+}," Phys. Rev. Lett. **107**, 023002.

Sturm, S., G. Werth, and K. Blaum, 2013, "Electron g-factor determinations in Penning traps," Ann. Phys. (Berlin) **525**, 620.

Sundrum, R., **1999**, "Towards an effective particle-string resolution of the cosmological constant problem," J. High Energy Phys. 07, 001.

Sushkov, A. O., W. J. Kim, D. A. R. Dalvit, and S. K. Lamoreaux, 2011a, "New experimental limits on non-Newtonian forces in the micrometer range," Phys. Rev. Lett. **107**, 171101.

Sushkov, A. O., W. J. Kim, D. A. R. Dalvit, and S. K. Lamoreaux, 2011b, "Observation of the thermal Casimir force," Nat. Phys. **7**, 230.

Sushkov, O. P., 2001, "Breit-interaction correction to the hyperfine constant of an external s electron in a many-electron atom," Phys. Rev. A **63**, 042504.

Sushkov, O. P., and V. V. Flambaum, 1978, "Parity breaking effects in diatomic molecules," ZhEFT **75**, 1208 [Sov. Phys. JETP **48**, 608 (1978)].

Sushkov, O. P., V. V. Flambaum, and I. B. Khriplovich, 1984, "Possibility of investigating P- and T-odd nuclear forces in atomic and molecular experiments," ZhETF **87**, 1521 [Sov. Phys. JETP **60**, 873 (1984)].

Svrcek, P., and E. Witten, **2006**, "Axions in string theory," J. High Energy Phys. 06, 051.

Swallows, M. D., T. H. Loftus, W. C. Griffith, B. R. Heckel, E. N. Fortson, and M. V. Romalis, 2013, "Techniques used to search for a permanent electric dipole moment of the ^{199}Hg atom and the implications for *CP* violation," Phys. Rev. A **87**, 012102.

Szymaniec, K., S. Eon Park, G. Marra, and W. Chałupczak, 2010, "First accuracy evaluation of the NPL-CsF2 primary frequency standard," Metrologia **47**, 363–376.

Talmadge, C., J.-P. Berthias, R. W. Hellings, and E. M. Standish, 1988, "Model-independent constraints on possible modifications of Newtonian gravity," Phys. Rev. Lett. **61**, 1159.

Tamm, C., N. Huntemann, B. Lipphardt, V. Gerginov, N. Nemitz, M. Kazda, S. Weyers, and E. Peik, 2014, "Cs-based optical frequency measurement using cross-linked optical and microwave oscillators," Phys. Rev. A **89**, 023820.

Tan, W.-H., S.-Q. Yang, C.-G. Shao, J. Li, A.-B. Du, B.-F. Zhan, Q.-L. Wang, P.-S. Luo, L.-C. Tu, and J. Luo, 2016, "New test of the gravitational inverse-square law at the submillimeter range with dual modulation and compensation," Phys. Rev. Lett. **116**, 131101.

Tarallo, M. G., T. Mazzoni, N. Poli, D. V. Sutyrin, X. Zhang, and G. M. Tino, 2014, "Test of Einstein equivalence principle for 0-spin and half-integer-spin atoms: Search for spin-gravity coupling effects," Phys. Rev. Lett. **113**, 023005.

Tarbutt, M. R., B. E. Sauer, J. J. Hudson, and E. A. Hinds, 2013, "Design for a fountain of YbF molecules to measure the electron's electric dipole moment," New J. Phys. **15**, 053034.

Tardiff, E. R., *et al.*, 2014, "The radon EDM apparatus," Hyperfine Interact. **225**, 197.

Taveras, V., and N. Yunes, 2008, "Barbero-Immirzi parameter as a scalar field: K-inflation from loop quantum gravity?," Phys. Rev. D **78**, 064070.

Taylor, T. R., 1990, "Dilaton, gaugino condensation and supersymmetry breaking," Phys. Lett. B **252**, 59.

Taylor, T. R., and G. Veneziano, 1988, "Dilaton couplings at large distances," Phys. Lett. B **213**, 450.

Terrano, W. A., E. G. Adelberger, J. G. Lee, and B. R. Heckel, 2015, "Short-range, spin-dependent interactions of electrons: A probe for exotic pseudo-goldstone bosons," Phys. Rev. Lett. **115**, 201801.

Terranova, F., and G. M. Tino, 2014, "Testing the a_μ anomaly in the electron sector through a precise measurement of h/M," Phys. Rev. A **89**, 052118.

Testera, G., *et al.*, 2015, "The AEgIS experiment," Hyperfine Interact. **233**, 13.

The Jefferson Lab PVDIS Collaboration, 2014, "Measurement of parity violation in electron-quark scattering," Nature (London) **506**, 67.

Thielking, J., M. V. Okhapkin, P. Glowacki, D. M. Meier, L. von der Wense, B. Seiferle, C. E. Düllmann, P. G. Thirolf, and E. Peik, 2018, "Laser spectroscopic characterization of the nuclear clock isomer ^{229m}Th," Nature (London) **556**, 321.

Thorne, K. S., and J. B. Hartle, 1985, "Laws of motion and precession for black holes and other bodies," Phys. Rev. D **31**, 1815.

Tino, G. M., 2000, "Testing the symmetrization postulate of quantum mechanics and the spin-statistics connection," Fortschr. Phys. **48**, 537.

Tino, G. M., 2001, "Spectroscopic tests of spin-statistics connection and symmetrization postulate of quantum mechanics," Phys. Scr. **T95**, 62.

Tino, G. M., and M. A. Kasevich, 2014, Eds., in "Atom interferometry," *Proceedings of the International School of Physics "Enrico Fermi," Course 188* (IOS Press, Amsterdam).

Tino, G. M., and F. Vetrano, 2007, "Is it possible to detect gravitational waves with atom interferometers?," Classical Quantum Gravity **24**, 2167.

Tino, G. M., *et al.*, 2013, "Precision gravity tests with atom interferometry in space," Nucl. Phys. B, Proc. Suppl. **243–244**, 203.

Tobar, M. E., *et al.*, 2013, "Testing local position and fundamental constant invariance due to periodic gravitational and boost using long-term comparison of the SYRTE atomic fountains and H-masers," Phys. Rev. D **87**, 122004.

Tokunaga, S. K., C. Stoeffler, F. Auguste, A. Shelkovnikov, C. Daussy, A. Amy-Klein, C. Chardonnet, and B. Darquié, 2013, "Probing weak force-induced parity violation by high-resolution mid-infrared molecular spectroscopy," Mol. Phys. **111**, 2363.

Touboul, P., *et al.*, 2017, "MICROSCOPE mission: first results of a space test of the Equivalence Principle," Phys. Rev. Lett. **119**, 231101.

Truppe, S., R. J. Hendricks, S. K. Tokunaga, H. J. Lewandowski, M. G. Kozlov, C. Henkel, E. A. Hinds, and M. R. Tarbutt, 2013, "A search for varying fundamental constants using hertz-level frequency measurements of cold CH molecules," Nat. Commun. **4**, 2600.

Truppe, S., H. J. Williams, M. Hambach, L. Caldwell, N. J. Fitch, E. A. Hinds, B. E. Sauer, and M. R. Tarbutt, 2017, "Molecules cooled below the Doppler limit," Nat. Phys. **13**, 1173.

Trzcinska, A., J. Jastrzebski, P. Lubinski, F. J. Hartmann, R. Schmidt, T. von Egidy, and B. Klos, 2001, "Neutron density distributions deduced from antiprotonic atoms," Phys. Rev. Lett. **87**, 082501.

Tsigutkin, K., D. Dounas-Frazer, A. Family, J. E. Stalnaker, V. V. Yashchuk, and D. Budker, 2009, "Observation of a large atomic parity violation effect in ytterbium," Phys. Rev. Lett. **103**, 071601.

Tsujikawa, S., 2013, "Quintessence: a review," Classical Quantum Gravity **30**, 214003.

Tullney, K., *et al.*, 2013, "Constraints on spin-dependent short-range interaction between nucleons," Phys. Rev. Lett. **111**, 100801.

Tureanu, Anca, 2013, "*CPT* and Lorentz invariance: Their relation and violation," J. Phys. Conf. Ser. **474**, 012031.

Turner, M. S., 1988, "Axions from SN1987A," Phys. Rev. Lett. **60**, 1797.

Turner, M. S., 1990, "Windows on the axion," Phys. Rep. **197**, 67.

Tyson, J. A., G. P. Kochanski, and I. P. Dell'Antonio, 1998, "Detailed mass map of CL 0024 + 1654 from strong lensing," Astrophys. J. Lett. **498**, L107.

Tzanavaris, P., M. T. Murphy, J. K. Webb, V. V. Flambaum, and S. J. Curran, 2007, "Probing variations in fundamental constants with radio and optical quasar absorption-line observations," Mon. Not. R. Astron. Soc. **374**, 634.

Tzanavaris, P., J. K. Webb, M. T. Murphy, V. V. Flambaum, and S. J. Curran, 2005, "Limits on variations in fundamental constants from 21-cm and ultraviolet quasar absorption lines," Phys. Rev. Lett. **95**, 041301.

Ubachs, W., J. Bagdonaite, E. J. Salumbides, M. T. Murphy, and L. Kaper, 2016, "Colloquium: Search for a drifting proton-electron mass ratio from H_2," Rev. Mod. Phys. **88**, 021003.

Ueda, Masahito, 2014, "Topological aspects in spinor Bose-Einstein condensates," Rep. Prog. Phys. **77**, 122401.

Ullmann, J., *et al.*, 2017, "High precision hyperfine measurements in bismuth challenge bound-state strong-field QED," Nat. Commun. **8**, 15484.

Ulmer, S., C. C. Rodegheri, K. Blaum, H. Kracke, A. Mooser, W. Quint, and J. Walz, 2011, "Observation of spin flips with a single trapped proton," Phys. Rev. Lett. **106**, 253001.

Ulmer, S., *et al.*, 2015, "High-precision comparison of the antiproton-to-proton charge-to-mass ratio," Nature (London) **524**, 196.

Ushijima, I., M. Takamoto, M. Das, T. Ohkubo, and H. Katori, 2015, "Cryogenic optical lattice clocks," Nat. Photonics **9**, 185.

Usukura, J., K. Varga, and Y. Suzuki, 1998, "Signature of the existence of the positronium molecule," Phys. Rev. A **58**, 1918.

Uzan, J.-P., 2011, "Varying constants, gravitation and cosmology," Living Rev. Relativity **14**, 2.

Uzan, J.-P., 2013, "Variation of fundamental constants on sub- and super-hubble scales: From the equivalence principle to the multiverse," in *American Institute of Physics Conference Series*, Vol. 1514, edited by M. P. Dabrowski, A. Balcerzak, and T. Denkiewicz (American Institute of Physics), p. 14.

Uzan, Jean-Philippe, 2015, "The stability of fundamental constants," C.R. Phys. **16**, 576.

Vainshtein, A. I., 1972, "To the problem of nonvanishing gravitation mass," Phys. Lett. B **39**, 393.

van Bibber, K., and G. Carosi, 2013, "Status of the ADMX and ADMX-HF experiments," in *Proceedings of the 8th Patras Workshop on Axions, WIMPs and WISPs*, Report No. DESY-PROC-2012-04, arXiv:1304.7803.

Van Tilburg, K., N. Leefer, L. Bougas, and D. Budker, 2015, "Search for ultralight scalar dark matter with atomic spectroscopy," Phys. Rev. Lett. **115**, 011802.

van Zoest, T., *et al.*, 2010, "Bose-Einstein condensation in microgravity," Science **328**, 1540.

Varga, K., 2014, "Comment on the 'Stability of the five-body bi-positronium ion Ps_2e^-'," [Phys. Lett. A 372 (2008) 6721] Phys. Lett. A **378**, 529.

Varga, K., J. Usukura, and Y. Suzuki, 1998, "Second bound state of the positronium molecule and biexcitons," Phys. Rev. Lett. **80**, 1876.

Vasilakis, G., J. M. Brown, T. W. Kornack, and M. V. Romalis, 2009, "Limits on new long range nuclear spin-dependent forces set with a K-^{3}He comagnetometer," Phys. Rev. Lett. **103**, 261801.

Vasil'ev, B. V., 1969, Zh. Eksp. Teor. Fiz. Pis'ma Red. **9**, 299.

Velyukhov, G. E., 1968, Zh. Eksp. Teor. Fiz. Pis'ma Red. **8**, 372.

Venema, B. J., P. K. Majumder, S. K. Lamoreaux, B. R. Heckel, and E. N. Fortson, 1992, "Search for a coupling of Earth's gravitational field to nuclear spins in atomic mercury," Phys. Rev. Lett. **68**, 135.

Vessot, R. F. C., M. W. Levine, E. M. Mattison, E. L. Blomberg, T. E. Hoffman, G. U. Nystrom, B. F. Farrel, R. Decher, P. B. Eby,

and C. R. Baugher, 1980, "Test of relativistic gravitation with a space-borne hydrogen maser," Phys. Rev. Lett. **45**, 2081.

Vetter, P. A., D. M. Meekhof, P. K. Majumder, S. K. Lamoreaux, and E. N. Fortson, 1995, "Precise test of electroweak theory from a new measurement of parity nonconservation in atomic thallium," Phys. Rev. Lett. **74**, 2658.

Vietze, L., P. Klos, J. Menendez, W. C. Haxton, and A. Schwenk, 2015, "Nuclear structure aspects of spin-independent WIMP scattering off xenon," Phys. Rev. D **91**, 043520.

Vilenkin, A., 1985, "Cosmic strings and domain walls," Phys. Rep. **121**, 263.

Volotka, A. V., D. A. Glazov, O. V. Andreev, V. M. Shabaev, I. I. Tupitsyn, and G. Plunien, 2012, "Test of many-electron QED effects in the hyperfine splitting of heavy high-Z ions," Phys. Rev. Lett. **108**, 073001.

Volotka, A. V., D. A. Glazov, G. Plunien, and V. M. Shabaev, 2013, "Progress in quantum electrodynamics theory of highly charged ions," Ann. Phys. (Berlin) **525**, 636.

Volotka, A. V., D. A. Glazov, V. M. Shabaev, I. I. Tupitsyn, and G. Plunien, 2014, "Many-electron QED corrections to the g factor of lithiumlike ions," Phys. Rev. Lett. **112**, 253004.

Volotka, A. V., and G. Plunien, 2014, "Nuclear polarization study: New frontiers for tests of QED in heavy highly charged ions," Phys. Rev. Lett. **113**, 023002.

von der Wense, L., *et al.*, 2016, "Direct detection of the ^{229}Th nuclear clock transition," Nature (London) **533**, 47.

von Lindenfels, D., *et al.*, 2013, "Experimental access to higher-order Zeeman effects by precision spectroscopy of highly charged ions in a Penning trap," Phys. Rev. A **87**, 023412.

Vretenar, D., G. A. Lalazissis, and P. Ring, 2000, "Neutron density distributions for atomic parity nonconservation experiments," Phys. Rev. C **62**, 045502.

Vutha, A. C., *et al.*, 2010, "Search for the electric dipole moment of the electron with thorium monoxide," J. Phys. B **43**, 074007.

Wagner, A., S. Sturm, F. Köhler, D. A. Glazov, A. V. Volotka, G. Plunien, W. Quint, G. Werth, V. M. Shabaev, and K. Blaum, 2013, "g factor of lithiumlike silicon ^{28}Si^{11+}," Phys. Rev. Lett. **110**, 033003.

Wagner, A., *et al.*, 2010, "Search for hidden sector photons with the ADMX detector," Phys. Rev. Lett. **105**, 171801.

Wagner, T. A., S. Schlamminger, J. H. Gundlach, and E. G. Adelberger, 2012, "Torsion-balance tests of the weak equivalence principle," Classical Quantum Gravity **29**, 184002.

Wall, T. E., A. M. Alonso, B. S. Cooper, A. Deller, S. D. Hogan, and D. B. Cassidy, 2015, "Selective production of Rydberg-Stark states of positronium," Phys. Rev. Lett. **114**, 173001.

Wan-Ping, Z., Z. Peng, and Q. Hao-Xue, 2015, "Detecting extra dimensions by hydrogen-like atoms," Open Physics **13**, 96.

Wansbeek, L. W., B. K. Sahoo, R. G. E. Timmermans, K. Jungmann, B. P. Das, and D. Mukherjee, 2008, "Atomic parity nonconservation in Ra$^+$," Phys. Rev. A **78**, 050501.

Warrington, R. B., C. D. Thompson, and D. N. Stacey, 1993, "A new measurement of parity-non-conserving optical rotation at 648 nm in atomic bismuth," Europhys. Lett. **24**, 641.

Wcisło, P., P. Morzyński, M. Bober, A. Cygan, D. Lisak, R. Ciuryło, and M. Zawada, 2016, "Experimental constraint on dark matter detection with optical atomic clocks," Nature Astron. **1**, 0009.

Webb, J. K., V. V. Flambaum, C. W. Churchill, M. J. Drinkwater, and J. D. Barrow, 1999, "Search for time variation of the fine structure constant," Phys. Rev. Lett. **82**, 884.

Webb, J. K., J. A. King, M. T. Murphy, V. V. Flambaum, R. F. Carswell, and M. B. Bainbridge, 2011, "Indications of a spatial variation of the fine structure constant," Phys. Rev. Lett. **107**, 191101.

Weinberg, S., 1978, "A new light boson?," Phys. Rev. Lett. **40**, 223.

Weinberg, Steven, 1976, "Gauge theory of *CP* nonconservation," Phys. Rev. Lett. **37**, 657.

Weinberg, Steven, 1989, "The cosmological constant problem," Rev. Mod. Phys. **61**, 1.

Weiss, David S., Fang Fang, and Jingbiao Chen, 2003, "Measuring the electric dipole moment of Cs and Rb in an optical lattice," in *Bulletin of the American Physical Society*, Vol. 48, No. 3, Abstract J1.008.

wen Chou, Chin, Christoph Kurz, David B. Hume, Philipp N. Plessow, David R. Leibrandt, and Dietrich Leibfried, 2017, "Preparation and coherent manipulation of pure quantum states of a single molecular ion," Nature (London) **545**, 203.

Weyl, H., 1950, "A remark on the coupling of gravitation and electron," Phys. Rev. **77**, 699.

Weyssenhoff, J., and A. Raabe, 1947, "Relativistic dynamics of spin-fluids and spin-particles," Acta Phys. Pol. **9**, 7.

Wheeler, J. A., 1946, "Polyelectrons," Ann. N.Y. Acad. Sci. **48**, 219.

Whitmore, J. B., and M. T. Murphy, 2015, "Impact of instrumental systematic errors on fine-structure constant measurements with quasar spectra," Mon. Not. R. Astron. Soc. **447**, 446.

Wichmann, E. H., 2001, "Symmetries and the connection between spin and statistics in rigorous quantum field theory," in *American Institute of Physics Conference Series*, Vol. 596 (American Institute of Physics), p. 201.

Wicht, A., J. M. Hensley, E. Sarajlic, and S. Chu, 2002, "A preliminary measurement of the fine structure constant based on atom interferometry," Phys. Scr. **T102**, 82.

Wiens, E., A. Y. Nevsky, and S. Schiller, 2016, "Resonator with ultrahigh length stability as a probe for equivalence-principle-violating physics," Phys. Rev. Lett. **117**, 271102.

Wilczek, F., 1978, "Problem of strong P and T invariance in the presence of instantons," Phys. Rev. Lett. **40**, 279.

Wilczek, F., 1982, "Axions and family symmetry breaking," Phys. Rev. Lett. **49**, 1549.

Wilczynska, M. R., J. K. Webb, J. A. King, M. T. Murphy, M. B. Bainbridge, and V. V. Flambaum, 2015, "A new analysis of fine-structure constant measurements and modelling errors from quasar absorption lines," Mon. Not. R. Astron. Soc. **454**, 3082.

Will, C. M., 2014, "The confrontation between general relativity and experiment," Living Rev. Relativity **17**, 4.

Williams, J., S.-W. Chiow, N. Yu, and H. Müller, 2016, "Quantum test of the equivalence principle and space-time aboard the international space station," New J. Phys. **18**, 025018.

Williams, J. G., S. G. Turyshev, and D. H. Boggs, 2004, "Progress in lunar laser ranging tests of relativistic gravity," Phys. Rev. Lett. **93**, 261101.

Williams, J. G., S. G. Turyshev, and D. H. Boggs, 2012, "Lunar laser ranging tests of the equivalence principle," Classical Quantum Gravity **29**, 184004.

Wilson, Kenneth G., 1970, "Operator-product expansions and anomalous dimensions in the Thirring model," Phys. Rev. D **2**, 1473.

Windberger, A., *et al.*, 2015, "Identification of the predicted $5s - 4f$ level crossing optical lines with applications to metrology and searches for the variation of fundamental constants," Phys. Rev. Lett. **114**, 150801.

Windpassinger, Patrick, and Klaus Sengstock, 2013, "Engineering novel optical lattices," Rep. Prog. Phys. **76**, 086401.

Wineland, D. J., 2013, "Nobel lecture: Superposition, entanglement, and raising Schrödinger's cat," Rev. Mod. Phys. **85**, 1103.

Wineland, D. J., J. J. Bollinger, D. J. Heinzen, W. M. Itano, and M. G. Raizen, 1991, "Search for anomalous spin-dependent forces using stored ion spectroscopy," Phys. Rev. Lett. **67**, 1735.

Wineland, D. J., and N. F. Ramsey, 1972, "Atomic deuterium maser," Phys. Rev. A **5**, 821.

Wolf, Fabian, Yong Wan, Jan C. Heip, Florian Gerbert, Chunyan Shi, and Piet O. Schmidt, 2016, "Non-destructive state detection for quantum logic spectroscopy of molecular ions," Nature (London) **530**, 457.

Wolf, P., F. Chapelet, S. Bize, and A. Clairon, 2006, "Cold atom clock test of Lorentz invariance in the matter sector," Phys. Rev. Lett. **96**, 060801.

Wolf, P., P. Lemonde, A. Lambrecht, S. Bize, A. Landragin, and A. Clairon, 2007, "From optical lattice clocks to the measurement of forces in the Casimir regime," Phys. Rev. A **75**, 063608.

Wolf, P., *et al.*, 2009, "Quantum physics exploring gravity in the outer solar system: the SAGAS project," Exp. Astron. **23**, 651.

Wood, C. S., S. C. Bennett, D. Cho, B. P. Masterson, J. L. Roberts, C. E. Tanner, and C. E. Wieman, 1997, "Measurement of parity non-conservation and an anapole moment in cesium," Science **275**, 1759.

Wu, C. S., E. Ambler, R. W. Hayward, D. D. Hoppes, and R. P. Hudson, 1957, "Experimental test of parity conservation in beta decay," Phys. Rev. **105**, 1413.

Wu, X., T. Gantner, M. Koller, M. Zeppenfeld, S. Chervenkov, and G. Rempe, 2017, "A cryofuge for cold-collision experiments with slow polar molecules," Science **358**, 645.

Yamaguchi, A., M. Kolbe, H. Kaser, T. Reichel, A. Gottwald, and E. Peik, 2015, "Experimental search for the low-energy nuclear transition in ^{229}Th with undulator radiation," New J. Phys. **17**, 053053.

Yamanaka, N., B. K. Sahoo, N. Yoshinaga, T. Sato, K. Asahi, and B. P. Das, 2017, "Probing exotic phenomena at the interface of nuclear and particle physics with the electric dipole moments of diamagnetic atoms: A unique window to hadronic and semi-leptonic *CP* violation," Eur. Phys. J. A **53**, 54.

Yamanaka, Nodoka, and Emiko Hiyama, **2016**, "Standard model contribution to the electric dipole moment of the deuteron, ^{3}H, and ^{3}He nuclei," J. High Energy Phys. 02, 067.

Yamazaki, T., A. Miyazaki, T. Suehara, T. Namba, S. Asai, T. Kobayashi, H. Saito, I. Ogawa, T. Idehara, and S. Sabchevski, 2012, "Direct observation of the hyperfine transition of ground-state positronium," Phys. Rev. Lett. **108**, 253401.

Yamazaki, Yasunori, and Stefan Ulmer, 2013, "*CPT* symmetry tests with cold $\bar{p}$ and antihydrogen," Ann. Phys. (Berlin) **525**, 493.

Yan, H., and W. M. Snow, 2013, "New limit on possible long-range parity-odd interactions of the neutron from neutron-spin rotation in liquid ^{4}He," Phys. Rev. Lett. **110**, 082003.

Yan, H., G. A. Sun, S. M. Peng, Y. Zhang, C. Fu, H. Guo, and B. Q. Liu, 2015, "Searching for new spin- and velocity-dependent interactions by spin relaxation of polarized ^{3}He gas," Phys. Rev. Lett. **115**, 182001.

Yan, Z.-C., W. Nörtershäuser, and G. W. F. Drake, 2008, "High precision atomic theory for Li and Be^{+}: QED shifts and isotope shifts," Phys. Rev. Lett. **100**, 243002; **102**, 249903(E) (2009).

Yang, C. N., 1950, "Selection rules for the dematerialization of a particle into two photons," Phys. Rev. **77**, 242.

Yang, S.-Q., B.-F. Zhan, Q.-L. Wang, C.-G. Shao, L.-C. Tu, W.-H. Tan, and J. Luo, 2012, "Test of the gravitational inverse square law at millimeter ranges," Phys. Rev. Lett. **108**, 081101.

Yerokhin, V. A., and Z. Harman, 2013, "Two-loop QED corrections with closed fermion loops for the bound-electron *g* factor," Phys. Rev. A **88**, 042502.

Yerokhin, V. A., P. Indelicato, and V. M. Shabaev, 2003, "Two-loop self-energy correction in high-Z hydrogenlike ions," Phys. Rev. Lett. **91**, 073001.

Yerokhin, V. A., and V. M. Shabaev, 2015, "Nuclear recoil effect in the Lamb shift of light hydrogenlike atoms," Phys. Rev. Lett. **115**, 233002.

Youdin, A. N., D. Krause, K. Jagannathan, L. R. Hunter, and S. K. Lamoreaux, 1996, "Limits on spin-mass couplings within the axion window," Phys. Rev. Lett. **77**, 2170.

Youn, S., 2016, "Axion research at CAPP/IBS," Int. J. Mod. Phys. Conf. Ser. **43**, 1660193.

Young, B. A., 1969, "Search for a gravity shift in the proton Larmor frequency," Phys. Rev. Lett. **22**, 1445.

Yu, N., and M. Tinto, 2011, "Gravitational wave detection with single-laser atom interferometers," Gen. Relativ. Gravit. **43**, 1943.

Yudin, V. I., A. V. Taichenachev, and A. Derevianko, 2014, "Magnetic-dipole transitions in highly-charged ions as a basis of ultra-precise optical clocks," Phys. Rev. Lett. **113**, 233003.

Yudin, V. I., A. V. Taichenachev, C. W. Oates, Z. W. Barber, N. D. Lemke, A. D. Ludlow, U. Sterr, Ch. Lisdat, and F. Riehle, 2010, "Hyper-Ramsey spectroscopy of optical clock transitions," Phys. Rev. A **82**, 011804.

Yunes, N., K. Yagi, and F. Pretorius, 2016, "Theoretical physics implications of the binary black-hole mergers GW150914 and GW151226," Phys. Rev. D **94**, 084002.

Zatorski, J., B. Sikora, S. G. Karshenboim, S. Sturm, F. Köhler-Langes, K. Blaum, C. H. Keitel, and Z. Harman, 2017, "Extraction of the electron mass from *g*-factor measurements on light hydrogenlike ions," Phys. Rev. A **96**, 012502.

Zel'dovich, Ya. B., 1957, "Electromagnetic interaction with parity violation," J. Exptl. Theoret. Phys. (U.S.S.R.) **33**, 1531 [http://www.jetp.ac.ru/cgi-bin/dn/e_006_06_1184.pdf] [Sov. Phys. JETP **6**, 1184 (1958)].

Zeldovich, Ya. B., 1959, "Parity nonconservation in the 1st order in the weak-interaction constant in electron scattering and other effects," J. Exptl. Theoret. Phys. (U.S.S.R.) **36**, 964 [http://www.jetp.ac.ru/cgi-bin/dn/e_009_03_0682.pdf] [Sov. Phys. JETP **9**, 682 (1959)].

Zelevinsky, T., S. Kotochigova, and J. Ye, 2008, "Precision test of mass-ratio variations with lattice-confined ultracold molecules," Phys. Rev. Lett. **100**, 043201.

Zhang, Ke, *et al.*, 2018, "Testing the universality of free fall at 10^{-10} level by comparing the atoms in different hyperfine states with Bragg diffraction," arXiv:1805.07758.

Zhitnitskii, A. R., 1980, "Weinberg's model of *CP* violation and T-odd correlations in weak decays," Sov. J. Nucl. Phys. **31**, 260.

Zhou, L., *et al.*, 2015, "Test of equivalence principle at 10^{-8} level by a dual-species double-diffraction Raman atom interferometer," Phys. Rev. Lett. **115**, 013004.

Zimmer, S., 2017, "Experimental search for the electric dipole moment of Xe-129," https://www.ag-heil.physik.uni-mainz.de/60_ENG_HTML.php.

Zwicky, F., 1933, "Die rotverschieb ung von extragalaktischen nebeln," Helv. Phys. Acta **6**, 110–127 [Gen. Relativ. Gravit. **41**, 207 (2009)].